

Site U1331¹

Expedition 320/321 Scientists²

Chapter contents

Background and objectives	1
Science summary	2
Operations	4
Lithostratigraphy	6
Biostratigraphy	11
Paleomagnetism	15
Geochemistry	17
Physical properties	18
Stratigraphic correlation and composite section	20
Downhole measurements	21
References	23
Figures	25
Tables	67

Background and objectives

Integrated Ocean Drilling Program (IODP) Site U1331 ($12^{\circ}04.088'N$, $142^{\circ}09.708'W$; 5116 meters below seafloor [mbsl]) (Fig. F1; Table T1) is the northwesternmost site drilled during the Pacific Equatorial Age Transect (PEAT) program (IODP Expedition 320/321). This site is situated $\sim 6^{\circ}$ (~ 700 km) north of the Clipperton Fracture Zone, $\sim 3^{\circ}$ (~ 350 km) south of the Clarion Fracture Zone, and ~ 170 km (90 nmi) east of the nearest previously drilled Ocean Drilling Program (ODP) Site 1221.

The survey for Site U1331 revealed a region of abyssal hills bound by a large volcanic rise to the east and several seamounts to the southwest. At Site U1331, the abyssal hills are more widely spaced than at the other PEAT sites and trend northwest rather than northeast. During the site survey we noted a change in trend of abyssal hills between Site U1331 and our next site (IODP Site U1332), perhaps associated with the Pacific plate reorganization that occurred at ~ 50 Ma (Rea and Dixon, 1983).

Prior to drilling, an interpretation of site survey seismic data (Fig. F2) indicated that Site U1331 might penetrate seismic reflectors P2 and P3 of Lyle et al. (2002). Sediment thickness, based on interval velocities from nearby ODP Leg 199 sites (Busch et al., 2006), was estimated to be ~ 187 m of sediment above basaltic basement.

One of the objectives of the combined PEAT science program is to obtain paleoceanographic records from the Pacific ocean during the time period around the Early Eocene Climatic Optimum (EECO) (Zachos et al., 2001; Shipboard Scientific Party, 2004), targeted by Site U1331. During Leg 199, a north-south transect was drilled across the equatorial region at ~ 56 Ma. Sites on this transect had generally drifted below the calcium carbonate compensation depth (CCD) by 52–53 Ma. Thus we presently lack calcareous sediments from the region of the equatorial circulation system during this time of maximum Cenozoic warmth (Zachos et al., 2001), elevated atmospheric $p\text{CO}_2$ concentrations (Lowenstein and Demicco, 2007), and a shallow early Eocene CCD estimated between 3200 and 3300 mbsl (Lyle, Wilson, Janecek, et al., 2002; Lyle et al., 2005; Rea and Lyle, 2005).

Site U1331 is located on crust with an estimated age of ~ 53 Ma to primarily intercept the interval between 53 and 50 Ma in basal carbonate sediments, an interval that was poorly sampled on the 56 Ma transect of Leg 199 and that had little carbonate recovery

¹Expedition 320/321 Scientists, 2010. Site U1331. In Pälike, H., Lyle, M., Nishi, H., Raffi, I., Gamage, K., Klaus, A., and the Expedition 320/321 Scientists, Proc. IODP, 320/321: Tokyo (Integrated Ocean Drilling Program Management International, Inc.).

doi:10.2204/iodp.proc.320321.103.2010

²Expedition 320/321 Scientists' addresses.



above the basal Paleocene–Eocene section. At Site U1331, the oldest sediments and basaltic seafloor of all Expedition 320/321 sites were sampled.

Average (noncarbonate) accumulation rates at this time were estimated to be moderate (Moore et al., 2004), showing only slight increases in some of the more northern sites on the Leg 199 latitudinal transect (ODP Sites 1215 and 1220) (Lyle, Wilson, Janecek, et al., 2002). Leg 199 records suggest that the very shallow CCD of this early Eocene time appears to deepen to the north, perhaps suggesting a northern source for bottom waters. Sites targeting this time interval would ideally give us sediments with sufficient biogenic material to better constrain the isotopic and biotic characteristics of the near-surface equatorial waters.

We positioned Site U1331 and the other PEAT sites south of the estimated paleoequatorial position at the target age in order to maximize the time that drill sites remain within the equatorial zone (i.e., $\pm 2^\circ$ of the Equator), to allow for some southward bias of the equatorial sediment mound relative to the hotspot frame of reference (Knappenberger, 2000), and to place the interval of maximum interest above the basal hydrothermal sediments. We located the site using the seafloor digital age grid from Müller et al. (1997), heavily modified and improved with additional magnetic anomaly picks from Petronotis (1991), Petronotis et al. (1994), and Deep Sea Drilling Project (DSDP)/ODP basement ages, as well as the magnetostratigraphic data compiled by Cande et al. (1989) and Cande and Kent (1995). From the digital age grid, each point is backrotated in time to zero age using the fixed-hotspot stage-poles from Koppers et al. (2001) and Engebretson et al. (1985) and the paleopole data from Sager and Pringle (1988). From the backtracked latitudes for each grid point we then obtained the paleoequator at the crustal age by contouring the paleolatitude on the original grid.

An additional important objective of the PEAT program is to provide a limited depth transect for several Cenozoic key horizons, such as the Eocene–Oligocene transition (Coxall et al., 2005). For this objective, Site U1331 will form the deepest paleodepth constraint. All Expedition 320/321 drill sites have in common the objective to improve and extend the extensive intercalibrated bio-, magneto-, chemo-, and astronomical stratigraphies for the Cenozoic (e.g., Shackleton et al., 2000; Pälike et al., 2006).

Science summary

Three holes were cored at Site U1331 ($12^\circ 04.088'N$, $142^\circ 09.708'W$; 5116 mbsl), which is the northwest-

ernmost site drilled during the PEAT program (Fig. F1; Table T1). In Hole U1331A, seafloor basalt is overlain by 187.02 m of pelagic sediment, containing radiolarian and nannofossil ooze with varying amounts of clay. The oldest sediment is of early Eocene age. For detailed coring activities, see “[Operations](#).”

The sediment column at Site U1331 has a strong resemblance to that of Site 1220 (Fig. F3) (Lyle, Wilson, Janecek, et al., 2002), but with noteworthy sharp erosive contacts concentrated within the upper two-thirds of the section (Fig. F4). A total of 7 m of Pleistocene–Pliocene clay overlies lower Oligocene to lower Eocene alternations of nannofossil ooze, radiolarian nannofossil ooze, and radiolarian oozes of varying clay and calcium carbonate content (see “[Lithostratigraphy](#)”), with a sharp lithologic change at the Eocene–Oligocene transition (~26 m core depth below seafloor [CSF]). The lowermost target interval in Hole U1331C is characterized by a ~20 m thick radiolarian ooze and porcellanite layer from 157 to 177 m CSF overlying a dominantly clayey radiolarian ooze and zeolitic clay with hydrothermal red staining from 177 to 187.5 m CSF deposited on top of a thin (187.6–188.5 m CSF in Hole U1331C) layer of calcareous ooze and zeolitic clay above the basalt. Some fine-grained basaltic fragments show fresh glassy chilled margins.

Carbonate content approaches 80% in the Oligocene nannofossil oozes in the upper part of the site and cycles between 0% and 40% in the middle Eocene section (see “[Geochemistry](#)”). A concentration of sharp erosive contacts occurs in the interval between 80 and 120 m CSF, with calcareous material dominating the basal portion of these contacts and then fining upward in grain size into radiolarian oozes. Rarely, the sediment above a sharp contact contains well-rounded clasts up to 1 cm in diameter (interval 320-U1331B-10H-6, 117–130 cm). The lithologic and stratigraphic characteristics of these sediments have been interpreted as gravity-driven deposits, possibly from nearby seamounts ~10 km to the south (Fig. F1B). Between ~177 and 187.2 m CSF, Cores 320-U1331A-22X, 320-U1331C-16H, and 17H achieved our site objective of recovering carbonate-bearing material from the time interval just following 52 Ma. All major microfossil groups were found in sediments from Site U1331, and they provide a consistent and coherent biostratigraphic succession from basement to below the surficial clay layer. Nannofossils are common in the Oligocene and lower Eocene but sporadic in sediments from the upper Eocene because of dissolution. Middle Eocene sediments commonly contain calcareous nannofossils punctuated by several barren intervals, notably below Zone



NP21 (radiolarian Zone RP19 equivalent), below Zone NP17, and between Zones NP15 and NP13 (radiolarian Zones RP12–RP8 equivalent). Radiolarians are common to abundant throughout the section. Radiolarian and nannofossil datums and their age determinations agree and range from nannofossil Zone NP12 in the basal sediment section (~51–53 m.y. before present) to Zones NP23/NP24 and radiolarian Zones RP8 just above basement through RP21 (late Oligocene, older than 25 Ma) in the uppermost section, below the Pleistocene clays. Both radiolarian and nannofossil assemblages contain reworked older components (deeper than ~50 m CSF) but within a coherent and ordered stratigraphy. Planktonic foraminifers are generally absent, except for sporadic occurrences often associated with sediment just above sharp lithologic contacts and also in the basal carbonate section (Zones E4/E5). Benthic foraminifers are generally rare and indicate lower bathyal to upper abyssal paleodepths. They are frequently found in the graded coarse sediment above the base of sharp contacts but indicate there is no apparent difference in the depth habitat between benthic foraminifers from just above sharp contacts and other parts of the section.

Apparent sedimentation rates, as implied by the biostratigraphic age determinations and aided by magnetostratigraphic polarity interpretations, vary throughout the section. The radiolarian-rich section between ~80 m CSF and basement was deposited at an average rate of 10 m/m.y., whereas the late middle Eocene to Oligocene section was deposited at a rate of ~4 m/m.y., with an apparent inflection between 60–80 m CSF. Porcellanite is located in an interval that spans a time of ~2–3 m.y. The presence of all major fossil groups as well as a detailed magnetostratigraphy will allow us to achieve one of the main PEAT objectives to arrive at an integrated Cenozoic stratigraphy and age calibration (e.g., Pälike et al., 2006).

A full physical property program was run on cores from all three holes, including Whole-Round Multi-sensor Logger (WRMSL) measurements of magnetic susceptibility, bulk density, *P*-wave velocity, and noncontact resistivity, along with natural gamma radiation (NGR), followed by discrete measurements of color reflectance, index moisture and density properties, sound velocities, and thermal conductivity. Bulk density measurements increase markedly in the carbonate-rich Oligocene section. Magnetic susceptibility measurements are variable throughout the section, allowing detailed correlation between different holes and picking of sharp contacts and clay layers by increased susceptibilities. NGR measurements are elevated by an order of magnitude in the surficial

clay layer and reach 130 counts per second (cps) at the seafloor, dropping to <5 cps deeper than 30 m CSF. Porosity values are generally high in radiolarian-rich sediments (80%) and decrease within the Oligocene carbonate section. Carbonate content is positively correlated with thermal conductivity. Discrete physical property measurements will prove useful to calibrate WRMSL velocity and density estimates and generally agree with WRMSL estimates, once appropriate correction factors are included for the core liner. Discrete velocities are significantly higher (50–100 m/s) than track measurements in the direction perpendicular to the split plane of the core section (*x*-axis), which is likely an artifact.

Using whole-round magnetic susceptibility measurements, Holes U1331A–U1331C can be spliced to form a continuous section to at least 140 m CSF or 150 m core composite depth (CCSF-A) (see “[Core composite depth scale](#)” in the “Methods” chapter), with no apparent gaps. Core expansion is ~15%. It is possible that Hole U1331C cores can provide an additional spliced section to the top of the porcellanite interval at ~157 m CSF. Below 149 m CCSF-A, it was only possible to tentatively correlate features in the track data down to Core 320-U1331A-17X for a total composite section to ~172 m CCSF-A.

A full range of paleomagnetic analyses was conducted on cores and samples from Site U1331. Our aims are to determine the magnetostratigraphy and study geomagnetic field behavior, environmental magnetism, and Pacific plate paleogeography. Shipboard analyses conducted suggest that a useful magnetic signal is preserved in almost all advanced piston corer (APC)-cored intervals. Preliminary comparison of biostratigraphic data and changes in magnetic paleodeclinations suggest the recovery of Oligocene magnetochrons to the base of the middle Eocene (Chron C21n; ~47 Ma). Paleomagnetic directions from discrete samples agree well with those from split-core results.

A standard shipboard suite of geochemical analyses of pore water and organic and inorganic sediment properties was conducted on samples from Site U1331, including a pilot study of high-resolution “Rhizon” pore water sampling, which does not require the cutting of whole rounds for squeezing. Carbonate coulometry yielded carbonate concentrations of ~80 wt% in the Oligocene nannofossil ooze and sporadic horizons with up to 40 wt% CaCO₃ in the middle Eocene radiolarian-rich oozes. Preliminary calcium carbonate determinations from the white, hydrothermally stained sediments just above basement (whole-round Sample 320-U1331C-17H-4, 83–84 cm) yielded low values of only 2–3 wt% CaCO₃. Alkalinity values range between 2.5 and 3 mM

throughout the section. Additional ephemeral samples were taken for shore-based microbiology and permeability studies.

Wireline logging provided valuable information to constrain the interval of porcellanite formation within the borehole, and further analysis will aid in interpretations of carbonate content and lithologies. Integration with the seismic data will allow further improvements with the regional seismic interpretations. Data from Site U1331 indicate that the top of seismic Horizon P2 (Lyle et al., 2002) correlates with the top of the chert section. Downhole temperature measurements with the advanced piston core temperature (APCT-3) tool, when combined with the thermal conductivity values obtained from the cores, indicate that Site U1331 had a thermal gradient of $13.4^{\circ}\text{C}/\text{km}$ and a heat flow of 10.3 mW/m^2 . This is within the range of lower values in the global heat flow data set for the eastern Pacific but significantly lower than values obtained for ODP Sites 1218 and 1219.

Highlights

Carbonate ooze in basal section

At Site U1331 we recovered a 1.2 m thick interval (lithologic Unit IV) of calcareous ooze with concretions and reddish color streaks, achieving one of the objectives for this site. The nannofossil ooze recovered in Sample 320-U1331A-22X-CC contains a moderately to poorly preserved assemblage of early Eocene planktonic foraminifers (planktonic foraminifer Zone E5). This moderately preserved assemblage was also observed in the basal section of Hole U1331C.

Stratigraphic integration

One of the primary objectives of the PEAT science program is the integration of different stratigraphic methodologies and tools. Site U1331 contains almost all major fossil groups (nannofossils, radiolarians, foraminifers, and diatoms), as well as an excellent magnetostratigraphy. The possibility of a cycle-by-cycle match between Sites U1331 and 1220 has been demonstrated using magnetic susceptibility and bulk density data, providing additional stratigraphic tie points and verification of the completeness of the stratigraphic section on a regional scale. Thus, Site U1331 will help us to achieve an integrated stratigraphy for the Cenozoic Pacific Ocean.

Eocene–Oligocene transition and depth transect

Site U1331 forms the oldest and deepest component of the PEAT depth transect component, which will

allow the study of critical intervals (such as the Eocene–Oligocene transition; see Coxall et al., 2005) and variations of the equatorial CCD. Site U1331 is estimated to have been $\sim 4.2 \text{ km}$ deep during the Eocene–Oligocene transition, $\sim 800 \text{ m}$ shallower than today. Sediments rapidly change from radiolarian ooze below the Eocene–Oligocene transition to nannofossil oozes above and will provide a tie point for calcium carbonate burial at $\sim 5^{\circ}$ paleolatitude.

Variations in the CCD

Site U1331 will provide important constraints for variations and depth of the CCD from the early Eocene to the late Oligocene. This site shows increased carbonate content and much increased mass accumulation rates approximately from the middle of Chron C18r to the base of Chron C19r during the middle Eocene and can be correlated to an interval of enhanced carbonate burial that was previously documented by Lyle et al. (2005) in Leg 199 cores.

Age transect of seafloor basalt

At Site U1331 we recovered what appear to be fresh fragments of seafloor basalt, aged between 52 and 53 Ma as estimated from biostratigraphic results. This material will, when combined with other PEAT basalt samples, be of importance for the study of basalt alteration by seawater and paleomagnetic properties of oceanic crust.

Operations

Unless otherwise noted, times are local ship time, which was Hawaii Standard Time (UTC – 10 h) for Site U1331.

Honolulu port call

Expedition 320 officially began when the first line was passed ashore to Pier 29 of Honolulu harbor at 1042 h on 5 March 2009. Following routine U.S. customs and immigration formalities, port call activities were initiated with the changing and crossover of Overseas Drilling Limited and IODP personnel. Expedition scientists boarded the ship on 6 March.

During the ~ 5 day port call, the usual food stocks and provisions were loaded and off-going freight disembarked. Items that were loaded in Honolulu included ~ 707 metric tons of marine gasoil, 147 short tons of bulk attapulgite, 7 joints of 20 inch casing, 16 joints of 16 inch casing, and 46 joints of $10\frac{3}{4}$ inch casing. Other significant items were two boxes of core liners and two reentry cone assemblies.

In accordance with the port call plan, customer service representatives came on the vessel to perform

maintenance and repair on the ship's elevator and the heating, ventilation, and air conditioning (HVAC) system. A Siemens engineer also performed upgrades to the throttle system program.

A number of shipboard tours were conducted for the IODP Science and Technology Panel, several classes from the University of Hawaii (USA), and National Science Foundation visitors. A replacement refrigerated food container had to be leased at the last moment because the 10 ft auxiliary unit located on the accommodation roof could not be repaired in the time available. The U.S. Coast Guard interrupted the loading of compressed gas cylinders on 9 March for nearly an hour to address concerns relating to the handling of these items at this facility.

Following the release of the last line from the pier at 1500 h on 10 March, the *JOIDES Resolution* exited the harbor. Outside the harbor, a small vessel came alongside to deliver a radioactive source and two neutron tools required for the logging effort. The vessel then departed at full speed to the first site (U1331) with an expected arrival the evening of 14 March.

Transit to Site U1331

The transit to the first site of Expedition 320 was made through generally moderate seas and swell with predominantly overcast skies and occasional showers signifying that we were under the influence of the Intertropical Convergence Zone (ITCZ). We began positioning over Site U1331 at 2330 h on 14 March 2009. The 1081 nmi voyage from Honolulu was accomplished at an average speed of 10.4 kt.

During the 4 day voyage the zero-speed module, which monitors shaft speed and direction, failed 1 h out of port and the breaker supplying power to starboard shaft Motor 17A and port shaft Motor 14B tripped offline 2 h before arriving on location.

Site U1331

Hole U1331A

Once the vessel was positioning over Site U1331, an operational test of the dynamic positioning (DP) system was undertaken. Concurrent with DP testing, the making up of the bottom-hole assembly (BHA) and spacing out of the core barrel and colletted delivery system were accomplished. As the drill string was deployed, the length of each joint of pipe was measured and the internal clearance of each tubular inspected in accordance with routine practices.

Prior to spud-in, the drill string was flushed and cleaned of rust particles by pumping down a clean-out plug and two round trips of an extended core barrel (XCB) core barrel. Depths reported in this

operations section are based on the measurements using the length of the drill string and are either drilling depth below rig floor (DRF) or drilling depth below seafloor (DSF).

Because the precision depth recorder was inoperative, the driller carefully extended the bit to tag the seafloor to verify the depth. Using the passive heave compensator, the bit was raised 10 m from this depth. Hole U1331A was spudded with the APC at 0750 h on 16 March 2009 (Table T1). The water depth calculated from the recovery of the first core was established as 5127.3 m DRF; the offset of the rig floor above sea level was 11.1 m, so the water depth as determined by drill string length was 5116.2 meters below sea level (mbsl).

Piston coring advanced the hole to 138.2 m DSF just above the chert layer suggested by the seismic record. We cored to 138.2 m DSF with APC Cores 1H through 15H and recovered 141.3 m of core (102%) (Table T1). Cores 1H through 11H were oriented with the FlexIt tools. Cores 12H through 15H were not oriented because the FlexIt tool was not deployed in anticipation of having to drill over stuck core barrels. The pullout force to recover the core barrels from the sediment gradually increased with depth and then decreased. We also switched to the standard, more durable steel core barrels starting with Core 12H instead of the nonmagnetic core barrels. To avoid damaging the APC, operations were then conservatively switched to the XCB corer.

XCB coring advanced from 138.2 m DSF to basement at ~190.6 m DSF. We cored a 52.4 m interval with Cores 15X through 21X and recovered 13.6 m (26%). For Cores 18X through 22X (157.3–190.6 m DSF), recovery was reduced by the presence of chert. We did manage to recover a short (0.42 m) section of the basal carbonate in the last core and bottomed out with a small sample of basalt. The total average recovery of APC/XCB coring in Hole U1331A was 81%.

Upon completion of the coring program, we conducted downhole logging, as detailed in “[Downhole measurements](#).“ Downhole logging completed one run to a total depth of the borehole with the “paleo”-combo tool string (NGR, gamma ray attenuation [GRA] density, and magnetic susceptibility). These data were used to guide the coring strategy in subsequent holes at this site. The planned second run with the Formation MicroScanner (FMS)-sonic tool was aborted because of problems with the logging winch.

Hole U1331B

After the bit was pulled above seafloor at 0820 h on 18 March 2009, the vessel was offset 20 m west of



Hole U1331A. Hole U1331B was spudded with the APC, and the recovery of the first core was used to calculate the seafloor depth as 5127.4 m DRF (5116.3 mbsl). The vertical offset to Hole U1331A was 5 m deeper to cover gaps between cores in the first hole. With APC Cores 1H through 17H, we advanced from 0 to 156.6 m DSF, cored 156.5 m, and recovered 163.13 m (104%). Five formation temperature measurements were made with the APCT-3 in Cores 2H, 3H, 5H, 7H, and 10H (19.6, 29.1, 48.1, 67.1, and 95.6 m DSF, respectively).

We switched to XCB coring for Core 18X (156.6–166.3 m DSF) but did not recover any core. Based on the drill, log, and core data from the first hole, we decided to drill with a center bit (without coring) through the chert interval (166.3–177.0 m DSF) and then attempt a single APC core in the sediment section below. APC Core 20H was attempted below the chert in the early Eocene basal carbonate section, but the corer was not able to penetrate the formation. We drilled ahead again without coring to 179.0 m DSF and one more XCB core was taken from 179.0–188.5 m DSF, but it did not recover any material. From 156.6 to 188.5 m DSF, we XCB cored 19.2 m but did not recover any material. An additional 12.7 m was drilled without coring. The bit was pulled free of the seafloor at 2220 h on 19 March, and the vessel was offset 20 m west of Hole U1331B.

Hole U1331C

The program for the third hole of the site was to fill in gaps in the sedimentary record from the first two holes by spot coring and to obtain any core from below the chert. Hole U1331C was spudded with the APC at 0155 h on 20 March 2009. The recovery of the first core was used to calculate the seafloor depth as 5128.0 m DRF (5116.9 mbsl). Cores 1H through 4H penetrated to 38.0 m DSF, and we recovered 39.2 m (103%). The interval from 38.0 to 59.0 m DSF was then drilled without coring, and Core 6H was taken from 59.0 to 68.5 m DSF (9.99 m recovered; 105%). We then drilled without coring from 68.5 to 92.5 m DSF and took APC Core 8H (92.5–102.0 m DSF; recovery = 9.21 m, 97%).

A short interval of 0.5 m was drilled to 102.5 m DSF, and Core 10H was taken from 102.5 to 112.0 m DSF, recovering 8.48 m (89%). The interval from 112.0 to 129.0 m DSF was drilled without coring, and Cores 2H through 14H were obtained from 129.0 to 157.5 m DSF (29.1 m recovered; 102%). Following a drilled interval of 19.5 m through a chert sequence (157.5–177.0 m DSF), a third attempt to core the short interval below the chert and above the top of basaltic oceanic crust was attempted.

This early Eocene section was one of the highest priority sections at this site and was poorly recovered in the previous two holes. This time the drillers successfully obtained this interval in APC Cores 17H and 18H (177.0–189.0 m DSF), coring 12.0 m and recovering 14.0 m (117%). Judging by the deformation of the cutting shoe and a bent 15 ft section of core barrel, it was surmised that Core 18H had more than vigorously encountered basement.

During spot coring in Hole U1331C, all piston cores up to and including Core 14H employed nonmagnetic core barrels and were oriented with the FlexIt tool. Standard steel barrels were used to obtain Cores 16H and 17H and did not use the orientation tool to avoid damaging it. We recovered 109.5 m (102%) in the cored interval of 107.0 m. An additional 82.0 m was drilled without coring. With the recovery of Core 17H, the decision was made to end coring at this site and to proceed to Site U1332.

After the drill string was pulled free of the seafloor at 1300 h on 21 March, the pipe trip was temporarily suspended for 1.5 h to accomplish the slipping and cutting of 115 ft of drilling line. Once drilling line maintenance was completed, tripping was resumed. The beacon was retrieved at 1500 h while the drill string was being recovered. At 0500 h on 22 March the drilling equipment was secured and the vessel departed for Site U1332.

Lithostratigraphy

Drilling at Site U1331 recovered a 189 m thick section of pelagic sediments overlying seafloor basalt. The uppermost ~6 m of the section is a late Neogene (~400 ka to 6 Ma based on radiolarian biostratigraphy and magnetostratigraphy) clay with radiolarians and micronodules (Fig. F4). These sediments are, in turn, underlain by ~94 m of Oligocene to late middle Eocene nannofossil and radiolarian ooze and ~87 m of early middle Eocene to early Eocene radiolarian ooze with alternations of nannofossil ooze, clay, and porcellanite. A thin (1.9 m thick) unit of early Eocene calcareous ooze and zeolite clay was recovered at the base of the sedimentary sequence above basalt. Approximately 15 m of the lithologic section was not recovered.

The sedimentary sequence at Site U1331 is divided into four major lithologic units, and two of these units are further divided into three subunits (Table T2; Fig. F4). Unit and subunit boundaries are defined by differences in lithology and measured physical properties. Lithologic differences, based on visual core descriptions and smear slide and thin section analysis (Figs. F5, F6; see “[Site U1331 thin sections](#)” and “[Site U1331 smear slides](#)” in “Core descrip-

tions"), are primarily attributable to varying distributions of biogenic components (e.g., nannofossils and radiolarians) and clay-sized lithogenic material with minor variations in manganese and iron oxide content. Lithologic descriptions are primarily based on sediments recovered in Hole U1331A, supplemented with observations from Holes U1331B and U1331C.

Unit I

Intervals: 320-U1331A-1H-1, 0 cm, through 2H-1, 85 cm; 320-U1331B-1H-1, 0 cm, through 1H-5, 52 cm; 320-U1331C-1H-1, 0 cm, through 1H-5, 107 cm

Depths: Hole U1331A = 0.0–6.05 m CSF; Hole U1331B = 0.0–6.52 m CSF; Hole U1331C = 0.0–7.07 m CSF

Age: late Neogene

Lithology: clay

The major lithology in Unit I is pale brown (10YR 4/3) to very dark gray (10YR 3/1) to dark brown (10YR 3/3) clay. Pale brown clay occurs in a distinct interval ~70 cm thick (in the upper meter of Hole U1331A). The clay in Unit I occurs with radiolarians and with radiolarians and micronodules as minor lithologic components. In Hole U1331A a ferromanganese crust with associated micronodules and encrusted pebbles occurs between 74 and 85 cm from the top of the sedimentary section. Bioturbation is generally minor in these sediments. Unit I is further characterized by high magnetic susceptibility, low GRA bulk densities, low L* reflectance (lightness; see "[Physical properties](#)" for additional reflectance information), and near-zero CaCO₃ content. The downhole transition into the underlying Unit II takes place over an interval that is ~5 cm thick.

Unit II

Intervals: 320-U1331A-2H-1, 85 cm, through 11H-CC, 22 cm; 320-U1331B-1H-5, 52 cm, through 11H-1, 150 cm; 320-U1331C-1H-5, 107 cm, through 8H-5, 16 cm

Depths: Hole U1331A = 6.05–99.52 m CSF; Hole U1331B = 6.52–97.10 m CSF; Hole U1331C = 7.07–98.66 m CSF

Age: early Oligocene to late middle Eocene

Lithology: alternations of nannofossil ooze and radiolarian ooze

The dominant lithologies in Unit II are pale brown (10YR 6/3) to very pale brown (10YR 7/3) nannofossil ooze, yellowish brown (10YR 5/4) to dark brown (10YR 3/3) radiolarian nannofossil ooze, and brown (10YR 5/3) to very dark brown (10YR 2/2) radiolarian ooze. Bioturbation is generally moderate to nonvisible in these sediments, and both gradual and sharp

contacts are observed between lithologies. Sharp contacts are often characterized by an inclined and irregular basal surface overlain by noticeably coarser grained, more carbonate-rich (including planktonic and benthic foraminifers), and opaque-coated sediments. The overlying materials grade from coarse to fine grained uphole.

Subunit IIa

Intervals: 320-U1331A-2H-1, 85 cm, through 4H-1, 140 cm; 320-U1331B-1H-5, 52 cm, through 3H-5, 35 cm; 320-U1331C-1H-5, 107 cm, through 3H-6, 2 cm

Depths: Hole U1331A = 6.05–25.60 m CSF; Hole U1331B = 6.52–25.95 m CSF; Hole U1331C = 7.07–26.52 m

Age: early Oligocene

Lithology: alternations of nannofossil ooze, radiolarian nannofossil ooze, and radiolarian ooze

The major lithologies in Subunit IIa are very pale brown (10YR 8/2) to brown (10YR 4/3) nannofossil ooze and pale brown (10YR 6/3) to yellowish brown (10YR 5/4) radiolarian nannofossil ooze. Pale brown (10YR 6/4) to light yellowish brown (10YR 6/3) radiolarian ooze with nannofossils are minor lithologies. Within the major lithologies, nannofossil ooze sometimes occurs with radiolarians or with diatoms and radiolarians as minor components. Radiolarian nannofossil ooze occurs with clay as a minor lithologic component, whereas radiolarian ooze occurs with clay or nannofossils as minor lithologic components. Alternations of nannofossil ooze with radiolarian nannofossil ooze and of radiolarian ooze with nannofossils occur on 5 cm to 1 m scales. Bioturbation is generally minor to nonvisible in these sediments, and both gradual and sharp contacts occur between lithologies. Sharp contacts are typically inclined and irregular surfaces with noticeably coarser grained, relatively carbonate-rich (including planktonic and benthic foraminifers), and opaque-coated overlying sediments that fine uphole. GRA bulk density, L*, and CaCO₃ contents all increase downhole at the Unit I/Subunit IIa boundary and maintain relatively high values until they decrease just above the Subunit IIa/IIb boundary (Fig. F4). Magnetic susceptibility is generally elevated but variable in Subunit IIa. The contact with underlying Subunit IIb takes place over a 5 cm interval.

Subunit IIb

Intervals: 320-U1331A-4H-1, 140 cm, through 8H-5, 119 cm; 320-U1331B-3H-5, 35 cm, through 8H-2, 76 cm; 320-U1331C-3H-6, 2 cm, to at least 6H-CC, 25 cm (boundary not cored in Hole U1331C)



Depths: Hole U1331A = 25.60–69.39 m CSF; Hole U1331B = 25.95–69.36 m CSF; Hole U1331C 26.52 to below 68.5 m CSF (boundary not cored in Hole U1331C)

Age: late to late middle Eocene

Lithology: alternations of clayey radiolarian ooze, radiolarian ooze, radiolarian nannofossil ooze, and nannofossil ooze

The absence of nannofossil ooze as a major lithology distinguishes Subunit IIb from Subunit IIa (and Sub-unit IIc; see below). The major lithologies in Subunit IIb are dark brown (10YR 3/3) clayey radiolarian ooze and yellowish brown (10YR 5/4) to dark brown (10YR 3/3) radiolarian ooze. Yellowish brown (10YR 5/4) to dark brown (10YR 3/3) radiolarian nannofossil ooze and radiolarian ooze with clay as well as yellowish brown (10YR 5/4) nannofossil ooze with radiolarians are minor lithologies. Bioturbation is generally minor to nonvisible in these sediments, and both gradual and sharp contacts are observed between lithologies. Sharp contacts are marked by inclined and irregular basal surfaces with noticeably coarser grained, more carbonate-rich (including planktonic and benthic foraminifers), and opaque-coated overlying coarse-grained sediments. Sediments grade toward finer grain sizes uphole. The transition from Subunit IIa to Subunit IIb is characterized by high-frequency, high-amplitude peaks in magnetic susceptibility, GRA bulk density, and L*. The underlying section shows generally low values for each of these series and for CaCO₃ content. Contact with the underlying Subunit IIc takes place over a 5 cm interval.

Subunit IIc

Intervals: 320-U1331A-8H-5, 119 cm, through 11H-CC, 22 cm; 320-U1331B-8H-2, 76 cm, through 11H-1A, 150 cm; top not cored in Hole U1331C but extends through 320-U1331C-8H-5, 16 cm

Depths: Hole U1331A = 69.39–99.52 m CSF; Hole U1331B = 69.36–97.10 m CSF; top of Hole U1331C not cored but extends through 98.66 m CSF

Age: middle Eocene

Lithology: alternations of nannofossil radiolarian ooze, radiolarian nannofossil ooze, and nannofossil ooze

The major lithologies in Subunit IIc are dark brown (10YR 3/3) to dark yellowish brown (10YR 5/3) nannofossil radiolarian ooze, dark brown (10YR 3/3) radiolarian nannofossil ooze, and yellowish brown (10YR 5/4) to dark brown (10YR 3/3) nannofossil ooze. Dark brown (10YR 3/3) radiolarian ooze with clay and very dark brown (10YR 2/2) radiolarian clay

are minor lithologies. Each of the major lithologies sometimes occurs with clay as a minor component. In addition, nannofossil ooze can be seen to occur with radiolarians as a minor component. Bioturbation is generally minor to nonvisible in these sediments, and both gradual and sharp contacts are observed between lithologies. Sharp contacts are common, with generally inclined and irregular basal surfaces and noticeably coarser grained, more carbonate rich (including planktonic and benthic foraminifers) overlying sediments that grade to a finer grain size uphole. Subunit IIc is characterized by relatively high L* and CaCO₃ content and slightly elevated GRA bulk densities. The contact between Subunit IIc and the underlying Unit III takes place over several centimeters.

Unit III

Intervals: 320-U1331A-11H-CC, 22 cm, through 22X-1, 11 cm; 320-U1331B-11H-150 cm, through at least 17H-CC, 40 cm (bottom not cored in Hole U1331B); 320-U1331C-8H-5, 16 cm, through 17H-3, 62 cm

Depths: Hole U1331A = 99.52–186.51 m CSF; Hole U1331B = 97.10 to at least 156.8 m CSF; Hole U1331C = 98.66–187.62

Age: early middle Eocene to early Eocene

Lithology: radiolarian ooze and radiolarian ooze with clay and with porcellanite

The dominant lithologies in Unit III are dark yellowish brown (10YR 4/4) to dark brown (10YR 3/3) radiolarian ooze and black (10YR 2/1) porcellanite. Bioturbation is generally minor to moderate in Sub-unit IIIa, minor in Subunit IIIb, and minor to absent (i.e., laminated) in Subunit IIIc. Both gradual and sharp contacts are observed between lithologies. Sharp irregular contacts with pronounced color change are particularly common in Subunit IIIa.

Subunit IIIa

Intervals: 320-U1331A-11H-CC, 11 cm, through 17X-CC, 37 cm; 320-U1331B-11H-1, 150 cm, through 17H-CC, 40 cm (bottom in Hole U1331B not cored); 320-U1331C-8H-5, 16 cm, through 14H-CC, 29 cm

Depths: Hole U1331A = 99.52–157.06 m CSF; Hole U1331B = 97.10–156.88 m CSF; Hole U1331C = 98.66–156.94 m CSF

Age: middle Eocene

Lithology: radiolarian ooze

The major lithology in Subunit IIIa is dark yellowish brown (10YR 4/4) to dark brown (10YR 3/3) radiolarian ooze. Dark yellowish brown (10YR 4/4) nannofossil radiolarian ooze, very dark grayish brown



(10YR 3/2) radiolarian ooze, and black (10YR 2/1) porcellanite are minor lithologies. Radiolarian ooze occurs with clay and nannofossils in varying amounts as minor components. Bioturbation is generally minor to moderate in these sediments. Sharp irregular contacts between lithologies of different color are common in the upper portion of this sub-unit. The sediments immediately overlying these contacts are noticeably coarser grained and more carbonate rich (including planktonic and benthic foraminifers) than those immediately below the contacts and grade into finer grained material uphole. Sub-unit IIIa is characterized by overall low magnetic susceptibility, GRA bulk density, L*, and CaCO₃ content, as well as logging magnetic susceptibility (Fig. F4). The contact with underlying Subunit IIIb was not sufficiently well recovered to be identified with confidence based on core observation, but it occurs near the top of Core 320-U1331A-18X based on drilling operations reports (see “Operations”) and down-hole logs (see “Downhole measurements”).

Subunit IIIb

Intervals: 320-U1331A-17X-CC, 37 cm, through at least 18X-1, 25 cm (bottom not recovered); not recovered in Hole U1331B; 320-U1331C-14H-CC, 29 cm, through 16H-1, 0 cm

Depths: Hole U1331A = 157.06–157.55 m CSF (bottom not cored in Hole U1331A); Hole U1331C = 156.94–177.00 m CSF

Age: early Eocene

Lithology: radiolarian ooze and porcellanite

Subunit IIIb is distinguished from Subunit IIIa (and IIIc; see below) based on the presence of porcellanite as a major lithology. The major lithologies in Sub-unit IIIb are dark brown (10YR 3/3) radiolarian ooze and black (10YR 2/1) porcellanite. Very dark brown (10YR 2/2) radiolarian clay and very dark brown (10YR 2/2) clayey radiolarian ooze are less important. Clay and opaques sometimes occur as minor components within radiolarian oozes. Oozes show minor bioturbation, and, where recovered without drilling disturbance, porcellanites are associated with intervals rich in clay.

Subunit IIIc

Intervals: top in Hole U1331A not cored, present in 320-U1331A-22X-1, 0 cm, through 22X-1, 11 cm; Subunit IIIc not cored in Hole U1331B; 320-U1331C-16H-1, 0 cm, through 17H-3, 62 cm

Depths: Top of Hole U1331A not cored to 186.51 m CSF; Hole U1331C = 177.00–187.62 m CSF

Age: early Eocene

Lithology: radiolarian ooze and clayey radiolarian ooze, radiolarian clay, and zeolite clay

The major lithologies in Subunit IIIc are dark brown (10YR 3/3), brown (10YR 4/3), and light yellowish brown (10YR 6/4) radiolarian ooze and dark yellowish brown clayey radiolarian ooze (10YR 3/4). Dark brown (10YR 3/3) radiolarian clay, dark yellowish brown (10YR 3/4) clayey radiolarian ooze, and dark brown (10YR 3/3) zeolite clay are minor lithologies. Bioturbation is minor to nonvisible in these sediments, and some intervals are distinctly laminated (e.g., Samples 320-U1331C-16H-2, 80–145 cm, and 16H-3, 80–120 cm). Only logging magnetic susceptibility data are available for comparison to the lithologic descriptions in Subunit IIIb. Formation magnetic susceptibility is highly variable, with high-amplitude short peaks likely associated with partially lithified porcellanite and clay-rich layers that characterize this subunit. The contact with underlying Unit IV occurs over a 10–15 cm interval containing centimeter-scale laminae.

Unit IV

Intervals: 320-U1331A-22X-1, 11 cm, through 22X-CC, 25 cm; Unit IV not cored in Hole U1331B; 320-U1331C-17X-3, 62 cm, through 17H-CC, 8 cm

Depths: Hole U1331A = 186.51–187.02 m CSF; Hole U1331C = 187.62–189.48 m CSF

Age: early Eocene

Lithology: calcareous ooze and zeolite clay

The major lithologies in Unit IV are light yellowish brown (10YR 6/4) calcareous ooze (composed of calcareous nannofossils and micrite) and very dark brown (10YR 2/2) zeolite clay. A basal 1.2 m thick interval of Unit IV was recovered in Hole U1331C and is characterized by calcareous ooze with concretions and reddish color streaks. Physical property data series show high variability within Unit IV consistent with the heterogeneous lithologies recovered.

Unit V

Intervals: 320-U1331A-22X-1-CC, 25 cm, through 22X-1-CC, 44 cm; not cored in Holes U1331B and U1331C

Depth: Hole U1331A = 187.02–187.21 m CSF

Age: early Eocene

Lithology: basalt

Fine-grained basaltic fragments from 1 to 5 cm in size were recovered at the base of Hole U1331A. Some of the recovered basalt shows a fresh glassy chilled margin (Fig. F7C, F7D). Thin section analysis indicates a sparsely phryic basalt mainly composed of phenocryst plagioclase (Sample 320-U1331A-22X-CC [Piece 1, 26–29 cm]) overlying a microphyric basalt mainly made of phenocryst of clinopyroxene



and plagioclase (Sample 320-U1331A-22X-CC [Piece 4, 37–44 cm]) (see “[Site U1331 Thin sections](#)” in “Core descriptions”). Minor minerals are olivine, opaque minerals, and glass.

Sediments across the Eocene–Oligocene transition

A downhole Eocene–Oligocene transition was recovered in all three holes drilled at Site U1331 (Fig. [F8](#)). The Eocene/Oligocene boundary sensu strictu is defined on the extinction of the planktonic foraminifer genus *Hantkenina* but cannot be identified at Site U1331 because although calcareous benthic foraminifers show good to very good preservation, the planktonic foraminifer assemblage is highly dissolved (see “[Biostratigraphy](#)”). Based on magnetostratigraphic and both radiolarian and nannofossil biostratigraphic results, however, the boundary falls somewhere between Section 320-U1331B-3H-5, 45 cm, and the upper part of Core 320-U1331B-4H, probably in Section 320-U1331B-3H-5 or 3H-6 (Fig. [F6](#)). The lithostratigraphy of the Eocene–Oligocene transition at Site U1331 defines the Subunit IIa/IIb boundary and is marked by a sharp (~5 cm interval) downhole transition from very pale brown nannofossil ooze to homogeneous dark brown clayey radiolarian ooze. An associated pronounced downhole increase occurs in magnetic susceptibility together with pronounced downhole decreases in GRA bulk density, L*, and CaCO₃ content (Figs. [F4](#), [F8](#)) (see “[Physical properties](#)”). These lithostratigraphic results for the Eocene–Oligocene transition at Site U1331 are consistent with those obtained from multiple sites drilled during Leg 199—in particular, with those of Site 1220 (Shipboard Scientific Party, 2002).

Gravity flow deposits

Throughout the sedimentary section drilled at Site U1331, sharp irregular contacts occur between lithologies (Table [T3](#); Fig. [F4](#)). Many are instantly recognizable by distinct changes in color (Table [T3](#); Figs. [F9](#), [F10](#)). Many of these sharp contacts are directly overlain by coarser grained, more carbonate rich (including planktonic and benthic foraminifers), and/or opaque-coated sediments than those below the contact. The overlying sediments fine up-hole (Figs. [F9](#), [F10](#)). In some cases, the coarse-grained sediments directly overlying the sharp contacts are multicolored and these contacts are often clearly of erosional origin (Figs. [F9](#), [F10](#)). Planktonic foraminifers are rare in sediments from Site U1331 because of seafloor dissolution below the shallow CCD during the Eocene. The occurrence of planktonic foraminifers above many of the sharp contacts is not consistent with a winnowing origin for the coarse-grained

intervals because this would require comparatively prolonged exposure on the seafloor. Instead, their presence in the coarse-grained intervals is indicative of improved preservation through rapid burial. For these reasons, the erosional contacts and overlying graded sediments are interpreted as the product of mass flow events, likely turbidity currents. The provenance of the inferred turbidites observed at Site U1331 is unknown, but their typically calcareous composition points to a source that lay above the CCD at the time that the reworked sediments were originally deposited, possibly the seamount lying a few kilometers to the south (present water depth at summit >500 m shallower than Site U1331) (Fig. [F3](#)).

A number of the turbidites identified in cores recovered at Site U1331 are sufficiently distinctive that they are readily correlated among two or all three sites drilled. One example is located ~0.5 m below the Unit I/Subunit IIa boundary (Fig. [F10](#)). Nannofossil biostratigraphy indicates that the sediments 7 cm below the basal scour of this turbidite seen in Hole U1331A are Oligocene in age, whereas the overlying clay (Unit I) at all three sites is substantially younger based on radiolarians (<6 Ma, most likely Pliocene–Pleistocene) (see “[Biostratigraphy](#)”). Magnetostratigraphic results support the existence of a hiatus somewhere between these two age control points (see “[Paleomagnetism](#)”). This hiatus is interpreted to fall at the base of the turbidite based on the erosional nature of its basal contact (Fig. [F10](#)).

The turbidites documented in sediments recovered from Site U1331 vary significantly in prominence. Many have barely discernible changes in grain size, whereas others contain sand- and even pebble-sized material. The coarsest grains observed occur within a partially lithified conglomerate that is surrounded by a ~1 cm thick sand layer overlying a clay horizon within the radiolarian oozes of Subunit IIc in Hole U1331B (Fig. [F9C](#)). The lithified conglomerate is ~7 cm in length. Thin section analysis indicates that centimeter-scale angular rip-up clasts of mudstone and millimeter- to micrometer-scale biogenic components are contained within a fine-grained, partially silicified clay matrix (microcrystalline quartz). The major biogenic components are benthic and planktonic foraminifers, radiolarian spines, and nannofossils. Foraminifers and nannofossils retain their calcareous composition (they have not been silicified), but foraminifer chambers are typically infilled with chalcedonic quartz.

Clay horizons and porcellanite

In Subunit IIc and Unit III, dark brown clay horizons occur within biogenic oozes at Site U1331 (Table [T4](#); Fig. [F11](#)). Some of the observed clay horizons are as-



sociated with sharp erosional boundaries and partial silicification of the associated coarser grained sediments (Fig. F11C). Clay horizons contain nannofossils, radiolarians, and, in particular, zeolite minerals in minor (<10%) amounts. Porcellanite pebbles and discrete layers are observed in sediments of middle Eocene age in Cores 320-U1331A-12H, 320-U1331B-11H, and 320-U1331C-10H (see “[Site U1331 smear slides](#)” in “Core descriptions”). Porcellanite layers 2 to 4 cm thick were recovered in Core 320-U1331A-19X from sediments of early middle Eocene age (see “[Site U1331 smear slides](#)” in “Core descriptions”). Massive or more frequent porcellanite layers are inferred to be present in the underlying 10–15 m interval where recovery was near zero based on the high-frequency, high-amplitude peaks in magnetic susceptibility data from downhole logging (Fig. F3).

Summary

At Site U1331, Eocene seafloor basalt is overlain by 187.2 m of pelagic sediments that are divided into four major lithologic units (Units I–IV); Units II and III are both divided into three subunits. Site U1331 sediments are dominated by radiolarian and nannofossil ooze with varying amounts of clay and can be correlated with Site 1220 using biostratigraphic and magnetostratigraphic results. Basal early middle Eocene sediments (Unit IV) are carbonate rich and overlain by a ~20 m thick radiolarian ooze–porcellanite interval. The middle Eocene sediment section (Hole U1331A; 49–158 m CSF) is dominated by radiolarian ooze with varying amounts of clay and nannofossil ooze and frequent turbidites. The late Eocene is characterized by radiolarian ooze with relatively less nannofossil ooze. The Eocene/Oligocene boundary is marked by a relatively sharp transition from dark brown radiolarian ooze beneath to pale brown nannofossil ooze with radiolarians above. A transition is indicated from siliceous sedimentation during the late Eocene to carbonate deposition during the early Oligocene, as observed previously in sediments from other sites in the region (e.g., ODP Sites 1218, 1219, and 1220 and DSDP Sites 161 and 162). This transition is interpreted to reflect deepening of the CCD associated with Antarctic glaciation (van Andel et al., 1975; Shipboard Scientific Party, 2002; Coxall et al., 2005).

Biostratigraphy

At Site U1331 we recovered a 187 m thick sequence of upper Oligocene–lower Eocene radiolarian clays, radiolarian clays with nannofossils, chert/porcellanite, and nannofossil ooze covered by Pliocene–Pleistocene clays. Radiolarian clays are the dominant lithology, with significant nannofossil ooze intervals in the

Oligocene and lower Eocene. A poorly recovered chert/porcellanite sequence occurs in the uppermost lower Eocene–middle Eocene. Radiolarians are present through most of the section and are well preserved in the Eocene. They provide a coherent high-resolution biochronology. Calcareous nannofossils are abundant and poor to moderately well preserved when present. Nannofossil datum and zonal determinations agree well with the radiolarian biostratigraphy; an integrated calcareous and siliceous microfossil biozonation is shown in Figure F12. A detailed age-depth plot including biostratigraphic and paleomagnetic datums is shown in Figure F13. Both radiolarian and nannofossil assemblages contain reworked older components, especially in the Oligocene section. Despite these allochthonous components, a coherent and ordered stratigraphy is apparent. Planktonic foraminifers are generally absent through most of the sequence but occur in several samples in the Oligocene and lower Eocene ooze lithologies. Benthic foraminifers are sporadically present and indicate lower bathyal to upper abyssal depths.

Calcareous nannofossils

Calcareous nannofossil biostratigraphy is based on analyses of core catcher samples from all three holes (U1331A–U1331C) and from samples from each core section in Hole U1331A. Depth positions and age estimates of biostratigraphic marker events are shown in Table T5. Nannofossils are abundant in the pale nannofossil oozes of the Oligocene and lower Eocene and are consistently present through significant portions of the middle Eocene (from 75.30 to 96.18 m CSF and 110.50 to 119.58 m CSF in Hole U1331A), where radiolarian ooze with clay lithology dominates. However, barren intervals are frequent through the Eocene section and from 119.90 (Hole U1331A) to 185.32 (Hole U1331C) m CSF nannofossils are completely absent. Where present in the radiolarian clay lithologies the nannofossils are common to abundant, but typically etched, and characterized by abundant disaggregated and/or fragmented placolith shields. Discoasters present in these assemblages appear to be less susceptible to dissolution. In the nannofossil ooze lithology, nannofossil preservation is moderate to poor.

The red clay in the uppermost portion of the section (0–6.3 m CSF) is barren of calcareous nannofossils. The interval from Samples 320-U1331B-1H-5, 100 cm, to 320-U1331A-4H-1, 110 cm (7.00–25.30 m CSF), is carbonate rich, and nannofossil Zones NP23–NP21 are recognized using the base of *Sphenolithus distentus* in Sample 320-U1331A-2H-4, 70 cm (10.38 m CSF), top of *Reticulofenestra umbilicus* in



Sample 320-U1331A-3H-6, 110 cm (23.29 m CSF), and top of *Coccolithus formosus* in Sample 320-U1331A-3H-CC (24.34 m CSF). Rare specimens resembling *Sphenolithus ciperoensis* were observed in Sample 320-U1331B-1H-CC, together with frequent *Sphenolithus predistentus* and *Triquetrorhabdulus longus*. We have not, however, applied the base of *S. ciperoensis* datum because of its absence from samples at similar, or shallower, depths from the top of Holes U1331A and U1331C. The rare occurrence of transitional *S. distentus*–*S. ciperoensis* morphologies suggests that the top of the Oligocene nannofossil-bearing lithology is in the vicinity of the Zone NP23/NP24 boundary. Reworked nannofossils of late Eocene to early Oligocene age are conspicuous between Samples 320-U1331A-2H-1, 147 cm (6.66 m CSF), and 2H-3, 70 cm (8.89 m CSF), coincident with coarse fining-upward sequences in the cores.

The interval from Samples 320-U1331A-4H-2, 70 cm (26.43 m CSF), to 9H-2, 60 cm (73.8 m CSF), is predominantly barren of calcareous nannofossils, but limited carbonate-bearing intervals containing nannofossils are present in each core. The tops of *Discoaster saipanensis* in Sample 320-U1331A-4H-7, 10 cm (33.30 m CSF), *Chiasmolithus grandis* in Sample 320-U1331A-6H-7, 9 cm (51.79 m CSF), and *Chiasmolithus solitus* in Sample 320-U1331A-8H-6, 50 cm (70.20 m CSF), and base of *Dictyococcites bisectus* in Sample 320-U1331A-6H-CC (52.60 m CSF) delineate nannofossil Zones NP22, NP21, and NP17 and an undifferentiated Zone NP18–NP20 interval. The Eocene/Oligocene boundary transition must lie between the top of *C. formosus* and top of *D. saipanensis* and is apparently complete at the resolution provided by the nannofossil biostratigraphy. Reworking is commonly found through this interval.

The interval from Samples 320-U1331A-9H-3, 60 cm (75.32 m CSF), to 13H-CC (119.58 m CSF) is largely nannofossiliferous. The base of *R. umbilicus* in Sample 320-U1331A-11H-4, 30 cm (94.68 m CSF), and top *Nannotetraena fulgens* in Sample 320-U1331A-13H-5, 70 cm (116.40 m CSF), indicate the presence of nannofossil Zones NP16 and NP15. These datums are further supported by the total range of *Discoaster bifax* (Samples 320-U1331A-8H-6, 50 cm, through 13H-2, 5 cm). The base and top of *D. bifax* were used by Bukry (1973) to define Subzone CP14a (along with alternative marker species), but modern calibrations are lacking and so these events were not included in the 320/321 timescale charts.

The interval from Samples 320-U1331A-14H-1, 70 cm (119.90 m CSF), to 320-U1331C-16H-CC (185.32 m CSF) is barren of calcareous nannofossils, although recovery in all three holes was poor between ~160 and 180 m CSF because of the presence of extensive

chert/porcellanite horizons. A short interval of white nannofossil ooze, lying directly on basalt, was recovered at the base of Holes U1331A and U1331C (Cores 320-U1331A-22X and 320-U1331C-17H). The top of *Tribrachiatus orthostylus*, which defines the Zone NP12/NP13 boundary, is located in Sample 320-U1331C-17H-3, 109 cm. This basal nannofossil ooze contains *Girgisia gammation*, *Discoaster lodoensis*, and *Toweius callosus*, indicating a position in uppermost Zone NP12 to lowermost Zone NP13.

Radiolarians

Radiolarians are common to abundant throughout the recovered section, except in the basal carbonate, where they are absent (Table T6, T7, T8). In the upper (Oligocene) part of the section (Cores 320-U1331A-1H through 3H), radiolarians show distinct signs of dissolution and fragmentation. In the Eocene section, however, preservation is good. Even within and below the Eocene chert/porcellanite interval near the base of the section, radiolarians are frequently abundant and well preserved.

The radiolarian stratigraphy and datum levels shown in Table T9 are based on Nigrini et al. (2006). In this work, 12 new species were named and a substantial number of new biostratigraphic datums were correlated with the paleomagnetic stratigraphy of Sites 1218–1220. The application of this stratigraphy to Site U1331 was made difficult by extensive reworking of older radiolarians into younger assemblages. The upper ~10 m of the section is likely to be Quaternary in age, as indicated by the presence of *Theocyrtium trachelium* in Sample 320-U1331A-1H-CC. However, the radiolarian assemblage in these sediments is dominated by species that range from Oligocene to early middle Eocene in age. Below this highly mixed interval, sediments are mid-Oligocene (Zone RP21) but also contain reworked lower Oligocene and Eocene species. To further complicate matters, the marker species for the base of the next younger zone (*Lynchocanoma elongata*; Zone RP22) is apparently present in the core catcher of Core 320-U1331A-2H but is not found in upper part of this core. The accompanying presence of *Lithocyclia angusta* and common *Dorcadospyris circulus*, as well as the absence of *Acrocubus octopyle*, *Calocyctella robusta*, and *Dorcadospyris scambos*, argue for placing the lower part of Core 320-U1331A-2H well within Zone RP21. We believe that this anomalous occurrence of what appears to be *L. elongata* may be a case of a brief iterative appearance, similar to that seen for *A. octopyle* and *Didymocyrtis tubaria* in Leg 199 material. Because of the pervasive mixing, first appearance datums are the more reliable.

The Eocene/Oligocene boundary is probably represented by a hiatus within the upper part of Core 320-U1331A-4H. The change in the assemblage from Zone RP20 in Core 320-U1331A-3H (Oligocene) to Zone RP19 in Core 4H is quite distinct in spite of the reworked older material. All radiolarian zones are represented down to Zone RP12 in Core 320-U1331A-16X; however, the amount of reworked material varies with depth (Fig. F14) as a result of the varying amount of downslope transport of sediments (see “[Lithostratigraphy](#)”) and the overall sediment accumulation rate. Near basement the reworking of older microfossils is difficult to detect.

Zones RP10 and RP9 were recovered in Cores 320-U1331A-19X, 20X, and 320-U1331C-16H below the chert/porcellanite interval. The Zone RP9/RP8 boundary lies just below Sample 320-U1331C-16H-4, 96–103 cm. Zone RP8 is the oldest radiolarian zone recovered at Site U1331. Based on correlation with paleomagnetic stratigraphy, this zonal boundary lies at ~50.9 Ma (older than indicated in the “[Methods](#)” chapter). Based on this correlation, the oldest sediment recovered containing radiolarians must be slightly older than 51 Ma.

Diatoms

Diatoms were examined in core catcher samples from Hole U1331A. Diatoms are typically rare with poor preservation or are absent from the samples examined. The exception is Sample 320-U1331-3H-CC, which contains few diatoms with moderate preservation. The assemblage consists of *Coscinodiscus marginatus*, *Coscinodiscus trochus*, and *Coscinodiscus excavatus*. The occurrence of *C. excavatus* allows assignment of this sample to the lowermost Oligocene *C. excavatus* Zone.

Also of note is the interval from Samples 320-U1331A-13H-CC through 16H-CC, which contains rare to common diatoms with poor preservation. Sample 320-U1331A-13H-CC contains rare specimens of *C. marginatus* and *Hemiaulus polymorphus*. The occurrences of *H. polymorphus* and *Triceratium schultzii* in Sample 320-U1331A-15H-CC suggest an Eocene age for the sample. Sample 15H-CC is of note as the diatoms are common but dominated by a to be determined pennate diatom.

Planktonic foraminifers

Core catchers were sampled from all three holes at Site U1331, and additional samples were taken in Hole U1331A (approximately one per core) from any light-colored sediment intervals, which we assumed had a higher carbonate content. Samples were, for the most part, completely barren of planktonic for-

minifers except for brief intervals in the Oligocene and early-middle Eocene when a carbonate-rich lithology was present. Thus, planktonic foraminifers were of limited use in the development of a high-resolution biostratigraphy and for correlation between holes. Depth positions and age estimates of biostratigraphic marker events identified are shown in Table T10. Abundances and estimates of preservation are presented in range chart format (Table T11). Where recovered, planktonic foraminifer assemblages are generally dissolved and moderately to poorly preserved, have relatively low species diversities (maximum = ~12 species), and include individuals that show evidence of recrystallization (i.e., are not glassy). The sporadic occurrence of planktonic foraminifers at this site is thought to be the result of dissolution because of the site’s position either below or close to the CCD.

In Sample 320-U1331A-2H-4, 49–51 cm, a moderately preserved Oligocene assemblage was recovered containing the marker species *Paragloborotalia opima*, indicating planktonic foraminifer Zones upper O2 through O5. Further differentiation of biozones between Zones O2 and O5 was hindered by the absence of key taxa (i.e., *Chiloguembelina cubensis*, *Subbotina angiporoides*, *Turborotalia ampliapertura*, and *Globigerina angulisuturalis*). The long-ranging Eocene-Oligocene taxa *Catapsydrax unicavus*, *Paragloborotalia nana*, *Turborotalia increbescens*, *Dentoglobigerina galavisi*, and *Globoquadrina euapertura* are also present. In Sample 320-U1331B-1H-CC, a poorly preserved fauna was recovered containing *P. nana*, *C. unicavus*, *G. euapertura*, and *Dentoglobigerina tripartita* along with a number of paragloborotaliids, but the lack of age-diagnostic taxa prevented a zonal assignment beyond a very broad estimate, based on taxa ranges, of Zones E13–O6. Nannofossil and radiolarian zonal assignments NP24 and RP21, respectively, suggest that the assemblage in Sample 320-U1331B-1H-CC is upper Oligocene.

Sample 320-U1331A-10H-2, 30–32 cm, contains a highly dissolved middle Eocene assemblage. The assemblage is dominated by robust globigerine forms. The genera *Morozovelloides* and *Globigerinatheka* are completely absent. The presence of *Turborotalia pomeroli* and *Acarinina bullbrookii* indicate that the assemblage falls within the upper part of planktonic foraminifer Zone E10 or within Zone E11, consistent with age estimates determined by nannofossil (Zone NP16) and radiolarian (Zone RP14) biostratigraphy. Single specimens of *Turborotalia frontosa* and *Dentoglobigerina pseudovenezuelana* found in Samples 320-U1331A-9H-CC and 10H-CC, respectively, indicate a broad planktonic foraminifer zonal range E7–E13 (middle Eocene) in keeping with the Zone



E10/E11 assignment for Sample 320-U1331A-10H-2, 30–32 cm.

The nannofossil ooze recovered at the base of Hole U1331A in Sample 320-U1331A-22X-CC contains a moderately to poorly preserved assemblage of early Eocene planktonic foraminifers. Species identified in the assemblage include *Morozovella aragonensis*, *Morozovella formosa*, *Morozovella lensiformis*, *Morozovella marginodentata*, *Acarinina pseudosubspherica*, *Acarinina soldadoensis*, *Acarinina wilcoxensis*, *Subbotina patagonica*, *Globanomalina planoconica*, *Cibicidoides grimsdalei*, and *Parasubbotina inaequespira*. Based on the presence of *M. aragonensis* and *Morozovella subbotinnae*, this assemblage is assigned to planktonic foraminifer Zone E5, consistent with the nannofossil Zone NP12 assignment for this sample. Similarly, at the base of Hole U1331C in Sample 320-U1331C-17H-CC, the basal carbonate contains an early Eocene planktonic foraminifer assemblage of approximately the same age (planktonic foraminifer Zones E4–E5). However, in contrast to Hole U1331A, the planktonic foraminifer assemblage recovered in Sample 320-U1331C-17H-CC is highly dissolved and contains only a small number of whole specimens and a large number of broken planktonic foraminifers, as well as numerous agglutinated and calcareous benthic foraminifers and fish remains (teeth, ootholiths, and bone fragments). Molds of planktonic foraminifers are also present but rapidly disintegrate when touched. Fauna is scarce but contains acarininids and subbotinids, whereas morozovellids are almost completely absent. Additional small sediment samples scraped from the surface of Section 320-U1331C-17H-3 between 77 and 105 cm during cleaning of the core surface contain moderately preserved foraminifer assemblages that were used to help further constrain the biostratigraphy. The assemblages are similar to those observed in Sample 320-U1331A-22X-CC (Table T10). Core 320-U1331C-17H is tentatively assigned to planktonic foraminifer Zone E5 based on the presence of *M. subbotinnae*, *M. aragonensis*, *M. formosa*, and *M. marginodentata* and the absence of *Subbotina velascoensis* and *Morozovella aqua*. However, only a single highly dissolved specimen of *M. aragonensis* was identified (in Sample 320-U1331C-17H-CC), and the assemblages in general correspond to Zones E4–E5.

In Hole U1331B, toothpick samples were taken from coarse-grained layers identified in Samples 320-U1331B-1H-5, 116 cm, 1H-7, 72 cm, 10H-2, 9 cm, 11H-2, 89 cm, and 11H-3, 18 cm, to determine the composition of the layers. Samples from coarse layers consistently yielded fish teeth, fish bone, and benthic and planktonic foraminifers in the >250 µm size fraction (with a planktonic:benthic foraminifer

ratio of ~1:2). In Samples 320-U1331B-1H-5, 116 cm, and 1H-7, 72 cm, only a few species such as *P. nana* and *C. unicavus* were identified, indicating a middle Eocene through Oligocene age. In Samples 320-U1331B-10H-2, 9 cm, 11H-2, 89 cm, and 11H-3, 18 cm, the presence of *P. nana*, *C. unicavus*, *Turborotalia possagnoensis*, and *Globigerinatheka index* indicates planktonic foraminifer Zones E11–E15, a range consistent with nannofossil and radiolarian biostratigraphic determinations. The ratio of planktonic to benthic foraminifers was higher in the <250 µm size fraction than in the >250 µm size fraction.

Benthic foraminifers

Benthic foraminifers were examined semiquantitatively in all three holes of Site U1331. Benthic foraminifers at this site were sporadically present, but they were common in several samples (e.g., 320-U1331A-2H-CC, 10H-CC, and 22H-CC). Preservation of foraminifer tests was generally moderate to poor. The occurrence of benthic foraminifers at this site is shown in Table T12.

The uppermost sample in Hole U1331A (Sample 320-U1331A-1H-CC; 5.14 m CSF) contains no benthic foraminifers. In Sample 320-U1331A-2H-CC (15.02 m CSF), *Oridorsalis umbonatus*, *Nuttallides umbonifera*, *Cibicidoides mundulus*, and *Globocassidulina subglobosa* are common, and *Cibicidoides havanensis* and *C. grimsdalei* are subordinate. A similar fauna was found in Samples 320-U1331B-1H-CC, 2H-CC, and 320-U1331C-1H-CC. Preservation of foraminifer tests is good to moderate. These Oligocene taxa indicate lower bathyal and abyssal paleodepths (van Morkhoven et al., 1986).

Samples 320-U1331A-3H-CC through 19X-CC (24.34–162.36 m CSF) contained only sporadic benthic foraminifers. Agglutinated forms, such as *Rhizammina* spp., *Spiroplectammina spectabilis*, and *Paratrochamminoides* spp., are found with some poorly preserved calcareous forms. Calcareous forms identified include *O. umbonatus*, *Nuttallides truempyi*, *Cibicidoides eoceanus*, and *C. grimsdalei* and are found in Samples 320-U1331A-10H-CC (90.51 m CSF), 320-U1331B-8H-CC (77.19 m CSF), 9H-CC (81.61 m CSF), and 320-U1331C-10H-CC (110.92 m CSF). Preservation of these foraminifer tests is moderate. These faunas suggest lower bathyal to abyssal paleodepth at this site in the middle Eocene.

Similar faunas were also found in Samples 320-U1331A-10H-7, 44–46 cm, and 10H-7, 47–49 cm (scrape samples), taken from a coarse-grained bed. *N. truempyi*, *O. umbonatus*, and *C. grimsdalei* are common, and *G. subglobosa*, *Gyroidinoides* spp., *Anomalinoides* sp., and *Alabamina* sp. are subordinate. There is no marked difference in the faunal association between



these scrape and core catcher samples. Qualitative observation suggests that the test size of benthic foraminifers in Sample 320-U1331A-10H-7, 47–49 cm, is slightly larger than that observed in Sample 10H-7, 44–46 cm. In addition, planktonic foraminifers were more abundant in these coarse-grained layers compared to other Eocene samples. The ratio of planktonic/planktonic + benthic foraminifers increased uphole (from 14 to 31) through this interval. These features suggest that calcareous foraminifers might have been transported by a turbidity current to their current location and were preserved by rapid burial, but there is no evidence that the transport is from a significantly shallower depth zone.

Early Eocene Sample 320-U1331A-22H-CC (187.18 m CSF) contains rare *O. umbonatus* and *N. truempyi*. In contrast, Sample 320-U1331C-17H-CC (189.51 m CSF) contains common *N. truempyi* and *Gyroidinoides* spp. with *G. subglobosa* and *O. umbonatus* subordinate. Calcite overgrowths were commonly observed on the test surface of calcareous forms. These taxa suggest a lower bathyal to abyssal paleodepth.

Paleomagnetism

We measured and analyzed the magnetic remanence of archive-half sections from 54 cores collected from the three holes at Site U1331, excluding core catcher sections and other sections dominated by coring disturbance. The natural remanent magnetization (NRM) of each section was measured before and after alternating-field (AF) demagnetization at 20 mT. When time permitted, NRM was also measured after 5, 10, and/or 15 mT steps.

We processed data extracted from the Laboratory Information Management System (LIMS) database by removing all measurements collected from disturbed intervals, which are listed in Table T13, and all measurements that were made within 5 cm of the section ends, which are biased by sample edge effects. Cleaned data are available for each hole by AF demagnetization level in Tables T14, T15, T16, T17, T18, T19, T20, T21, T22, T23, T24, and T25.

For data from the 20 mT demagnetization step, we computed the mean paleomagnetic direction for stable polarity intervals from each core using Fisher statistics, with data from reversed polarity intervals inverted (Table T26). By subtracting the mean declination from each observed declination, the azimuth of the core can be approximately reoriented back into geographic coordinates. After this reorientation, normal polarity intervals have ~0° declination and reversed polarity intervals have ~180° declination. Based on the Pacific apparent polar wander path (APWP) (e.g., Beaman et al., 2007; Petronotis et al.,

1994), the declination for Oligocene and Eocene age sediments from Site U1331 is expected to be about 0° during normal polarity intervals. Hence, this reorientation method should provide a good estimate for placing the cores in their true geographical coordinates. Reoriented declinations are provided for Holes U1331A–U1331C in Tables T18, T22, and T25, respectively, for data collected after AF demagnetization at 20 mT.

In the absence of other evidence, this reorientation method would lead to a magnetic polarity ambiguity in which one might be unable to differentiate between magnetic north and magnetic south. By mapping the paleomagnetic declination downhole among holes, using distinct polarity reversal sequences within a single core, and taking advantage of biostratigraphic age constraints, it is fairly straightforward to determine a continuous polarity stratigraphy downhole and hence to obtain the correct azimuthal orientation of the core. This only breaks down when significant coring gaps occur or when rotation occurs between pieces within a single core, which is the case for all cores collected with the XCB. Hence XCB cores are not reoriented, nor can we confidently determine polarity from these because the inclination is generally too shallow at paleoequatorial sites, like all of the sites cored during this expedition.

We also attempted to reorient the cores using FlexIt tool data, but tool failures and other complications resulted in these data being considered only as a secondary method for orienting cores. Additional evaluation of the FlexIt tool during Expedition 321 indicated that the relative orientation from one core to the next was consistent and typically aided with reorienting the cores. For Site U1331, FlexIt orientation data proved useful in determining the polarity for the interval from 140 to 160 m CSF in Holes U1331B and U1331C, which otherwise had ambiguous polarity.

We also measured NRM, mass, and bulk magnetic susceptibility for 101 discrete paleomagnetic samples, with one sample collected about every section from Hole U1331A. Of these, 88 samples were subjected to progressive AF demagnetization up to 60 mT with a few samples demagnetized to 80 mT. The other 13 samples were progressively thermally demagnetized at room temperature, 90°C, and then from 150° to 600°C at 50°C steps. Remanence measurements and characteristic remanent magnetization (ChRM) directions computed using principal component analysis (PCA) are given in Tables T27 and T28, respectively. Magnetic susceptibilities and masses, along with volumes estimated using moisture and density (MAD) data (see “Physical proper-



ties"), are given in Table T29. This table also gives susceptibilities from whole-core data for the intervals corresponding to where the discrete samples were taken. These are used for checking the scale factor, 0.68×10^{-5} (see "Paleomagnetism" in the "Methods" chapter), for converting whole-core raw susceptibility meter measurements into true volume-normalized susceptibility values.

Results

Downhole variations in paleomagnetic data from split-core and discrete samples and magnetic susceptibility data from whole-core and discrete samples are shown in Figures F15, F16, and F17. Site U1331 cores contain a substantial drilling overprint, as is typical for cores from DSDP, ODP, and IODP (e.g., Shipboard Scientific Party, 2002). The overprint is primarily a viscous isothermal remanent magnetization (IRM), which results from the sediments residing inside the relatively magnetic BHA, drill pipe, and steel core barrel (and, to a lesser extent, the non-magnetic core barrel) for about 15 to 45 min from the time it is collected until it is removed from the core barrel on the rig floor.

The most obvious evidence of the overprint is the steep inclination (typically $\sim 70^\circ$ – 80°) measured prior to demagnetization. After AF demagnetization at 10 to 20 mT, the inclination becomes very shallow in general, as expected for sediments deposited near the Equator. The declinations are also overprinted, although it is often possible to discern the primary declination prior to demagnetization. The remanent magnetic intensities (prior to demagnetization) are also partially overprinted, as is evident by the manner in which they mimic magnetic susceptibility (Fig. F18). This happens because the viscous IRM magnetizes many of the magnetic grains, making the NRM prior to demagnetization a proxy for magnetic mineral concentration, similar to magnetic susceptibility. After demagnetization, the magnetically soft IRM is removed and the remaining NRM varies as a function of magnetic mineral concentration and paleomagnetic field strength, thus diverging from susceptibility, which does not depend on paleomagnetic field strength.

Following removal of the drilling overprint, a stable component of magnetization is resolved for AF demagnetization between 15 and 60 mT and for thermal demagnetization between 300° and $\sim 580^\circ\text{C}$ (Fig. F19). We interpret this ChRM to be the primary depositional remanent magnetization. Discrete samples have ChRM directions, as determined by PCA, that commonly differ by only a few degrees from the coeval intervals from the split-core samples, for which the 20 mT results are used as an estimate of

the ChRM. This indicates that any overprint is successfully removed by AF demagnetization up to 20 mT, with few exceptions, and so the NRM following 20 mT demagnetization is a reliable indicator of the ChRM for most intervals. Within a few narrow intervals, the inclinations remain steep even after demagnetization, indicating the drilling overprint still dominates in these intervals. For example, the 20 mT split-core data from 78.3 to 81.3 m CSF in Hole U1331A have an average inclination of 63° and the ChRM direction cannot be reliably resolved for discrete samples from this interval. A similar result was obtained for the coeval interval in Hole U1331B, so the result cannot be attributed to drilling deformation. More likely, it is related to lithology, with the interval being extremely homogeneous as opposed to the bioturbated interval above and below it. We suggest this interval may represent a turbidite that was only weakly and incoherently magnetized during deposition. Hence the drilling overprint makes a much more significant contribution.

It is likely that some small overprint remains in many intervals even after magnetic cleaning because the inclinations are not symmetrically distributed about zero. Instead, they are biased several degrees toward positive values, which could possibly result from a Brunhes field overprint or a drilling overprint. For example, the mean inclination for reversed polarity sediments from Hole U1331B that are Chron C12r age is 1.4° , whereas normal polarity sediments that are Chron 13n age have a mean inclination of 16.8° . Regardless, any overprint is sufficiently small that variations in inclination can be used to aid in determining the polarity even though the mean inclination at the site is very shallow. In such cases, reversed polarity intervals consistently have slightly shallower inclination than normal polarity intervals, as in the example for Chron C12r and C13n. Declination is, however, the primary parameter used for polarity determination, as it changes by $\sim 180^\circ$ across polarity reversals (Figs. F15, F16, F17, F20).

Magnetostratigraphy

Interpretation of the magnetostratigraphy is relatively uncomplicated, except for a few intervals (Table T30; Fig. F20). In particular, the upper 8 m of sediment record a sequence of magnetozones (N1 to R3) (see Fig. F20 for magnetozone definitions) that is tentatively interpreted to span from Chron C2An.2r in the upper part of Zone R3 to Chron C2r in Magnetozone R1. The upper normal polarity magnetozone (N1) may be partly Chron C2n and partly Chron C1n (Brunhes) because a manganese horizon occurs in interval 320-U1331A-1H-1, 74–85 cm, indicating



there was a period with no or extremely low deposition (see “[Lithostratigraphy](#)”). The interpretation of this upper sequence of magnetozones is based mainly on mixed radiolarian assemblages in the core catcher of Core 320-U1331A-1H that range in age from Pleistocene to late Miocene and on the existence of an erosional contact overlain by a turbidite(?) that occurs from 6.6 to 7.6 m CSF in the individual holes or at 8.11 m CCSF-A (see Table [T30](#)). This contact is within Magnetozone R3. Nannofossils belonging to Biozone NP23 (early Oligocene) are identified 7 cm below the contact. Below the erosional contact, the polarity sequence from the lower part of Magneto-zones R3 through N6 is unambiguously correlated to Chrons C10r through C13n. Given this sequence of reversals, the erosional contact at 8.11 m CCSF-A depth represents a nearly 26 m.y. long hiatus.

Other complications result from erosional contacts with overlying units that are likely turbidites (see “[Lithostratigraphy](#)”). These mainly confound interpretation in an interval from about 28 to 38 m CSF (between Magnetozones R6 and N10, which correspond to Chrons C13r and C17n.1n).

A final complication occurs for the interval below ~130 m CSF owing to discontinuous core recovery, coring deformation, and porcellanite layers. Nonetheless, we did record long intervals of constant polarity and two reversals, one at ~149 m CSF and the other at ~179 m CSF (see Table [T30](#)). A third reversal was observed at 186 m CSF in Core 320-U1331C-17H, but we consider it a somewhat suspicious result as the core had sustained minor coring deformation and because the drilling overprint could not be fully removed. Because of the discontinuous record and the difficulty with azimuthal core orientation, the reversal at 149 m CSF could correspond to either the Chron C20r/C21n or C21n/C21r reversal. The Chron C21n/C21r interpretation is in better agreement with biostratigraphic constraints, but the FlexIt orientation supports the Chron C20r/C21n interpretation, so that is the preferred interpretation (Table [T30](#)). Using inclination data, we interpret the reversal at 179 m CSF as a reversed polarity magnetozone (inclinations that are negative to near 0°) overlying a normal polarity magnetozone (inclinations that are slightly positive). Given that the seafloor at the site is Chron C23r age (~52 Ma), the reversal at 179 m CSF must be the Chron C21r/C22n, C22r/C23n.1n, or C23n.1r/C23n.2n reversal. The older ages are more compatible with biostratigraphic constraints. Hence we correlate the reversal with Chron C23n.1r/C23n.2n. Likewise, if the apparent reversal at 186 m is real, it would most likely correspond to the Chron C23n.2n/C23r boundary.

Geochemistry

Sediment gases sampling and analysis

Headspace gas samples were taken at a frequency of one sample per core in Hole U1331A as part of the routine environmental protection and safety monitoring program. All headspace gas sample analyses resulted in nondetectable levels of methane (C_1 ; <1 ppmv) with no higher hydrocarbons, consistent with the low organic carbon content of these sediments.

Interstitial water sampling and chemistry

Twenty-one interstitial water samples were collected using the traditional whole-round squeezing approach (Table [T31](#)). In addition, 14 samples were collected using Rhizon samplers from Section 320-U1331B-1H-6 at 10 cm spacing (Table [T32](#)). This section, with a visible color change at ~95 cm, corresponding to a change in calcium carbonate content, was chosen as a test of the logistics of this sampling on the *JOIDES Resolution*. Rhizon samplers were inserted through the core liner at an angle of ~55° along the length of the section so that they would not contact the typically disturbed core material near the core liner on either side (Fig. [F21A](#)). The section was positioned so the Rhizon samplers were in the vertical plane, with the sampler tubes exiting toward the top of the section (Fig. [F21A](#)). The samplers yielded 12 mL of fluid in the first 30 min, and water flow rate and total yield did not vary with depth in the section (Fig. [F21B](#)). We observed cracking in the sediment core as fluid collection proceeded (Fig. [F21A](#)), and visual observation raised concern that water near the core liner may be drawn into the sediment with time.

Chemical constituents were determined according to the procedures outlined in “[Geochemistry](#)” in the “Methods” chapter. We treated the results from the squeezed samples (Table [T31](#)) and Rhizon samples (Table [T32](#)) as single profiles with depth. Chlorinity shows relatively little variability with depth, with values ranging mainly from 555 to 565 mM (Fig. [F22](#)). Alkalinity ranges from 2.5 to 3.1 mM. Slightly lower alkalinites were observed in the uppermost 30 m CSF and between 80 and 120 m CSF. Sulfate concentrations are relatively constant and near seawater values throughout. Low alkalinites and high sulfate concentrations indicate that organic matter supply is not sufficient to drive redox conditions to sulfate reduction. The relatively low regeneration of organic carbon is also indicated by low dissolved phosphate concentrations, below detection limit in all but the uppermost ~25 m CSF. Because of the high sulfate concentrations, dissolved Ba concentra-



tions are low and relatively homogeneous, with values between 1.5 and 2.0 μM . Concentrations of dissolved silicate increase with depth from ~450 to ~800 μM .

Calcium and magnesium concentrations show similar patterns with depth, with values ranging from 9 to 11 mM and 46 to 53 mM, respectively (Fig. F22). Lithium, boron, and strontium concentrations vary between 21 and 28 μM , 410 and 490 μM , and 70 and 82 μM , respectively, have pronounced minima between 10 and 20 m CCSF-A, and subsequently decrease with depth (Fig. F23).

Bulk sediment geochemistry: major and minor elements

Selected bulk sediment samples at Site U1331 were analyzed for major and minor elements to target a distinct lithologic transition (180–190 m CSF in Hole U1331C) at relatively high resolution (~1 m). We analyzed concentrations of silicon, aluminum, iron, manganese, magnesium, calcium, sodium, potassium, titanium, phosphorus, copper, chromium, scandium, strontium, vanadium, yttrium, and zirconium (Table T33) by inductively coupled plasma–atomic emission spectroscopy (ICP-AES). The notable results are discussed below.

SiO_2 ranges between 7 and 80 wt%, showing a general decrease from 180 to 188 m CSF and a slight increase to 190 m CSF. Concentrations of Al_2O_3 range from 0.4 to 11 wt% with peaks around 187 and 189 m CSF, which are separated by a distinct minimum, also present in SiO_2 . A similar pattern is revealed by TiO_2 (0.01–0.6 wt%), K_2O (0.25–2 wt%), Zr (18–186 ppm), and Sc (0.6–40 ppm).

Iron and manganese show high concentrations between 186 and 188 m CSF of up to 15 and >0.2 wt% for Fe_2O_3 and MnO , respectively. Similar trends are shown by copper (50 to >140 ppm) and vanadium (0–150 ppm). The peak concentrations of Mn and Cu could not be quantified because they exceeded the calibrated range (Table T33).

Calcium (CaO) ranges from 0.4 to 40 wt%, with the maximum value corresponding to the minimum in SiO_2 and Al_2O_3 . Strontium concentrations range from 60 to >700 ppm, showing a similar pattern compared to CaO . Magnesium varies between 0.3 and 9 wt%, with peak values between 186 and 187 m CSF. In summary, the bulk geochemistry of the selected interval of Site U1331 reflects the varying lithology of the sediments.

Bulk sediment geochemistry: sedimentary inorganic and organic carbon

Calcium carbonate (CaCO_3), inorganic carbon (IC), and total carbon (TC) concentrations were determined on sediment samples from Hole U1331A (Table T34; Fig. F24). CaCO_3 concentrations ranged between <1 and 82 wt%. From ~6 to 24 m CSF, CaCO_3 concentrations are high (34–82 wt%), with values <1% in the uppermost ~6 m CSF. From 26 to 70 m CSF, CaCO_3 concentrations are low, with some spikes at 33.8 and ~50–53 m CSF. Higher CaCO_3 concentrations of 16 to 63 wt% are present between 70 and 93 m CSF. Below 94 m CSF, CaCO_3 concentrations are generally low, with higher concentrations of 18–26 wt% present at ~115–119 m CSF. Variations in CaCO_3 concentrations correspond to lithostratigraphic variations (see “[Lithostratigraphy](#)”).

Total organic carbon (TOC) concentrations were determined by two methods, normal and acidification (see “[Geochemistry](#)” in the “Methods” chapter) (Table T34; Fig. F24). TOC concentrations determined by using the normal method range from <0.1 to 1.7 wt%. These values may be overestimates because they are determined as a small difference between two numbers comparable in magnitude. This results in poor precision because of error propagation in very low TOC and high- CaCO_3 sediments. For example, determining a TOC value of 0.2 wt% from a sample with 10 wt% TC, with the TC value having an error of 0.03 wt% (0.3% relative standard deviation [RSD]) and IC values each having a nominal error of 0.04 wt% (0.4% RSD), results in an absolute error for TOC of ± 0.05 wt% or 25% RSD. Therefore, we analyzed TOC using carbonate-free sediments after treatment by acidification. TOC concentrations by this acidification method are very low throughout the sediment column, with values ranging from below the detection limit (<0.03 wt%) to 0.05 wt% (Fig. F24).

Physical properties

Physical properties at Site U1331 were measured on whole cores, split cores, and discrete samples. WRMSL (GRA bulk density, magnetic susceptibility, *P*-wave velocity, and electrical noncontact resistivity [NCR]), thermal conductivity, and NGR measurements comprised the whole-core measurements. Compressional wave velocity measurements on split cores and MAD analyses on discrete core samples were made at a frequency of one per undisturbed section in Cores 320-U1331A-1H through 22X. Compressional wave velocities were measured toward the



bottom of sections. MAD analyses were located 10 cm downsection from carbonate analyses (see “[Geochemistry](#)”). Lastly, the Section Half Multi-sensor Logger (SHMSL) was used to measure spectral reflectance on archive-half sections.

Density and porosity

Two methods were used to evaluate wet bulk density at Site U1331. GRA provided an estimate from whole cores (Fig. [F25](#)). MAD samples gave a second, independent measure of wet bulk density, along with providing dry bulk density, grain density, water content, and porosity from discrete samples (Table [T35](#)). MAD and GRA bulk density measurements display the same trends and are also similar in absolute values through the entire section (Fig. [F26B](#)). In general, wet bulk density values are 0.2 g/cm³ higher than GRA bulk density, which has been attributed to the GRA coefficient used in data processing combined with the attenuation coefficient of the radiolarian-rich sediments (Lyle et al., 2002). This offset was confirmed by measuring water as a standard, which gave a value of 1.2 g/cm³. All GRA data have been corrected for this offset. Cross-plots of wet and dry bulk density versus interpolated GRA density (Fig. [F27](#)) show excellent correlation between MAD and GRA data.

Generally, wet bulk density corresponds to changes in lithology. Density is higher in Subunits IIa and IIc, which are relatively high in CaCO₃ (see “[Lithostratigraphy](#)”). Wet bulk density is ~1.25 g/cm³ from the seafloor to the base of Unit I. Values increase to 1.6 g/cm³ in Subunit IIa, which is characterized by high CaCO₃ weight percent. Bulk density decreases in Subunit IIb to values of 1.2 g/cm³. In Subunit IIc, where CaCO₃ content reaches 50 wt%, bulk density increases to ~1.35 g/cm³. Bulk density is 1.2 g/cm³ in Subunits IIIa–IIIc. These units are predominantly radiolarian ooze and show very little variation in bulk density values. Bulk density increases in a short interval at the base of the cored section that corresponds with the APC-cored sections that recovered carbonate-rich sediment.

Variation in grain density in Hole U1331A generally matches changes in lithology (Fig. [F26C](#)). Grain density averages 2.4 g/cm³ in Unit I in Hole U1331A. In Subunit IIa it increases to 2.7 g/cm³, coinciding with the increase in CaCO₃. In the upper section of Subunit IIb grain density decreases to 2.2 g/cm³ and becomes highly variable through the rest of the succession, ranging from 2.2 to 2.9 g/cm³. This variation is expected to be related to variations in radiolarian content (opal = 2.2 g/cm³) and that of carbonate material (calcite = 2.7 g/cm³).

Porosity averages 83% through much of the succession. Porosity and water content vary inversely with wet bulk density (Fig. [F26A](#)). Porosity decreases to a minimum of 50% in the clay-rich upper Eocene section of Subunit IIa. The highest porosity (91%) is present in the radiolarian clay of Unit II at 65 m CSF.

Magnetic susceptibility

Whole-core magnetic susceptibility measurements correlate well with the major differences in lithology and changes in bulk physical properties (Fig. [F25B](#)). Magnetic susceptibility values in Unit I are relatively high. A significant decrease in susceptibility marks the top of Unit II at ~5 m CSF. Magnetic susceptibility values are low in Subunit IIa, averaging 10×10^{-5} SI, with a gradual rise into Subunit IIb. The highest susceptibility in Subunit IIb (28.9×10^{-5} SI) is reached at ~46 m CSF, after which values decrease toward the top of Subunit IIc. Through Subunit IIc susceptibility increases gradually from 6×10^{-5} to 25×10^{-5} SI. In Unit III magnetic susceptibility gradually decreases and then increases again, from $\sim 20 \times 10^{-5}$ to 10×10^{-5} SI, at the top of Unit IV where the record ends.

Variations in magnetic susceptibility are thought to correspond to alternations between nannofossil ooze (lower magnetic susceptibility) and clayey nannofossil ooze (higher magnetic susceptibility). The increase in susceptibility toward the base of Unit III is expected to relate to the presence of chert in the succession.

Compressional wave velocity

Shipboard results

Compressional wave velocity was measured by the *P*-wave logger (PWL) on all whole cores from Holes U1331A–U1331C and by the insertion and contact probe systems on split cores from Hole U1331A (Table [T36](#)), allowing determination of velocities in the *y*-, *z*-, and *x*-directions. Whole-core and split-core data follow similar trends, with key features occurring at similar locations (Fig. [F28](#)); however, values are offset with a difference of ~50 m/s between PWL and discrete *z*- and *y*-directions and a difference of ~100 m/s for the *x*-direction. This is thought to have resulted from excessive wetting of sediment to ensure a measurement could be taken on the split cores, a water-rich rind inside the core liner, and possible variations in pressure/probe contact between the PWL and discrete *x*-direction transducers.

Slight downhole trends in velocity generally follow changes in lithology and bulk properties (Fig. [F28](#)). Velocity (PWL) increases with depth in Unit I to the Eocene/Oligocene boundary. From 5 m CSF, near the



base of Unit I, to 10 m CSF, near the top of Unit II, velocity decreases to 1440–1450 m/s. Overall, velocity gradually increases with depth in Unit II. Small internal variations in velocity may reflect alternations in lithology. Unit III is marked by fairly uniform velocities (~1470 m/s), again with internal variation most likely attributed to changes in lithology. Data are not available for the chert-rich lower part of Unit III. Limited data for Unit IV give the highest velocities seen in this section (~1485 m/s).

The lack of consistent downhole velocity trends in Hole U1331A is partly explained by the cross-plot of velocity and wet bulk density (Fig. F29). Unit I has increasing density with slightly decreasing velocity. Subunits IIa and IIc comprise radiolarian ooze and variable carbonate nannofossil components; these continue this trend of increasing density with decreasing velocity. Subunit IIb follows a similar but much weaker trend with much more scatter, whereas Subunit IIIa shows more limited variation of velocity with density; both have higher velocities than neighboring units.

Postcruise correction

During the initial sampling of Hole U1337A, it was observed that *x*-direction velocities are consistently higher than other velocities and that PWL velocities are consistently low for Hole U1337A and all holes drilled at Sites U1331–U1336. It was determined that the high *x*-directed velocities are the result of using an incorrect value for the system delay associated with the contact probe (see “Physical properties” in the “Site U1337” chapter). Critical parameters used in this correction are system delay = 19.811 µs, liner thickness = 2.7 mm, and liner delay = 1.26 µs. PWL velocities were corrected for Hole U1337A by adding a constant value that would produce a reasonable velocity of water (~1495 m/s) for the quality assurance/quality control (QA/QC) liner (see “Physical properties” in the “Site U1337” chapter). These corrections have not been applied to the velocity data presented in this chapter.

Natural gamma radiation

NGR was measured on all whole cores at Site U1331 (Fig. F25). The highest NGR values are present at the seafloor (~130 cps). NGR values remain high through Unit I and the top of Unit II, where they average 8.5 cps. Below 30 m CSF, values drop to ~5 cps throughout Units II–IV; this is relatively higher than the 1 cps values noted during Leg 199 and is expected to be the result of the use of a new, more sensitive NGR track that records at a higher resolution. A number of spikes in NGR occur in Units II–IV; these appear to correspond to sharp boundaries iden-

tified in the lithologic core descriptions. The steplike feature in Hole U1331A at ~78 m is an artifact resulting from a baseline shift of unknown origin that occurred during the analysis of cores from Hole U1331A.

Thermal conductivity

Thermal conductivity was measured on the third section of each core from Hole U1331A (Table T37). Thermal conductivity shows a strong dependence on porosity in Unit I (Fig. F30) but seems otherwise unaffected by porosity. Decreased conductivity occurs with increasing porosity as increased interstitial spacing attenuates the applied current from the probe. Thermal conductivity is almost constant through Units II–IV (~0.74 W/[m·K]), except for a notable increase to 0.82 W/(m·K) near the Unit II/III boundary.

Reflectance spectroscopy

Spectral reflectance was measured on split archive section halves from Holes U1331A–U1331C using the SHMSL (Fig. F31). The parameters L* (black–white), a* (green–red), and b* (blue–yellow) follow changes in lithology, with variations in L* and b* correlating very well to carbonate content, density, and magnetic susceptibility measurements. The parameter a* has a very limited relationship with lithologic variation downhole. Carbonate-rich sediments are found in Subunits IIa and IIc; these intervals are represented by a distinct increase in L* and b* values in these sections. Subunit IIa shows the highest L* and b* values (70 and 17, respectively), corresponding to the increased carbonate content (shown by geochemistry data) above the Eocene/Oligocene boundary. These increases in L*, a*, and b* clearly respond to lithology, where carbonate-rich sections are light brown-gray and radiolarian-rich sections are darker brown.

Stratigraphic correlation and composite section

All cores from Site U1331 were initially depth-shifted on the basis of magnetic susceptibility and GRA bulk density data collected at 5 cm resolution with the Special Task Multisensor Logger (STMSL; “fast track”) soon after recovery. Data from the STMSL were used to monitor and direct coring in Holes U1331B and U1331C in real time to provide complete recovery and construction of the composite section. Several intervals between Holes U1331A and U1331B did not overlap sufficiently to cover gaps between cores. Thus, coring of Hole U1331C was designed to cover



the missing intervals, as well as to provide additional material for high-resolution studies. The coring effort in Hole U1331C was successful at covering gaps between cores in Holes U1331A and U1331B to ~134 m CSF (149 m CCSF-A). Below 149 m CCSF-A it was only possible to tentatively correlate features in the track data to Core 320-U1331A-17X for a total composite section of ~172 m (Fig. F32). The correlation between the three holes for the chosen parameters was good or, in some depth intervals, excellent. The gaps between successive cores are on the order of 1 to 2 m, with a maximum of 2.5 m.

The correlation was refined once magnetic susceptibility and GRA density were available at 2.5 cm resolution from the WRMSL. NGR and color reflectance data were also available from the NGR track and the SHMSL (see “Physical properties”). Magnetic susceptibility proved most useful for correlating between holes at Site U1331. Features in the magnetic susceptibility are well aligned among Holes U1331A–U1331C to 140 m CCSF-A, as these cores were not significantly stretched, squeezed, or disturbed during the coring process (Fig. F32). Offsets and composite depths are listed in Table T38. Good weather conditions during the entire occupation of Site U1331 led to excellent recovery and fairly small coring gaps in all three holes. Chert intervals caused poor core recovery below ~160 m CSF.

Following construction of the composite depth section at Site U1331, a single spliced record was assembled for the aligned cores to 172 m CCSF-A. Sections of core used for the splice are identified in Table T39. The spliced composite section mainly consists of sections from Holes U1331A and U1331B. Four segments from Hole U1331C were needed in the splice to fill core breaks in Holes U1331A and U1331B (Fig. F32). Cores from Site U1331 provide a continuous stratigraphic sequence to ~149 m CCSF-A with four potential gaps at ~39.7, ~45.8, ~115.0, and ~143.7 m CCSF-A. Preliminary paleomagnetic reversal stratigraphy (see “Paleomagnetism”) suggests that the hole to hole correlation based on magnetic susceptibility data in the interval between ~32.6 and ~44.0 m CCSF-A might be affected by the occurrence of a sharp erosional contact in the radiolarian ooze that is overlain by multiple graded beds with multi-colored coarse sand grains. This interval is easily recognized as a sharp peak in the magnetic susceptibility data at 38.45 m CCSF-A at 320-U1331B-4H-5, 90 cm, and 320-U1331C-4H-6, 34 cm. Below ~150 m CCSF-A the shipboard composite splice is not well constrained and might need postcruise refinement. We avoided intervals with significant disturbance or distortion and intervals where whole-round samples

for interstitial water chemistry and microbiology were taken (see “Paleomagnetism;” Table T13).

The Site U1331 splice can be used as a sampling guide to recover a single sedimentary sequence between 0 and 172 m CCSF-A, although it is advisable to overlap a few decimeters from different holes when sampling to accommodate anticipated ongoing development of the depth scale. Stretching and compression of sedimentary features in aligned cores indicates distortion of the cored sequence. Because much of the distortion occurs within individual cores on depth scales of <9 m, it was not possible to align every single feature in the magnetic susceptibility, GRA, NGR, and color reflectance records. However, at crossover points along the splice (Table T39), care was taken to align highly identifiable features from cores in each hole.

A growth factor of 1.10 is calculated by linear regression for all holes at Site U1331, indicating a 10% increase in CCSF-A relative to CSF depth (Fig. F33). We used this value to calculate the CCSF-B (see “Corrected core composite depth scale” in the “Methods” chapter) depths presented in Table T38 to aid in the calculation of mass accumulation rates.

Sedimentation rates

All the principal biostratigraphies, plus a set of ~30 paleomagnetic reversals, are defined in Holes U1331A–U1331C (Table T40; see “Biostratigraphy” and “Paleomagnetism”). Paleomagnetic reversals are used to calculate the average linear sedimentation rates (LSRs) for Site U1331 using the CCSF-B scale through most of the section. Calcareous nanofossils, foraminifers, and radiolarians are present throughout the entire section and were used in addition to the magnetostratigraphy in establishing age control (Fig. F13). The LSR at Site U1331 in the radiolarian oozes of lithologic Units II and III decreases from ~16 m/m.y. in the middle Eocene part of the section to 5.5 m/m.y. in the late Eocene and to 3.2 m/m.y. in the early Oligocene (Fig. F13). Based on a simple linear interpolation from the sediment surface (assumed to be zero age) and Chron C2n (Table T40), the clays of lithologic Unit I (see “Lithostratigraphy”) have a LSR of 2.7 m/m.y.

Downhole measurements

Logging operations

Downhole logging measurements in Hole U1331A were made after completion of APC/XCB coring to a total depth of 190.6 m DSF. In preparation for logging, the hole was flushed with a 65 bbl sweep of high viscosity mud and the go-devil was dropped to



open the lockable flapper valve. The hole was then displaced with 80 bbl of mud, and the bit was pulled up to ~80 m DSF. No tight spots were encountered during the reaming. The deployment of two tool strings (modified triple combination [triple combo] and FMS-sonic) was planned for Hole U1331A; however, because of difficulties with the wireline winch unit during deployment of the first tool string, the second tool string (FMS-sonic) was not deployed.

On 18 March 2009, the modified triple combo tool string (magnetic susceptibility, density, and NGR) (Fig. F34) was lowered and logged to 191 m wireline log depth below seafloor (WSF) and reached the bottom of the hole. The hole was then logged to seafloor. The tools provided continuous and good quality log data. The borehole diameter was 10 inches (25.4 cm) near the base of the hole, increasing to >18 inches (~45.7 cm) above 131 m WSF. The depth of the chert-rich interval was identified in the logs, which allowed the coring strategy in Holes U1331B and U1331C to be adjusted to maximize recovery of the target sediment interval beneath the chert.

Both the wireline winch and the wireline heave compensator (WHC) had problems during the logging operation. The WHC was initialized just after entering the open hole, but the flying head on the piston/pulley system moved up to its maximum extent and stayed there, rather than oscillating about the middle point as it would under normal operation. Initial troubleshooting failed to fix the WHC, and given the relatively calm sea state (<1 m heave), the hole was logged without heave compensation. As a result of the fully extended WHC piston, apparent logging depths (wireline log depth below rig floor [WRF]) for this hole are ~6–7 m deeper than expected. The cause of the WHC problem was later found to be the Vickers valve, which switches the hydraulic system to alternately move the piston up or down.

On the upward logging pass, logging speed became erratic because the winch motor and clutch was slipping under the weight of the cable and tool string. The upward pass was completed, although cable speed remained erratic. At one point it was difficult to raise the tool string at all. Logging operations were terminated because of the risk to the second tool string (FMS-sonic).

The wireline depth to seafloor was determined from the step increase in gamma ray values at the sediment/water interface to be at 5133.5 m WRF; the drillers mudline depth used for establishing core depth was 5127.3 m DRF.

Logging units

Hole U1331A was divided into three units on the basis of the logs (Fig. F35). The uplog was used as the reference to establish the wireline log matched depth below seafloor (WMSF) depth scale.

Logging Unit 1: base of drill pipe to 157 m WMSF

Unit 1 is characterized by low gamma ray values (between 2 and 6 gAPI), low and uniform density values (~1.25 g/cm³), low magnetic susceptibility, and a wide hole diameter. Logged density values are slightly higher than MAD bulk density measurements, probably because of core expansion (Fig. F35). NGR values were logged through the pipe, and these data were corrected by a factor of 3.5 to account for attenuation by the thickness of the drill pipe (Figs. F35, F36). Gamma ray values are similar to the open hole except in the top 1 m of the hole, where values reach 54 gAPI.

Logging Unit 2: 157–175 m WMSF

Unit 2 is characterized by a series of peaks to higher gamma, density, magnetic susceptibility, and photoelectric factor (PEF) values than those found in Unit 1 (Fig. F33). This is consistent with harder and less porous material than is found in Units 1 and 3. Drilling and coring data from this section indicate it is a porcellanite-rich interval (See “[Lithostratigraphy](#)”).

Logging Unit 3: 175–189 m WMSF

Unit 3 is similar to Unit 1 both in the absolute density, gamma radiation, and susceptibility values and in the relatively uniform log response. Susceptibility and conductivity logs increase in the lowermost 2 m of the hole and probably represent a different lithology; they may also be affected by the underlying basaltic basement.

Heat flow

Heat flow at Site U1331 was determined according to the procedure of Pribnow et al. (2000). Five APCT-3 temperature measurements in Hole U1331B ranged from 1.88°C at 19.6 m to 2.86°C at 95.6 m, giving a geothermal gradient of 13.4°C/km (Fig. F37; Table T41). Seafloor temperature was ~1.5°C. Thermal conductivity under in situ conditions was estimated from laboratory-determined thermal conductivity using the method of Hyndman et al. (1974) (see “[Physical properties](#)” in the “Methods” chapter). Calculated in situ values are ~2% lower than measured laboratory values. Thermal resistance was then



calculated by cumulatively adding the inverse of the in situ thermal conductivity values over depth intervals downhole (Fig. F37). Heat flow was obtained from the linear fit between temperature and thermal resistance (Fig. F37). The heat flow estimate for Site U1331 is 10.3 mW/m², which is lower than heat flow values from nearby Sites 1218, 1219, and 1220 but within the range of the lower values in the global heat flow data set for the eastern Pacific (Pollack et al., 1993).

References

- Amante, C., and Eakins, B.W., 2008. *ETOPO1 1 Arc-Minute Global Relief Model: Procedures, Data Sources and Analysis*: Washington, DC (DOC/NOAA/NESDIS/NGDC).
- Beaman, M., Sager, W.W., Acton, G.D., Lanci, L., and Pares, J., 2007. Improved Late Cretaceous and early Cenozoic paleomagnetic apparent polar wander path for the Pacific plate. *Earth Planet. Sci. Lett.*, 262(1–2): 1–20. doi:10.1016/j.epsl.2007.05.036
- Bukry, D., 1973. Low-latitude coccolith biostratigraphic zonation. In Edgar, N.T., Saunders, J.B., et al., *Init. Repts. DSDP*, 15: Washington, DC (U.S. Govt. Printing Office), 685–703. doi:10.2973/dsdp.proc.15.116.1973
- Busch, W.H., Vanden Berg, M.D., and Masau, P.E., 2006. Velocity and density of Paleogene equatorial sediments: variation with sediment composition. In Wilson, P.A., Lyle, M., and Firth, J.V. (Eds.), *Proc. ODP, Sci. Results*, 199: College Station, TX (Ocean Drilling Program), 1–31. doi:10.2973/odp.proc.sr.199.226.2006
- Cande, S.C., and Kent, D.V., 1995. Revised calibration of the geomagnetic polarity timescale for the Late Cretaceous and Cenozoic. *J. Geophys. Res.*, 100(B4):6093–6095. doi:10.1029/94JB03098
- Cande, S.C., LaBrecque, J.L., Larson, R.L., Pitmann, W.C., III, Golovchenko, X., and Haxby, W.F., 1989. *Magnetic Lineations of the World's Ocean Basins*. AAPG Map Ser., 13.
- Coxall, H.K., Wilson, P.A., Pälike, H., Lear, C.H., and Backman, J., 2005. Rapid stepwise onset of Antarctic glaciation and deeper calcite compensation in the Pacific Ocean. *Nature (London, U. K.)*, 433(7021):53–57. doi:10.1038/nature03135
- Engebretson, D.C., Cox, A., and Gordon, R.G., 1985. *Relative Motions between Oceanic and Continental Plates in the Pacific Basin*. Spec. Pap.—Geol. Soc. Am., 206.
- Hyndman, R.D., Erickson, A.J., and Von Herzen, R.P., 1974. Geothermal measurements on DSDP Leg 26. In Davies, T.A., Luyendyk, B.P., et al., *Init. Repts. DSDP*, 26: Washington, DC (U.S. Govt. Printing Office), 451–463. doi:10.2973/dsdp.proc.26.113.1974
- Knappenberger, M., 2000. Sedimentation rates and Pacific plate motion calculated using seismic cross sections of the Neogene equatorial sediment bulge [M.Sc. thesis]. Boise State Univ., Idaho.
- Koppers, A.A.P., Phipps Morgan, J., Morgan, J.W., and Staudigel, H., 2001. Testing the fixed hotspot hypothesis using ⁴⁰Ar/³⁹Ar age progressions along seamount trails. *Earth Planet. Sci. Lett.*, 185(3–4):237–252. doi:10.1016/S0012-821X(00)00387-3
- Lyle, M., Liberty, L., Moore, T.C., Jr., and Rea, D.K., 2002. Development of a seismic stratigraphy for the Paleogene sedimentary section, central tropical Pacific Ocean. In Lyle, M., Wilson, P.A., Janecek, T.R., et al., *Proc. ODP, Init. Repts.*, 199: College Station, TX (Ocean Drilling Program), 1–21. doi:10.2973/odp.proc.ir.199.104.2002
- Lyle, M., Olivarez Lyle, A., Backman, J., and Tripati, A., 2005. Biogenic sedimentation in the Eocene equatorial Pacific—the stuttering greenhouse and Eocene carbonate compensation depth. In Lyle, M., Wilson, P.A., Janecek, T.R., et al., *Proc. ODP, Init. Repts.*, 199: College Station, TX (Ocean Drilling Program), 1–35. doi:10.2973/odp.proc.sr.199.219.2005
- Lyle, M.W., Pälike, H., Moore, T.C., Mitchell, N., and Backman, J., 2006. *Summary Report of R/V Roger Revelle Site Survey AMAT03 to the IODP Environmental Protection and Safety Panel (EPSP) in Support for Proposal IODP626*: Southampton, U.K. (Univ. Southampton). <http://eprints.soton.ac.uk/45921/>
- Lyle, M., Wilson, P.A., Janecek, T.R., et al., 2002. *Proc. ODP, Init. Repts.*, 199: College Station, TX (Ocean Drilling Program). doi:10.2973/odp.proc.ir.199.2002
- Lowenstein, T.K., and Demicco, R.V., 2007. Elevated Eocene atmospheric CO₂ and subsequent decline. *Science*, 313(5795):1928. doi:10.1126/science.1129555
- Moore, T.C., Jr., Backman, J., Raffi, I., Nigrini, C., Sanfilippo, A., Pälike, H., and Lyle, M., 2004. Paleogene tropical Pacific: clues to circulation, productivity, and plate motion. *Paleoceanography*, 19(3):PA3013. doi:10.1029/2003PA000998
- Müller, R.D., Roest, W.R., Royer, J.-Y., Gahagan, L.M., and Slater, J.G., 1997. Digital isochrons of the world's ocean floor. *J. Geophys. Res.*, 102(B2):3211–3214. doi:10.1029/96JB01781
- Nigrini, C., Sanfilippo, A., and Moore, T.C., Jr., 2006. Cenozoic radiolarian biostratigraphy: a magnetobiostratigraphic chronology of Cenozoic sequences from ODP Sites 1218, 1219, and 1220, equatorial Pacific. In Wilson, P.A., Lyle, M., and Firth, J.V. (Eds.), *Proc. ODP, Sci. Results*, 199: College Station, TX (Ocean Drilling Program), 1–76. doi:10.2973/odp.proc.sr.199.225.2006
- Pälike, H., Norris, R.D., Herrle, J.O., Wilson, P.A., Coxall, H.K., Lear, C.H., Shackleton, N.J., Tripati, A.K., and Wade, B.S., 2006. The heartbeat of the Oligocene climate system. *Science*, 314(5807):1894–1898. doi:10.1126/science.1133822
- Petronotis, K.E., 1991. Paleomagnetic studies of the skewness of Pacific plate marine magnetic anomalies 25–32R: implications for anomalous skewness and the motion of the Pacific plate and hotspots [Ph.D. thesis]. Northwestern Univ., Evanston, IL.
- Petronotis, K.E., Gordon, R.G., and Acton, G.D., 1994. A 57 Ma Pacific plate paleomagnetic pole determined from a skewness analysis of crossings of marine magnetic anomaly 25r. *Geophys. J. Int.*, 118(3):529–554. doi:10.1111/j.1365-246X.1994.tb03983.x



- Pollack, H.N., Hurter, S.J., and Johnson, J.R., 1993. Heat flow from the earth's interior: analysis of the global data set. *Rev. Geophys.*, 31(3):267–280. [doi:10.1029/93RG01249](https://doi.org/10.1029/93RG01249)
- Pribnow, D.F.C., Kinoshita, M., and Stein, C.A., 2000. *Thermal Data Collection and Heat Flow Recalculations for ODP Legs 101–180*: Hanover, Germany (Inst. Joint Geosci. Res., Inst. Geowiss. Gemeinschaftsauf. [GGA]). <http://www-odp.tamu.edu/publications/heatflow/ODPReprt.pdf>
- Rea, D.K., and Dixon, J.M., 1983. Late Cretaceous and Paleogene tectonic evolution of the North Pacific Ocean. *Earth Planet. Sci. Lett.*, 65(1):145–166. [doi:10.1016/0012-821X\(83\)90196-6](https://doi.org/10.1016/0012-821X(83)90196-6)
- Rea, D.K., and Lyle, M.W., 2005. Paleogene calcite compensation depth in the eastern subtropical Pacific: answers and questions. *Paleoceanography*, 20(1):PA1012. [doi:10.1029/2004PA001064](https://doi.org/10.1029/2004PA001064)
- Sager, W.W., and Pringle, M.S., 1988. Mid-Cretaceous to early Tertiary apparent polar wander path of the Pacific plate. *J. Geophys. Res., [Solid Earth]*, 93(B10):11753–11771. [doi:10.1029/JB093iB10p11753](https://doi.org/10.1029/JB093iB10p11753)
- Shackleton, N.J., Hall, M.A., Raffi, I., Tauxe, L., and Zachos, J., 2000. Astronomical calibration age for the Oligocene–Miocene boundary. *Geology*, 28(5):447–450. [doi:10.1130/0091-7613\(2000\)28<447:ACAFTO>2.0.CO;2](https://doi.org/10.1130/0091-7613(2000)28<447:ACAFTO>2.0.CO;2)
- Shipboard Scientific Party, 2002. Leg 199 summary. In Lyle, M., Wilson, P.A., Janecek, T.R., et al., *Proc. ODP, Init. Repts.*, 199: College Station, TX (Ocean Drilling Program), 1–87. [doi:10.2973/odp.proc.ir.199.101.2002](https://doi.org/10.2973/odp.proc.ir.199.101.2002)
- Shipboard Scientific Party, 2003. Site 1223. In Stephen, R.A., Kasahara, J., Acton, G.D., et al., *Proc. ODP, Init. Repts.*, 200: College Station, TX (Ocean Drilling Program), 1–159. [doi:10.2973/odp.proc.ir.200.103.2003](https://doi.org/10.2973/odp.proc.ir.200.103.2003)
- Shipboard Scientific Party, 2004. Leg 208 summary. In Zachos, J.C., Kroon, D., Blum, P., et al., *Proc. ODP, Init. Repts.*, 208: College Station, TX (Ocean Drilling Program), 1–112. [doi:10.2973/odp.proc.ir.208.101.2004](https://doi.org/10.2973/odp.proc.ir.208.101.2004)
- van Andel, T.H., 1975. Mesozoic/Cenozoic calcite compensation depth and the global distribution of calcareous sediments. *Earth Planet. Sci. Lett.*, 26(2):187–194. [doi:10.1016/0012-821X\(75\)90086-2](https://doi.org/10.1016/0012-821X(75)90086-2)
- van Morkhoven, F.P.C.M., Berggren, W.A., and Edwards, A.S., 1986. *Cenozoic Cosmopolitan Deep-Water Benthic Foraminifera*. Bull. Cent. Rech. Explor.—Prod. Elf-Aquitaine, Mem. 11.
- Zachos, J., Pagani, M., Sloan, L., Thomas, E., and Billups, K., 2001. Trends, rhythms, and aberrations in global climate 65 Ma to present. *Science*, 292(5517):686–693. [doi:10.1126/science.1059412](https://doi.org/10.1126/science.1059412)

Publication: 30 October 2010
MS 320321-103

Figure F1. A. ETOPO1 (Amante and Eakins, 2008) bathymetric overview map of Site U1331 and PEAT drilling locations, with previous ODP and DSDP sites. B. Swath map bathymetry for Site U1331 region from the AMAT-03 site survey. Black labels = seismic shotpoints, white labels = bathymetric contours. Orange line = seismic Line PEAT1C-sl-8 (Fig. F2). F.Z. = fracture zone.

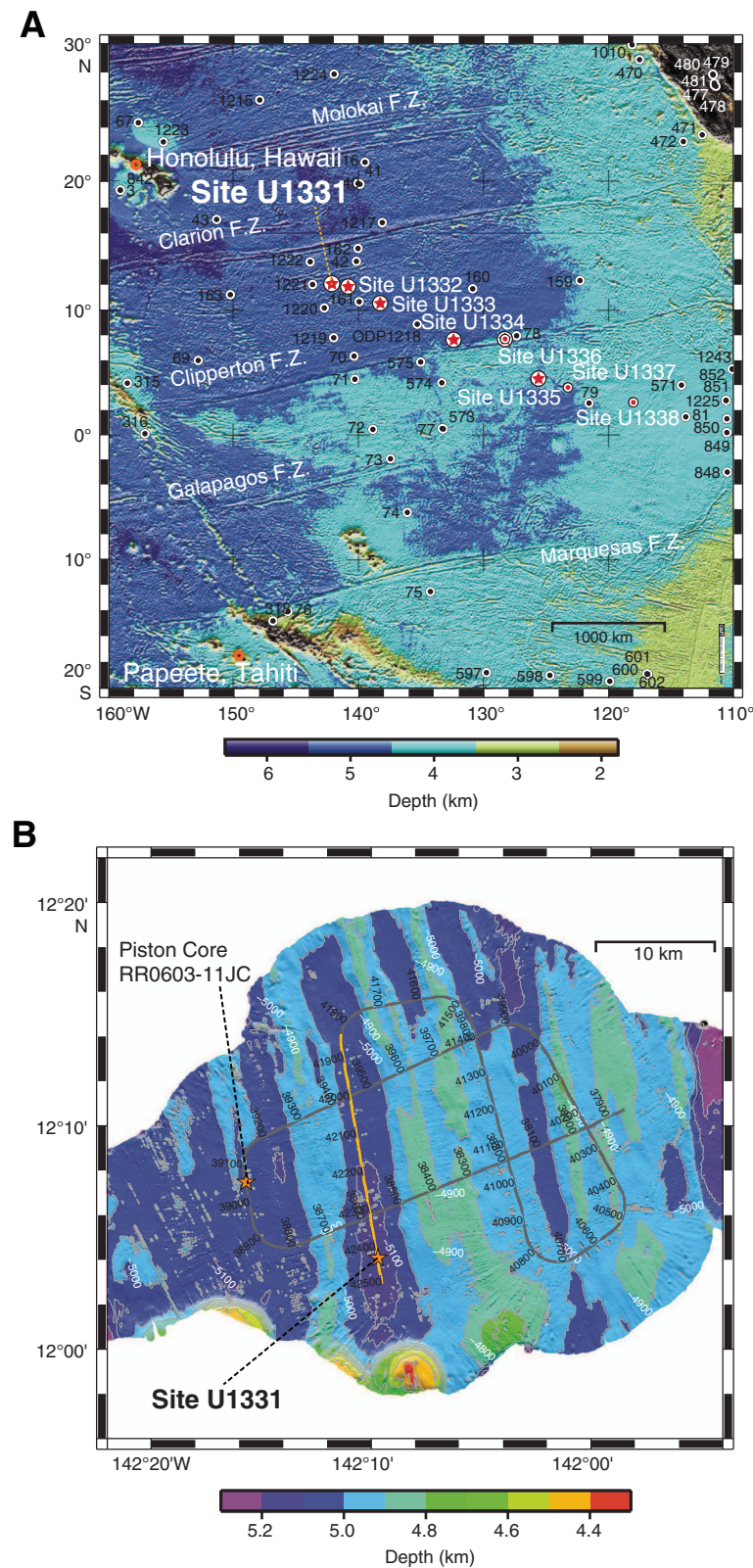


Figure F2. Seismic reflection profile PEAT-1C (Site U1331) Line 8 from the 48-channel seismic reflection survey, annotated in shotpoints (Lyle et al., 2006). Data are filtered, stacked, and migrated. Line 8 goes down the western abyssal valley at the site. Site was located where basal reflections appeared less strong to minimize possible cherts. Tentative conversion from two-way traveltime to depth uses velocity model of Busch et al. (2006). P2, P3 = seismic reflectors of Lyle et al. (2002). All times are Universal Time Coordinated (UTC). TD = total depth.

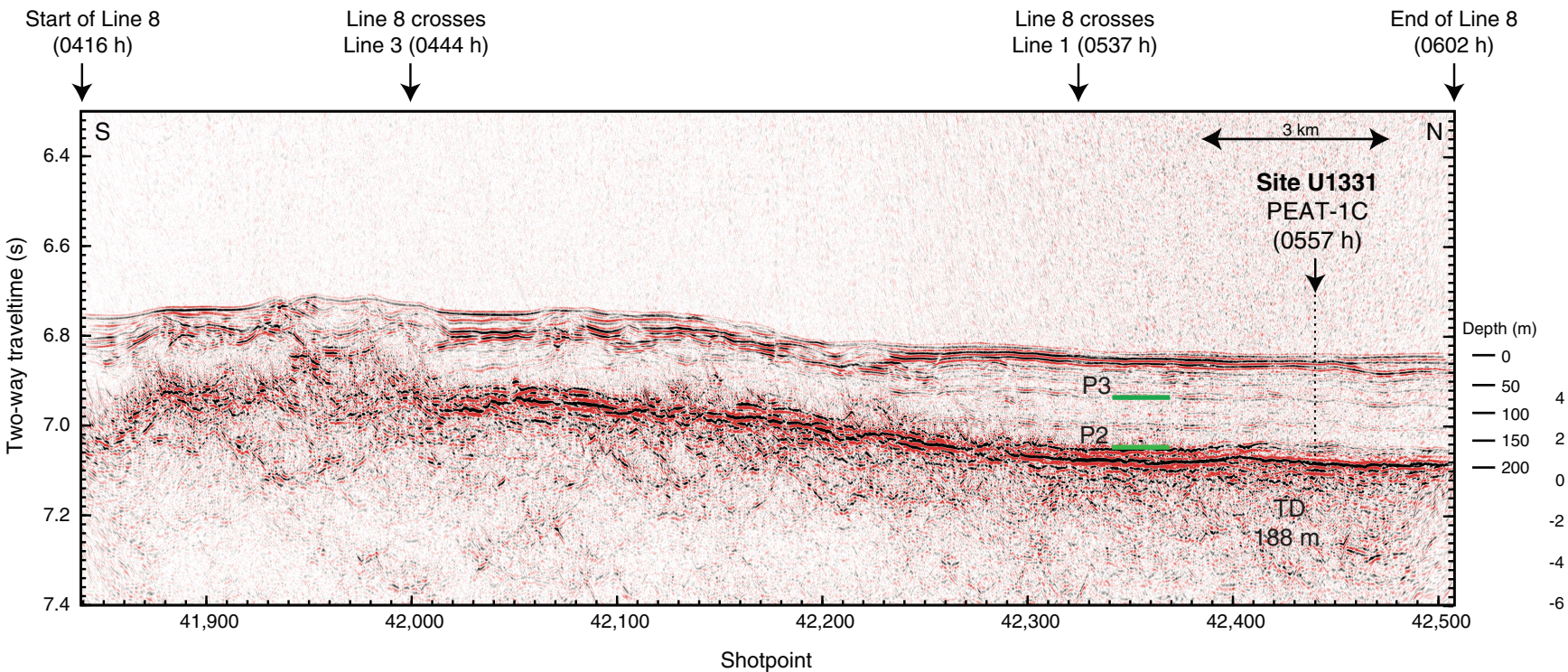


Figure F3. Site U1331 summary.

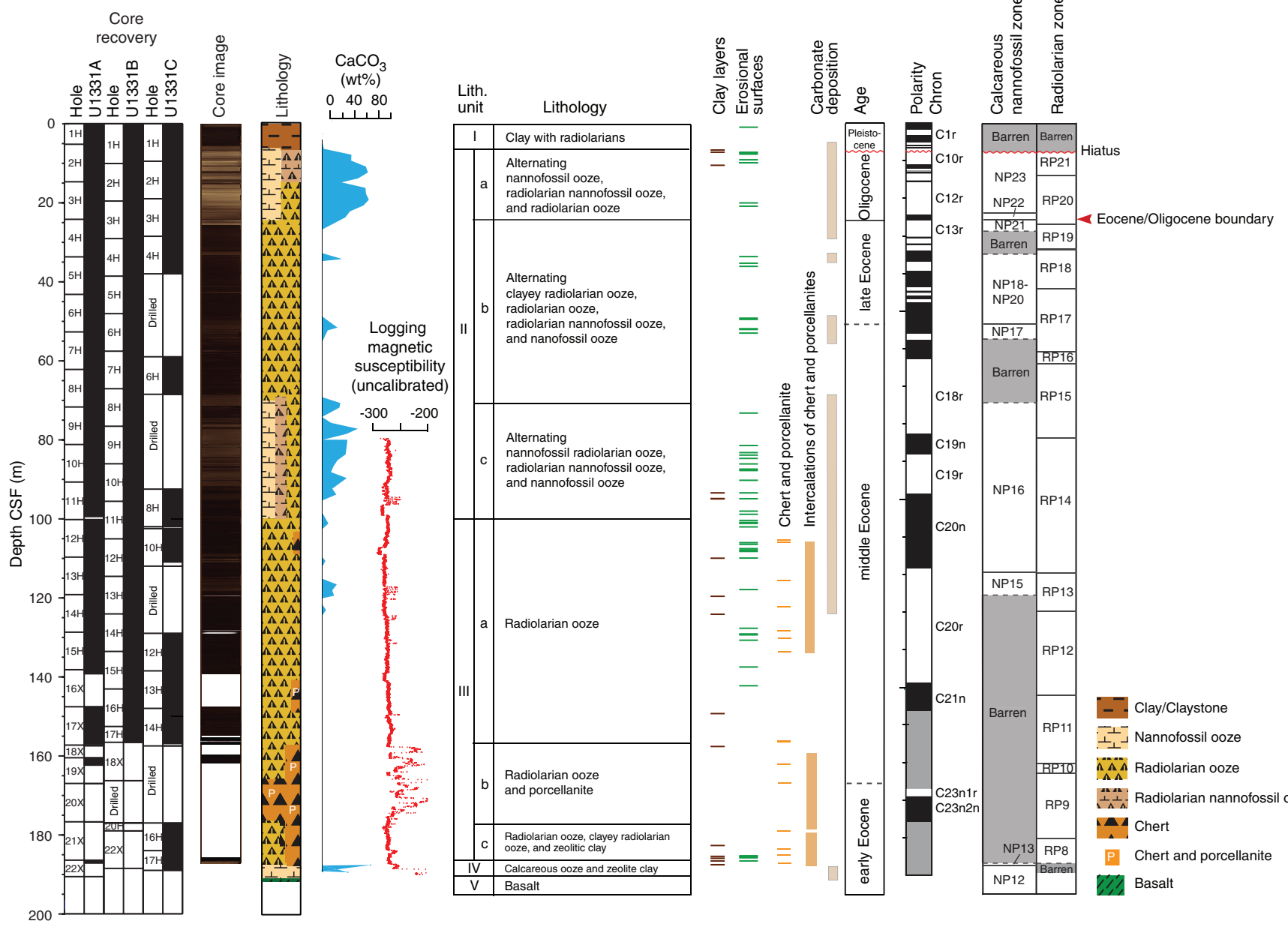


Figure F4. Lithologic summary, Site U1331. L* = reflectance value of sediment as defined in the LAB color model. See the “**Methods**” chapter for biozone definitions.

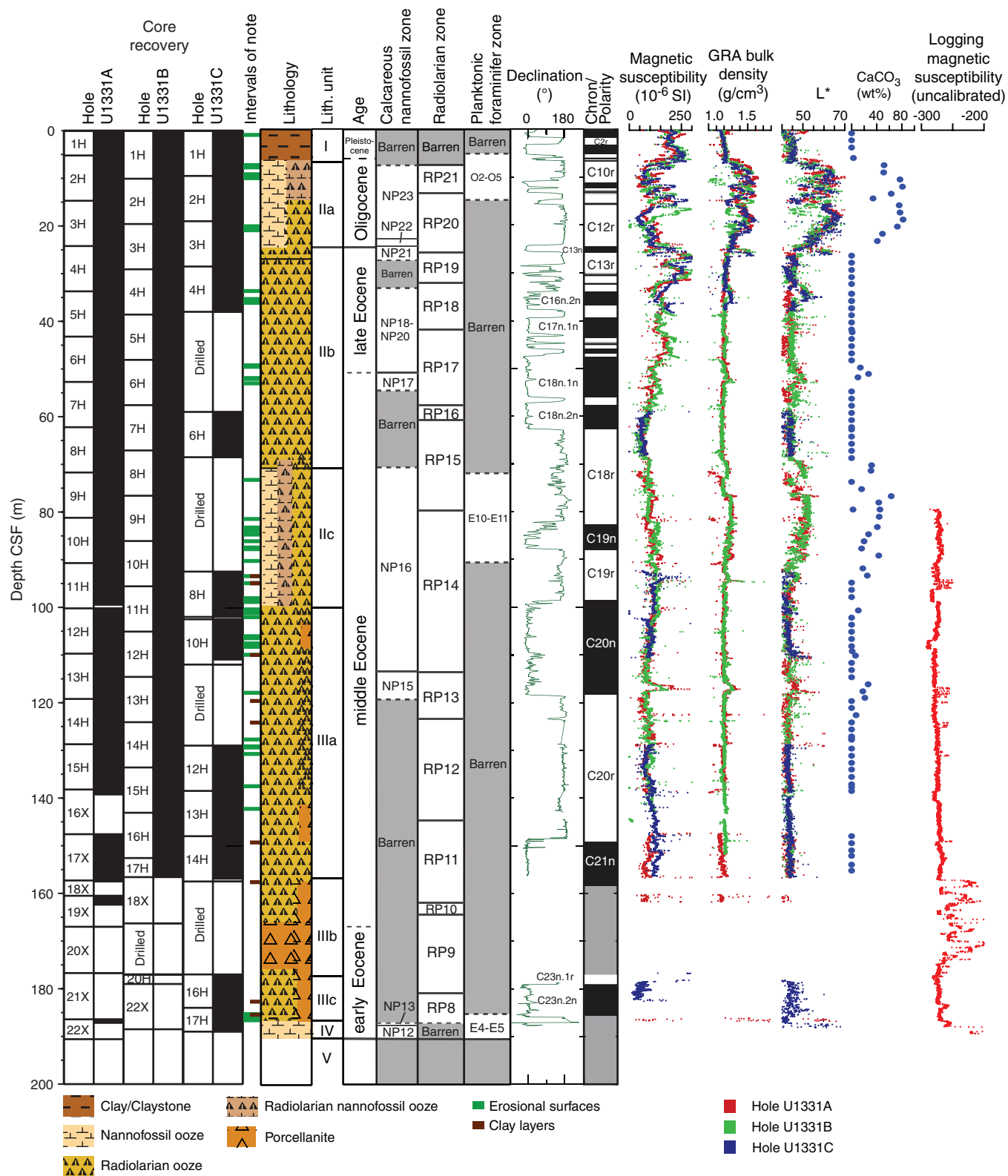


Figure F5. Smear slide photomicrographs of selected representative lithologies, Site U1331. Left image = plane-polarized light, right image = cross-polarized light. A. Nannofossil ooze (Sample 320-U1331B-3H-4, 149 cm). B. Nannofossil ooze with diatoms and radiolarians (Sample 320-U1331A-3H-6, 90 cm). C. Radiolarian nannofossil ooze with clay (Sample 320-U1331B-10H-1, 70 cm). D. Radiolarian ooze (Sample 320-U1331C-16H-2, 67 cm).

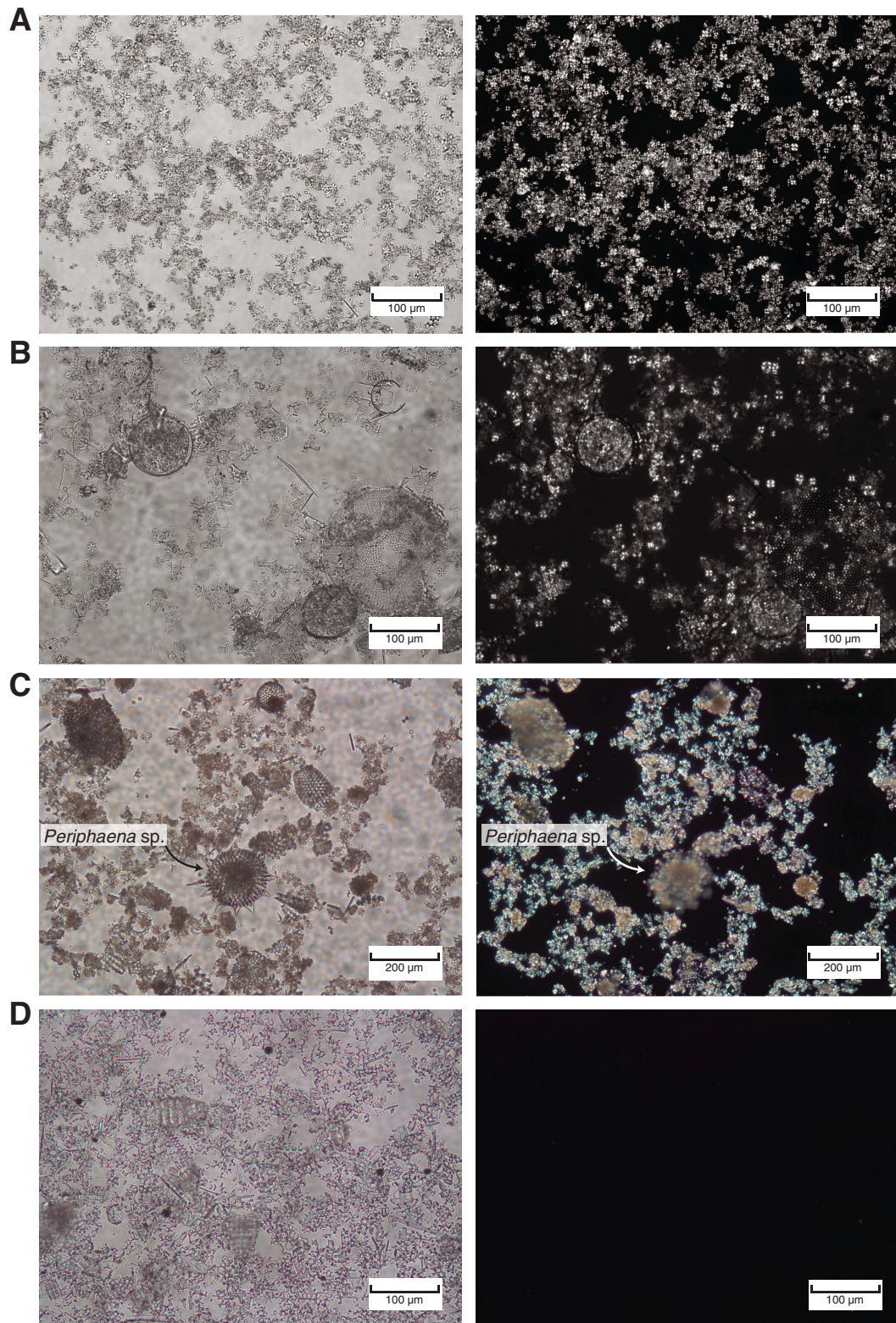


Figure F6. Photomicrographs of selected representative lithologies, Site U1331. Left image = plane-polarized light, right image = cross-polarized light. A. Smear slide, zeolite clay (Sample 320-U1331B-3H-4, 149 cm). Note euhedral cruciform crystal of philipsite. B. Thin section, porcellanite (Sample 320-U1331A-14H-3, 53 cm). C. Thin section, porcellanite (Sample 320-U1331A-18X-1, 7–10 cm). D. Thin section, porcellanite (Sample 320-U1331A-19X-1, 52–61 cm). Note layering in porcellanite samples.

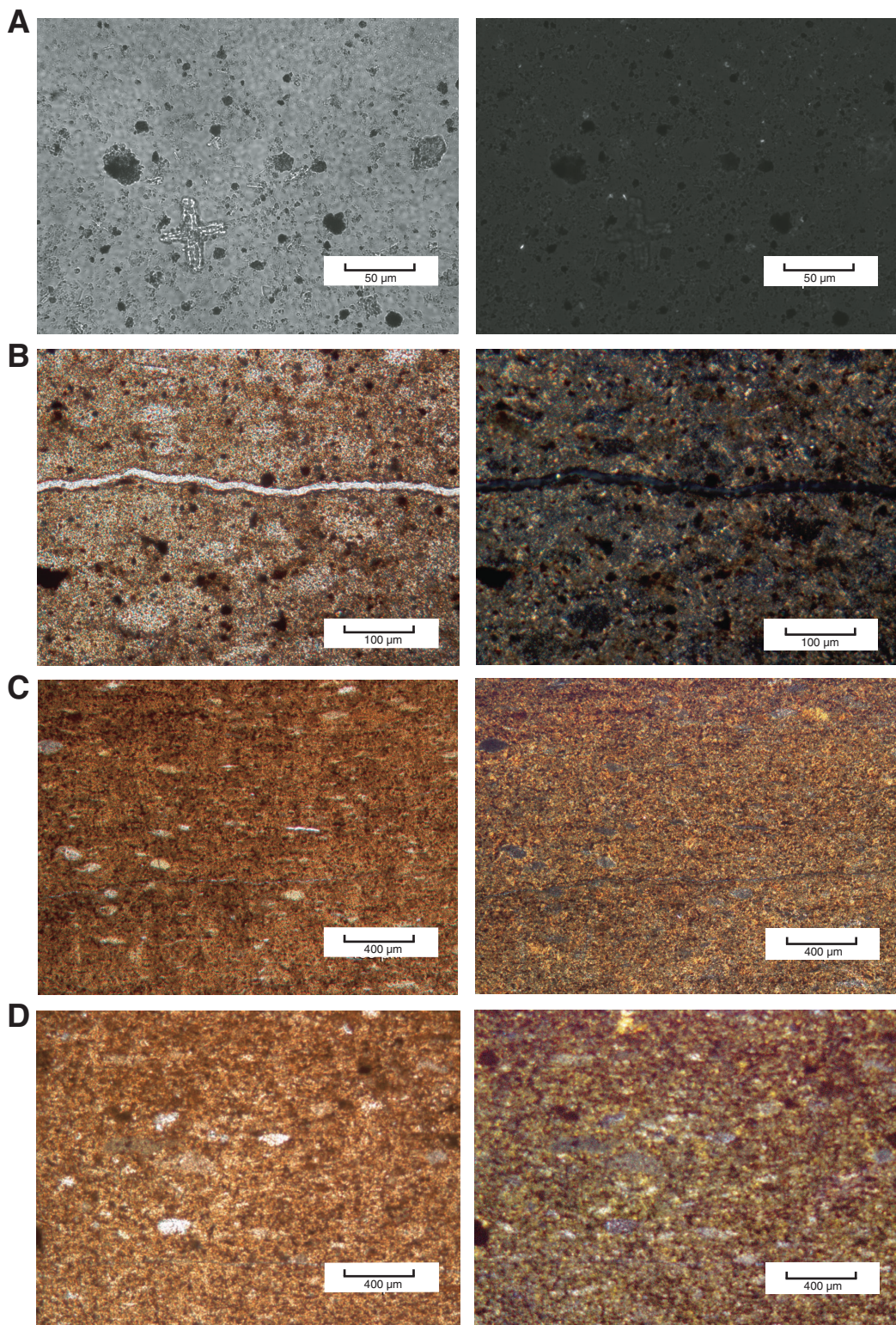


Figure F7. Thin section photomicrographs. Left image = plane-polarized light, right image = cross-polarized light. A, B. Conglomerate (Sample 320-U1331B-10H-6, 120–128 cm). Foraminifers, fish teeth, and coarse mud clasts (up to 2 cm diameter) are visible. Calcareous benthic foraminifer with calcite test walls but chambers infilled by diagenetic silica shown in B. C. Interior of basement basalt (Sample 320-U1331A-22X-CC, 37–44 cm) D. Chilled margin of basement basalt, same sample as C. Glass matrixes are comparatively fresh. Plg = plagioclase feldspar, Cpx = clinopyroxene, Chl = chlorite, Alt. glass = altered glass.

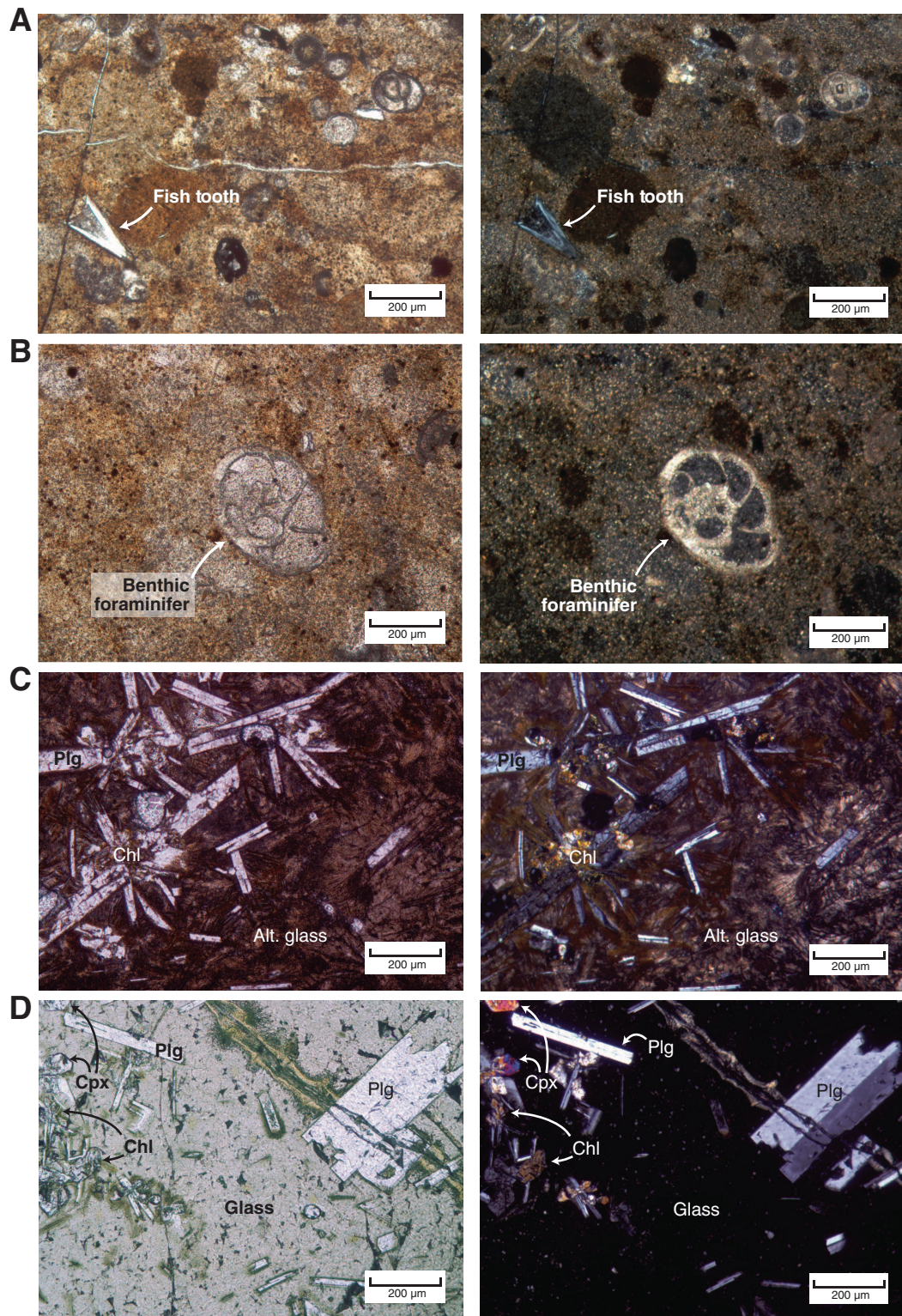


Figure F8. Line scan images and magnetic susceptibility of Eocene/Oligocene boundary. A. Hole U1331A. B. Hole U1331B. C. Hole U1331C.

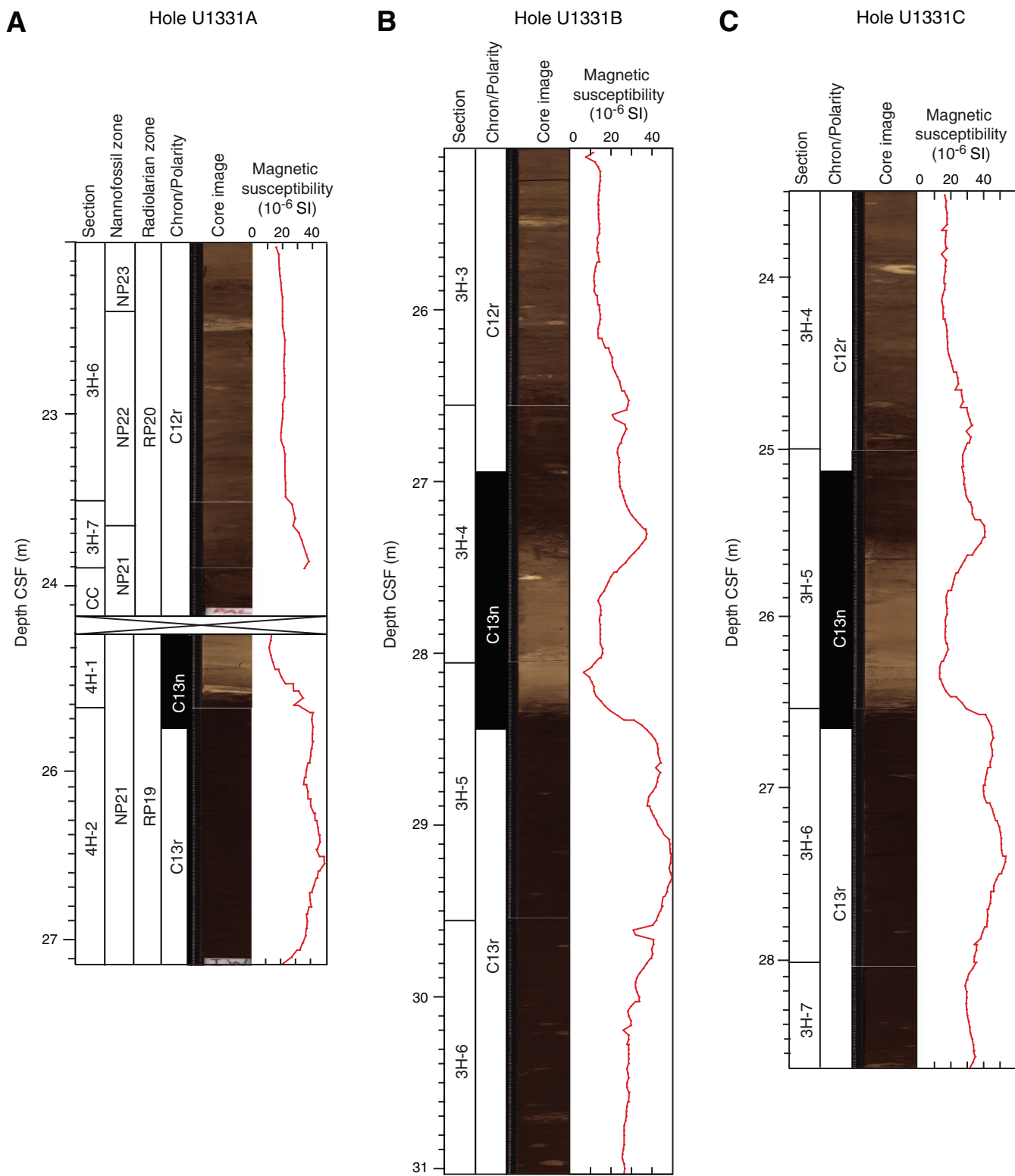


Figure F9. Line scan images of inferred turbidite deposits. A. Interval 320-U1331B-1H-7, 67–76 cm. Subunit IIa. B. Interval 320-U1331B-4H-5, 0–9 cm. Subunit IIb. C. Interval 320-U1331B-10H-6, 117–130 cm. Subunit IIc. D. Interval 320-U1331A-11H-4, 32–46 cm. A, B, and D show obvious basal scour and fining-upward sequences. C shows a partially lithified conglomerate containing large (up to 2 cm) angular to subrounded mud clasts (inferred rip-up clasts), carbonate microfossils, and sands surrounded by unconsolidated multicolored sands similar to those seen in B.

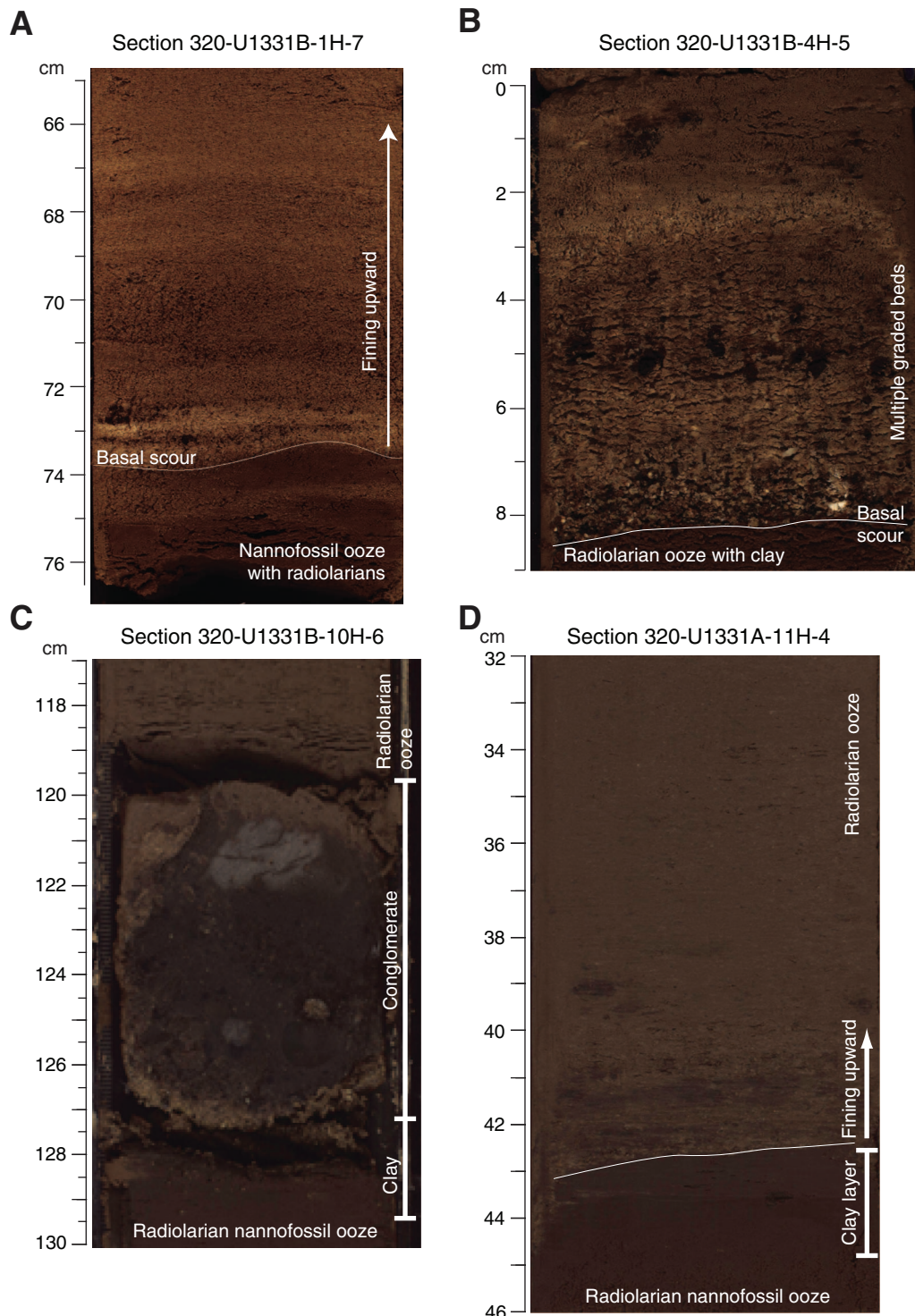


Figure F10. Line scan images of turbidite and probable hiatus located ~0.5 m below the Unit I/Subunit IIa boundary. Magnetostratigraphic interpretation of this interval draws on these lithostratigraphic results (see “Paleomagnetism”). For Chron C2An.2r, correlation to GPTS is uncertain. A. Interval 320-U1331B-1H-5, 26–149 cm. B. Intervals 320-U1331A-2H-1, 54–150 cm, and 2H-2, 0–28 cm. C. Intervals 320-U1331C-1H-5, 65–150 cm, and 1H-6, 0–38 cm. Dashed line indicates basal scour in all holes. Solid line represents Unit I/Subunit IIa boundary.

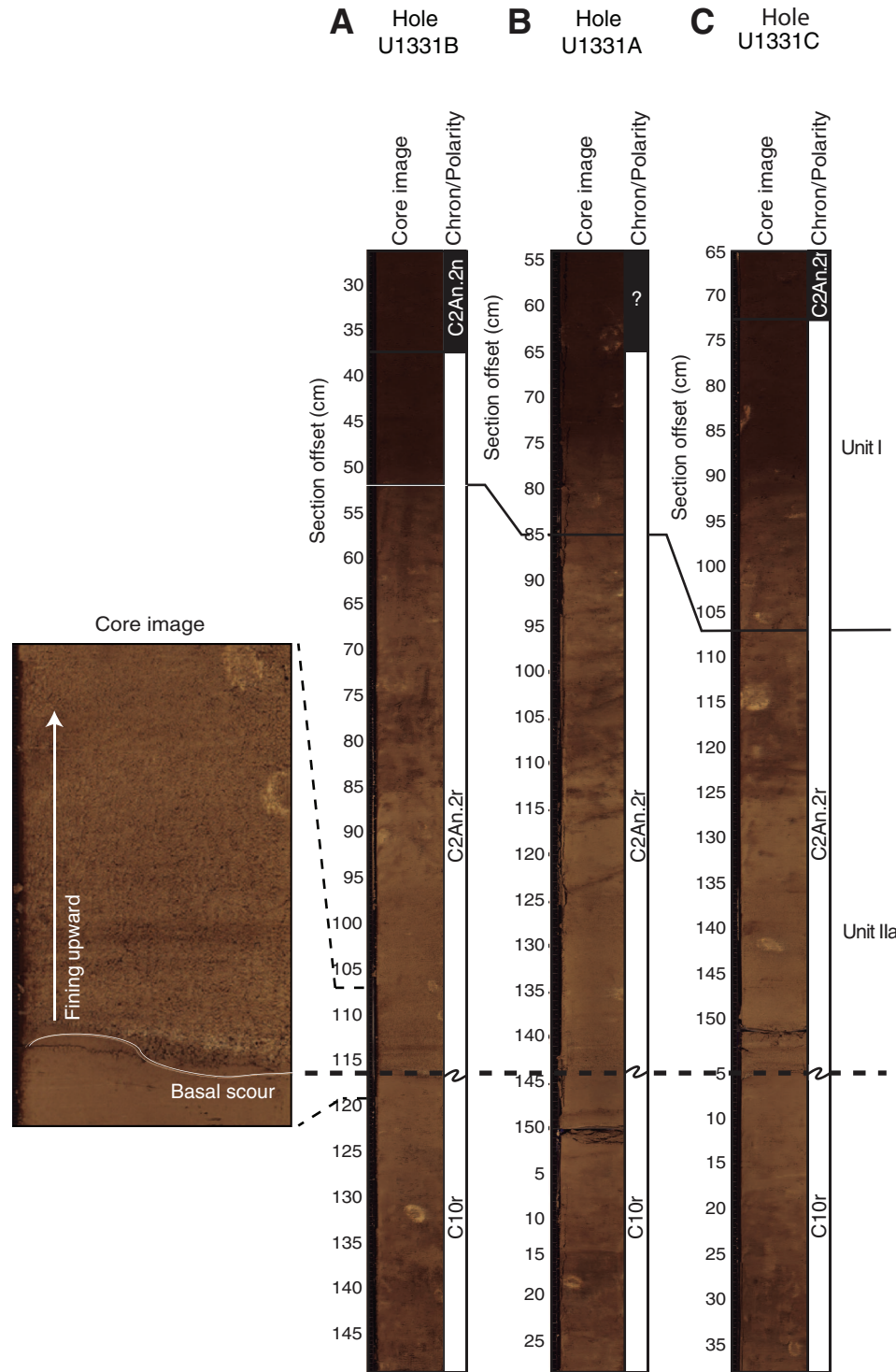


Figure F11. Line scan images. A. Soft unconsolidated clay layer, Subunit IIIc (interval 320-U1331C-17H-2, 25–53 cm). B. Clay layer with a partially lithified interval, Subunit IIIa (interval 320-U1331B-16H-5, 0–20 cm). C. Clay layer containing porcellanite horizon, Subunit IIIc (interval 320-U1331C-16H-4, 102–122 cm).

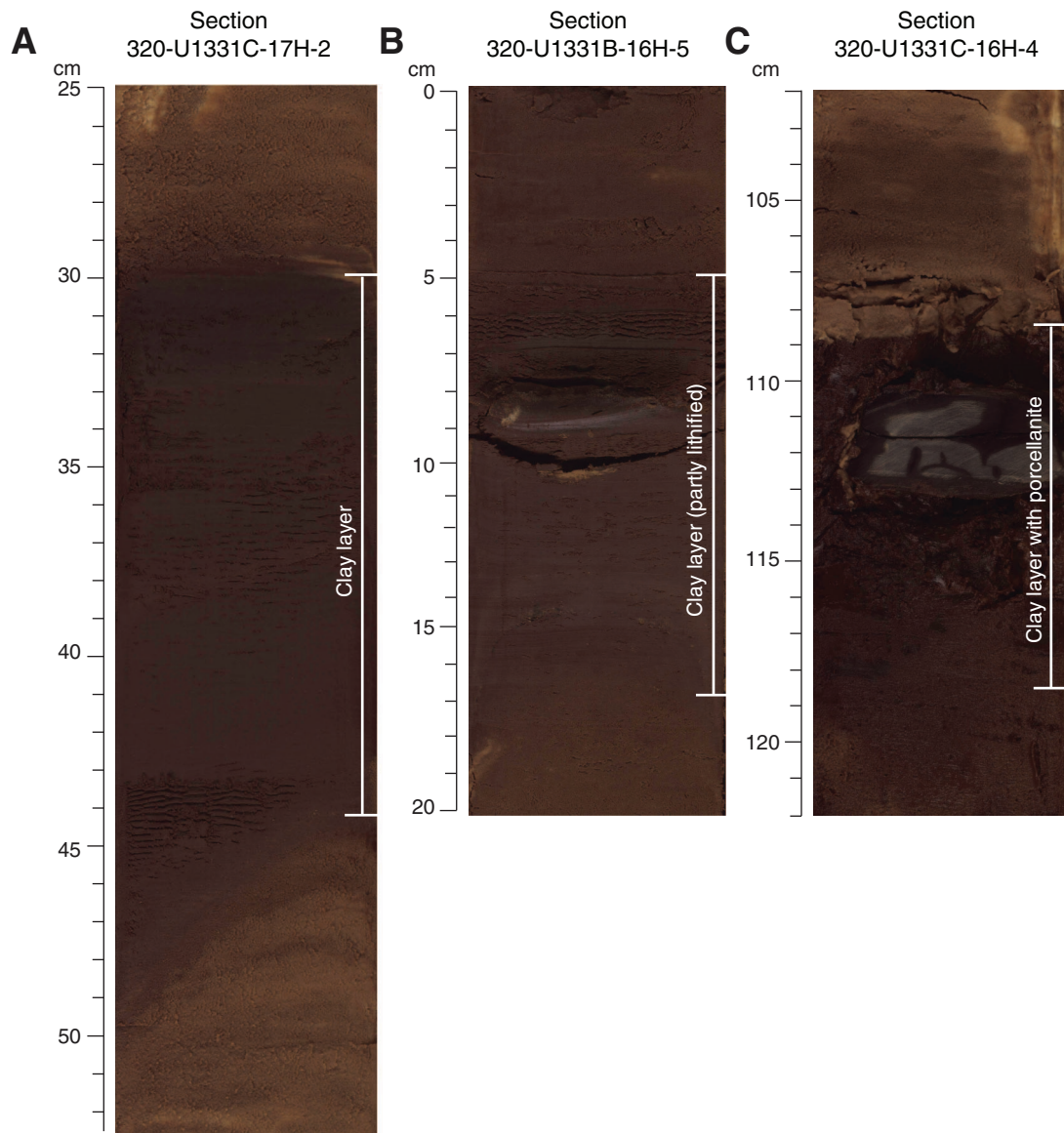


Figure F12. Integrated calcareous and siliceous microfossil biozonation, Site U1331. Calcareous microfossil zonation was limited by the presence of extensive barren intervals; dashed zonal boundaries indicate stratigraphic extent of calcareous microfossil assemblages consistent with a particular zonal assignment.

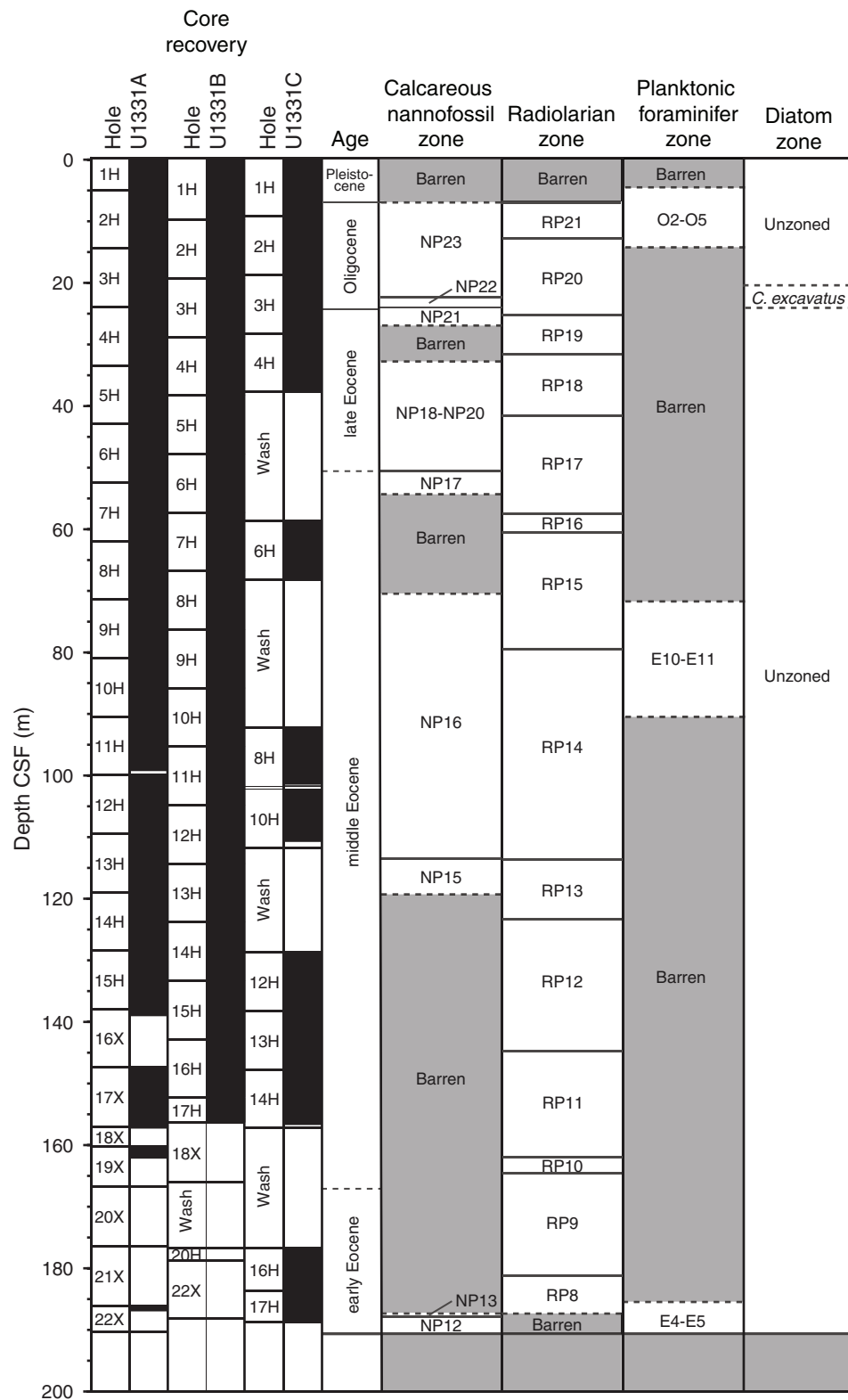


Figure F13. Age-depth curve, linear sedimentation rates, and chronostratigraphic markers, Site U1331.

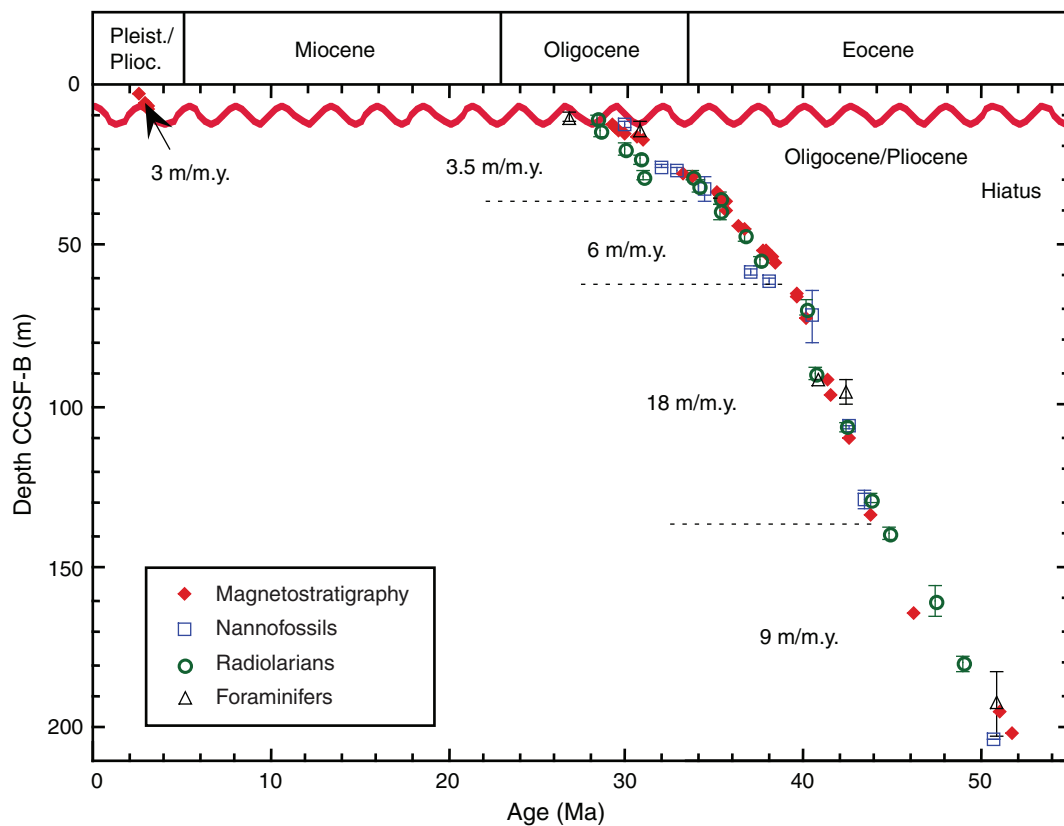


Figure F14. Reworked radiolarian microfossils, Site U1331. Qualitative estimate of amount of admixed older radiolarians in an assemblage ranges from 0 (no reworked material) to 3 (>10 reworked specimens per slide) (see the “**Methods**” chapter).

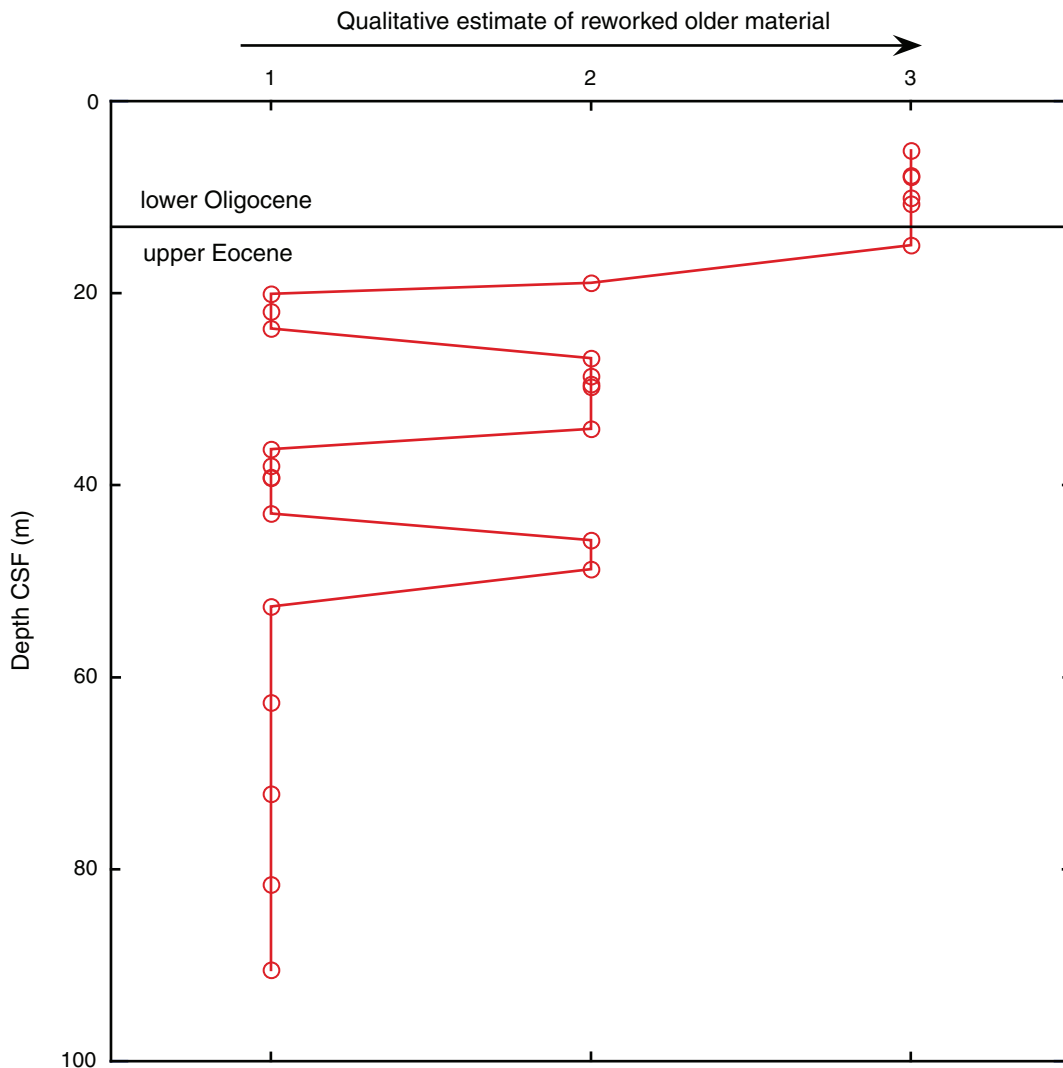


Figure F15. Summary of magnetic susceptibility and paleomagnetic results, Hole U1331A. Red wavy line = long hiatus. PCA = principal component analysis.

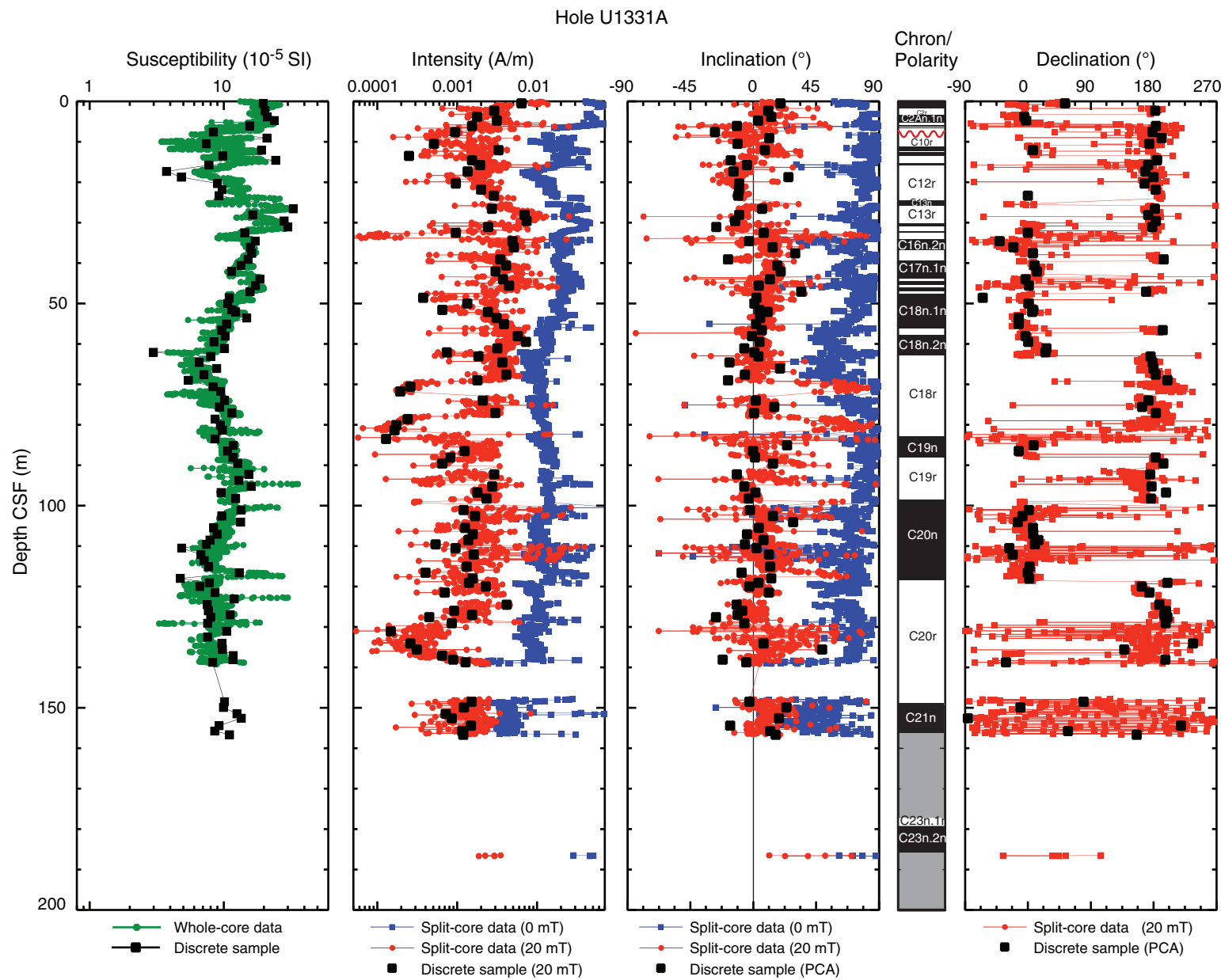


Figure F16. Summary of magnetic susceptibility and paleomagnetic results, Hole U1331B. Red wavy line = long hiatus.

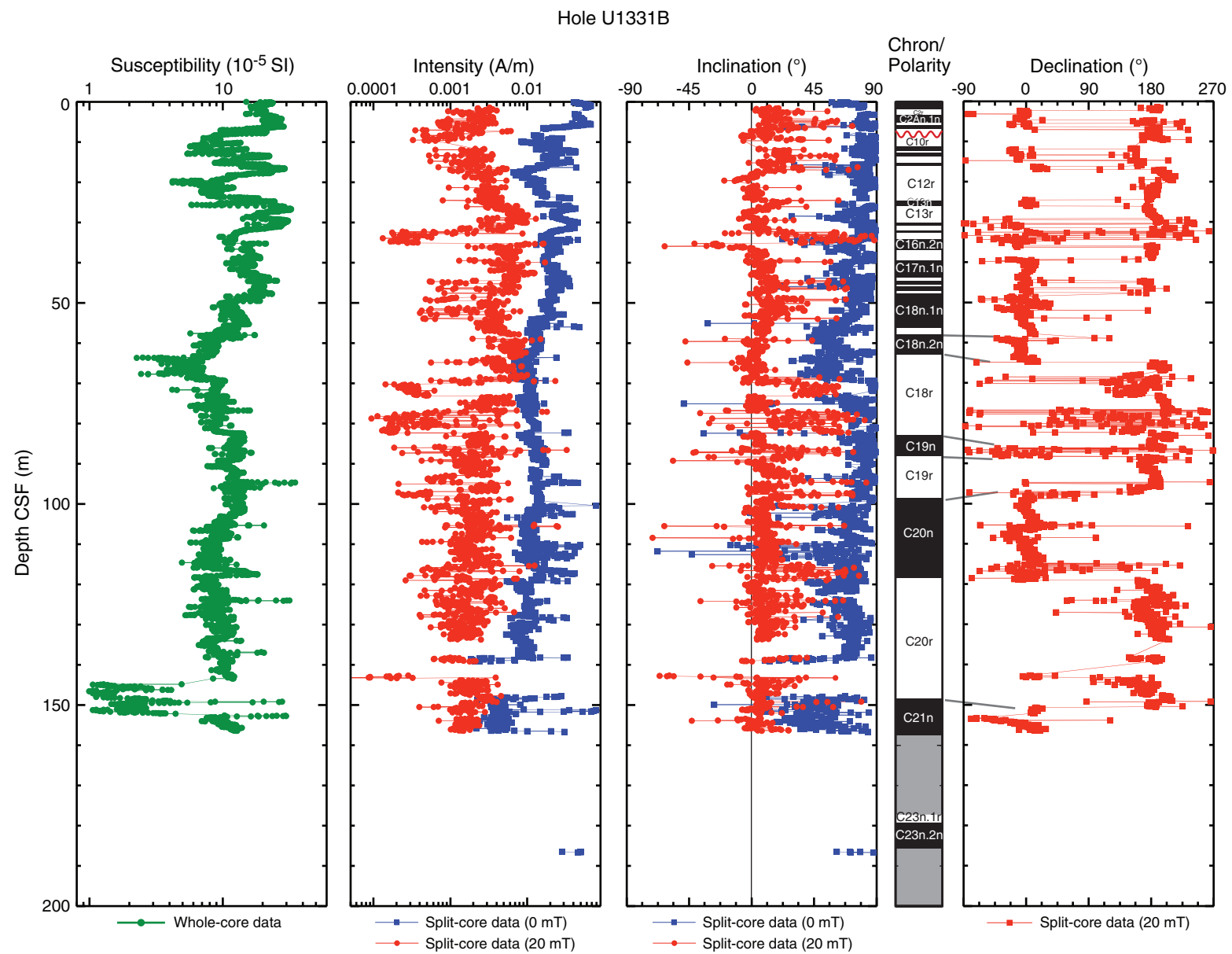


Figure F17. Summary of magnetic susceptibility and paleomagnetic results, Hole U1331C. Red wavy line = long hiatus.

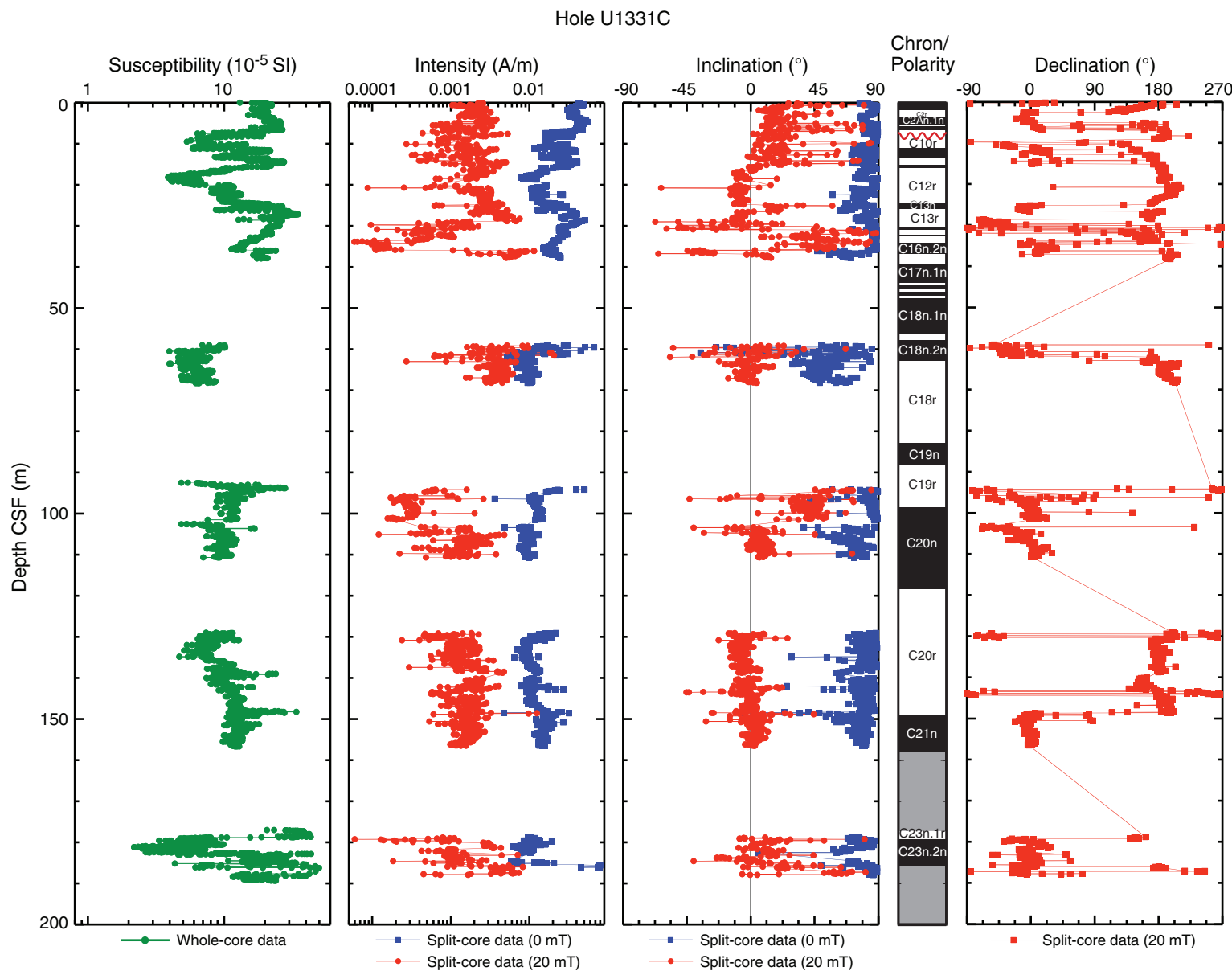


Figure F18. Magnetic susceptibility and NRM intensity (prior to demagnetization) for an interval from Hole U1331A. The similarity indicates both are providing proxies for magnetic mineral concentration (see text).

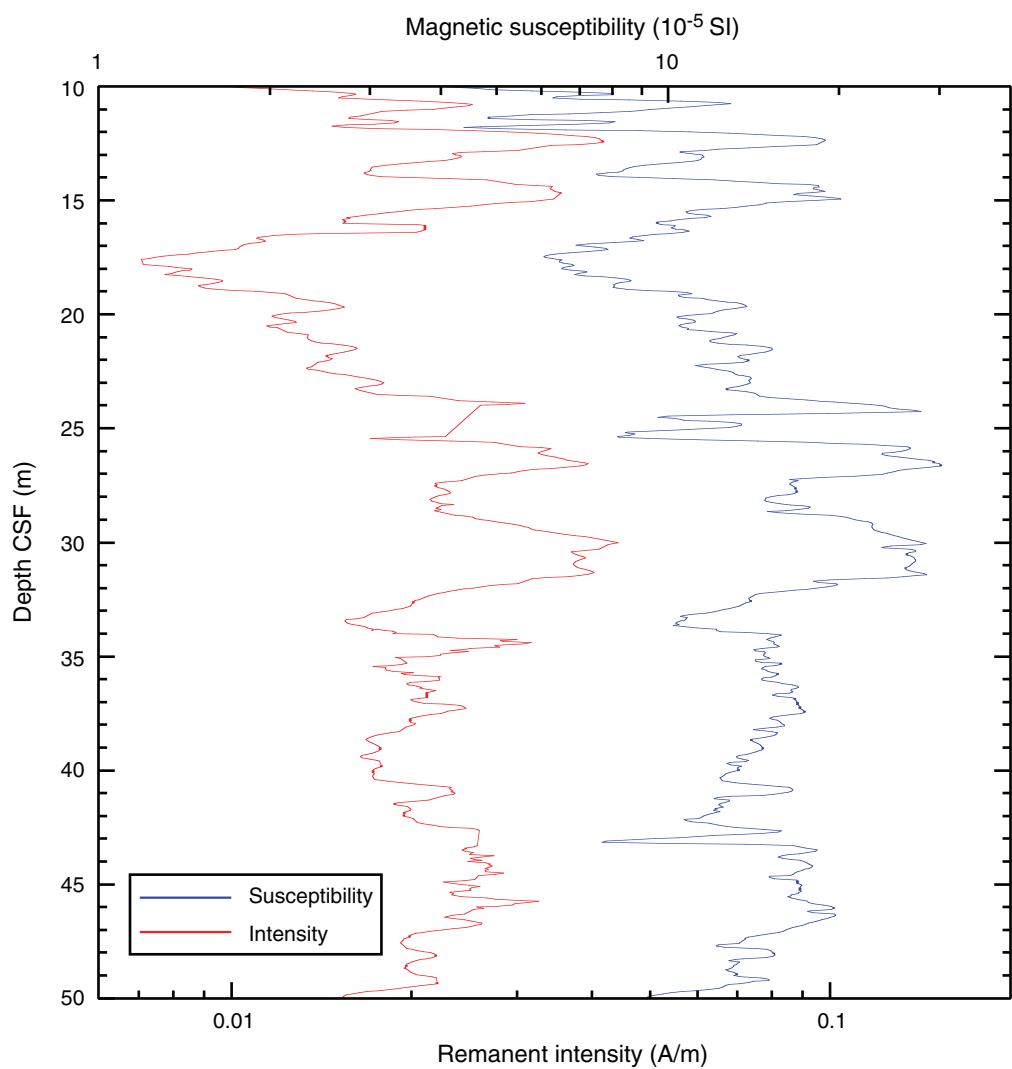


Figure F19. Alternating-field and thermal demagnetization (demag) results for four discrete samples. Left plot shows vector endpoints of paleomagnetic directions on vector demagnetization diagrams or modified Zijderveld plots (squares = inclinations, circles = declinations), right plot shows intensity variation with progressive demagnetization. All four vector demagnetization diagrams illustrate removal of a steep drilling overprint by about 15 mT or 300°C, with the remaining magnetization providing a well-resolved characteristic remanent magnetization. A. Sample 320-U1331A-5H-5, 85 cm (40.54 m CSF). B. Sample 320-U1331A-8H-2, 85 cm (64.54 m CSF). C. Sample 320-U1331A-8H-3, 85 cm (66.07 m CSF). D. Sample 320-U1331A-10H-3, 85 cm (85.08 m CSF). NRM = natural remanent magnetization.

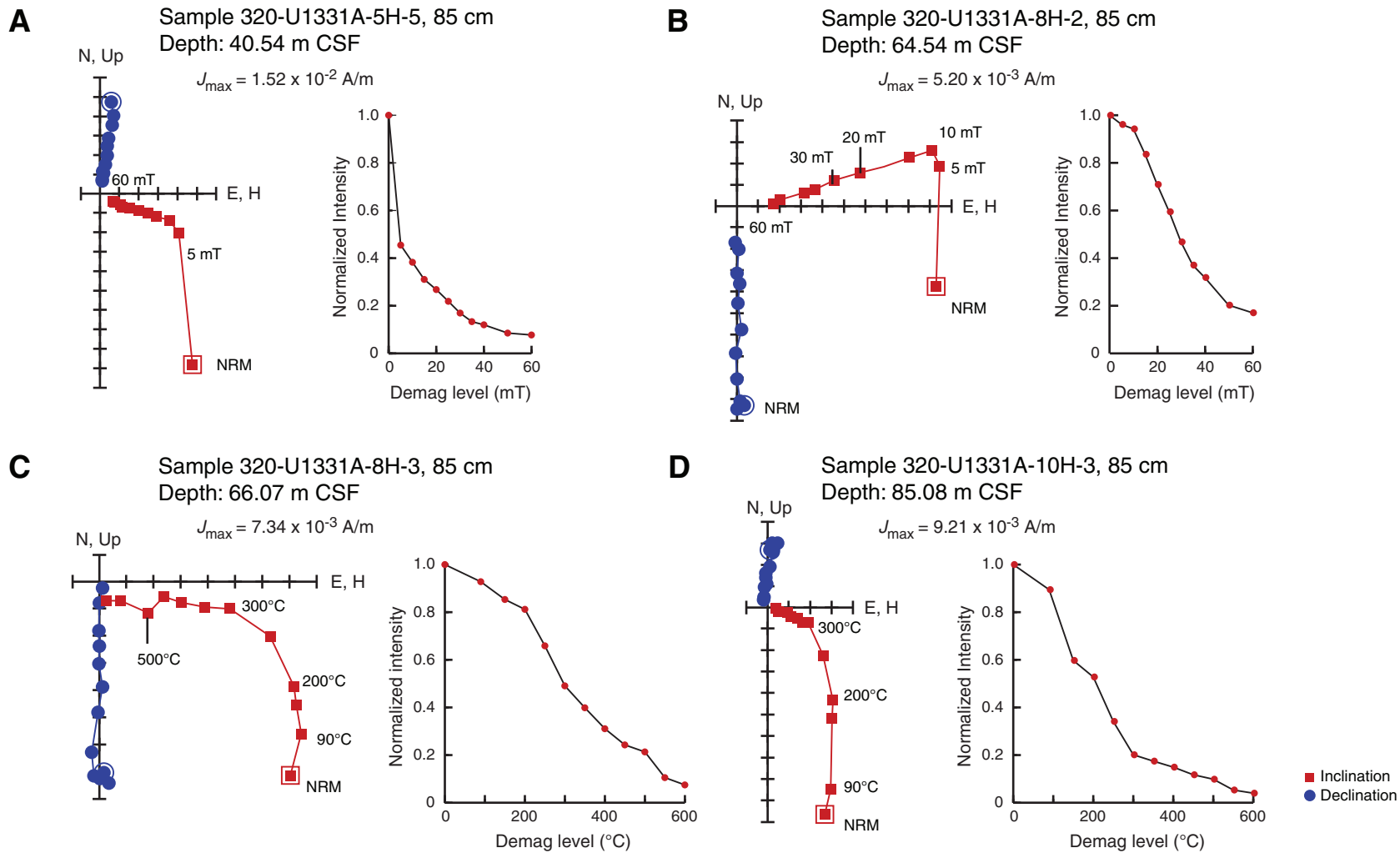


Figure F20. Latitude of the virtual geomagnetic pole (VGP). A. 0–100 m depth. North latitudes = normal polarity, south latitudes = reversed polarity. ([Continued on next page](#))

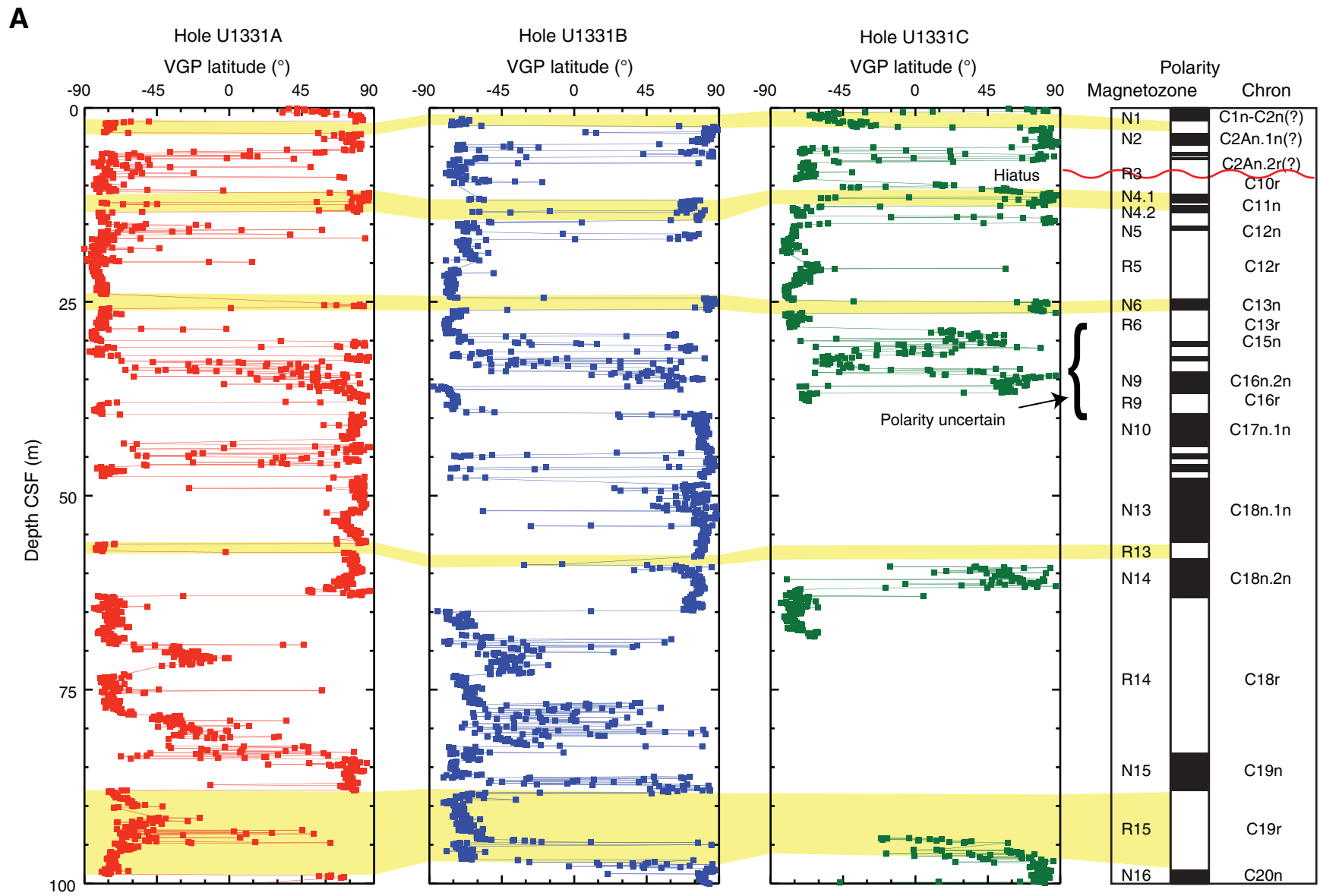


Figure F20 (continued). B. 100–200 m depth.

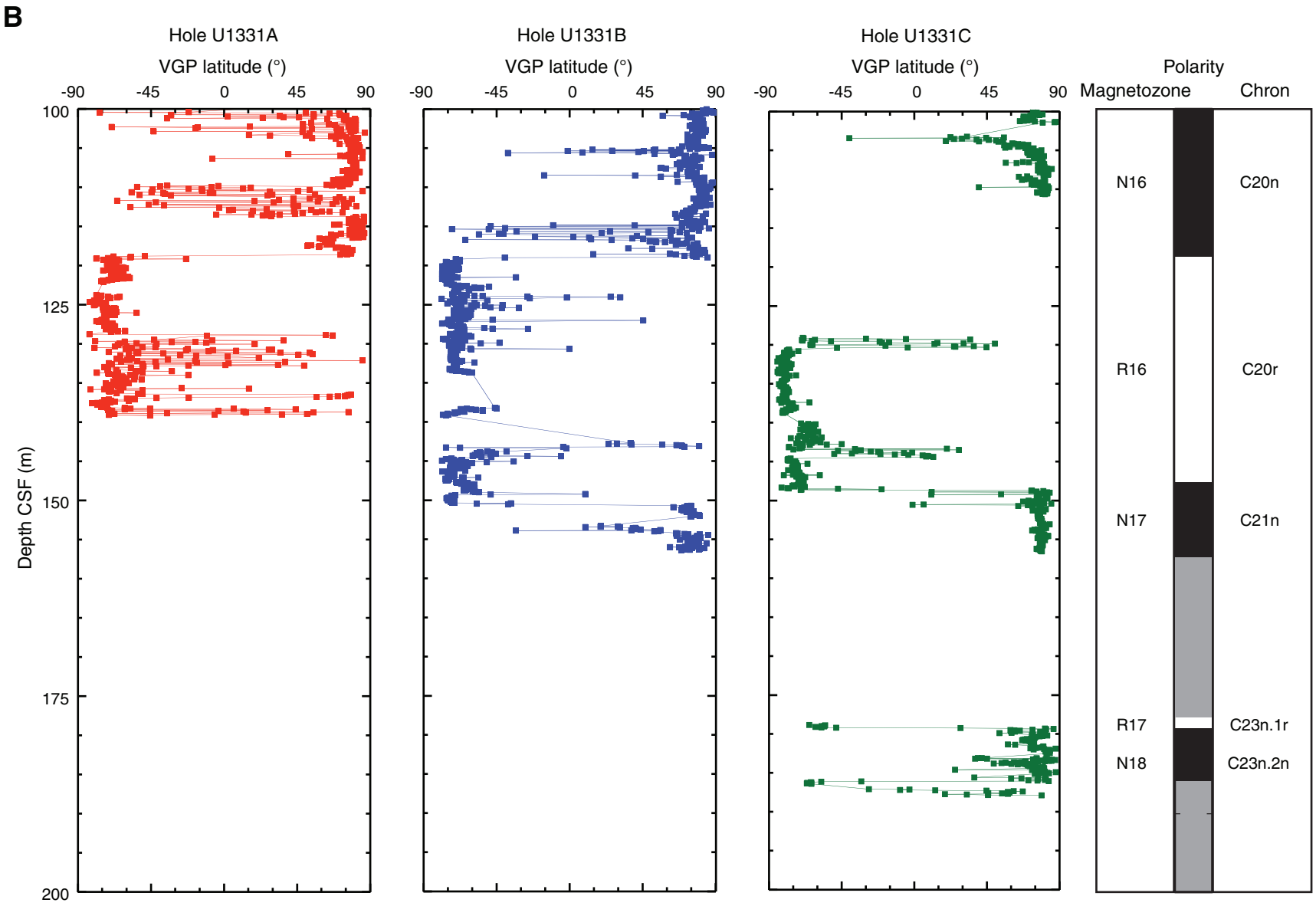


Figure F21. A. Rhizon sampling of Section 320-U133B-1H-6, showing close-up of the interval from ~85 to 110 cm. This section had a pronounced color change at ~95 cm. ([Continued on next page.](#))

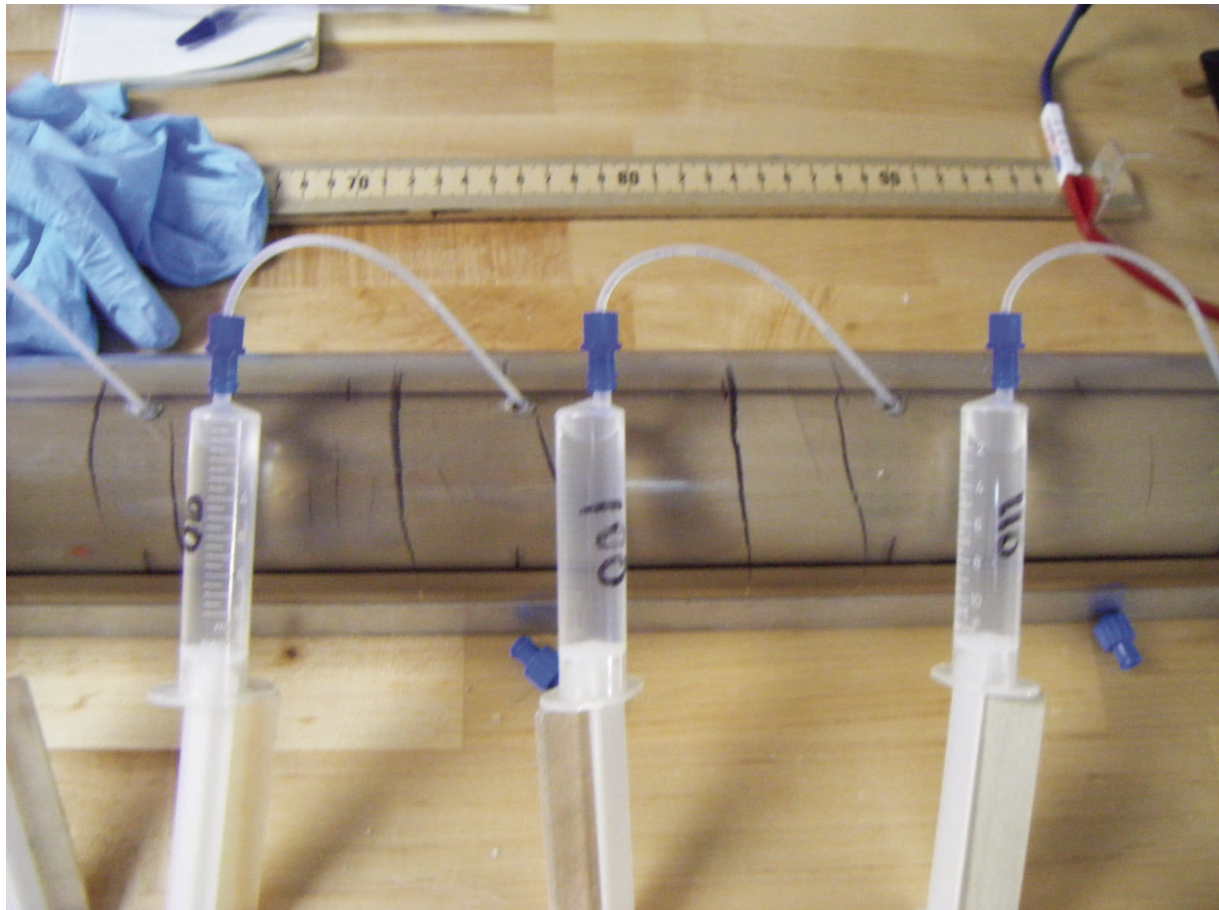
A

Figure F21 (continued). B. Water yield vs. time since insertion for Rhizon sampling of Section 320-U1331B-1H-6. Solid diamonds = yield for Rhizons inserted from 10 to 90 cm, open circles = Rhizons inserted from 100 to 140 cm. 12 mL was the maximum volume of the syringe.

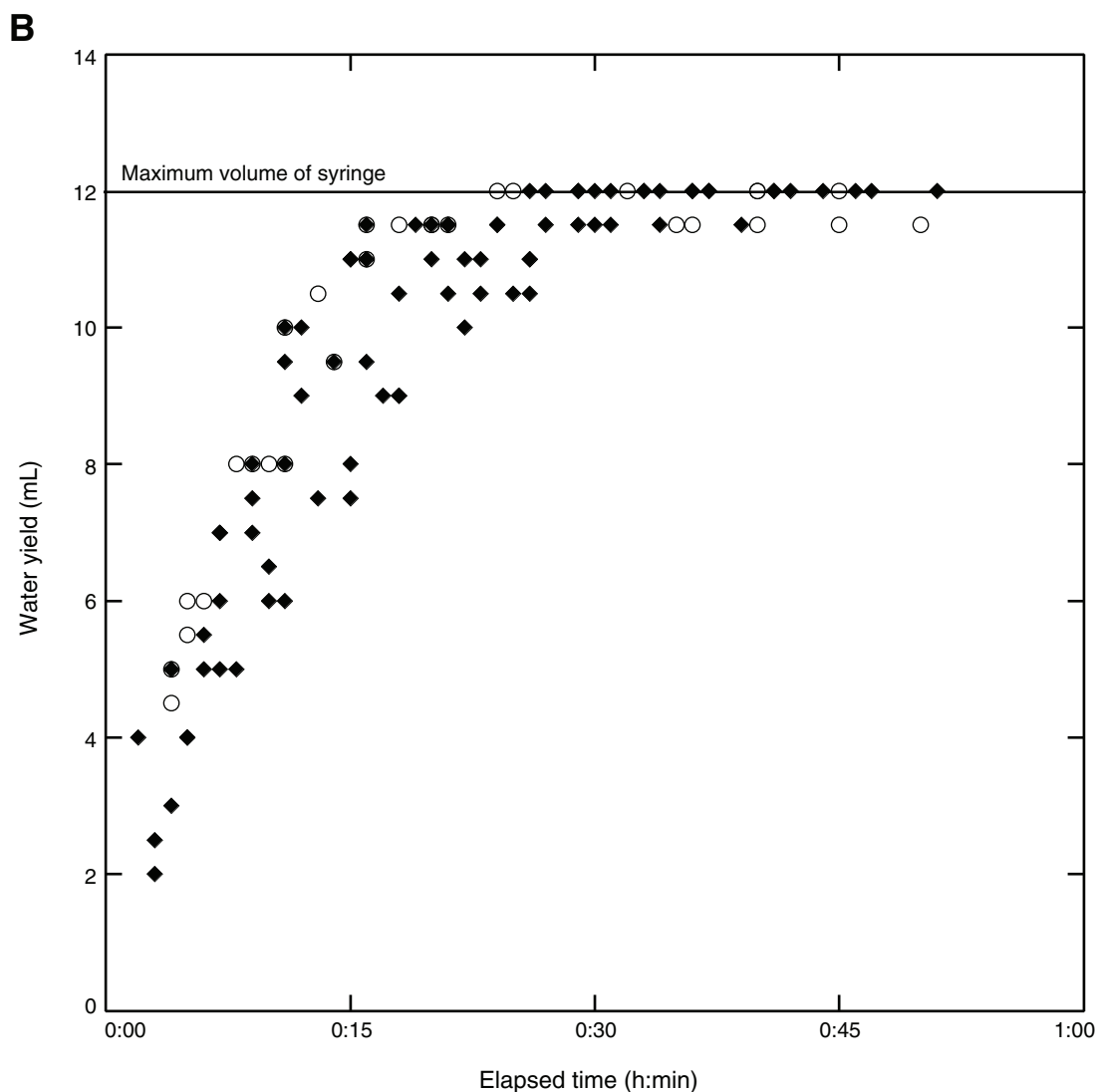


Figure F22. Interstitial water chemistry, Site U1331. Values below the detection limit (0.6 μM for HPO_4^{2-}) are plotted as zero. Hole U1331B samples (plotted as open symbols) include Rhizon samples. Apparent offsets between samples from Holes U1331A and U1331B reflect CSF depth scale differences between holes. (See “[Lithostratigraphy](#)” for information on unit boundaries.)

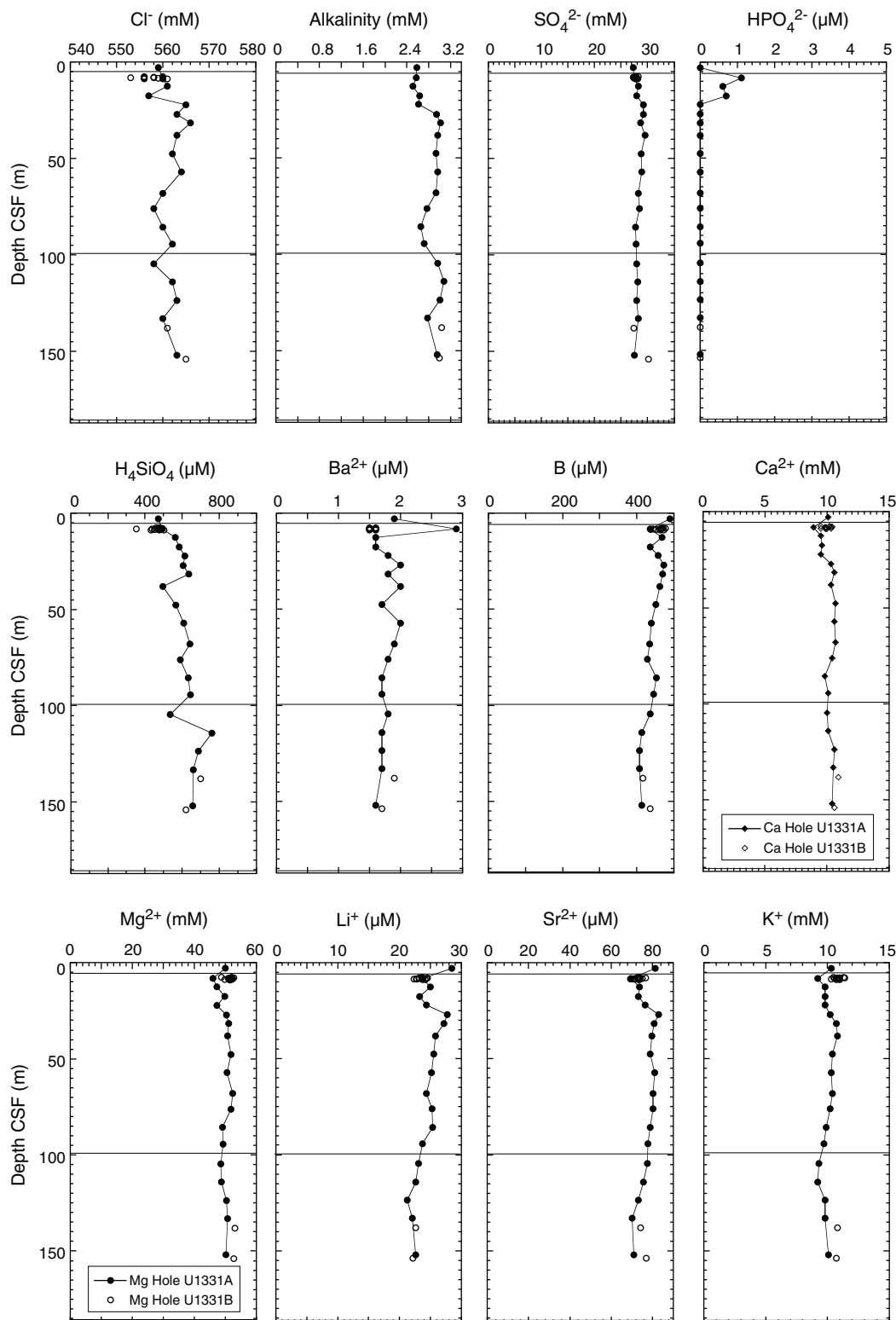


Figure F23. Interstitial water chemistry, Hole U1331C.

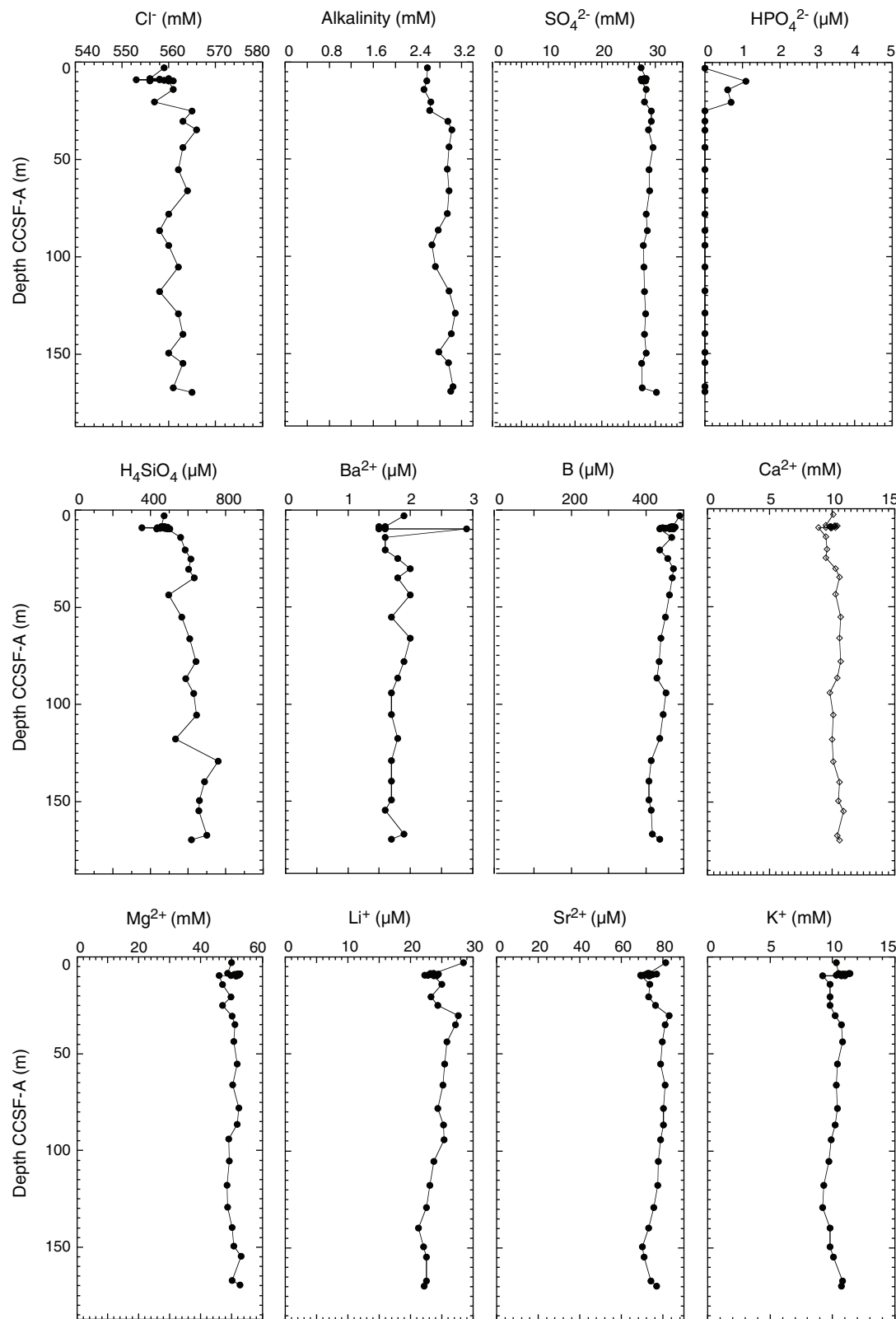


Figure F24. Calcium carbonate (CaCO_3), inorganic carbon (IC), total carbon (TC), and total organic carbon (TOC) determined by normal and acidification methods in sediments from Hole U1331A. (See “[Lithostratigraphy](#)” for information on unit boundaries.)

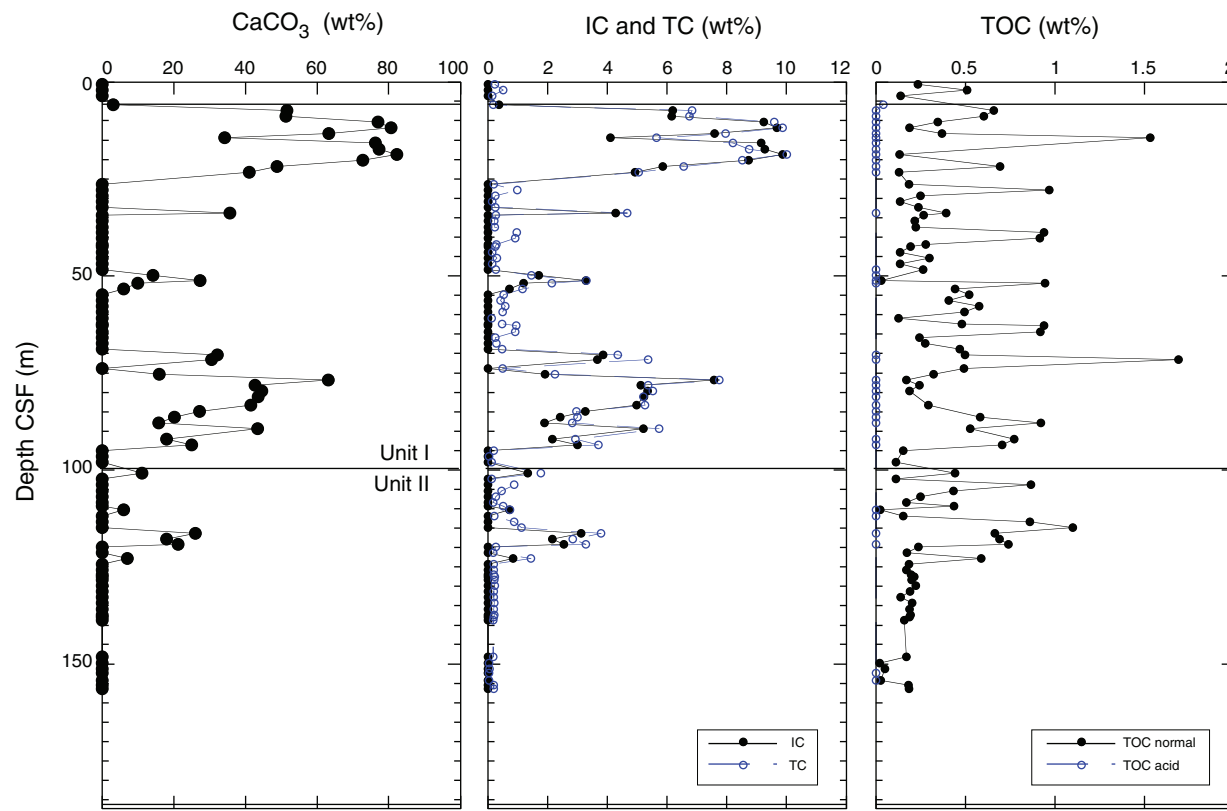


Figure F25. Whole-Round Multisensor Logger (WRMSL) and natural gamma radiation (NGR) data, Holes U1331A-U1331C. Hole U1331B and U1331C data are plotted using offsets (0.5 and 1 g/cm³ for gamma ray attenuation [GRA] bulk density; 10 × 10⁻⁵ and 20 × 10⁻⁵ SI for magnetic susceptibility; 100 and 200 m/s for P-wave velocity; 10 and 20 cps for NGR).

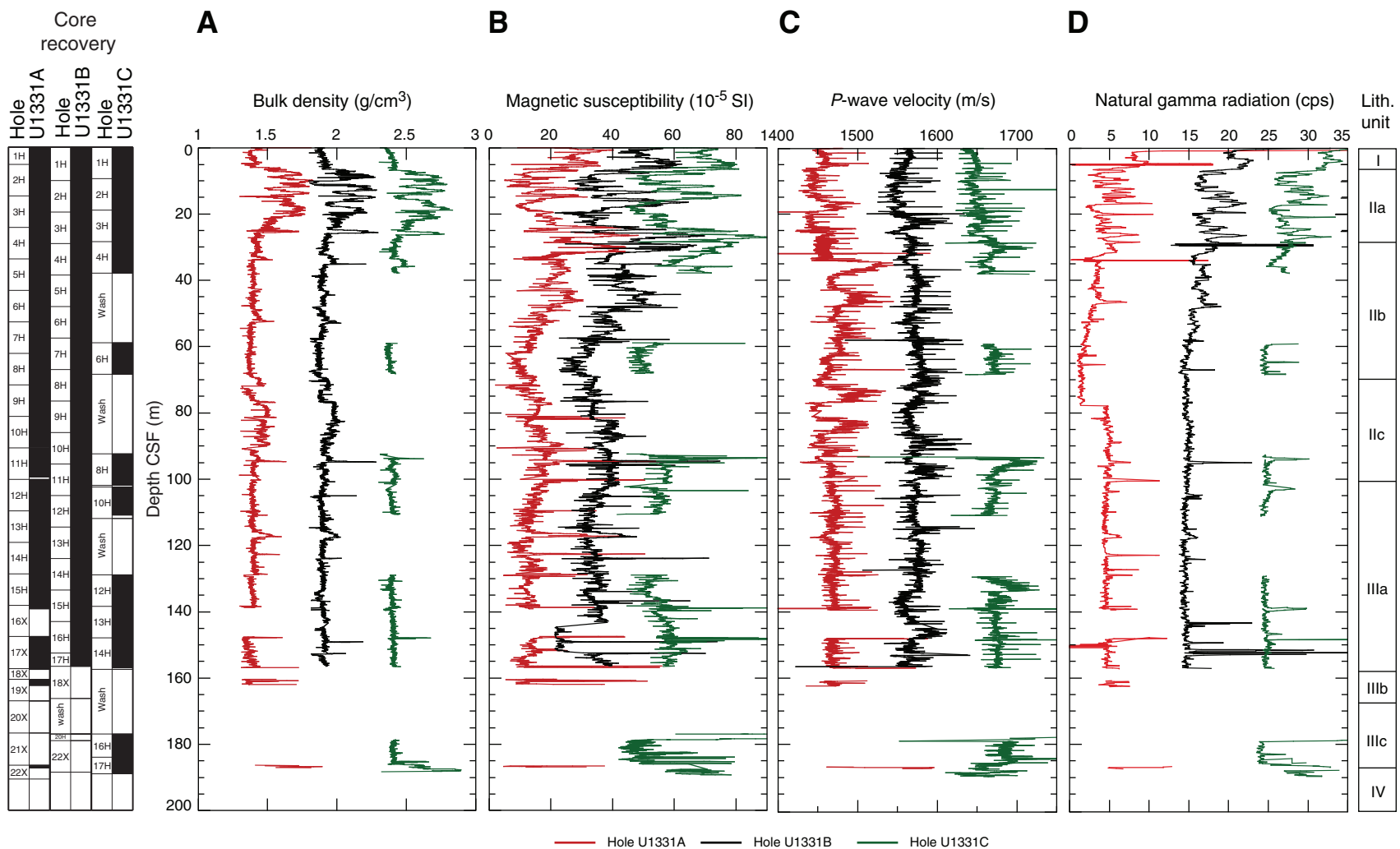


Figure F26. Moisture and density measurements, Hole U1331A. A. Porosity and water content. B. MAD and GRA bulk density. C. Grain density.

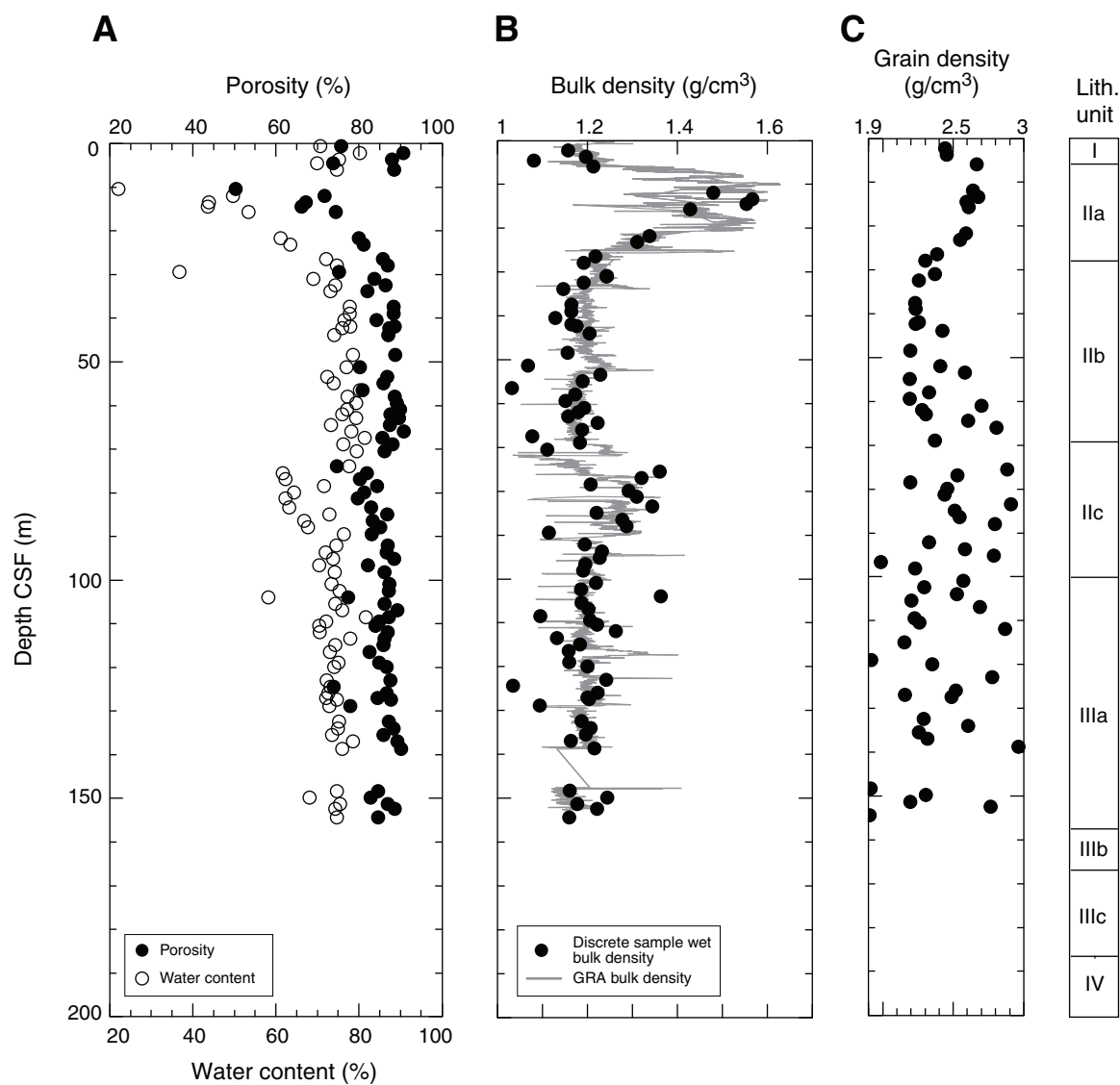


Figure F27. Moisture and density (MAD) analysis of discrete samples, Hole U1331A. Gamma ray attenuation (GRA) density interpolated with a 20 cm wide Gaussian window.

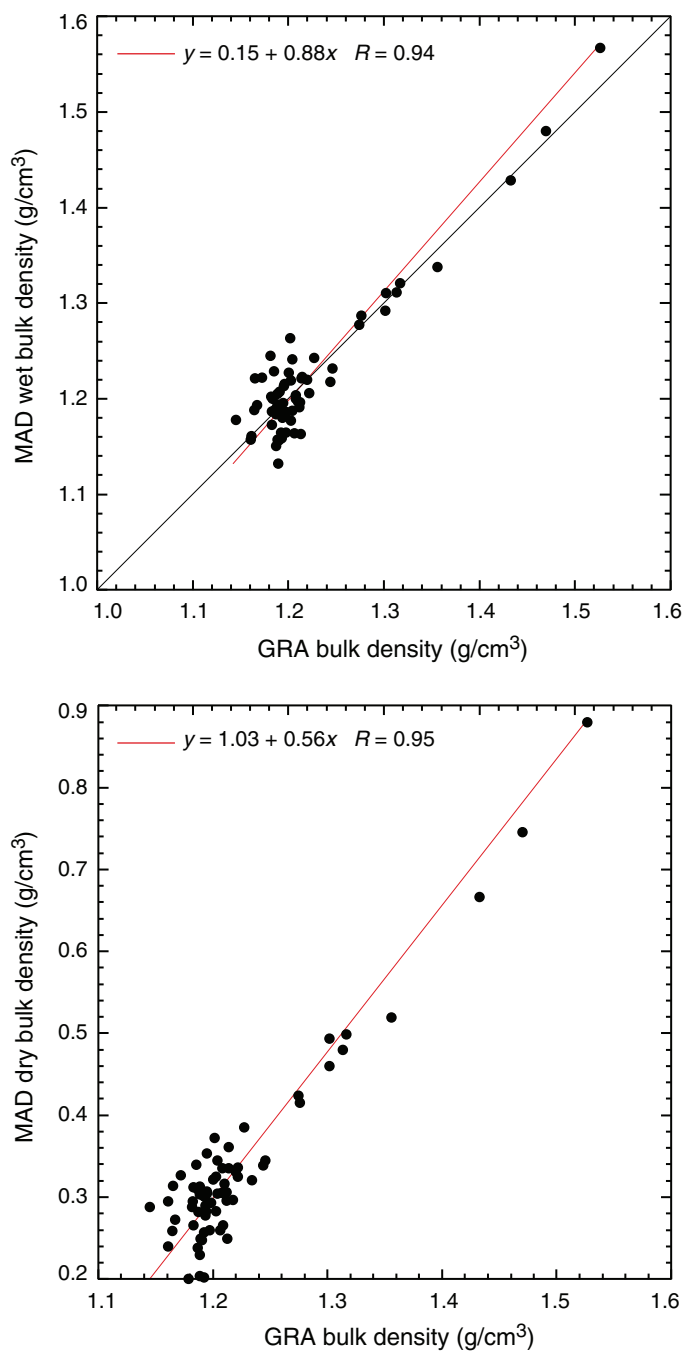


Figure F28. Compressional wave velocity from the *P*-wave logger (PWL) and discrete velocity measurements on split core from Hole U1331A, using the contact probe for *x*-axis measurements and insertion probes for *y*- and *z*-axis measurements. (see “[Compressional wave velocity](#)” for a note on postcruise velocity correction.)

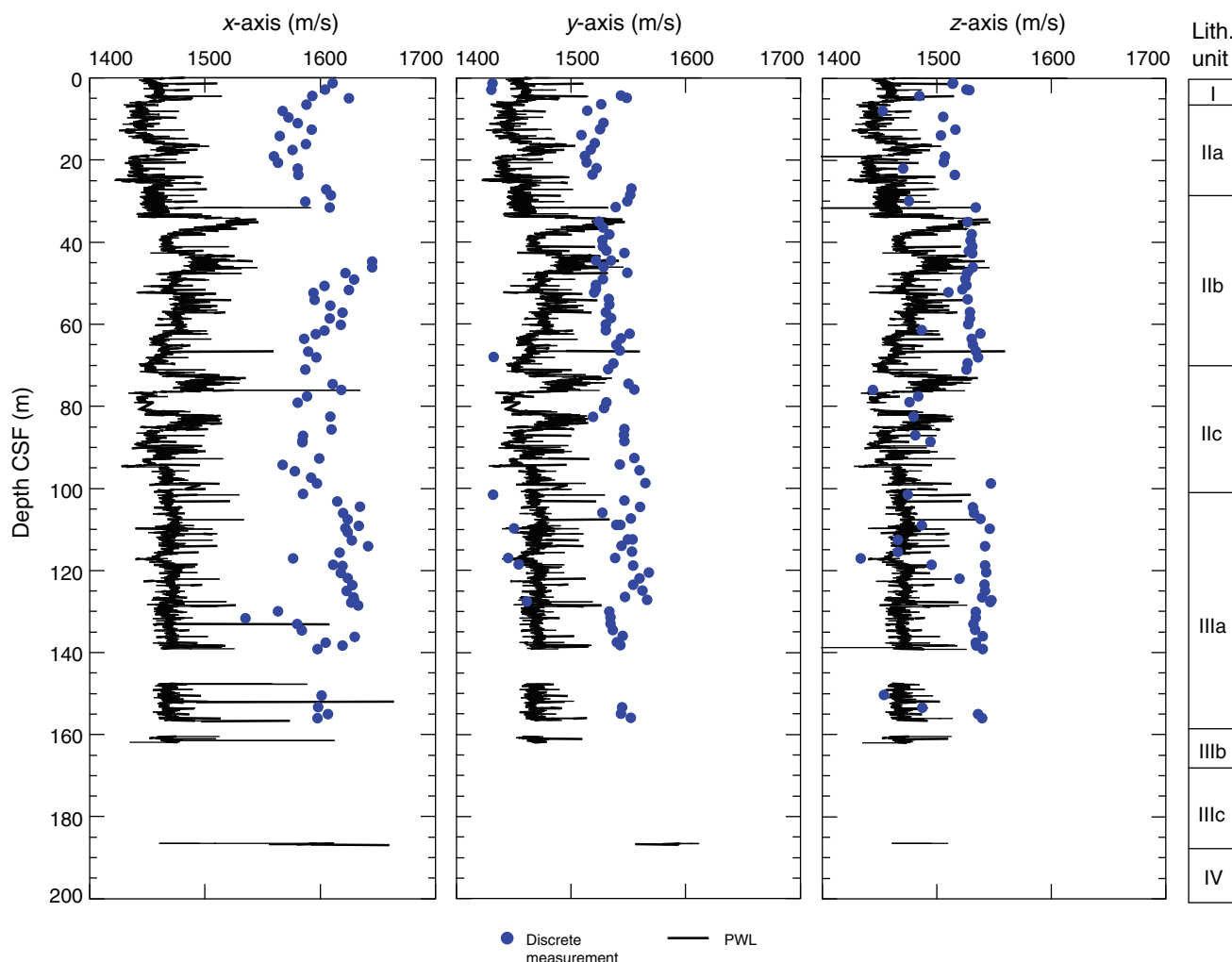


Figure F29. Compressional wave velocity from the *P*-wave logger (PWL) plotted with wet bulk density (MAD measurements).

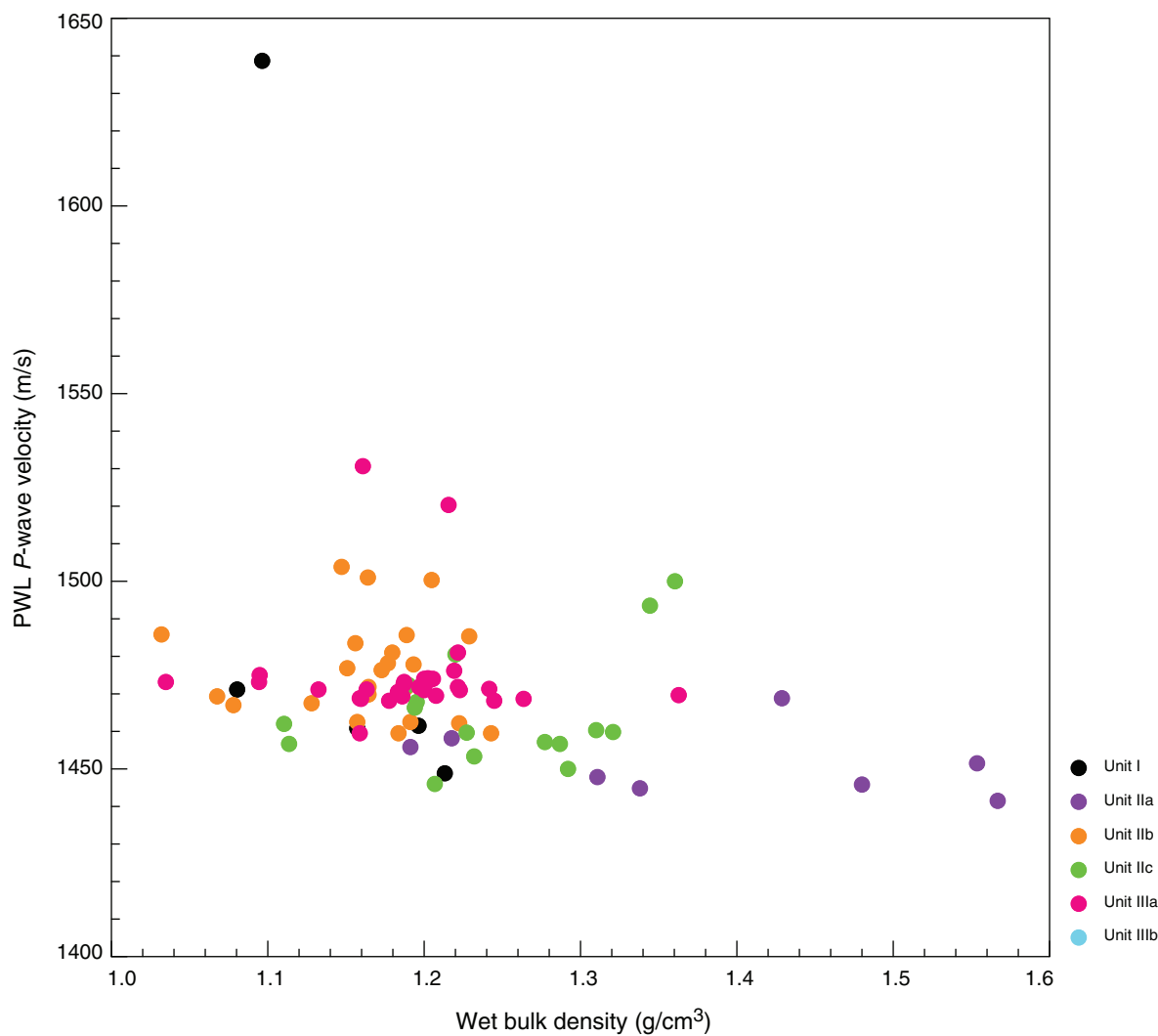


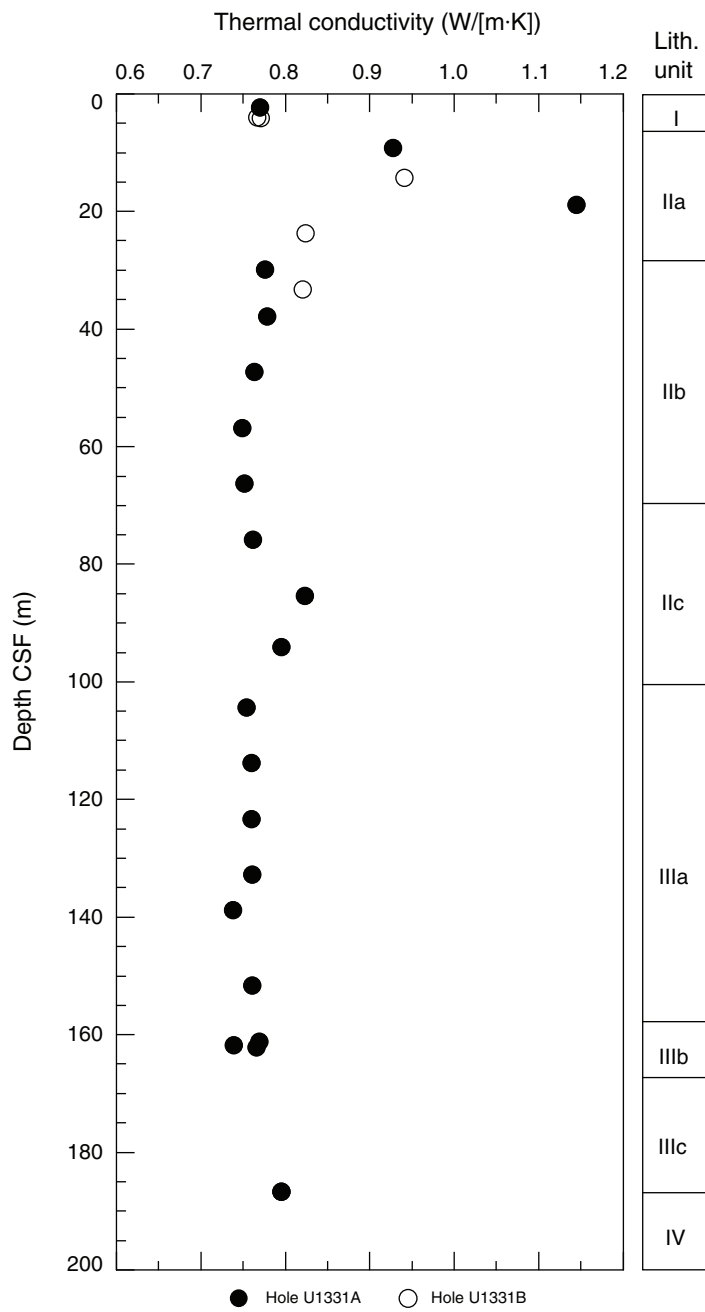
Figure F30. Thermal conductivity measurements, Holes U1331A and U1331B.

Figure F31. Reflectance spectrophotometer (RSC) data, Holes U1331A–U1331C. RSC for Holes U1331B and U1331C have been offset (20 and 40 for L^* ; 5 and 10 for a^* ; 10 and 20 for b^*) for core to core comparison. L^* , a^* , b^* = reflectance value of sediment as defined in the LAB color model.

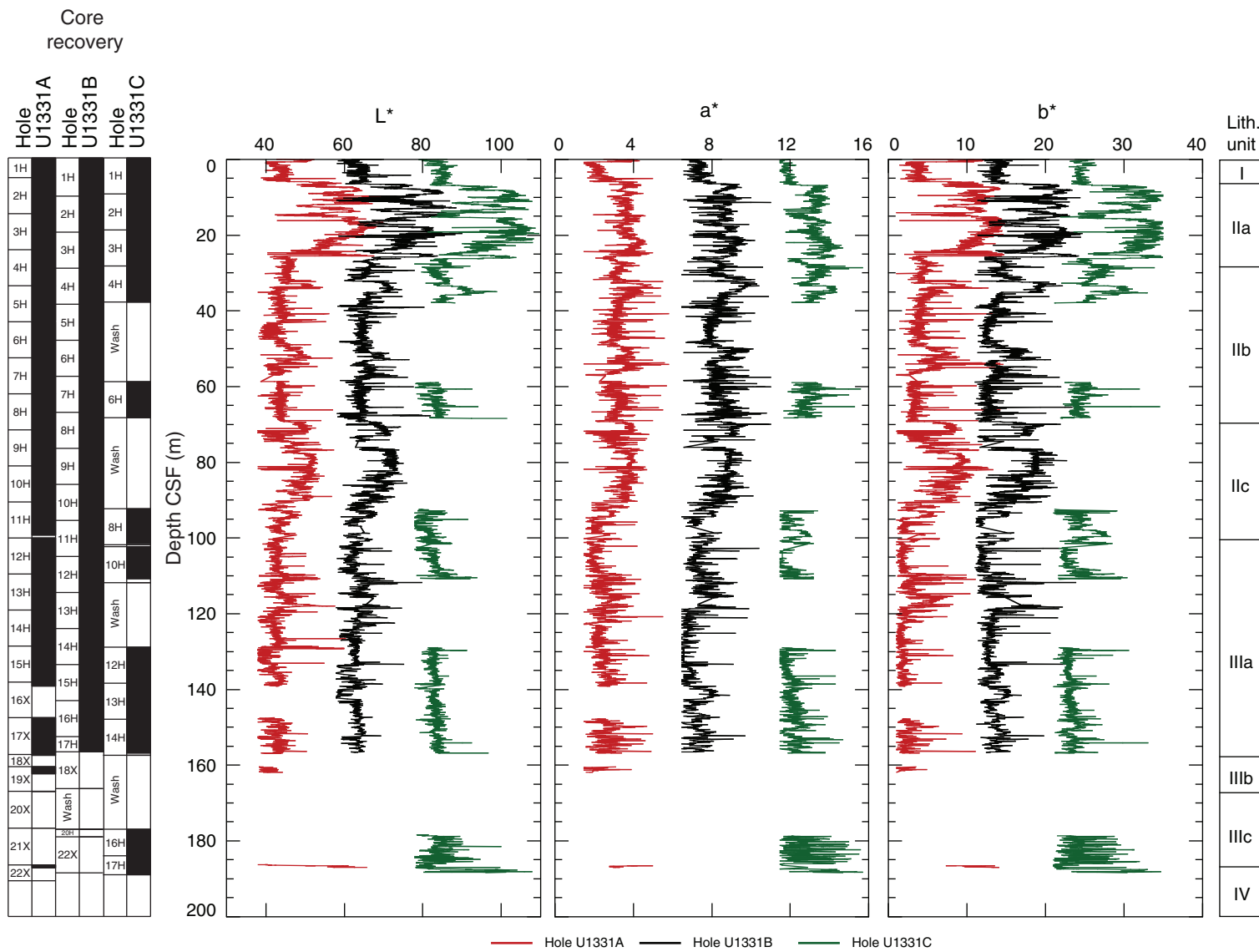


Figure F32. Magnetic susceptibility data, Site U1331. Top panel = spliced section with core breaks (triangles) and hole designations, bottom panel = Holes U1331A (red), U1331B (blue), and U1331C (green), offset from each other by a constant (300×10^{-6} SI). A. 0–50 CCSF-A. ([Continued on next three pages.](#))

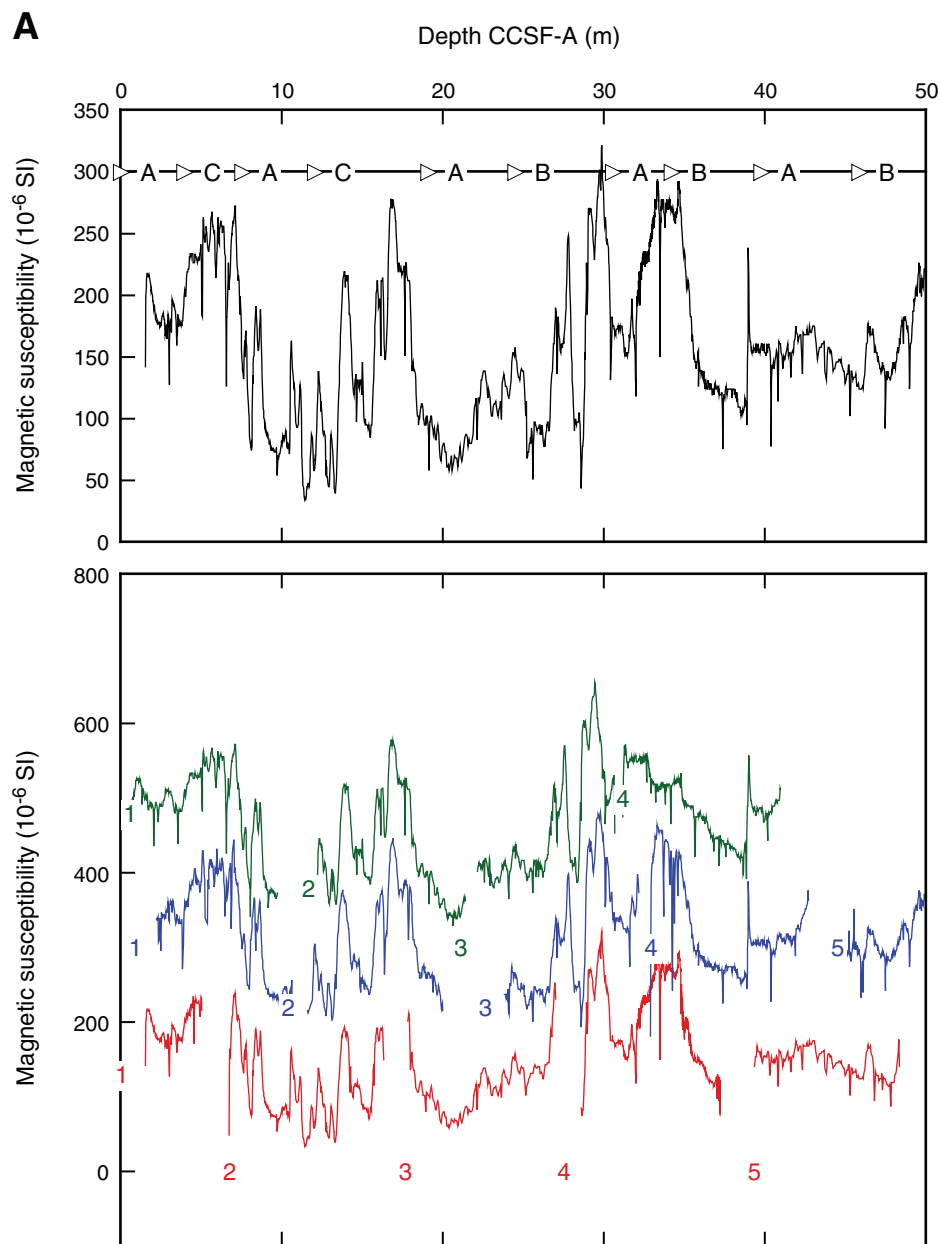


Figure F32 (continued). B. 50–100 CCSF-A. (Continued on next page.)

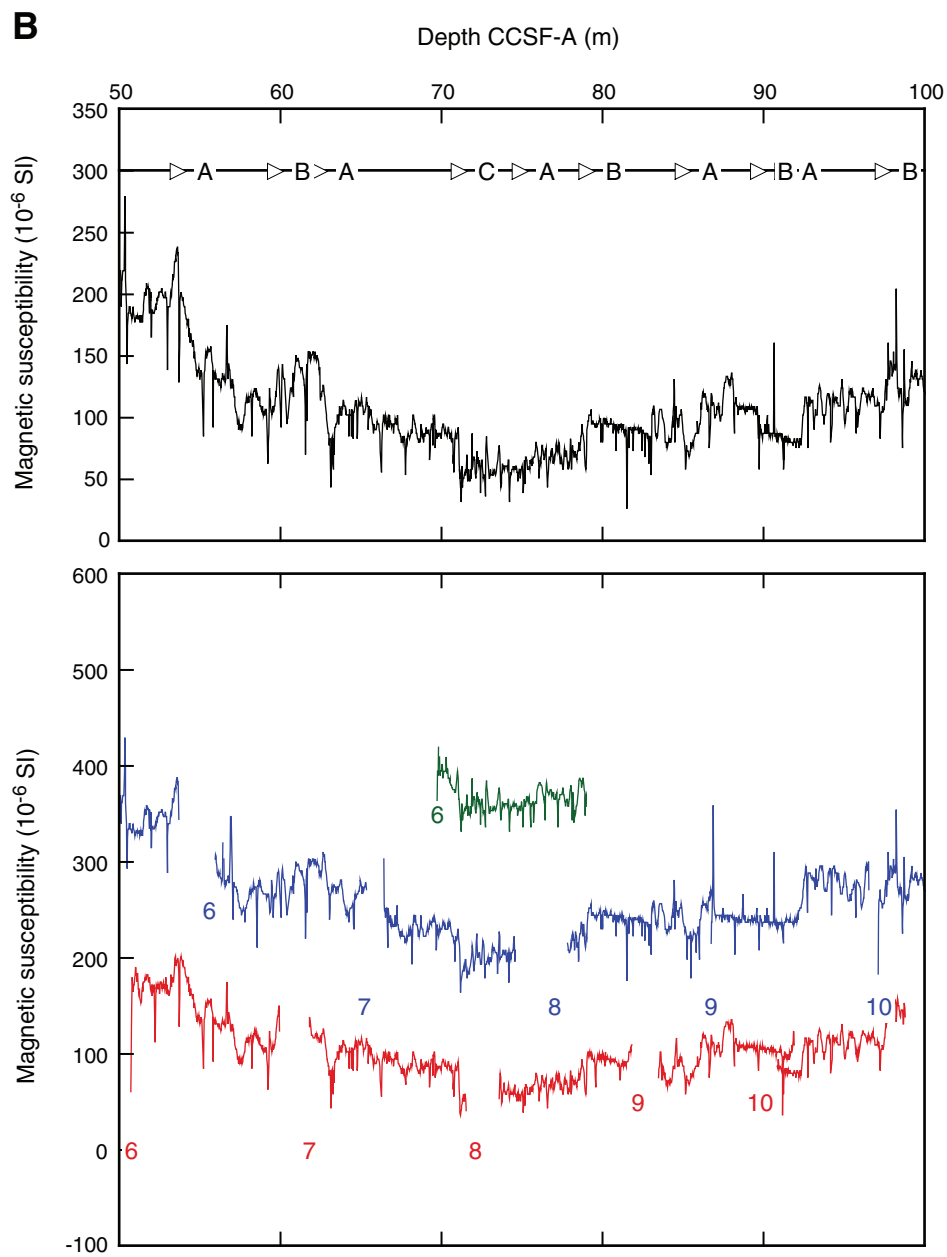


Figure F32 (continued). C. 100–150 CCSF-A. (Continued on next page.)

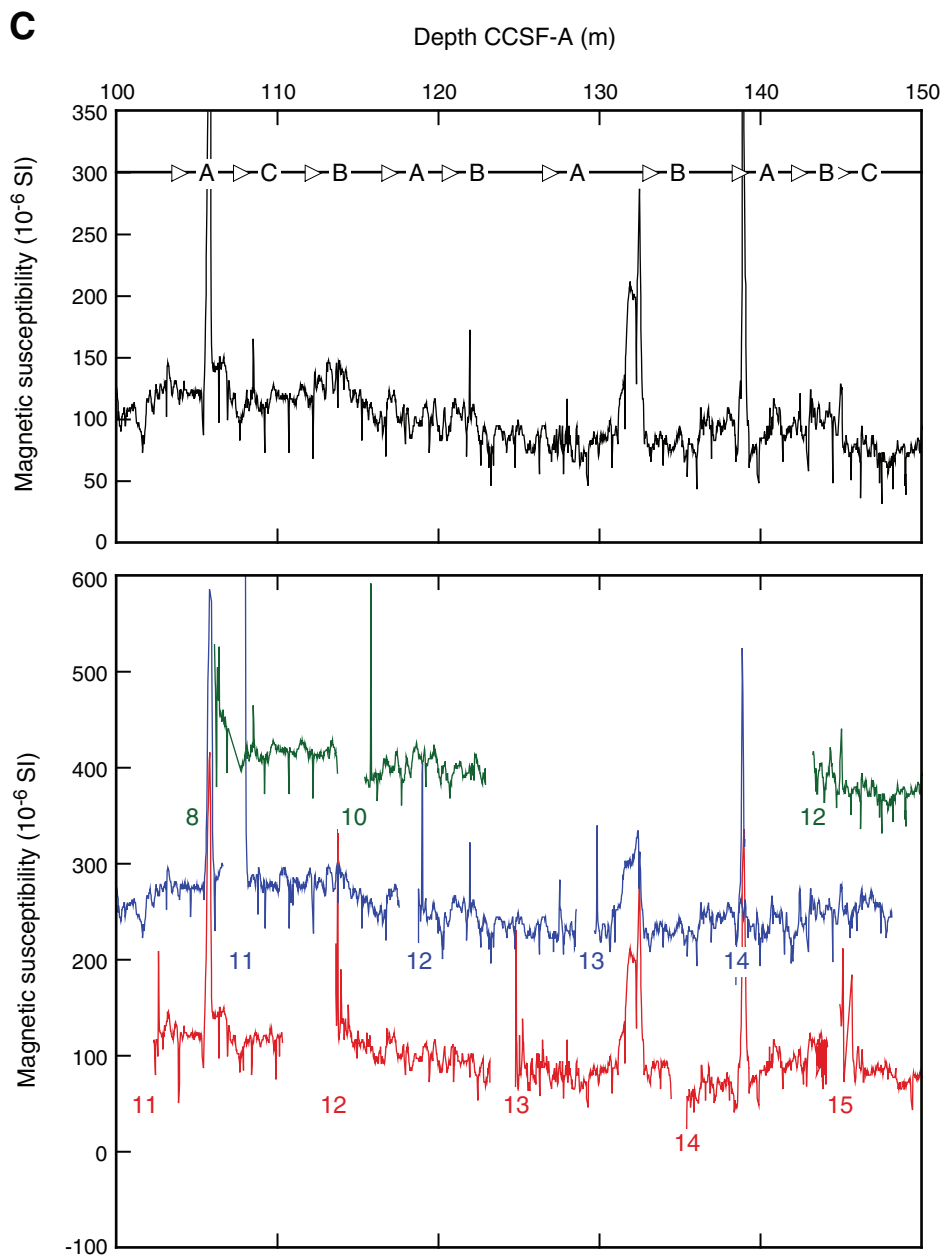


Figure F32 (continued). D. 150–200 CCSF-A.

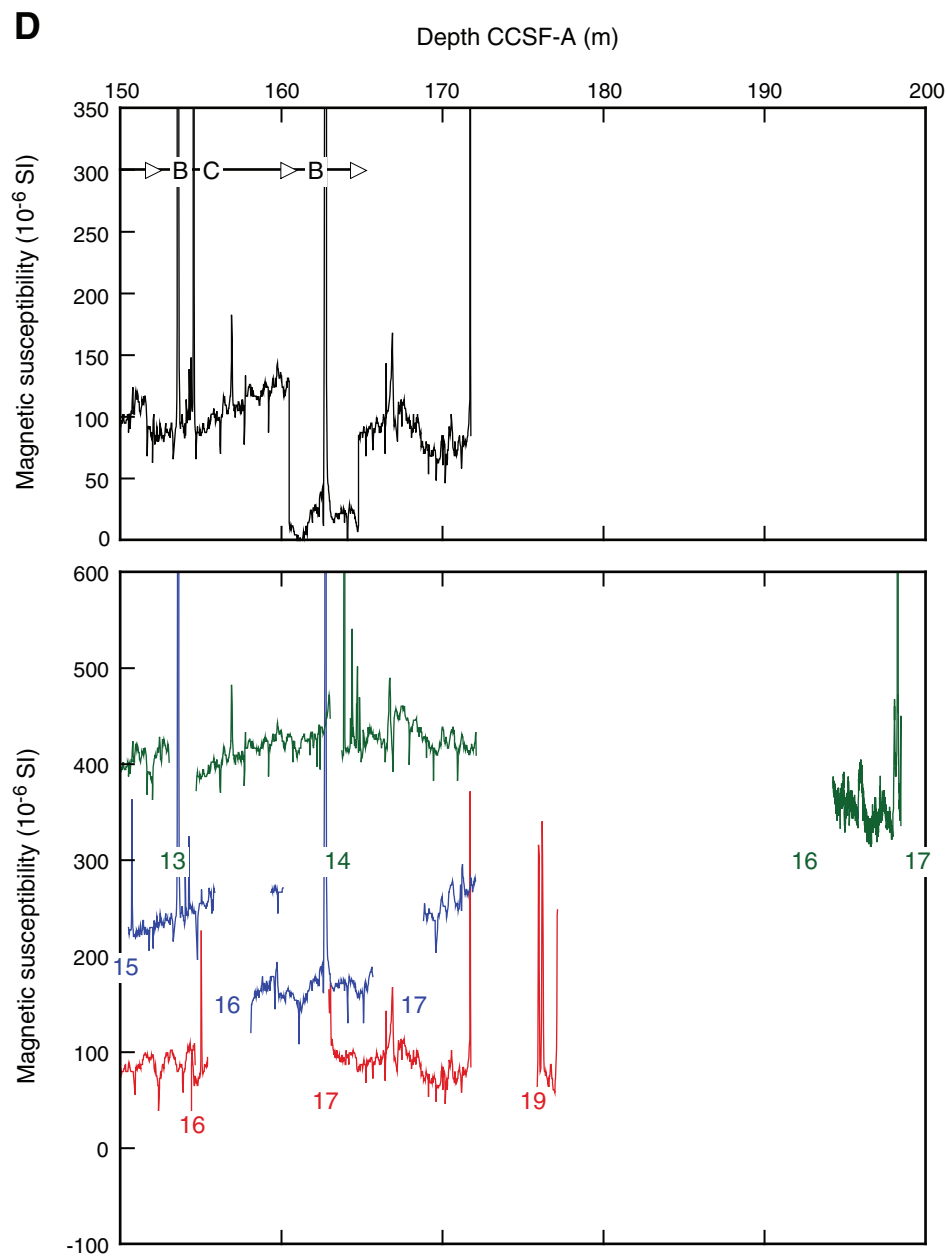


Figure F33. CSF depth vs. CCSF-A depth for tops of cores, Site U1331. Growth factor = slope of the regression line.

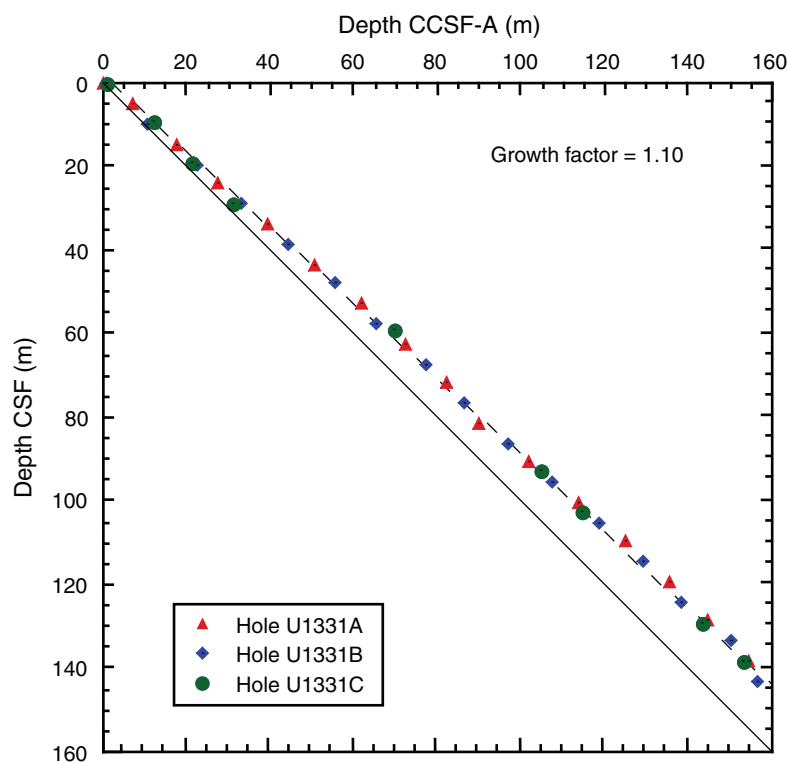


Figure F34. Logging operations summary diagram. A. Modified triple combination tool string run in Hole U1331A. B. Depth intervals of downlog and uplog (main) passes. HNGS = Hostile Environment Gamma Ray Sonde, HLDS = Hostile Environment Litho-Density Sonde, MSS = Magnetic Susceptibility Sonde.

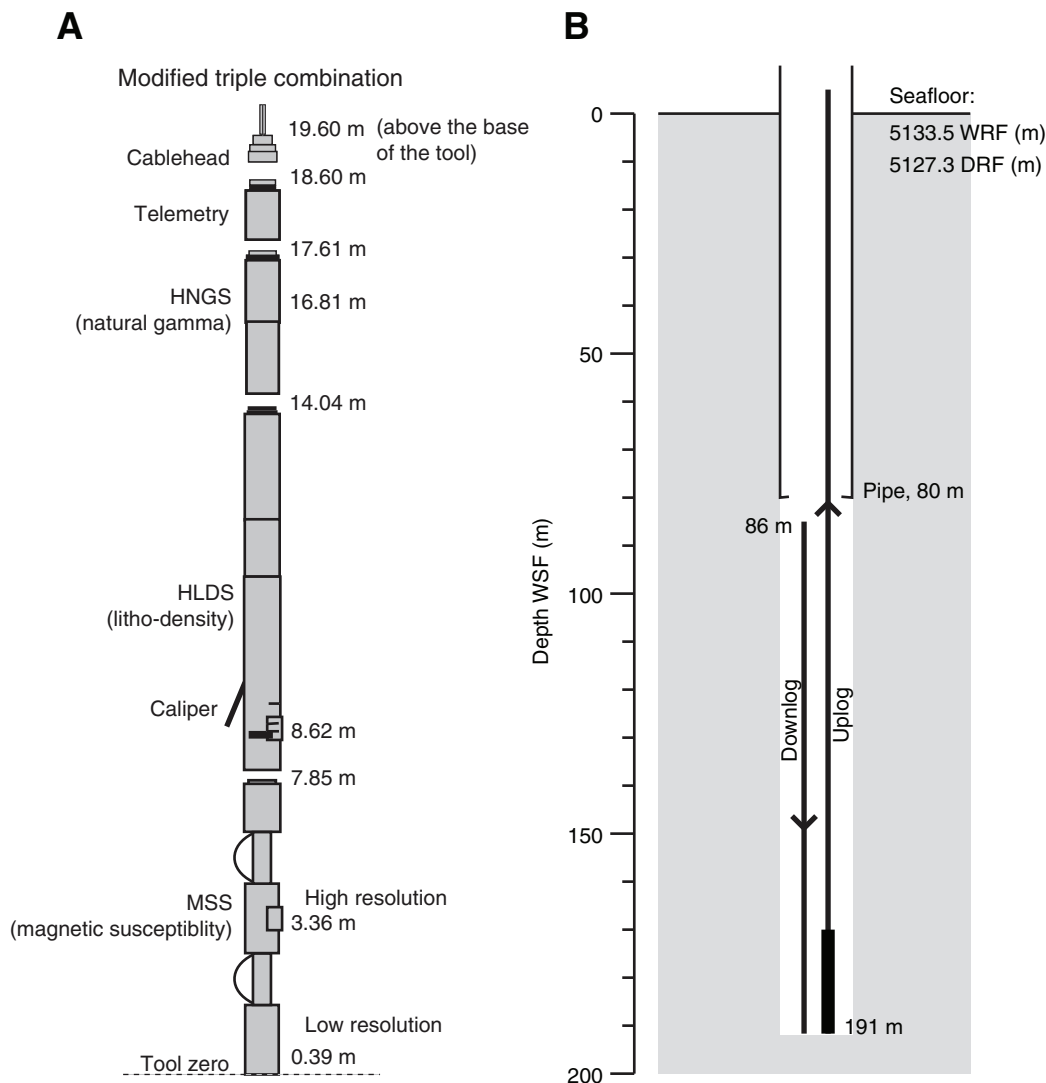


Figure F35. Downhole logs, Hole U1331A. Logging units are described in text. Chert-rich Unit 2 is characterized by higher density, magnetic susceptibility, and gamma radiation than the oozes of Units 1 and 3. uncal. = uncalibrated. MAD = moisture and density, PEF = photoelectric effect.

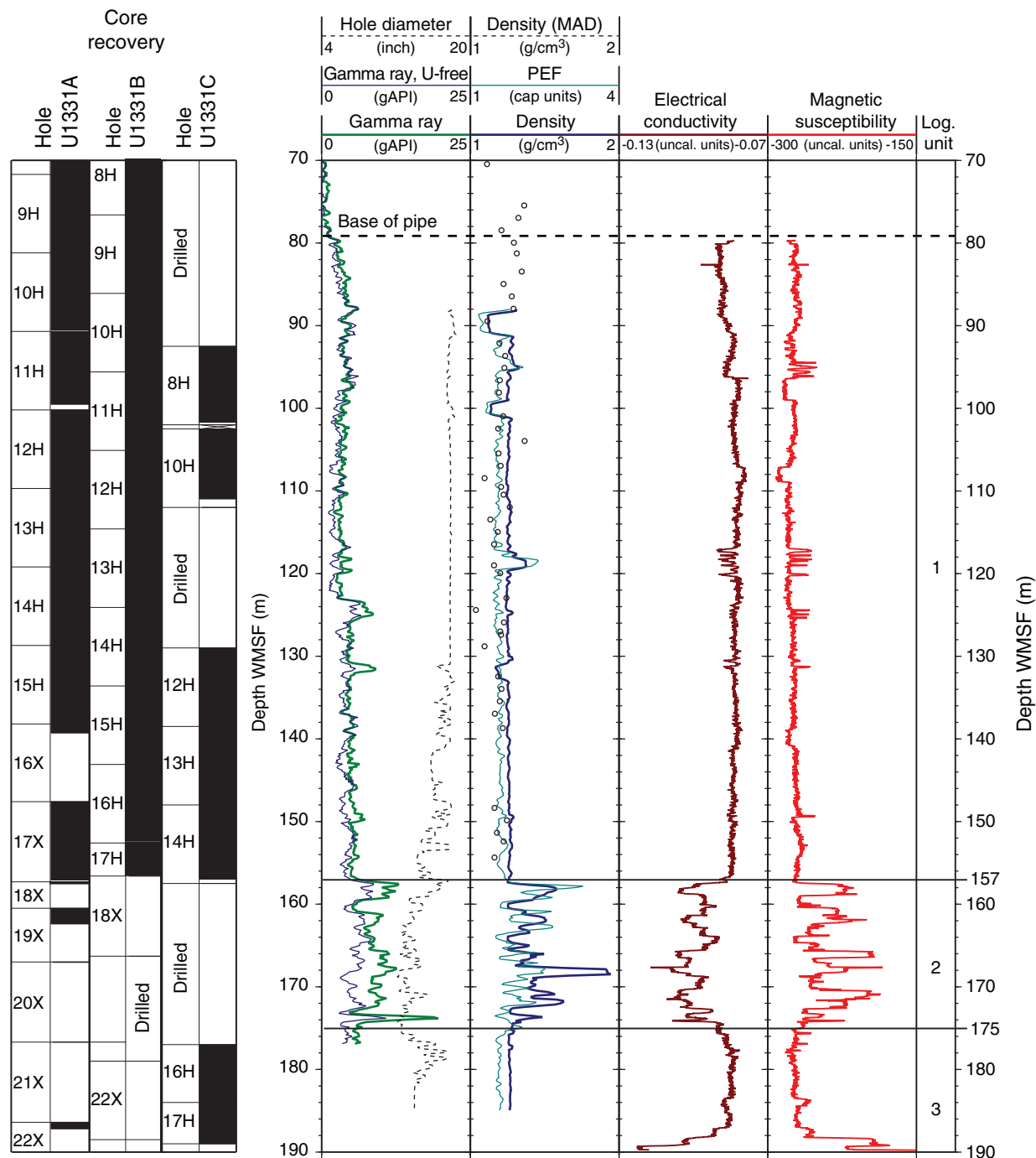


Figure F36. Natural gamma radiation data, Hole U1331A. Data above 78 m WMSF have been corrected for attenuation through the thickness of the metal drill pipe.

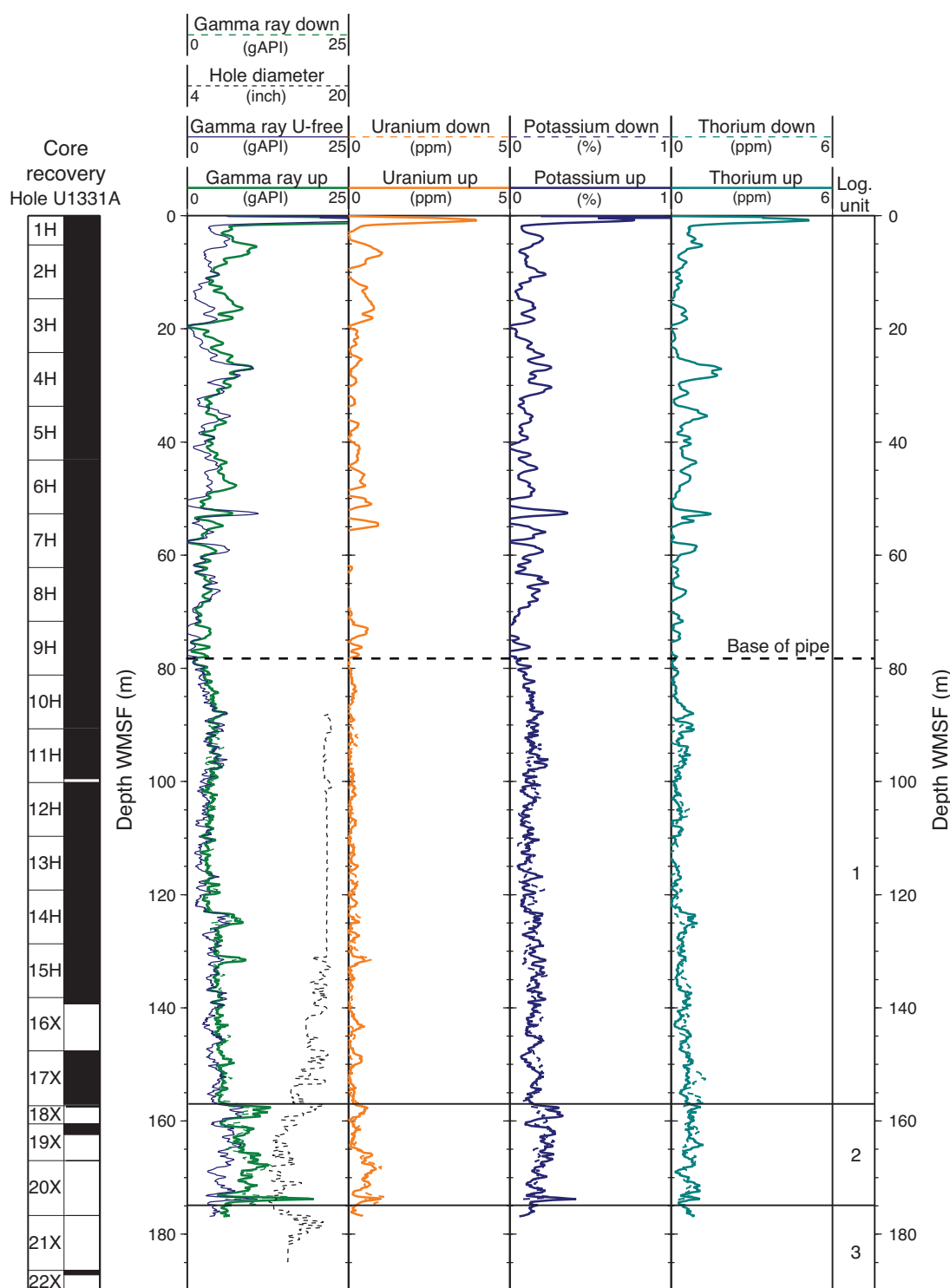


Figure F37. Heat flow calculation, Hole U1331A. A. Sediment temperatures. B. Thermal resistance based on laboratory thermal conductivity data. C. Bullard plot where heat flow is calculated from a linear fit of the temperature data. APCT-3 = advanced piston corer temperature tool.

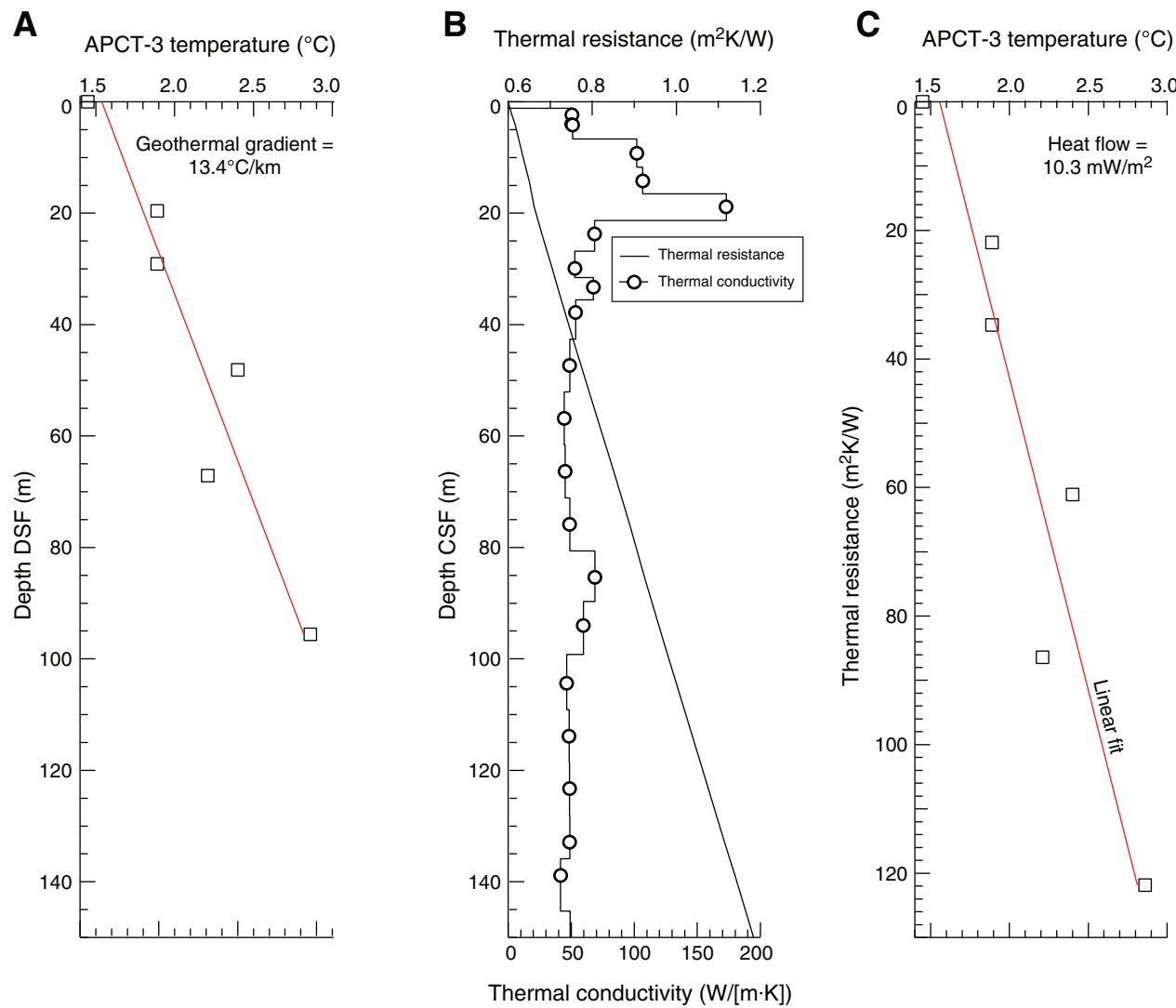


Table T1. Coring summary, Site U1331. (See table notes.) (Continued on next page.)

Site U1331									
Time on site (h): 173.5 (2330 h, 14 March–0500 h, 22 March 2009)									
Hole U1331A									
Latitude: 12°4.088'N Longitude: 142°9.696'W Time on hole (h): 80.8 (2330 h, 14 March–0820 h, 18 March 2009) Seafloor (drill pipe measurement below rig floor, m DRF): 5127.3 Distance between rig floor and sea level (m): 11.1 Water depth (drill pipe measurement from sea level, mbsl): 5116.2 Total depth (drill pipe measurement from rig floor, m DRF): 5317.9 Total penetration (drilling depth below seafloor, m DSF): 190.6 Total length of cored section (m): 190.6 Total core recovered (m): 155.1 Core recovery (%): 81 Total number of cores: 22									
Hole U1331B									
Latitude: 12°4.088'N Longitude: 142°9.709'W Time on hole (h): 38.0 (0820 h, 18 March–2200 h, 19 March 2009) Seafloor (drill pipe measurement below rig floor, m DRF): 5127.4 Distance between rig floor and sea level (m): 11.1 Water depth (drill pipe measurement from sea level, mbsl): 5116.3 Total depth (drill pipe measurement from rig floor, m DRF): 5315.9 Total penetration (drilling depth below seafloor, m DSF): 188.5 Total length of cored section (m): 175.8 Total core recovered (m): 163.0 Core recovery (%): 93 Total number of cores: 20									
Hole U1331C									
Latitude: 12°4.089'N Longitude: 142°9.720'W Time on hole (h): 54.7 (2200 h, 19 March–0500 h, 22 March 2009) Seafloor (drill pipe measurement below rig floor, m DRF): 5128.0 Distance between rig floor and sea level (m): 11.1 Water depth (drill pipe measurement from sea level, mbsl): 5116.9 Total depth (drill pipe measurement from rig floor, m DRF): 5315.9 Total penetration (drilling depth below seafloor, m DSF): 189.0 Total length of cored section (m): 107.0 Total core recovered (m): 109.5 Core recovery (%): 102 Total number of cores: 12									
Core	Date (2009)	Local time (h)	Depth DSF (m)			Depth CSF (m)			
			Top of cored interval	Bottom of cored interval	Interval advanced (m)	Top of cored interval	Bottom of cored interval	Length of core recovered (m)	Recovery (%)
320-U1331A-									
1H	16 Mar	0830	0.0	5.2	5.2	0.0	5.2	5.19	100
2H	16 Mar	1000	5.2	14.7	9.5	5.2	15.1	9.87	104
3H	16 Mar	1115	14.7	24.2	9.5	14.7	24.4	9.69	102
4H	16 Mar	1245	24.2	33.7	9.5	24.2	34.2	9.99	105
5H	16 Mar	1410	33.7	43.2	9.5	33.7	43.0	9.32	98
6H	16 Mar	1535	43.2	52.7	9.5	43.2	52.7	9.45	99
7H	16 Mar	1655	52.7	62.2	9.5	52.7	62.7	9.95	105
8H	16 Mar	1816	62.2	71.7	9.5	62.2	72.2	10.02	105
9H	16 Mar	1956	71.7	81.2	9.5	71.7	81.7	9.96	105
10H	16 Mar	2202	81.2	90.7	9.5	81.2	90.5	9.33	98
11H	16 Mar	2330	90.7	100.2	9.5	90.7	99.5	8.82	93
12H	17 Mar	0045	100.2	109.7	9.5	100.2	110.2	10.00	105
13H	17 Mar	0220	109.7	119.2	9.5	109.7	119.6	9.93	105
14H	17 Mar	0350	119.2	128.7	9.5	119.2	129.3	10.08	106
15H	17 Mar	0530	128.7	138.2	9.5	128.7	138.6	9.90	104
16X	17 Mar	0710	138.2	147.6	9.4	138.2	139.3	1.10	12
17X	17 Mar	0830	147.6	157.3	9.7	147.6	157.1	9.46	98
18X	17 Mar	0955	157.3	160.5	3.2	157.3	157.6	0.25	8
19X	17 Mar	1200	160.5	167.0	6.5	160.5	162.4	1.91	29
20X	17 Mar	1355	167.0	176.7	9.7	167.0	167.1	0.06	1



Table T1 (continued).

Core	Date (2009)	Local time (h)	Depth DSF (m)			Depth CSF (m)			Length of core recovered (m)	Recovery (%)
			Top of cored interval	Bottom of cored interval	Interval advanced (m)	Top of cored interval	Bottom of cored interval			
21X	17 Mar	1505	176.7	186.4	9.7	176.7	176.7	0.00	0	
22X	17 Mar	1635	186.4	190.6	4.2	186.4	187.2	0.80	19	
			Advanced total: 190.6						155.08	81
			Total interval cored: 190.6							
320-U1331B-										
1H	18 Mar	1200	0.0	10.1	10.1	0.0	10.1	10.09	100	
2H	18 Mar	1345	10.1	19.6	9.5	10.1	20.1	10.03	106	
3H	18 Mar	1530	19.6	29.1	9.5	19.6	29.5	9.94	105	
4H	18 Mar	1650	29.1	38.6	9.5	29.1	39.2	10.07	106	
5H	18 Mar	1820	38.6	48.1	9.5	38.6	48.1	9.50	100	
6H	18 Mar	1945	48.1	57.6	9.5	48.1	58.3	10.15	107	
7H	18 Mar	2150	57.6	67.1	9.5	57.6	67.2	9.61	101	
8H	18 Mar	2305	67.1	76.6	9.5	67.1	77.2	10.09	106	
9H	19 Mar	0030	76.6	86.1	9.5	76.6	86.7	10.05	106	
10H	19 Mar	0225	86.1	95.6	9.5	86.1	96.1	10.04	106	
11H	19 Mar	0400	95.6	105.1	9.5	95.6	105.7	10.10	106	
12H	19 Mar	0530	105.1	114.6	9.5	105.1	115.0	9.92	104	
13H	19 Mar	0700	114.6	124.1	9.5	114.6	124.4	9.81	103	
14H	19 Mar	0825	124.1	133.6	9.5	124.1	134.0	9.93	105	
15H	19 Mar	0950	133.6	143.1	9.5	133.6	143.6	10.02	105	
16H	19 Mar	1255	143.1	152.6	9.5	143.1	152.5	9.40	99	
17H	19 Mar	1410	152.6	156.6	4.0	152.6	156.9	4.28	107	
18X	19 Mar	1600	156.6	166.3	9.7	156.6	156.6	0.00	0	
19D			*****Drilled from 166.3 to 177.0 m DSF*****							
20H	19 Mar	1905	177.0	177.0	0.0	177.0				0.00
21D			*****Drilled from 177.0 to 179.0 m DSF*****							
22X	19 Mar	2040	179.0	188.5	9.5	179.0				0.01
			Advanced total: 188.5						163.04	93
			Total interval cored: 175.8							
320-U1331C-										
1H	20 Mar	0235	0.0	9.5	9.5	0.0	9.5	9.46	100	
2H	20 Mar	0430	9.5	19.0	9.5	9.5	19.5	10.02	105	
3H	20 Mar	0640	19.0	28.5	9.5	19.0	28.8	9.77	103	
4H	20 Mar	0810	28.5			9.5	28.5	38.5	9.99	105
5D			*****Drilled from 38.0 to 59.0 m DSF*****							
6H	20 Mar	1230	59.0	92.5	9.5	59.0	68.5	9.54	100	
7D			*****Drilled from 68.5 to 92.5 m DSF*****							
8H	20 Mar	1930	92.5	102.5	9.5	92.5	101.7	9.21	97	
9D			*****Drilled from 102.0 to 102.5 m DSF*****							
10H	20 Mar	2045	102.5	129.0	9.5	102.5	111.0	8.48	89	
11D			*****Drilled from 112.0 to 129.0 m DSF*****							
12H	21 Mar	0030	129.0	138.5	9.5	129.0	139.1	10.05	106	
13H	21 Mar	0130	138.5	148.0	9.5	138.5	148.6	10.09	106	
14H	21 Mar	0345	148.0	177.0	9.5	148.0	156.9	8.94	94	
15D			*****Drilled from 157.5 to 177.0 m DSF*****							
16H	21 Mar	0850	177.0	184.0	7.0	177.0	185.46	8.46	121	
17H	21 Mar	1040	184.0	189.0	5.0	184.0	189.53	5.53	111	
			Advanced total: 189.0						109.54	102
			Total interval cored: 107.0							

Notes: DRF = drilling depth below rig floor, DSF = drilling depth below seafloor, CSF = core depth below seafloor. H = APC core, X = XCB core.
 Local time = UTC – 10 h.

Table T2. Lithologic unit boundaries, Site U1331. (See table notes.)

Unit	Core, section, interval (cm)	Depth CSF (m)	Core, section, interval (cm)	Depth CSF (m)	Core, section, interval (cm)	Depth CSF (m)
	320-U1331A-		320-U1331B-		320-U1331C-	
I	2H-1, 85	6.05	1H-5, 52	6.52	1H-5, 107	7.07
IIa	4H-1, 140	25.6	3H-5, 35	25.95	3H-6, 2	26.52
IIb	8H-5, 119	69.39	8H-2, 76	69.36	6H-CC, 25*	68.5
IIc	11H-CC, 22	99.52	11H-1, 150	97.1	8H-5, 16	98.66
IIIa	17X-CC, 37	157.06	17H-CC, 40*	156.88	14H-CC, 29	156.94
IIIb	18X-1, 25*	157.55	—	—	16H-1, 0	177
IIIc	22X-1, 11	186.51	—	—	17X-3, 62	187.62
IV	22X-CC, 25	187.02	—	—	17X-CC, 8	189.48
V	22X-CC, 44	187.21	—	—	—	—

Notes: Interval/depth are given for basal boundary of each unit. * = unit extends through at least given interval and depth, but boundary was not cored. — = unit not cored.

Table T3. Prominent lithologic horizons: sharp boundaries, Site U1331. (See table notes.)

Unit	Core, section, interval (cm)	Depth CSF (m)	Note	Core, section, interval (cm)	Depth CSF (m)	Note	Core, section, interval (cm)	Depth CSF (m)	Note
	320-U1331A-			320-U1331B-			320-U1331C-		
I	1H-1, 74	0.74	Top of Mn crust						
IIa	2H-1, 143	6.63	Sharp boundary*	1H-5, 117	7.18	Sharp boundary*	1H-6, 5	7.56	Sharp boundary*
	2H-3, 80	9.00	Sharp boundary	1H-7, 74	9.75	Sharp boundary	3H-2, 32	20.78	Sharp boundary
	3H-4, 73	19.93	Sharp boundary						
IIb	6H-4, 143	49.13	Erosional contact*	4H-5, 9	35.21	Sharp boundary	4H-4, 77	33.55	Sharp boundary
	6H-7, 9	51.79	Erosional contact*	6H-1, 133	49.43	Sharp boundary	4H-6, 36	35.99	Sharp boundary
				6H-3, 90	52.00	Sharp boundary			
				6H-4, 32	52.92	Sharp boundary			
IIc	10H-2, 111–112	83.82	Sharp inclined contact*	8H-5, 6	73.17	Sharp boundary			
	10H-3, 39–44	84.64	Sharp inclined contact*	9H-4, 25	81.37	Sharp boundary			
	10H-5, 13–15	87.35	Sharp inclined contact*	9H-5, 55	83.18	Sharp boundary			
	10H-7, 42–49	90.19	Sharp inclined contact*	9H-7, 39	86.03	Sharp boundary			
	11H-4, 43	95.25	Sharp boundary	10H-2, 10	87.70	Sharp boundary			
				10H-5, 127	93.37	Sharp boundary			
				10H-6, 127	94.87	Sharp boundary			
				11H-2, 91	98.01	Sharp boundary			
				11H-3, 22	98.82	Sharp boundary			
IIIa	12H-1, 14	100.34	Sharp color contact	11H-4, 79	100.89	Sharp boundary	12H-1, 28–35	129.35	Sharp boundary
	12H-1, 92	101.12	Sharp contact†	11H-5, 40	102.00	Sharp boundary	12H-6, 119	137.49	Sharp boundary
	12H-5, 22	106.42	Sharp contact†	12H-1, 88	105.98	Sharp boundary			
	12H-7, 21	107.91	Sharp contact†	12H-2, 90	107.50	Sharp boundary	12H-CC, 1	138.84	Sharp boundary
	12H-6, 50	108.20	Sharp contact†	13H-3, 27	117.87	Sharp boundary	13H-3, 73	142.23	Sharp boundary
	12H-7, 67	109.87	Sharp contact†	14H-3, 56	127.66	Sharp boundary			
	17X-CC, 22	138.84	Sharp boundary	14H-4, 51	129.11	Sharp boundary			
				14H-5, 60	130.70	Sharp boundary			
IIIc	22X-1, 21	186.61	Sharp boundary				17H-1, 132	185.32	Sharp boundary
							17H-1, 144	185.44	Sharp boundary
							17H-2, 29	185.79	Sharp boundary

Notes: * = sharp inclined contact overlain by coarse-grained material (e.g., foraminifers and/or oxides), † = sharp irregular contact defined by color change.



Table T4. Prominent lithologic horizons: clay horizons, Site U1331.

Unit	Core, section, interval (cm)			Lithology	Core, section, interval (cm)			Lithology	Core, section, interval (cm)			Lithology
	Top	Bottom	Base depth CSF (m)		Top	Bottom	Base depth CSF (m)		Top	Bottom	Base depth CSF (m)	
IIc	320-U1331A- 17H-2, 42	17H-2, 44	94.82	Radiolarian clay	320-U1331B- 10H-6, 127	10H-6, 129	94.89	Zeolite clay	320-U1331C-			
IIIa	13H-1, 0	13H-CC, 21	119.57	Radiolarian clay with nannofossils	13H-7, 40	13H-7, 51	124.11	Clay with zeolite and nannofossils				
IIIb	18X-1, 0	18X-1, 32	157.62	Radiolarian clay	16H-5, 5	16H-5, 17	149.27	Clay (partly lithified)				
IIIc	22X-1, 6	22X-1, 21	186.61	Clay					16H-4, 108	16H-4, 119	182.69	Radiolarian clay
									17H-2, 132	17H-2, 144	185.44	Zeolite clay
									17H-2, 29	17H-2, 44	185.94	Zeolite clay
									17H-2, 65	17H-3, 55	187.55	Zeolite clay



Table T5. Calcareous nannofossil datums, Site U1331. (See table note.)

Core, section, interval (cm)	Top	Bottom	Marker species	Age (Ma)	Depth CSF (m)			
					Top	Bottom	Midpoint	±
320-U1331A-	320-U1331A-	2H-4, 70	B <i>Sphenolithus distentus</i>	30.0	10.40	11.90	11.15	0.75
		3H-5, 110	T <i>Reticulofenestra umbilicus</i>	32.0	21.80	23.30	22.55	0.75
		3H-6, 110	T <i>Coccolithus formosus</i>	32.9	23.30	24.34	23.82	0.52
		4H-1, 110	T <i>Discoaster saipanensis</i>	34.4	25.30	33.30	29.30	4.00
		6H-5, 70	T <i>Chiasmolithus grandis</i>	37.1	49.90	51.79	50.85	0.95
		6H-CC	B <i>Dictyococcites bisectus</i>	38.0	52.60	53.00	52.80	0.20
		7H-1, 30	T <i>Chiasmolithus solitus</i>	40.4	54.50	70.20	62.35	7.85
		7H-2, 30	T <i>Discoaster bifax</i>	—	54.50	70.20	62.35	7.85
		11H-4, 30	B <i>Reticulofenestra umbilicus</i> >14 µm	42.5	94.68	96.18	95.43	0.75
		13H-2, 5	T <i>Nannotetra fulgens</i>	43.4	111.25	116.40	113.83	2.58
		13H-2, 5	B <i>Discoaster bifax</i>	—	111.25	116.40	113.83	2.58
320-U1331C-	320-U1331C-	17H-3, 100	T <i>Tribrachiatus orthostylus</i>	50.7	188.00	188.09	188.05	0.05
17H-3, 109	17H-3, 109							

Note: B = bottom, T = top.

Table T6. Preservation and relative abundance of radiolarians, Hole U1331A. This table is available in an [oversize format](#).

Table T7. Preservation and relative abundance of radiolarians, Hole U1331B. (See table notes.) (Continued on next page.)

Core, section, interval (cm)	Radiolarian zone	Radiolarian preservation											
		Abundance			Mixing			Preservation			Relative abundance		
		A	F	C	M	R	VR	R	R	R	R	R	Max
320-U1331B-1H-6, 38–40	RP22 (middle)	C	M	R	R	R	R	R	R	R	R	R	3
1H-CC	RP20	C	M	R	R	R	R	R	R	R	R	R	3
2H-CC	RP19	A	M	R	R	R	R	R	R	R	R	R	1
3H-CC	RP18	A	G	R	R	R	R	R	R	R	R	R	2
4H-CC	RP17	A	M	R	R	R	R	R	R	R	R	R	1
5H-CC	RP14	A	G	R	R	R	VR	R	R	R	R	R	1
9H-CC		A	G	R	R	R	R	R	R	R	R	R	1
10H-CC	RP12	A	G	R	R	R	R	R	R	R	R	R	1
11H-CC	RP11	A	G	R	R	R	R	R	R	R	R	R	1
12H-CC													
13H-CC													
14H-CC													
15H-CC													
16H-CC													
17H-CC													

Notes: Abundance: A = abundant, F = frequent, C = common, R = rare, VR = very rare, ? = identification uncertain. Preservation: G = good, M = moderate. Mixing: blank = no mixing of older specimens detected, 1 = 1–3 reworked specimens detected, 2 = 3–10 reworked specimens detected, 3 = >10 reworked specimens detected.



Table T7 (continued).

Core, section, interval (cm)	Anomalous and/or highly weathered zones											
	Zones with anomalous lithologies				Zones with anomalous mineralogy				Zones with anomalous geochemistry			
	RP22 (middle)	RP20	RP19	RP18	RP17	RP14	RP12	RP11	RP10	RP9	RP8	
320-U1331B-1H-6, 38–40	C	M	M	M	M	R	R	R	R	R	R	R
1H-CC	C	M	M	M	M	R	R	R	R	R	R	R
2H-CC	A	M	M	G	G	R	R	R	R	R	R	R
3H-CC	A	A	G	G	G	R	R	R	R	R	R	R
4H-CC	A	A	G	G	G	R	R	R	R	R	R	R
5H-CC	A	A	G	G	G	R	R	R	R	R	R	R
9H-CC	A	A	G	G	G	R	R	R	R	R	R	R
10H-CC	A	A	G	G	G	R	R	R	R	R	R	R
11H-CC	A	A	G	G	G	R	R	R	R	R	R	R
12H-CC	A	A	G	G	G	R	R	R	R	R	R	R
13H-CC	A	A	G	G	G	R	R	R	R	R	R	R
14H-CC	A	A	G	G	G	R	R	R	R	R	R	R
15H-CC	A	A	G	G	G	R	R	R	R	R	R	R
16H-CC	A	A	G	G	G	R	R	R	R	R	R	R
17H-CC	A	A	G	G	G	R	R	R	R	R	R	R



Table T8. Preservation and relative abundance of radiolarians, Hole U1331C. (See table notes.) (Continued on next page.)

Core, section, interval (cm)	Radiolarian zone										
	RP20					RP12					
	Abundance					Abundance					
320-U1331C- 1H-CC	C	M	<i>Amphicraspedium murrayanum</i>			R	<i>Cryptocarpium ornatum</i>			<i>Diplolegma somphum</i>	
2H-CC	A	G	<i>Anthocyrtoma</i> spp.			R	<i>Dorcadospyris circulus</i>			<i>Dorcadospyris copeletta</i>	
3H-CC	A	G	R	R	R	R	<i>Dorcadospyris craticula</i>			<i>Dorcadospyris ombros</i> (upper)	
4H-CC	A	G	R	R	R	R	<i>Dorcadospyris pseudopapilio</i>			<i>Eucyrtidium plesiadiaphanes</i>	
6H-CC	A	G	R	R	R	R	<i>Dorcadospyris tiedelli</i>			<i>Eusyringium fistilligerum</i>	
8H-CC	A	G	R	R	R	R	<i>Eusyringium lagena</i>			<i>Lamptonium fab. chaunothorax</i>	
10H-CC	A	G	R	R	R	R	<i>Lamptonium constrictum</i>			<i>Lamponium pennatum</i>	
16H-2, 52-59	A	G	R	R	R	R	<i>Lithocyrtis vespertilio</i>			<i>Lithocyrtis ocellus</i> gr.	
16H-4, 96-103	A	G	VR	R	R	R	<i>Lithocyrtis angusta</i>			<i>Lophocyrtis exitelus</i>	
16H-5, 113-120	A	G	VR	R	R	R	<i>Lophocyrtis hadra</i>			<i>Lophocyrtis pegeatum</i>	
16H-CC	A	G	VR	R	R	R	<i>Lychnocanoma amphitrite</i>			<i>Lychnocanoma auxilla</i>	
17H-1, 125-132	C	M	VR	R	R	R	<i>Lychnocanoma babyonis</i>			<i>Lychnocanoma pileus</i>	
17H-1, 141-148	A	G	VR	R	R	R	<i>Periphæna delta</i>			<i>Periphæna delta</i>	
17H-2, 8-15	A	G	VR	R	R	R	<i>Phormocystis cubensis</i>			<i>Phormocystis striata exquisita</i>	
17H-2, 49-50	A	G	VR	R	R	R	<i>Podocystis ampla</i>			<i>Podocystis ampla</i>	

Notes: Abundance: A = abundant, F = frequent, C = common, R = rare, VR = very rare. Preservation: G = good, M = moderate. Mixing: blank = no mixing of older specimens detected, 1 = 1–3 reworked specimens detected, 2 = 3–10 reworked specimens detected, 3 = >10 reworked specimens detected.

Table T8 (continued).

Core, section, interval (cm)	Abundance	Precession length	Precession amplitude	Sedimentation rate	Spatial pattern	Threading frequency	Threading amplitude	Threading period	Threading ratio	Zonation	Amplitude
320-U1331C-1H-CC	A	R	R	R	R	R	R	R	R	R	R
2H-CC	A	F	R	R	R	R	R	R	R	R	R
3H-CC	A	R	R	R	R	R	R	R	R	R	R
4H-CC	A	R	R	R	R	R	R	R	R	R	R
6H-CC	A	R	R	R	R	R	R	R	R	R	R
8H-CC	A	R	R	R	R	R	R	R	R	R	R
10H-CC	A	R	R	R	R	R	R	R	R	R	R
16H-2, 52–59	A	R	R	R	R	R	R	R	R	R	R
16H-4, 96–103	A	R	R	R	R	R	R	R	R	R	R
16H-5, 113–120	A	R	R	R	R	R	R	R	R	R	R
16H-CC	A	R	R	R	R	R	R	R	R	R	R
17H-1, 125–132	C	R	R	R	R	R	R	R	R	R	R
17H-1, 141–148	A	R	R	R	R	R	R	R	R	R	R
17H-2, 8–15	A	R	R	R	R	R	R	R	R	R	R
17H-2, 49–50	A	R	R	R	R	R	R	R	R	R	R
<hr/>											
Radiolumin zone											
RP20											
RP19											
RP18											
RP15											
RP14											
RP13											
RP12											



Table T9. Radiolarian datums, Site U1331. (See table note.)

Geologic age	Zone	Marker species	Age (Ma)	Core, section, interval (cm)		Depth CSF (m)			
				Top	Bottom	Top	Bottom	Midpoint	±
upper Oligocene	RP21	<i>B. T. annosa</i>	28.33	320-U1331A-2H-2, 104-106	320-U1331A-2H-4, 104-106	7.75	10.75	9.25	1.50
		<i>T. triceros > D. ateuchus</i>	28.60	2H-4, 104-106	2H-CC	10.75	14.81	12.78	2.03
		<i>B. D. ateuchus</i>	29.50	2H-4, 104-106	2H-CC	10.75	14.81	12.78	2.03
		<i>B. D. circulus</i>	29.96	2H-CC	3H-3, 126-128	14.81	18.97	16.89	2.08
		<i>T. L. crux</i>	30.13	2H-CC	3H-3, 126-128	14.81	18.97	16.89	2.08
		<i>B. E. plesiadiaphanes</i>	30.57	2H-CC	3H-3, 126-128	14.81	18.97	16.89	2.08
		<i>B. L. pegetrum</i>	30.68	2H-CC	3H-3, 126-128	14.81	18.97	16.89	2.08
lower Oligocene	RP20	<i>T. L. oberhaensliae</i>	30.74	3H-3, 126-129	3H-5, 121-124	18.97	21.92	20.45	1.48
		<i>B. D. spinosa</i>	30.84	3H-3, 126-129	3H-5, 121-124	18.97	21.92	20.45	1.48
		<i>T. D. pseudopapilio</i>	30.84	3H-3, 126-129	3H-5, 121-124	18.97	21.92	20.45	1.48
		<i>T. C. gravida</i>	30.89	3H-5, 121-124	3H-CC	21.92	24.12	23.02	1.10
		<i>B. T. tuberosa</i>	31.00	3H-CC	4H-2, 104-106	24.12	26.75	25.44	1.31
		<i>B. D. pseudopapilio</i>	31.00	3H-CC	4H-2, 104-106	24.12	26.75	25.44	1.31
		<i>B. C. gravida</i>	31.01	3H-CC	4H-2, 104-106	24.12	26.75	25.44	1.31
		<i>B. L. crux</i>	31.01	3H-CC	4H-2, 104-106	24.12	26.75	25.44	1.31
		<i>T. C. anekathen</i>	33.65	3H-CC	4H-2, 104-106	24.12	26.75	25.44	1.31
		<i>T. L. jacchia</i>	33.69	3H-CC	4H-2, 104-106	24.12	26.75	25.44	1.31
upper Eocene	RP19	<i>T. D. armadillo</i>	33.69	3H-CC	4H-2, 104-106	24.12	26.75	25.44	1.31
		<i>T. L. amphitrite</i>	33.75	3H-CC	4H-2, 104-106	24.12	26.75	25.44	1.31
		<i>L. aristotelis > L. angusta</i>	33.82	3H-CC	4H-2, 104-106	24.12	26.75	25.44	1.31
		<i>B. L. angusta</i>	34.13	4H-2, 104-106	4H-4, 104-106	26.75	29.75	28.25	1.50
		<i>T. C. bandycia</i>	34.62	4H-2, 104-106	4H-4, 104-106	26.75	29.75	28.25	1.50
		<i>B. L. hadra</i>	35.34	4H-CC	5H-2, 104-106	33.95	36.25	35.10	1.15
		<i>T. L. turgidum</i>	35.77	4H-CC	5H-2, 104-106	33.95	36.25	35.10	1.15
		<i>T. L. amphitrite</i>	36.50	5H-4, 104-106	5H-CC	39.25	42.77	41.01	1.76
		<i>B. C. bandycia</i>	36.74	5H-4, 104-106	5H-CC	39.25	42.77	41.01	1.76
		<i>B. L. jacchia</i>	37.07	5H-4, 104-106	5H-CC	39.25	42.77	41.01	1.76
middle Eocene	RP18	<i>B. T. lochites</i>	37.52	6H-2, 105-107	6H-4, 105-107	45.75	48.75	47.25	1.50
		<i>B. C. azyx</i>	37.52	6H-2, 105-107	6H-4, 105-107	45.75	48.75	47.25	1.50
		<i>T Anthocytoma spp.</i>	37.92	6H-4, 105-107	6H-CC	48.75	52.46	50.61	1.85
		<i>B. T. bromia</i>	38.07	6H-4, 105-107	6H-CC	48.75	52.46	50.61	1.85
		<i>B. T. tetricantha</i>	38.12	6H-4, 105-107	6H-CC	48.75	52.46	50.61	1.85
		<i>T. D. anastasis</i>	38.45	6H-CC	7H-2, 95-97	52.46	55.16	53.81	1.35
		<i>B. C. turris</i>	38.67	6H-CC	7H-2, 95-97	52.46	55.16	53.81	1.35
		<i>B. L. aristotelis gr.</i>	39.73	7H-2, 95-97	7H-4, 95-97	55.16	58.16	56.66	1.50
		<i>B. D. anastasis</i>	39.98	7H-4, 95-97	7H-CC	58.16	62.49	60.33	2.17
		<i>B. P. goetheana</i>	40.16	7H-4, 95-97	7H-CC	58.16	62.49	60.33	2.17
middle Eocene	RP17	<i>T. L. biaurita</i>	40.36	8H-4, 104-106	8H-CC	67.75	72	69.88	2.13
		<i>P. mitra > P. chalara</i>	40.70	9H-4, 105-107	9H-CC	77.26	81.47	79.37	2.10
		<i>T. P. trachodes</i>	41.23	10H-2, 95-97	10H-4, 95-97	83.66	86.66	85.16	1.50
		<i>B. P. chalara</i>	41.54	10H-4, 95-97	10H-CC	86.66	90.29	88.48	1.82
		<i>B. C. ornatum</i>	42.10	10H-CC	11H-3, 106-108	90.29	93.95	92.12	1.83
		<i>B. S. triconiscus</i>	42.40	11H-3, 106-108	11H-5, 106-108	93.95	96.95	95.45	1.50
		<i>T. E. lagena</i>	42.69	11H-5, 106-108	11H-CC	96.95	99.32	98.14	1.19
		<i>B. T. perpumila</i>	42.97	11H-CC	12H-2, 106-108	99.32	102.77	101.05	1.73
		<i>T. P. helenae</i>	43.05	12H-2, 106-108	12H-4, 106-108	102.77	105.77	104.27	1.50
		<i>B. P. trachodes</i>	43.22	12H-4, 106-108	12H-CC	105.77	109.99	107.88	2.11
middle Eocene	RP14	<i>B. Z. cimelium</i>	43.35	12H-4, 106-108	12H-CC	105.77	109.99	107.88	2.11
		<i>P. sinuosa > P. mitra</i>	43.84	13H-2, 104-106	13H-4, 104-106	112.25	115.25	113.75	1.50
		<i>B. P. helenae</i>	44.15	13H-4, 104-106	13H-CC	115.25	119.38	117.32	2.06
		<i>T. P. phyxis</i>	44.44	13H-CC	14H-2, 104-106	119.38	121.72	120.55	1.17
		<i>P. phyxis > P. ampla</i>	44.77	14H-2, 104-106	14H-4, 104-106	121.72	124.72	123.22	1.50
		<i>T. T. venezuelensis</i>	45.16	14H-4, 104-106	14H-CC	124.72	128.58	126.65	1.93
		<i>T. T. anaclasta</i>	45.62	14H-CC	15H-2, 94-96	128.58	131.15	129.87	1.28
		<i>T. T. cryptocephala</i>	46.01	15H-2, 94-96	15H-4, 94-96	131.15	134.15	132.65	1.50
		<i>B. T. orthotenes</i>	46.16	15H-CC	16X-1, 50-52	138.47	139.71	139.09	0.62
		<i>T. T. hirsuta</i>	46.19	15H-CC	16X-1, 50-52	138.47	138.71	138.59	0.12
middle Eocene	RP12	<i>B. P. phyxis</i>	46.44	16X-1, 50-52	16X-CC	138.71	139.27	138.99	0.28
		<i>B. R. ornatum</i>	47.42	16X-CC	17X-2, 104-106	139.27	150.15	144.71	5.44
		<i>B. T. triacantha</i>	47.42	16X-CC	17X-2, 104-106	139.27	150.15	144.71	5.44
		<i>B. E. lagena</i>	47.42	16X-CC	17X-2, 104-106	139.27	150.15	144.71	5.44
		<i>T. P. striata striata</i>	48.14	17X-4, 104-106	19X-CC	153.15	162.1	157.63	4.47
middle Eocene	RP11	<i>B. D. mongolfieri</i>	48.50	19X-2, 25-27	19X-CC	161.75	162.1	161.93	0.17
		<i>T. nigriniae > T. cryptocephala</i>	49.00	19X-CC	20X-CC	162.1	167.02	164.56	2.46

Note: B = bottom, T = top.

Table T10. Planktonic foraminifer datums, Site U1331. (See table note.)

Core, section, interval (cm)	Top	Bottom	Marker species	Age (Ma)	Depth CSF (m)			
					Top	Bottom	Midpoint	±
320-U1331A-2H-2, 89–91	320-U1331A-2H-4, 49–51	T <i>Paragloborotalia opima</i>		26.9	7.59	10.19	8.89	1.29
2H-4, 49–51	2H-CC, 23–28	B <i>Paragloborotalia opima</i>		30.8	10.19	15.02	12.61	2.42
9H-CC, 16–21	10H-2, 30–32	T <i>Acarinina bullbrookii</i>		40.8	81.61	83.00	82.31	0.70
10H-2, 30–32	10H-CC, 21–26	B <i>Turborotalia pomeroli</i>		42.4	83.00	90.48	86.74	3.74
20X-CC, 2–6	22X-CC, 38–43	T <i>Morozovella subbotinae</i>		50.8	167.02	187.15	177.09	10.08
22X-CC, 38–43	—	B <i>Morozovella aragonensis</i>		<52.3	187.15	—	187.15	—

Note: T = top, B = bottom.

Table T11. Distribution of planktonic foraminifers, Site U1331. (See table notes.) (Continued on next two pages.)

Table T11 (continued). (Continued on next page.)



Table T11 (continued).

Notes: Preservation: M = moderate, P = poor, B = barren. Abundance: D = dominant, A = abundant, F = few, P = present, R = rare.

Table T12. Distribution of benthic foraminifers, Site U1331. (See table notes.) (Continued on next page.)

Core, section interval (cm)	Depth CSF (m)	Preservation	Bathymetry	<i>Abyssamina poagi</i>	<i>Abyssamina quadrata</i>	<i>Alabamina</i> sp.	<i>Anomalinoides</i> sp.	<i>Astronion</i> sp.	<i>Bigenerina</i> sp.	<i>Bolivina</i> sp.	<i>Buliminella midwayensis</i>	<i>Buliminella parvula</i>	<i>Buliminella</i> sp.	<i>Cibicidoides eocanus</i>	<i>Cibicidoides grimsdalei</i>	<i>Cibicidoides havanensis</i>	<i>Cibicidoides mundulus</i>	<i>Cibicidoides praemundulus</i>	<i>Cibicidoides</i> sp. A	<i>Cibicidoides</i> sp. B	<i>Cibicidoides</i> sp. C	<i>Cibicidoides</i> sp. indet.	<i>Dentalina</i> spp.	<i>Gaudryina pyramidata</i>	<i>Globocassidulina subglobosa</i>	<i>Gloospira goldensis</i>	<i>Gloospira irregularis</i>	<i>Gyroidinoides soldanii</i>	<i>Gyroidinoides</i> sp. A	<i>Gyroidinoides</i> sp. B	<i>Gyroidinoides</i> sp. indet.	<i>Haplophragmoides walteri</i>	<i>Karriella chapapotensis</i>
320-U1331A-																																	
1H-CC, 15–20	5.17	—																															
2H-CC, 23–28	15.05	M	LB-A																														
3H-CC, 24–29	24.37	P	LB-A																														
4H-CC, 21–26	34.17	—																															
5H-CC, 22–27	43.00	P																															
6H-CC, 16–21	52.63	—																															
7H-CC, 13–18	62.63	—																															
8H-CC, 19–24	72.20	P																															
9H-CC, 16–21	81.64	M																															
10H7, 44–46	90.15	M	LB-A		R	R	R	R																									
10H7, 47–49	90.18	M	LB-A	R	R	R	R	R																									
10H-CC, 21–26	90.51	M	LB-A	—																													
11H-CC, 17–22	99.50	—																															
12H-CC, 18–23	110.18	P																															
13H-CC, 22–27	119.61	P																															
14H-CC, 17–22	128.76	—																															
15H-CC, 0–5	138.48	P																															
16X-CC, 32–37	139.60	—																															
19X-CC, 28–33	162.39	—																															
22X-CC, 38–43	187.18	P	LB-A		R																												
320-U1331B-																																	
1H-CC, 30–32	10.08	M	LB-A																														
2H-CC, 37–39	20.12	M	LB-A																														
3H-CC, 34–36	29.53	P																															
4H-CC, 21–23	39.16	—																															
5H-CC, 28–30	48.09	—																															
6H-CC, 32–33	58.24	—																															
7H-CC, 17–19	67.20	—																															
8H-CC, 26–28	77.18	M	LB-A	R																													
9H-CC, 0–2	86.64	M	LB-A																														
10H-CC, 23–25	96.13	P																															
11H-CC, 28–30	102.55	—																															
12H-CC, 7–9	114.99	—																															
13H-CC, 22–24	124.40	—																															
14H-CC, 21–23	134.02	—																															
15H-CC, 16–18	143.61	P																															
16H-CC, 30–32	152.49	—																															
17H-CC, 38–40	156.87	P																															
320-U1331C-																																	
1H-CC, 24–26	9.45	—																															
2H-CC, 21–23	19.51	M	LB-A																														
3H-CC, 14–16	28.74	—																															
4H-CC, 14–16	38.48	P																															
6H-CC, 23–25	68.53	—																															
8H-CC, 25–27	101.78	P																															
10H-CC, 20–22	110.92	M	LB-A	R																													
12H-CC, 20–22	139.04	—																															
13H-CC, 24–26	148.58	—																															
14H-CC, 20–22	156.86	P																															
16H-CC, 8–10	185.35	—																															
17H-CC, 8–13	189.51	P	LB-A	R																													

Notes: — = presence of specimens found during other observations (other size fractions or planktonic foraminifer analysis). Preservation: M = moderate, P = poor. LB = lower Bathyal zone, A = Abyssal zone. Abundance: D = dominant, A = abundant, F = frequent, R = rare.



Table T12 (continued).

Core, section, interval (cm)	Depth CSF (m)	<i>Lenticulina</i> spp.	<i>Nodosaria</i> spp.	<i>Nonion affine</i>	<i>Nonion havanensis</i>	<i>Nuttallides truempyi</i>	<i>Nuttallides umbonifer</i>	<i>Ondorsalis umbonatus</i>	<i>Paratrochamminoides</i> sp.	<i>Pleurostomella</i> sp.	<i>Pullenia bulloides</i>	<i>Pullenia osloensis</i>	<i>Pullenia quinqueloba</i>	<i>Pullenia salisburyi</i>	<i>Pullenia subcarinata</i>	<i>Pullenia</i> sp. A	<i>Pyrulina</i> spp.	<i>Quadrimorphina profunda</i>	<i>Recurvoides</i> spp.	<i>Reophax</i> sp.	<i>Reticulophragmium amplectens</i>	<i>Siphonodosaria antillae</i>	<i>Siphonodosaria</i> sp. indet.	<i>Sphaeroidina bulloides</i>	<i>Spiralectammina spectabilis</i>	<i>Spirosgmoinella compressa</i>	Tube-shaped agglutinated foraminifer
320-U1331A-																											
1H-CC, 15–20	5.17																										F
2H-CC, 23–28	15.05	R	A	A	P		R	R				R														P	
3H-CC, 24–29	24.37																										P
4H-CC, 21–26	34.17																										P
5H-CC, 22–27	43.00																										P
6H-CC, 16–21	52.63																										P
7H-CC, 13–18	62.63																										P
8H-CC, 19–24	72.20																										P
9H-CC, 16–21	81.64	R	R	R	A	—																					
10H7, 44–46	90.15																										
10H7, 47–49	90.18																										
10H-CC, 21–26	90.51																										
11H-CC, 17–22	99.50																										
12H-CC, 18–23	110.18																										
13H-CC, 22–27	119.61																										
14H-CC, 17–22	128.76																										
15H-CC, 0–5	138.48																										
16X-CC, 32–37	139.60																										
19X-CC, 28–33	162.39																										
22X-CC, 38–43	187.18																										
320-U1331B-																											
1H-CC, 30–32	10.08	R	R	A																							
2H-CC, 37–39	20.12																										
3H-CC, 34–36	29.53																										
4H-CC, 21–23	39.16																										
5H-CC, 28–30	48.09																										
6H-CC, 32–33	58.24																										
7H-CC, 17–19	67.20																										
8H-CC, 26–28	77.18																										
9H-CC, 0–2	86.64																										
10H-CC, 23–25	96.13																										
11H-CC, 28–30	102.55																										
12H-CC, 7–9	114.99																										
13H-CC, 22–24	124.40																										
14H-CC, 21–23	134.02																										
15H-CC, 16–18	143.61																										
16H-CC, 30–32	152.49																										
17H-CC, 38–40	156.87																										
320-U1331C-																											
1H-CC, 24–26	9.45																										
2H-CC, 21–23	19.51																										
3H-CC, 14–16	28.74																										
4H-CC, 14–16	38.48																										
6H-CC, 23–25	68.53																										
8H-CC, 25–27	101.78																										
10H-CC, 20–22	110.92	R	R	A																							
12H-CC, 20–22	139.04																										
13H-CC, 24–26	148.58																										
14H-CC, 20–22	156.86																										
16H-CC, 8–10	185.35																										
17H-CC, 8–13	189.51	R	D	F																							

Table T13. Coring-disturbed intervals and gaps, Site U1331. (See table notes.)

Core, section interval (cm)	Type of disturbance	Core, section interval (cm)	Type of disturbance
320-U1331A-		2H-1, 0-120	Slurry
1H-1, 0-5	Top of core	2H-1, 127-150	Void
1H-2, 144-150	Interstitial water	3H-1, 0-121	Slurry
2H-1, 0-5	Top of core	5H-1, 0-63	Slurry
2H-2, 145-150	Interstitial water	5H-1, 63-64	Void
2H-5, 145-150	Interstitial water	6H-1, 0-40	Slurry
3H-1, 0-20	Top of core	7H-1, 0-120	Soupy
3H-2, 0-8	Expansion/voids	8H-1, 0-54	Slurry
3H-2, 145-150	Interstitial water	8H-1, 54-72	Void
3H-5, 145-150	Interstitial water	8H-1, 72-81	Expansion
4H-1, 0-110	Top of core	9H-1, 0-5	Top of core
4H-2, 145-150	Interstitial water	10H-1, 0-5	Top of core
4H-5, 145-150	Interstitial water	10H-5, 118-127	Conglomerate
5H-3, 145-150	Interstitial water	11H-1, 0-20	Top of core
6H-3, 145-150	Interstitial water	12H-1, 0-5	Top of core, chert
7H-1, 137-140	Slurry/void	12H-1, 18-19	Chert
7H-3, 145-150	Interstitial water	13H-1, 0-24	Top of core
7H-4, 140-150	Gamage sample	13H-1, 117-117	Chert
8H-3, 145-150	Interstitial water	15H-1, 0-20	Top of core
9H-1, 0-110	Top of core	15H-4, 91-92	Void
9H-1, 110-130	Expansion	15H-4, 110-150	Flow-in
9H-3, 145-150	Interstitial water	15H-5, 0-150	Flow-in
10H-1, 0-104	Top of core	15H-6, 0-150	Flow-in
10H-3, 145-150	Interstitial water	15H-7, 0-5	Flow-in
10H-4, 140-150	Gamage sample	16H-1, 0-40	Chert
11H-1, 0-60	Top of core	16H-1, 0-62	Slurry
11H-3, 145-150	Interstitial water	17H-1, 0-65	Top of core
12H-1, 0-16	Top of core	320-U1331C-	
12H-3, 145-150	Interstitial water	1H-1, 0-12	Coring disturbance
13H-3, 145-150	Interstitial water	2H-1, 0-30	Coring disturbance
14H-3, 52-57	Chert	3H-1, 0-106	Coring disturbance
14H-3, 145-150	Interstitial water	4H-1, 0-10	Coring disturbance
14H-8, 17-22	Paleontology sample	8H-1, 0-138	Soupy
15H-1, 0-5	Top of core	8H-2, 79-150	Mild coring disturbance
15H-1, 29-67	Void	8H-4, 25-26	Expansion crack
15H-1, 67-75	Slurry	10H-1, 0-70	Coring disturbance
15H-3, 145-150	Interstitial water	12H-1, 0-4	Chert
15H-4, 140-150	Gamage sample	13H-1, 0-150	Chert/coring disturbance
17X-1, 0-23	Top of core, chert	14H-1, 0-30	Chert/disturbed
17X-3, 135-150	Interstitial water and Gamage sample	16H-1, 0-150	Chert/disturbed
18X-1, 0-32	Top of core, chert	16H-2, 0-30	Chert/disturbed
19X-1, 0-4	Top of core, chert	16H-4, 110-150	Chert nodule and disturbed
19X-1, 0-28	Chert	17H-2, 95-150	Mild coring disturbance
20X-1, 0-5	Top of core, chert	17H-3, 95-150	Coring disturbance
22X-1, 0-6	Top of core, chert	17H-4, 0-90	Coring disturbance
320-U1331B-			
1H-1, 0-135	Disturbed		

Notes: When interval listed is 0-150 cm, entire section is included even if true section length is <150 cm. Top of core = myriad forms of voids, disturbance, and debris from uphole that affect top portion of most cores. For that reason, probably the top 20 cm or so of all cores should be avoided. Gamage sample = whole-round sample taken for K. Gamage.



Table T14. Paleomagnetic data from archive-half sections, Hole U1331A, at 0 mT AF demagnetization. ([See table notes](#).)

Core, section	Offset (m)	Depth CSF (m)	Declination (°)	Inclination (°)	Intensity (A/m)	Time (s)
320-U1331A-						
1H-1	0.10	0.10	19.1	58.0	4.068E-02	3320133135.92150
1H-1	0.15	0.15	1.3	64.1	4.362E-02	3320133141.24962
1H-1	0.20	0.20	1.1	68.5	4.369E-02	3320133146.56212
1H-1	0.25	0.25	7.1	69.7	4.630E-02	3320133151.89025
1H-1	0.30	0.30	7.2	69.9	4.891E-02	3320133157.21837
1H-1	0.35	0.35	2.7	75.4	4.670E-02	3320133162.54650
1H-1	0.40	0.40	1.9	72.0	4.851E-02	3320133167.85900
1H-1	0.45	0.45	1.3	66.7	5.396E-02	3320133173.18712
1H-1	0.50	0.50	0.3	69.4	5.594E-02	3320133178.51525
1H-1	0.55	0.55	0.6	73.5	5.637E-02	3320133183.84337
1H-1	0.60	0.60	357.1	73.2	5.732E-02	3320133189.17150
1H-1	0.65	0.65	20.1	64.5	6.132E-02	3320133194.48400
1H-1	0.70	0.70	354.3	60.5	5.859E-02	3320133199.81212
1H-1	0.75	0.75	294.6	71.3	6.205E-02	3320133205.14025
1H-1	0.80	0.80	317.5	81.1	6.148E-02	3320133210.46837
1H-1	0.85	0.85	338.2	79.0	6.529E-02	3320133215.79650
1H-1	0.90	0.90	342.0	79.3	6.665E-02	3320133221.12462
1H-1	0.95	0.95	336.6	78.5	6.795E-02	3320133226.43712
1H-1	1.00	1.00	329.6	79.2	6.770E-02	3320133231.76525
1H-1	1.05	1.05	331.9	79.5	6.603E-02	3320133237.09337
1H-1	1.10	1.10	330.8	79.5	6.434E-02	3320133242.42150
1H-1	1.15	1.15	329.4	79.3	6.386E-02	3320133247.73400
1H-1	1.20	1.20	332.4	80.5	6.273E-02	3320133253.06212
1H-1	1.25	1.25	335.0	80.4	6.222E-02	3320133258.39025
1H-1	1.30	1.30	337.9	80.4	6.131E-02	3320133263.71837
1H-1	1.35	1.35	338.2	79.0	6.018E-02	3320133269.04650
1H-1	1.40	1.40	335.1	77.3	5.827E-02	3320133274.37462
1H-3	0.10	3.10	116.0	83.9	4.170E-02	3320141022.76525
1H-3	0.15	3.15	24.5	88.3	4.511E-02	3320141028.09337
1H-3	0.20	3.20	323.0	83.9	4.647E-02	3320141033.42150
1H-3	0.25	3.25	320.0	81.0	4.696E-02	3320141038.74962
1H-3	0.30	3.30	319.7	79.4	4.677E-02	3320141044.07775
1H-3	0.35	3.35	322.3	78.3	4.637E-02	3320141049.40587
1H-3	0.40	3.40	322.8	78.9	4.455E-02	3320141054.71837
1H-3	0.45	3.45	318.6	79.7	4.244E-02	3320141060.04650
1H-3	0.50	3.50	323.9	80.9	4.276E-02	3320141065.37462
1H-3	0.55	3.55	324.4	81.0	4.363E-02	3320141070.70275
1H-3	0.60	3.60	317.5	79.3	4.341E-02	3320141076.03087
1H-3	0.65	3.65	316.3	79.4	4.304E-02	3320141081.34337
1H-3	0.70	3.70	318.5	79.7	4.266E-02	3320141086.67150
1H-3	0.75	3.75	317.9	79.3	4.246E-02	3320141091.99962
1H-3	0.80	3.80	315.8	79.4	4.247E-02	3320141097.31212
1H-3	0.85	3.85	314.5	81.2	4.331E-02	3320141102.64025
1H-3	0.90	3.90	312.9	82.5	4.578E-02	3320141107.96837
1H-3	0.95	3.95	313.0	82.5	4.775E-02	3320141113.29650
1H-3	1.00	4.00	315.4	79.3	4.904E-02	3320141118.62462
1H-3	1.05	4.05	314.0	78.0	4.986E-02	3320141123.95275
1H-3	1.10	4.10	313.3	78.0	4.987E-02	3320141129.26525
1H-3	1.15	4.15	309.3	79.6	5.044E-02	3320141134.59337
1H-3	1.20	4.20	305.0	80.3	5.056E-02	3320141139.92150
1H-3	1.25	4.25	305.3	80.0	5.121E-02	3320141145.24962
1H-3	1.30	4.30	305.6	79.1	5.249E-02	3320141150.57775
1H-3	1.35	4.35	308.9	78.7	5.270E-02	3320141155.90587
1H-3	1.40	4.40	311.2	77.9	5.245E-02	3320141161.21837
1H-4	0.10	4.60	314.0	77.8	5.473E-02	3320144019.65587
1H-4	0.15	4.65	313.2	78.1	5.450E-02	3320144024.98400
1H-4	0.20	4.70	314.0	78.2	5.378E-02	3320144030.29650
1H-4	0.25	4.75	313.8	78.1	5.349E-02	3320144035.62462
1H-4	0.30	4.80	311.9	77.6	5.219E-02	3320144040.98400
1H-4	0.35	4.85	312.4	76.6	4.984E-02	3320144046.31212
1H-4	0.40	4.90	327.9	77.5	4.952E-02	3320144051.64025
2H-1	0.10	5.30	141.7	74.2	3.845E-02	3320146085.28087

Notes: Time = since 1 January 1904. Only a portion of this table appears here. The complete table is available in [ASCII](#).



Table T15. Paleomagnetic data from archive-half sections, Hole U1331A, at 5 mT AF demagnetization. ([See table notes.](#)) ([Continued on next three pages.](#))

Core, section	Offset (m)	Depth CSF (m)	Declination (°)	Inclination (°)	Intensity (A/m)	Time (s)
320-U1331A-						
1H-1	0.10	0.10	18.3	15.5	2.036E-02	3320133908.17150
1H-1	0.15	0.15	1.0	23.6	1.976E-02	3320133913.48400
1H-1	0.20	0.20	354.7	26.0	1.507E-02	3320133918.81212
1H-1	0.25	0.25	357.9	26.2	1.411E-02	3320133924.14025
1H-1	0.30	0.30	358.6	27.8	1.453E-02	3320133929.46837
1H-1	0.35	0.35	355.9	32.4	1.175E-02	3320133934.79650
1H-1	0.40	0.40	349.0	28.3	1.335E-02	3320133940.12462
1H-1	0.45	0.45	353.0	24.8	1.681E-02	3320133945.45275
1H-1	0.50	0.50	352.8	28.2	1.681E-02	3320133950.76525
1H-1	0.55	0.55	349.9	39.5	1.429E-02	3320133956.09337
1H-1	0.60	0.60	343.0	39.2	1.469E-02	3320133961.42150
1H-1	0.65	0.65	13.5	25.1	2.020E-02	3320133966.74962
1H-1	0.70	0.70	358.4	3.4	2.097E-02	3320133972.06212
1H-1	0.75	0.75	302.2	16.6	1.779E-02	3320133977.39025
1H-1	0.80	0.80	308.2	43.8	1.230E-02	3320133982.71837
1H-1	0.85	0.85	308.1	50.4	1.394E-02	3320133988.04650
1H-1	0.90	0.90	313.3	52.2	1.538E-02	3320133993.37462
1H-1	0.95	0.95	315.9	51.0	1.670E-02	3320133998.68712
1H-1	1.00	1.00	313.2	50.3	1.704E-02	3320134004.01525
1H-1	1.05	1.05	312.2	50.7	1.607E-02	3320134009.34337
1H-1	1.10	1.10	312.1	49.6	1.523E-02	3320134014.67150
1H-1	1.15	1.15	311.9	48.2	1.482E-02	3320134019.98400
1H-1	1.20	1.20	310.5	52.2	1.357E-02	3320134025.31212
1H-1	1.25	1.25	314.5	51.3	1.346E-02	3320134030.64025
1H-1	1.30	1.30	314.4	50.6	1.321E-02	3320134035.96837
1H-1	1.35	1.35	315.3	49.7	1.332E-02	3320134041.29650
1H-1	1.40	1.40	317.6	44.5	1.415E-02	3320134046.60900
1H-3	0.10	3.10	130.3	36.8	7.660E-03	3320141552.12462
1H-3	0.15	3.15	134.9	59.0	6.388E-03	3320141557.45275
1H-3	0.20	3.20	289.2	77.4	5.795E-03	3320141562.76525
1H-3	0.25	3.25	316.8	52.8	7.183E-03	3320141568.09337
1H-3	0.30	3.30	304.1	45.4	8.055E-03	3320141573.42150
1H-3	0.35	3.35	314.2	40.1	8.693E-03	3320141578.74962
1H-3	0.40	3.40	315.0	41.3	8.299E-03	3320141584.07775
1H-3	0.45	3.45	309.0	44.7	6.894E-03	3320141589.39025
1H-3	0.50	3.50	313.5	49.8	6.448E-03	3320141594.71837
1H-3	0.55	3.55	311.3	53.4	6.411E-03	3320141600.04650
1H-3	0.60	3.60	312.8	48.0	7.064E-03	3320141605.37462
1H-3	0.65	3.65	310.0	44.4	7.364E-03	3320141610.68712
1H-3	0.70	3.70	310.2	44.0	7.110E-03	3320141616.01525
1H-3	0.75	3.75	312.0	42.1	7.395E-03	3320141621.34337
1H-3	0.80	3.80	308.3	41.0	7.559E-03	3320141626.67150
1H-3	0.85	3.85	311.8	44.2	7.093E-03	3320141631.99962
1H-3	0.90	3.90	306.1	55.0	6.573E-03	3320141637.32775
1H-3	0.95	3.95	303.3	58.3	7.049E-03	3320141642.65587
1H-3	1.00	4.00	309.2	46.0	8.411E-03	3320141647.96837
1H-3	1.05	4.05	307.5	36.1	9.865E-03	3320141653.29650
1H-3	1.10	4.10	309.0	33.0	9.420E-03	3320141658.62462
1H-3	1.15	4.15	307.6	36.6	8.983E-03	3320141663.93712
1H-3	1.20	4.20	306.2	40.1	8.834E-03	3320141669.26525
1H-3	1.25	4.25	304.9	40.1	8.982E-03	3320141674.59337
1H-3	1.30	4.30	306.1	39.7	9.364E-03	3320141679.92150
1H-3	1.35	4.35	305.2	38.3	9.657E-03	3320141685.24962
1H-3	1.40	4.40	305.1	37.8	9.825E-03	3320141690.57775
1H-4	0.10	4.60	315.1	32.2	1.126E-02	3320144309.20275
1H-4	0.15	4.65	316.9	36.2	1.054E-02	3320144314.53087
1H-4	0.20	4.70	315.1	36.9	1.025E-02	3320144319.85900
1H-4	0.25	4.75	315.0	37.0	1.011E-02	3320144325.18712
1H-4	0.30	4.80	313.2	35.6	1.031E-02	3320144330.49962
1H-4	0.35	4.85	310.5	32.1	1.023E-02	3320144335.82775
1H-4	0.40	4.90	320.1	40.2	8.264E-03	3320144341.15587
2H-1	0.10	5.30	159.0	30.3	9.123E-03	3320147487.98400
2H-1	0.15	5.35	176.2	40.0	1.012E-02	3320147493.31212
2H-1	0.20	5.40	212.7	80.0	8.919E-03	3320147498.64025
2H-1	0.25	5.45	79.9	55.0	1.243E-02	3320147503.96837
2H-1	0.30	5.50	84.7	40.9	2.068E-02	3320147509.28087

Table T15 (continued). (Continued on next page.)

Core, section	Offset (m)	Depth CSF (m)	Declination (°)	Inclination (°)	Intensity (A/m)	Time (s)
2H-1	0.35	5.55	63.8	75.5	1.628E-02	3320147514.60900
2H-1	0.40	5.60	230.3	63.8	1.990E-02	3320147519.93712
2H-1	0.45	5.65	229.8	77.2	1.018E-02	3320147525.26525
2H-1	0.50	5.70	93.3	58.5	8.706E-03	3320147530.57775
2H-1	0.55	5.75	142.4	26.5	1.286E-02	3320147535.90587
2H-1	0.60	5.80	132.8	6.9	1.790E-02	3320147541.23400
2H-1	0.65	5.85	302.4	79.0	4.682E-03	3320147546.56212
2H-1	0.70	5.90	276.5	45.6	7.622E-03	3320147551.89025
2H-1	0.75	5.95	273.8	63.5	5.901E-03	3320147557.21837
2H-1	0.80	6.00	291.6	46.3	4.833E-03	3320147562.53087
2H-1	0.85	6.05	305.2	42.1	3.079E-03	3320147567.85900
2H-1	0.90	6.10	10.8	45.9	4.405E-03	3320147573.18712
2H-1	0.95	6.15	277.8	22.5	5.689E-03	3320147578.51525
2H-1	1.00	6.20	244.3	-21.4	4.013E-02	3320147583.84337
2H-1	1.05	6.25	76.5	-48.2	2.506E-02	3320147589.15587
2H-1	1.10	6.30	252.4	-53.4	1.567E-03	3320147594.48400
2H-1	1.15	6.35	310.0	1.1	7.403E-03	3320147599.81212
2H-1	1.20	6.40	283.9	50.0	3.079E-03	3320147605.14025
2H-1	1.25	6.45	271.2	41.0	5.738E-03	3320147610.46837
2H-1	1.30	6.50	209.8	61.5	5.097E-03	3320147615.78087
2H-1	1.35	6.55	207.5	52.4	2.675E-03	3320147621.10900
2H-1	1.40	6.60	253.0	49.7	2.103E-03	3320147626.43712
2H-2	0.10	6.80	266.3	50.0	6.036E-03	3320155948.28087
2H-2	0.15	6.85	274.7	31.9	6.720E-03	3320155953.60900
2H-2	0.20	6.90	283.0	57.3	5.787E-03	3320155958.92150
2H-2	0.25	6.95	267.7	46.2	5.368E-03	3320155964.24962
2H-2	0.30	7.00	257.4	60.4	3.014E-03	3320155969.57775
2H-2	0.35	7.05	279.6	51.8	3.622E-03	3320155974.90587
2H-2	0.40	7.10	289.9	57.5	3.785E-03	3320155980.23400
2H-2	0.45	7.15	291.1	44.8	4.782E-03	3320155985.54650
2H-2	0.50	7.20	295.7	52.0	4.224E-03	3320155990.87462
2H-2	0.55	7.25	18.7	71.6	3.617E-03	3320155996.20275
2H-2	0.60	7.30	341.7	60.8	6.891E-03	3320156001.53087
2H-2	0.65	7.35	256.1	48.3	7.433E-03	3320156006.84337
2H-2	0.70	7.40	279.1	45.6	3.336E-03	3320156012.17150
2H-2	0.75	7.45	55.6	73.7	1.946E-03	3320156017.49962
2H-2	0.80	7.50	112.4	67.1	7.918E-04	3320156022.81212
2H-2	0.85	7.55	295.5	24.1	1.251E-03	3320156028.14025
2H-2	0.90	7.60	164.1	29.7	1.294E-03	3320156033.46837
2H-2	0.95	7.65	241.2	22.8	1.610E-03	3320156038.78087
2H-2	1.00	7.70	321.9	16.0	1.635E-03	3320156044.10900
2H-2	1.05	7.75	313.7	7.8	1.348E-03	3320156049.43712
2H-2	1.10	7.80	259.3	8.6	1.020E-03	3320156054.76525
2H-2	1.15	7.85	273.6	2.9	1.362E-03	3320156060.09337
2H-2	1.20	7.90	274.2	6.8	1.150E-03	3320156065.40587
2H-2	1.25	7.95	270.9	-3.9	1.234E-03	3320156070.73400
2H-2	1.30	8.00	272.6	-17.9	1.340E-03	3320156076.06212
2H-2	1.35	8.05	272.5	-22.1	9.674E-04	3320156081.39025
2H-2	1.40	8.10	270.9	-12.9	1.249E-03	3320156086.71837
2H-3	0.10	8.30	86.4	10.8	3.986E-03	3320160236.23400
2H-3	0.15	8.35	72.0	19.7	2.711E-03	3320160241.56212
2H-3	0.20	8.40	135.3	6.2	1.780E-03	3320160246.89025
2H-3	0.25	8.45	230.5	6.8	2.934E-03	3320160252.21837
2H-3	0.30	8.50	256.8	40.9	1.914E-03	3320160257.54650
2H-3	0.35	8.55	98.5	77.6	1.581E-03	3320160262.87462
2H-3	0.40	8.60	357.5	74.6	1.567E-03	3320160268.18712
2H-3	0.45	8.65	329.1	75.2	1.825E-03	3320160273.51525
2H-3	0.50	8.70	151.9	85.3	1.619E-03	3320160278.84337
2H-3	0.55	8.75	74.4	88.0	1.489E-03	3320160284.15587
2H-3	0.60	8.80	85.0	74.7	1.327E-03	3320160289.48400
2H-3	0.65	8.85	122.0	65.4	1.018E-03	3320160294.81212
2H-3	0.70	8.90	134.8	64.4	1.094E-03	3320160300.14025
2H-3	0.75	8.95	95.8	44.8	1.541E-03	3320160305.46837
2H-3	0.80	9.00	268.6	36.5	2.593E-03	3320160310.78087
2H-3	0.85	9.05	279.8	13.7	7.728E-03	3320160316.10900
2H-3	0.90	9.10	285.9	17.1	7.005E-03	3320160321.43712
2H-3	0.95	9.15	279.1	25.9	4.378E-03	3320160326.76525
2H-3	1.00	9.20	290.0	30.7	2.633E-03	3320160332.09337
2H-3	1.05	9.25	286.6	31.9	2.794E-03	3320160337.42150

Table T15 (continued). (Continued on next page.)

Core, section	Offset (m)	Depth CSF (m)	Declination (°)	Inclination (°)	Intensity (A/m)	Time (s)
2H-3	1.10	9.30	280.2	26.7	3.187E-03	3320160342.73400
2H-3	1.15	9.35	284.4	44.5	2.057E-03	3320160348.06212
2H-3	1.20	9.40	275.6	53.4	1.896E-03	3320160353.39025
2H-3	1.25	9.45	273.9	48.5	1.960E-03	3320160358.71837
2H-3	1.30	9.50	282.6	22.3	3.197E-03	3320160364.04650
2H-3	1.35	9.55	288.5	22.0	4.053E-03	3320160369.35900
2H-3	1.40	9.60	289.0	36.6	3.955E-03	3320160374.68712
2H-4	0.10	9.80	267.5	-9.9	2.332E-03	3320164451.85900
2H-4	0.15	9.85	309.1	-5.6	2.150E-03	3320164457.17150
2H-4	0.20	9.90	309.5	17.0	1.300E-03	3320164462.49962
2H-4	0.25	9.95	290.8	37.3	7.724E-04	3320164467.82775
2H-4	0.30	10.00	281.5	44.8	9.640E-04	3320164473.15587
2H-4	0.35	10.05	275.5	62.5	1.069E-03	3320164478.48400
2H-4	0.40	10.10	257.8	55.6	1.088E-03	3320164483.79650
2H-4	0.45	10.15	286.2	40.5	1.283E-03	3320164489.12462
2H-4	0.50	10.20	284.9	53.4	1.197E-03	3320164494.45275
2H-4	0.55	10.25	299.0	43.0	1.822E-03	3320164499.78087
2H-4	0.60	10.30	286.1	42.0	2.765E-03	3320164505.10900
2H-4	0.65	10.35	261.1	47.8	2.098E-03	3320164510.42150
2H-4	0.70	10.40	283.9	62.2	1.156E-03	3320164515.74962
2H-4	0.75	10.45	246.7	19.8	1.313E-03	3320164521.07775
2H-4	0.80	10.50	256.7	24.4	2.240E-03	3320164526.40587
2H-4	0.85	10.55	160.7	38.4	1.620E-03	3320164531.73400
2H-4	0.90	10.60	181.2	49.6	1.364E-03	3320164537.06212
2H-4	0.95	10.65	291.9	54.7	2.242E-03	3320164542.37462
2H-4	1.00	10.70	270.8	44.8	2.913E-03	3320164547.70275
2H-4	1.05	10.75	284.9	40.0	2.925E-03	3320164553.03087
2H-4	1.10	10.80	289.3	26.7	3.530E-03	3320164558.35900
2H-4	1.15	10.85	306.7	47.4	2.799E-03	3320164563.68712
2H-4	1.20	10.90	129.1	74.2	2.766E-03	3320164568.99962
2H-4	1.25	10.95	124.2	40.8	3.353E-03	3320164574.32775
2H-4	1.30	11.00	115.0	40.3	3.320E-03	3320164579.65587
2H-4	1.35	11.05	108.2	41.3	3.350E-03	3320164584.98400
2H-4	1.40	11.10	97.7	36.5	3.942E-03	3320164590.29650
2H-5	0.10	11.30	111.9	34.5	3.523E-03	3320167891.73400
2H-5	0.15	11.35	110.6	39.5	2.952E-03	3320167897.06212
2H-5	0.20	11.40	110.2	41.4	3.060E-03	3320167902.39025
2H-5	0.25	11.45	111.7	42.1	3.533E-03	3320167907.70275
2H-5	0.30	11.50	107.7	32.3	4.889E-03	3320167913.03087
2H-5	0.35	11.55	107.1	20.0	7.196E-03	3320167918.35900
2H-5	0.40	11.60	101.0	14.9	7.256E-03	3320167923.68712
2H-5	0.45	11.65	106.0	37.6	3.802E-03	3320167929.01525
2H-5	0.50	11.70	115.8	42.1	3.379E-03	3320167934.34337
2H-5	0.55	11.75	113.5	39.2	3.399E-03	3320167939.65587
2H-5	0.60	11.80	111.3	34.9	3.561E-03	3320167944.98400
2H-5	0.65	11.85	108.7	35.4	3.657E-03	3320167950.31212
2H-5	0.70	11.90	108.6	41.3	4.402E-03	3320167955.64025
2H-5	0.75	11.95	114.2	33.6	6.316E-03	3320167960.96837
2H-5	0.80	12.00	115.4	31.2	8.439E-03	3320167966.28087
2H-5	0.85	12.05	112.6	31.3	8.412E-03	3320167971.60900
2H-5	0.90	12.10	116.1	38.0	7.066E-03	3320167976.93712
2H-5	0.95	12.15	132.8	67.9	4.475E-03	3320167982.26525
2H-5	1.00	12.20	306.9	82.9	4.345E-03	3320167987.59337
2H-5	1.05	12.25	285.2	73.1	4.773E-03	3320167992.90587
2H-5	1.10	12.30	260.6	80.9	5.001E-03	3320167998.23400
2H-5	1.15	12.35	157.7	76.4	5.284E-03	3320168003.56212
2H-5	1.20	12.40	122.4	76.6	5.248E-03	3320168008.89025
2H-5	1.25	12.45	114.0	80.7	5.055E-03	3320168014.21837
2H-5	1.30	12.50	110.6	42.4	8.103E-03	3320168019.53087
2H-5	1.35	12.55	110.5	36.0	9.537E-03	3320168024.85900
2H-5	1.40	12.60	109.6	35.6	8.946E-03	3320168030.18712
2H-6	0.10	12.80	148.4	38.0	1.161E-02	3320170730.64025
2H-6	0.15	12.85	135.9	62.8	3.943E-03	3320170735.96837
2H-6	0.20	12.90	119.8	59.8	3.340E-03	3320170741.28087
2H-6	0.25	12.95	123.0	49.3	3.843E-03	3320170746.60900
2H-6	0.30	13.00	124.4	48.2	4.187E-03	3320170751.93712
2H-6	0.35	13.05	131.7	42.0	4.835E-03	3320170757.26525
2H-6	0.40	13.10	123.8	41.6	4.771E-03	3320170762.59337
2H-6	0.45	13.15	123.0	37.4	5.109E-03	3320170767.90587

Table T15 (continued).

Core, section	Offset (m)	Depth CSF (m)	Declination (°)	Inclination (°)	Intensity (A/m)	Time (s)
2H-6	0.50	13.20	134.7	47.0	4.190E-03	3320170773.23400
2H-6	0.55	13.25	147.0	52.7	3.313E-03	3320170778.56212
2H-6	0.60	13.30	136.6	59.7	2.797E-03	3320170783.89025
2H-6	0.65	13.35	179.0	73.1	2.228E-03	3320170789.21837
2H-6	0.70	13.40	239.8	64.3	2.034E-03	3320170794.54650
2H-6	0.75	13.45	258.5	58.8	2.095E-03	3320170799.85900
2H-6	0.80	13.50	265.1	42.5	2.319E-03	3320170805.18712
2H-6	0.85	13.55	278.0	41.1	2.263E-03	3320170810.51525
2H-6	0.90	13.60	276.4	32.5	2.281E-03	3320170815.84337
2H-6	0.95	13.65	276.3	27.9	2.834E-03	3320170821.15587
2H-6	1.00	13.70	275.6	30.3	2.536E-03	3320170826.48400
2H-6	1.05	13.75	280.1	27.2	2.729E-03	3320170831.81212
2H-6	1.10	13.80	290.0	24.9	3.466E-03	3320170837.14025
2H-6	1.15	13.85	274.6	30.8	3.075E-03	3320170842.46837
2H-6	1.20	13.90	273.9	31.2	2.741E-03	3320170847.79650
2H-6	1.25	13.95	274.8	30.4	2.946E-03	3320170853.10900
2H-6	1.30	14.00	275.6	34.7	3.141E-03	3320170858.43712
2H-6	1.35	14.05	276.0	42.4	3.080E-03	3320170863.76525
2H-6	1.40	14.10	280.4	41.3	3.569E-03	3320170869.09337

Notes: Time = since 1 January 1904. This table is also available in [ASCII](#).



Table T16. Paleomagnetic data from archive-half sections, Hole U1331A, at 10 mT AF demagnetization. (See table notes.)

Core, section	Offset (m)	Depth CSF (m)	Declination (°)	Inclination (°)	Intensity (A/m)	Time (s)
320-U1331A-						
1H-1	0.10	0.10	15.3	6.6	1.584E-02	3320134560.17150
1H-1	0.15	0.15	3.2	13.3	1.613E-02	3320134565.49962
1H-1	0.20	0.20	357.7	12.7	1.205E-02	3320134570.82775
1H-1	0.25	0.25	358.7	9.9	1.084E-02	3320134576.15587
1H-1	0.30	0.30	359.2	11.2	1.016E-02	3320134581.48400
1H-1	0.35	0.35	357.4	11.1	8.273E-03	3320134586.79650
1H-1	0.40	0.40	348.6	8.1	9.327E-03	3320134592.12462
1H-1	0.45	0.45	353.6	7.4	1.186E-02	3320134597.45275
1H-1	0.50	0.50	352.8	8.0	1.139E-02	3320134602.78087
1H-1	0.55	0.55	347.9	17.4	7.854E-03	3320134608.10900
1H-1	0.60	0.60	341.7	15.6	8.515E-03	3320134613.43712
1H-1	0.65	0.65	13.3	6.5	1.390E-02	3320134618.74962
1H-1	0.70	0.70	360.0	-12.4	1.751E-02	3320134624.07775
1H-1	0.75	0.75	300.6	-3.3	1.289E-02	3320134629.40587
1H-1	0.80	0.80	292.1	4.0	5.782E-03	3320134634.73400
1H-1	0.85	0.85	296.8	12.1	5.877E-03	3320134640.04650
1H-1	0.90	0.90	307.2	13.3	6.759E-03	3320134645.37462
1H-1	0.95	0.95	310.3	13.4	7.726E-03	3320134650.70275
1H-1	1.00	1.00	310.6	13.0	7.820E-03	3320134656.03087
1H-1	1.05	1.05	310.1	13.5	7.252E-03	3320134661.35900
1H-1	1.10	1.10	309.8	10.6	6.879E-03	3320134666.68712
1H-1	1.15	1.15	309.4	10.8	6.772E-03	3320134671.99962
1H-1	1.20	1.20	310.8	11.4	6.005E-03	3320134677.32775
1H-1	1.25	1.25	312.2	12.7	5.395E-03	3320134682.65587
1H-1	1.30	1.30	311.4	13.3	5.411E-03	3320134687.98400
1H-1	1.35	1.35	310.9	13.0	5.627E-03	3320134693.31212
1H-1	1.40	1.40	310.6	11.7	6.409E-03	3320134698.62462
1H-3	0.10	3.10	129.8	2.3	6.229E-03	3320142524.70275
1H-3	0.15	3.15	133.3	11.5	4.697E-03	3320142530.01525
1H-3	0.20	3.20	137.1	56.4	1.187E-03	3320142535.34337
1H-3	0.25	3.25	312.3	35.3	2.168E-03	3320142540.67150
1H-3	0.30	3.30	305.0	17.5	3.730E-03	3320142545.99962
1H-3	0.35	3.35	311.9	13.8	4.469E-03	3320142551.32775
1H-3	0.40	3.40	312.6	14.7	4.191E-03	3320142556.65587
1H-3	0.45	3.45	310.6	15.7	3.442E-03	3320142561.96837
1H-3	0.50	3.50	313.5	23.2	2.083E-03	3320142567.29650
1H-3	0.55	3.55	307.7	25.6	2.264E-03	3320142572.62462
1H-3	0.60	3.60	310.6	21.5	2.990E-03	3320142577.95275
1H-3	0.65	3.65	306.2	17.1	3.575E-03	3320142583.28087
1H-3	0.70	3.70	307.9	15.7	3.259E-03	3320142588.59337
1H-3	0.75	3.75	308.7	15.3	3.482E-03	3320142593.92150
1H-3	0.80	3.80	308.1	15.1	3.645E-03	3320142599.24962
1H-3	0.85	3.85	310.7	16.3	3.298E-03	3320142604.57775
1H-3	0.90	3.90	280.8	39.0	1.939E-03	3320142609.89025
1H-3	0.95	3.95	296.2	41.8	2.281E-03	3320142615.21837
1H-3	1.00	4.00	306.4	26.0	3.941E-03	3320142620.54650
1H-3	1.05	4.05	310.7	11.7	6.421E-03	3320142625.87462
1H-3	1.10	4.10	308.5	9.9	5.541E-03	3320142631.20275
1H-3	1.15	4.15	306.7	11.3	4.837E-03	3320142636.53087
1H-3	1.20	4.20	303.6	14.2	4.486E-03	3320142641.84337
1H-3	1.25	4.25	303.8	15.2	4.765E-03	3320142647.17150
1H-3	1.30	4.30	305.5	14.9	4.946E-03	3320142652.49962
1H-3	1.35	4.35	304.4	13.7	5.202E-03	3320142657.82775
1H-3	1.40	4.40	304.4	13.6	5.323E-03	3320142663.14025
1H-4	0.10	4.60	315.5	10.6	6.741E-03	3320144644.78087
1H-4	0.15	4.65	316.3	14.0	6.090E-03	3320144650.09337
1H-4	0.20	4.70	315.7	13.7	5.862E-03	3320144655.42150
1H-4	0.25	4.75	315.2	13.6	5.755E-03	3320144660.74962
1H-4	0.30	4.80	313.4	12.3	6.051E-03	3320144666.07775
1H-4	0.35	4.85	310.2	6.6	6.224E-03	3320144671.40587
1H-4	0.40	4.90	321.6	11.1	3.784E-03	3320144676.71837
2H-1	0.10	5.30	172.4	16.3	3.827E-03	3320148152.20275
2H-1	0.15	5.35	160.8	17.4	9.871E-03	3320148157.53087

Notes: Time = since 1 January 1904. Only a portion of this table appears here. The complete table is available in [ASCII](#).

Table T17. Paleomagnetic data from archive-half sections, Hole U1331A, at 15 mT AF demagnetization. (See table notes.) (Continued on next three pages.)

Core, section	Offset (m)	Depth CSF (m)	Declination (°)	Inclination (°)	Intensity (A/m)	Time (s)
320-U1331A-						
1H-1	0.10	0.10	13.2	6.7	1.300E-02	3320135021.67150
1H-1	0.15	0.15	5.7	12.2	1.360E-02	3320135026.99962
1H-1	0.20	0.20	2.1	12.5	1.125E-02	3320135032.31212
1H-1	0.25	0.25	1.4	10.7	9.986E-03	3320135037.64025
1H-1	0.30	0.30	2.6	11.5	9.335E-03	3320135042.96837
1H-1	0.35	0.35	356.6	11.9	7.457E-03	3320135048.29650
1H-1	0.40	0.40	352.4	8.6	7.988E-03	3320135053.60900
1H-1	0.45	0.45	356.8	7.6	1.033E-02	3320135058.93712
1H-1	0.50	0.50	355.5	7.6	9.884E-03	3320135064.26525
1H-1	0.55	0.55	352.0	14.7	6.873E-03	3320135069.57775
1H-1	0.60	0.60	348.0	14.9	7.202E-03	3320135074.90587
1H-1	0.65	0.65	13.4	8.6	1.219E-02	3320135080.23400
1H-1	0.70	0.70	2.7	-12.0	1.543E-02	3320135085.56212
1H-1	0.75	0.75	302.0	-4.0	1.072E-02	3320135090.87462
1H-1	0.80	0.80	289.2	5.8	4.238E-03	3320135096.20275
1H-1	0.85	0.85	297.6	9.9	4.067E-03	3320135101.53087
1H-1	0.90	0.90	310.4	12.1	4.868E-03	3320135106.85900
1H-1	0.95	0.95	313.6	12.0	5.759E-03	3320135112.17150
1H-1	1.00	1.00	313.4	11.6	5.815E-03	3320135117.49962
1H-1	1.05	1.05	313.0	12.4	5.312E-03	3320135122.82775
1H-1	1.10	1.10	312.3	11.1	5.074E-03	3320135128.15587
1H-1	1.15	1.15	312.7	8.6	4.926E-03	3320135133.48400
1H-1	1.20	1.20	314.0	9.6	4.339E-03	3320135138.81212
1H-1	1.25	1.25	319.2	11.3	3.743E-03	3320135144.12462
1H-1	1.30	1.30	317.2	11.7	3.818E-03	3320135149.45275
1H-1	1.35	1.35	316.9	11.7	3.960E-03	3320135154.78087
1H-1	1.40	1.40	315.4	10.4	4.619E-03	3320135160.10900
1H-3	0.10	3.10	134.0	-0.4	5.381E-03	3320143018.07775
1H-3	0.15	3.15	133.3	4.0	5.061E-03	3320143023.40587
1H-3	0.20	3.20	128.1	46.7	9.308E-04	3320143028.73400
1H-3	0.25	3.25	292.0	27.0	1.461E-03	3320143034.04650
1H-3	0.30	3.30	300.4	16.2	2.570E-03	3320143039.37462
1H-3	0.35	3.35	307.5	11.0	3.671E-03	3320143044.70275
1H-3	0.40	3.40	311.9	12.4	3.360E-03	3320143050.03087
1H-3	0.45	3.45	309.9	13.6	2.682E-03	3320143055.35900
1H-3	0.50	3.50	309.7	17.8	1.769E-03	3320143060.67150
1H-3	0.55	3.55	302.6	25.2	1.611E-03	3320143065.99962
1H-3	0.60	3.60	311.1	20.0	2.268E-03	3320143071.32775
1H-3	0.65	3.65	307.8	15.8	2.689E-03	3320143076.65587
1H-3	0.70	3.70	307.6	13.7	2.542E-03	3320143081.98400
1H-3	0.75	3.75	308.7	13.5	2.704E-03	3320143087.29650
1H-3	0.80	3.80	319.1	10.7	3.463E-03	3320143092.62462
1H-3	0.85	3.85	308.9	13.3	2.600E-03	3320143097.95275
1H-3	0.90	3.90	292.4	27.3	1.601E-03	3320143103.28087
1H-3	0.95	3.95	292.7	46.2	1.760E-03	3320143108.60900
1H-3	1.00	4.00	318.5	24.2	3.006E-03	3320143113.93712
1H-3	1.05	4.05	307.7	12.1	4.805E-03	3320143119.24962
1H-3	1.10	4.10	308.3	8.2	4.521E-03	3320143124.57775
1H-3	1.15	4.15	307.2	9.2	3.924E-03	3320143129.90587
1H-3	1.20	4.20	305.1	11.7	3.643E-03	3320143135.23400
1H-3	1.25	4.25	303.8	13.3	3.837E-03	3320143140.54650
1H-3	1.30	4.30	304.9	13.2	3.964E-03	3320143145.87462
1H-3	1.35	4.35	304.5	12.1	4.189E-03	3320143151.20275
1H-3	1.40	4.40	304.1	12.0	4.276E-03	3320143156.53087
1H-4	0.10	4.60	315.0	8.6	5.471E-03	3320145046.56212
1H-4	0.15	4.65	316.0	11.0	4.904E-03	3320145051.89025
1H-4	0.20	4.70	315.2	11.7	4.713E-03	3320145057.21837
1H-4	0.25	4.75	314.8	11.7	4.578E-03	3320145062.53087
1H-4	0.30	4.80	313.2	10.4	4.832E-03	3320145067.85900
1H-4	0.35	4.85	309.9	5.4	5.033E-03	3320145073.18712
1H-4	0.40	4.90	315.3	7.7	3.115E-03	3320145078.51525
2H-1	0.10	5.30	145.8	56.6	4.177E-03	3320148742.49962
2H-1	0.15	5.35	137.7	21.7	1.429E-02	3320148747.82775
2H-1	0.20	5.40	135.9	33.6	2.285E-03	3320148753.15587
2H-1	0.25	5.45	88.3	11.8	3.606E-03	3320148758.46837
2H-1	0.30	5.50	91.4	11.0	9.266E-03	3320148763.79650

Table T17 (continued). (Continued on next page.)

Core, section	Offset (m)	Depth CSF (m)	Declination (°)	Inclination (°)	Intensity (A/m)	Time (s)
2H-1	0.35	5.55	37.6	53.1	6.100E-03	3320148769.12462
2H-1	0.40	5.60	231.0	49.9	9.490E-03	3320148774.45275
2H-1	0.45	5.65	236.3	28.6	3.231E-03	3320148779.76525
2H-1	0.50	5.70	80.2	8.5	3.075E-03	3320148785.09337
2H-1	0.55	5.75	139.1	-4.7	8.558E-03	3320148790.42150
2H-1	0.60	5.80	134.1	-10.6	1.387E-02	3320148795.74962
2H-1	0.65	5.85	318.8	-35.5	7.474E-04	3320148801.07775
2H-1	0.70	5.90	290.5	2.1	3.073E-03	3320148806.39025
2H-1	0.75	5.95	301.5	3.8	1.714E-03	3320148811.71837
2H-1	0.80	6.00	298.7	-11.5	3.344E-03	3320148817.04650
2H-1	0.85	6.05	315.6	-35.8	2.589E-03	3320148822.37462
2H-1	0.90	6.10	18.7	-10.5	2.261E-03	3320148827.70275
2H-1	0.95	6.15	263.2	-22.7	3.022E-03	3320148833.01525
2H-1	1.00	6.20	249.2	-26.0	2.833E-02	3320148838.34337
2H-1	1.05	6.25	51.4	-55.2	1.829E-02	3320148843.67150
2H-1	1.10	6.30	45.0	-52.4	3.370E-03	3320148848.99962
2H-1	1.15	6.35	305.1	-13.9	2.964E-03	3320148854.32775
2H-1	1.20	6.40	246.8	5.6	1.255E-03	3320148859.65587
2H-1	1.25	6.45	279.5	27.3	3.343E-03	3320148864.96837
2H-1	1.30	6.50	199.2	57.2	2.624E-03	3320148870.29650
2H-1	1.35	6.55	159.1	31.6	8.054E-04	3320148875.62462
2H-1	1.40	6.60	338.2	-11.6	6.159E-04	3320148880.93712
2H-2	0.10	6.80	292.4	-7.6	5.285E-03	3320157305.09337
2H-2	0.15	6.85	292.3	-5.6	5.661E-03	3320157310.42150
2H-2	0.20	6.90	298.8	11.8	3.555E-03	3320157315.74962
2H-2	0.25	6.95	277.0	8.0	3.765E-03	3320157321.07775
2H-2	0.30	7.00	275.6	-2.4	2.115E-03	3320157326.40587
2H-2	0.35	7.05	286.1	-9.6	2.392E-03	3320157331.71837
2H-2	0.40	7.10	291.2	-5.8	2.776E-03	3320157337.04650
2H-2	0.45	7.15	288.5	-2.3	3.219E-03	3320157342.37462
2H-2	0.50	7.20	290.2	-1.5	2.884E-03	3320157347.70275
2H-2	0.55	7.25	305.0	5.2	1.686E-03	3320157353.01525
2H-2	0.60	7.30	323.0	32.2	2.883E-03	3320157358.34337
2H-2	0.65	7.35	263.3	28.0	3.553E-03	3320157363.67150
2H-2	0.70	7.40	267.3	16.4	1.589E-03	3320157368.99962
2H-2	0.75	7.45	306.4	17.7	6.585E-04	3320157374.32775
2H-2	0.80	7.50	283.2	-7.0	6.894E-04	3320157379.64025
2H-2	0.85	7.55	290.1	-4.3	1.016E-03	3320157384.96837
2H-2	0.90	7.60	155.4	7.4	6.127E-04	3320157390.29650
2H-2	0.95	7.65	247.6	6.2	1.298E-03	3320157395.62462
2H-2	1.00	7.70	318.8	3.5	1.524E-03	3320157400.95275
2H-2	1.05	7.75	312.7	-0.8	1.200E-03	3320157406.28087
2H-2	1.10	7.80	256.1	-7.2	9.304E-04	3320157411.59337
2H-2	1.15	7.85	273.3	-6.8	1.141E-03	3320157416.92150
2H-2	1.20	7.90	274.0	-4.7	9.759E-04	3320157422.24962
2H-2	1.25	7.95	271.6	-9.1	1.057E-03	3320157427.57775
2H-2	1.30	8.00	273.0	-20.0	1.099E-03	3320157432.90587
2H-2	1.35	8.05	272.7	-22.5	9.039E-04	3320157438.21837
2H-2	1.40	8.10	270.9	-15.4	1.108E-03	3320157443.54650
2H-3	0.10	8.30	330.5	-10.8	6.787E-04	3320161253.73400
2H-3	0.15	8.35	0.8	-20.6	4.921E-04	3320161259.06212
2H-3	0.20	8.40	180.0	-57.3	7.964E-04	3320161264.39025
2H-3	0.25	8.45	245.3	-12.6	2.308E-03	3320161269.71837
2H-3	0.30	8.50	299.0	-11.4	5.634E-04	3320161275.03087
2H-3	0.35	8.55	290.4	15.3	4.307E-04	3320161280.35900
2H-3	0.40	8.60	302.5	2.0	5.680E-04	3320161285.68712
2H-3	0.45	8.65	300.6	6.6	6.520E-04	3320161291.01525
2H-3	0.50	8.70	281.8	7.0	4.271E-04	3320161296.34337
2H-3	0.55	8.75	284.4	1.8	4.604E-04	3320161301.65587
2H-3	0.60	8.80	293.7	-4.2	2.536E-04	3320161306.98400
2H-3	0.65	8.85	129.1	-81.4	1.983E-04	3320161312.31212
2H-3	0.70	8.90	226.1	-64.3	1.517E-04	3320161317.64025
2H-3	0.75	8.95	94.6	-8.1	5.785E-04	3320161322.96837
2H-3	0.80	9.00	270.4	-2.6	1.916E-03	3320161328.29650
2H-3	0.85	9.05	281.4	-6.1	6.646E-03	3320161333.60900
2H-3	0.90	9.10	286.3	-4.9	6.476E-03	3320161338.93712
2H-3	0.95	9.15	287.5	-7.1	4.123E-03	3320161344.26525
2H-3	1.00	9.20	292.2	-13.1	2.591E-03	3320161349.59337
2H-3	1.05	9.25	284.3	-10.5	2.613E-03	3320161354.92150

Table T17 (continued). (Continued on next page.)

Core, section	Offset (m)	Depth CSF (m)	Declination (°)	Inclination (°)	Intensity (A/m)	Time (s)
2H-3	1.10	9.30	282.4	-8.9	2.875E-03	3320161360.23400
2H-3	1.15	9.35	282.7	-8.8	2.305E-03	3320161365.56212
2H-3	1.20	9.40	285.4	-6.5	1.494E-03	3320161370.89025
2H-3	1.25	9.45	285.0	-8.5	1.656E-03	3320161376.21837
2H-3	1.30	9.50	286.0	-6.9	3.034E-03	3320161381.53087
2H-3	1.35	9.55	290.0	-4.2	3.401E-03	3320161386.85900
2H-3	1.40	9.60	287.7	1.6	3.512E-03	3320161392.18712
2H-4	0.10	9.80	274.3	-26.1	2.180E-03	3320165593.98400
2H-4	0.15	9.85	305.8	-24.3	2.163E-03	3320165599.29650
2H-4	0.20	9.90	312.7	-22.2	9.512E-04	3320165604.62462
2H-4	0.25	9.95	284.8	-14.8	8.421E-04	3320165609.95275
2H-4	0.30	10.00	280.0	-11.8	8.724E-04	3320165615.28087
2H-4	0.35	10.05	279.4	-7.6	7.075E-04	3320165620.60900
2H-4	0.40	10.10	276.2	-6.1	8.290E-04	3320165625.92150
2H-4	0.45	10.15	279.7	-7.7	1.172E-03	3320165631.24962
2H-4	0.50	10.20	283.8	-7.0	1.059E-03	3320165636.57775
2H-4	0.55	10.25	290.5	-3.1	1.283E-03	3320165641.90587
2H-4	0.60	10.30	279.5	1.8	2.079E-03	3320165647.23400
2H-4	0.65	10.35	276.4	-3.5	1.691E-03	3320165652.54650
2H-4	0.70	10.40	290.8	-18.0	1.149E-03	3320165657.87462
2H-4	0.75	10.45	280.1	-12.1	9.792E-04	3320165663.20275
2H-4	0.80	10.50	260.3	-6.4	1.302E-03	3320165668.53087
2H-4	0.85	10.55	232.3	11.7	6.133E-04	3320165673.85900
2H-4	0.90	10.60	204.0	3.6	7.793E-04	3320165679.17150
2H-4	0.95	10.65	283.0	5.0	1.104E-03	3320165684.49962
2H-4	1.00	10.70	277.3	4.1	2.142E-03	3320165689.82775
2H-4	1.05	10.75	291.7	-3.0	3.153E-03	3320165695.15587
2H-4	1.10	10.80	289.9	-6.4	3.470E-03	3320165700.48400
2H-4	1.15	10.85	294.3	-7.2	1.732E-03	3320165705.81212
2H-4	1.20	10.90	138.6	17.7	4.759E-04	3320165711.12462
2H-4	1.25	10.95	116.2	9.5	1.268E-03	3320165716.45275
2H-4	1.30	11.00	115.4	18.5	1.300E-03	3320165721.78087
2H-4	1.35	11.05	107.9	15.6	1.454E-03	3320165727.10900
2H-4	1.40	11.10	102.0	12.2	2.289E-03	3320165732.42150
2H-5	0.10	11.30	108.6	13.4	2.017E-03	3320169069.28087
2H-5	0.15	11.35	108.2	16.7	1.538E-03	3320169074.60900
2H-5	0.20	11.40	107.5	22.4	1.793E-03	3320169079.93712
2H-5	0.25	11.45	110.5	18.0	2.003E-03	3320169085.26525
2H-5	0.30	11.50	117.1	11.6	2.635E-03	3320169090.59337
2H-5	0.35	11.55	110.0	3.3	3.277E-03	3320169095.92150
2H-5	0.40	11.60	106.2	1.4	3.188E-03	3320169101.23400
2H-5	0.45	11.65	114.4	8.2	1.572E-03	3320169106.56212
2H-5	0.50	11.70	113.0	12.2	1.821E-03	3320169111.89025
2H-5	0.55	11.75	112.1	14.4	1.943E-03	3320169117.21837
2H-5	0.60	11.80	110.9	14.2	2.152E-03	3320169122.53087
2H-5	0.65	11.85	108.5	14.4	2.188E-03	3320169127.85900
2H-5	0.70	11.90	109.2	17.1	2.426E-03	3320169133.18712
2H-5	0.75	11.95	107.6	12.9	4.353E-03	3320169138.51525
2H-5	0.80	12.00	113.3	12.1	5.135E-03	3320169143.84337
2H-5	0.85	12.05	113.1	11.5	5.109E-03	3320169149.15587
2H-5	0.90	12.10	116.6	7.8	3.568E-03	3320169154.48400
2H-5	0.95	12.15	133.6	16.5	6.827E-04	3320169159.81212
2H-5	1.00	12.20	286.8	3.3	1.394E-03	3320169165.14025
2H-5	1.05	12.25	287.8	1.1	2.185E-03	3320169170.46837
2H-5	1.10	12.30	284.9	5.3	1.457E-03	3320169175.79650
2H-5	1.15	12.35	106.7	23.7	6.825E-04	3320169181.10900
2H-5	1.20	12.40	257.4	55.0	3.950E-04	3320169186.43712
2H-5	1.25	12.45	63.3	47.2	3.338E-04	3320169191.76525
2H-5	1.30	12.50	112.9	11.0	3.398E-03	3320169197.09337
2H-5	1.35	12.55	110.6	9.8	4.469E-03	3320169202.42150
2H-5	1.40	12.60	110.7	10.2	4.381E-03	3320169207.73400
2H-6	0.10	12.80	130.8	17.3	4.330E-03	3320171735.78087
2H-6	0.15	12.85	107.7	16.1	1.605E-03	3320171741.10900
2H-6	0.20	12.90	113.1	12.8	1.888E-03	3320171746.43712
2H-6	0.25	12.95	114.4	12.5	2.140E-03	3320171751.74962
2H-6	0.30	13.00	116.0	14.2	2.267E-03	3320171757.07775
2H-6	0.35	13.05	113.7	15.2	2.496E-03	3320171762.40587
2H-6	0.40	13.10	111.7	12.6	3.223E-03	3320171767.73400
2H-6	0.45	13.15	115.2	13.2	3.258E-03	3320171773.04650

Table T17 (continued).

Core, section	Offset (m)	Depth CSF (m)	Declination (°)	Inclination (°)	Intensity (A/m)	Time (s)
2H-6	0.50	13.20	117.3	16.3	2.750E-03	3320171778.37462
2H-6	0.55	13.25	127.3	19.0	1.635E-03	3320171783.70275
2H-6	0.60	13.30	153.8	39.4	6.066E-04	3320171789.03087
2H-6	0.65	13.35	112.4	11.3	4.893E-04	3320171794.35900
2H-6	0.70	13.40	314.1	30.7	4.275E-04	3320171799.68712
2H-6	0.75	13.45	288.9	16.2	3.714E-04	3320171804.99962
2H-6	0.80	13.50	291.6	-11.0	4.641E-04	3320171810.32775
2H-6	0.85	13.55	281.8	-0.9	1.594E-03	3320171815.65587
2H-6	0.90	13.60	292.8	-2.0	1.085E-03	3320171820.98400
2H-6	0.95	13.65	292.4	-5.6	1.348E-03	3320171826.31212
2H-6	1.00	13.70	292.8	-7.2	1.309E-03	3320171831.64025
2H-6	1.05	13.75	292.3	-8.5	1.388E-03	3320171836.95275
2H-6	1.10	13.80	293.9	-6.7	1.626E-03	3320171842.28087
2H-6	1.15	13.85	288.6	-4.4	1.451E-03	3320171847.60900
2H-6	1.20	13.90	287.0	-5.3	1.495E-03	3320171852.93712
2H-6	1.25	13.95	289.3	-4.7	1.566E-03	3320171858.26525
2H-6	1.30	14.00	288.7	-2.0	1.387E-03	3320171863.57775
2H-6	1.35	14.05	290.9	2.5	1.151E-03	3320171868.90587
2H-6	1.40	14.10	285.8	1.7	2.368E-03	3320171874.23400

Notes: Time = since 1 January 1904. This table is also available in [ASCII](#).



Table T18. Paleomagnetic data from archive-half sections, Hole U1331A, at 20 mT AF demagnetization. (See table notes.)

Core, section	Offset (m)	Depth CSF (m)	Declination (°)	Inclination (°)	Intensity (A/m)	Time (s)	Declination		
							Core mean (°)	Geographical coordinates	
								0°–360°	-90°–270°
320-U1331A-									
1H-1	0.10	0.10	11.5	6.4	1.108E-02	3320135496.57775	318.76	52.7	52.7
1H-1	0.15	0.15	6.9	11.5	1.176E-02	3320135501.90587	318.76	48.1	48.1
1H-1	0.20	0.20	2.6	12.6	1.034E-02	3320135507.23400	318.76	43.8	43.8
1H-1	0.25	0.25	1.7	11.8	8.614E-03	3320135512.56212	318.76	42.9	42.9
1H-1	0.30	0.30	2.5	11.4	8.434E-03	3320135517.89025	318.76	43.7	43.7
1H-1	0.35	0.35	356.0	11.5	6.509E-03	3320135523.20275	318.76	37.2	37.2
1H-1	0.40	0.40	354.1	8.4	6.880E-03	3320135528.53087	318.76	35.3	35.3
1H-1	0.45	0.45	356.6	7.7	9.076E-03	3320135533.85900	318.76	37.8	37.8
1H-1	0.50	0.50	350.6	7.7	8.459E-03	3320135539.18712	318.76	31.8	31.8
1H-1	0.55	0.55	351.0	14.4	5.956E-03	3320135544.51525	318.76	32.2	32.2
1H-1	0.60	0.60	347.8	14.6	6.212E-03	3320135549.82775	318.76	29.0	29.0
1H-1	0.65	0.65	15.8	8.5	1.048E-02	3320135555.15587	318.76	57.0	57.0
1H-1	0.70	0.70	3.0	-13.7	1.357E-02	3320135560.48400	318.76	44.2	44.2
1H-1	0.75	0.75	300.2	-4.6	9.556E-03	3320135565.81212	318.76	341.4	-18.6
1H-1	0.80	0.80	290.0	2.0	3.231E-03	3320135571.14025	318.76	331.2	-28.8
1H-1	0.85	0.85	296.0	12.7	3.252E-03	3320135576.45275	318.76	337.2	-22.8
1H-1	0.90	0.90	305.7	11.1	3.764E-03	3320135581.78087	318.76	346.9	-13.1
1H-1	0.95	0.95	311.8	11.4	4.584E-03	3320135587.10900	318.76	353.0	-7.0
1H-1	1.00	1.00	312.3	10.6	4.631E-03	3320135592.43712	318.76	353.5	-6.5
1H-1	1.05	1.05	311.5	11.2	4.237E-03	3320135597.76525	318.76	352.7	-7.3
1H-1	1.10	1.10	310.9	10.2	4.034E-03	3320135603.07775	318.76	352.1	-7.9
1H-1	1.15	1.15	311.4	7.0	3.917E-03	3320135608.40587	318.76	352.6	-7.4
1H-1	1.20	1.20	315.5	8.8	3.257E-03	3320135613.73400	318.76	356.7	-3.3
1H-1	1.25	1.25	314.5	9.5	3.032E-03	3320135619.06212	318.76	355.7	-4.3
1H-1	1.30	1.30	314.8	10.4	2.999E-03	3320135624.39025	318.76	356.0	-4.0
1H-1	1.35	1.35	315.2	10.4	3.153E-03	3320135629.70275	318.76	356.4	-3.6
1H-1	1.40	1.40	313.5	9.5	3.650E-03	3320135635.03087	318.76	354.7	-5.3
1H-2	0.10	1.60	315.1	12.9	4.284E-03	3320139673.43712	318.76	356.3	-3.7
1H-2	0.15	1.65	329.5	18.2	2.686E-03	3320139678.76525	318.76	10.7	10.7
1H-2	0.20	1.70	313.9	39.5	1.078E-03	3320139684.07775	318.76	355.1	-4.9
1H-2	0.25	1.75	131.9	46.0	6.514E-04	3320139689.40587	318.76	173.1	173.1
1H-2	0.30	1.80	121.0	20.8	1.354E-03	3320139694.73400	318.76	162.2	162.2
1H-2	0.35	1.85	138.1	23.4	1.167E-03	3320139700.04650	318.76	179.3	179.3
1H-2	0.40	1.90	151.9	3.9	1.308E-03	3320139705.37462	318.76	193.1	193.1
1H-2	0.45	1.95	141.8	5.0	1.605E-03	3320139710.70275	318.76	183.0	183.0
1H-2	0.50	2.00	140.3	2.5	1.791E-03	3320139716.03087	318.76	181.5	181.5
1H-2	0.55	2.05	142.7	4.1	1.932E-03	3320139721.35900	318.76	183.9	183.9
1H-2	0.60	2.10	145.9	3.7	2.267E-03	3320139726.67150	318.76	187.1	187.1
1H-2	0.65	2.15	145.3	6.6	2.381E-03	3320139731.99962	318.76	186.5	186.5
1H-2	0.70	2.20	139.9	8.4	3.229E-03	3320139737.32775	318.76	181.1	181.1
1H-2	0.75	2.25	142.2	9.7	3.637E-03	3320139742.65587	318.76	183.4	183.4
1H-2	0.80	2.30	141.3	7.2	3.631E-03	3320139747.98400	318.76	182.5	182.5
1H-2	0.85	2.35	138.4	6.3	3.494E-03	3320139753.29650	318.76	179.6	179.6
1H-2	0.90	2.40	134.4	7.3	3.222E-03	3320139758.62462	318.76	175.6	175.6
1H-2	0.95	2.45	134.2	11.6	2.937E-03	3320139763.95275	318.76	175.4	175.4
1H-2	1.00	2.50	136.0	12.2	2.740E-03	3320139769.28087	318.76	177.2	177.2
1H-2	1.05	2.55	133.3	8.8	2.890E-03	3320139774.60900	318.76	174.5	174.5
1H-2	1.10	2.60	133.8	8.0	2.938E-03	3320139779.93712	318.76	175.0	175.0
1H-2	1.15	2.65	138.0	7.6	2.890E-03	3320139785.24962	318.76	179.2	179.2
1H-2	1.20	2.70	134.6	6.2	2.765E-03	3320139790.57775	318.76	175.8	175.8
1H-2	1.25	2.75	135.2	4.0	2.648E-03	3320139795.90587	318.76	176.4	176.4
1H-2	1.30	2.80	133.9	3.3	3.143E-03	3320139801.23400	318.76	175.1	175.1
1H-2	1.35	2.85	134.9	3.1	3.533E-03	3320139806.54650	318.76	176.1	176.1
1H-2	1.40	2.90	134.3	3.0	3.482E-03	3320139811.87462	318.76	175.5	175.5
1H-3	0.10	3.10	133.8	-1.5	4.268E-03	3320143476.64025	318.76	175.0	175.0
1H-3	0.15	3.15	134.0	0.3	4.053E-03	3320143481.96837	318.76	175.2	175.2
1H-3	0.20	3.20	135.0	27.9	8.503E-04	3320143487.29650	318.76	176.2	176.2
1H-3	0.25	3.25	283.8	19.4	1.469E-03	3320143492.62462	318.76	325.0	-35.0
1H-3	0.30	3.30	299.3	12.4	2.417E-03	3320143497.95275	318.76	340.5	-19.5
1H-3	0.35	3.35	314.9	9.9	2.989E-03	3320143503.26525	318.76	356.1	-3.9
1H-3	0.40	3.40	311.3	11.4	2.694E-03	3320143508.59337	318.76	352.5	-7.5

Notes: Time = since 1 January 1904. Only a portion of this table appears here. The complete table is available in [ASCII](#).

Table T19. Paleomagnetic data from archive-half sections, Hole U1331B, at 0 mT AF demagnetization. ([See table notes](#).)

Core, section	Offset (m)	Depth CSF (m)	Declination (°)	Inclination (°)	Intensity (A/m)	Time (s)
320-U1331B-						
1H-1	1.40	1.40	199.7	88.0	4.458E-02	3320363637.84337
1H-2	0.10	1.60	6.7	82.7	3.262E-02	3320364430.26525
1H-2	0.15	1.65	153.7	89.8	4.092E-02	3320364435.57775
1H-2	0.20	1.70	172.6	87.4	4.325E-02	3320364440.90587
1H-2	0.25	1.75	182.4	87.5	4.326E-02	3320364446.23400
1H-2	0.30	1.80	205.7	87.0	4.354E-02	3320364451.54650
1H-2	0.35	1.85	205.4	87.4	4.350E-02	3320364456.87462
1H-2	0.40	1.90	204.8	87.9	4.374E-02	3320364462.20275
1H-2	0.45	1.95	217.9	88.2	4.458E-02	3320364467.53087
1H-2	0.50	2.00	259.9	88.6	4.513E-02	3320364472.85900
1H-2	0.55	2.05	295.6	88.7	4.571E-02	3320364478.17150
1H-2	0.60	2.10	275.5	88.9	4.067E-02	3320364483.49962
1H-2	0.65	2.15	82.4	89.0	4.198E-02	3320364488.82775
1H-2	0.70	2.20	173.0	87.6	4.599E-02	3320364494.15587
1H-2	0.75	2.25	319.7	87.8	4.794E-02	3320364499.48400
1H-2	0.80	2.30	344.3	85.1	4.919E-02	3320364504.81212
1H-2	0.85	2.35	349.8	82.2	4.987E-02	3320364510.14025
1H-2	0.90	2.40	347.1	80.1	4.999E-02	3320364515.45275
1H-2	0.95	2.45	348.2	78.8	4.972E-02	3320364520.78087
1H-2	1.00	2.50	347.4	79.2	4.821E-02	3320364526.10900
1H-2	1.05	2.55	349.2	81.4	4.592E-02	3320364531.43712
1H-2	1.10	2.60	353.2	81.4	4.578E-02	3320364536.76525
1H-2	1.15	2.65	347.6	81.6	4.665E-02	3320364542.07775
1H-2	1.20	2.70	350.1	81.5	4.531E-02	3320364547.40587
1H-2	1.25	2.75	352.1	81.3	4.483E-02	3320364552.73400
1H-2	1.30	2.80	346.8	80.5	4.456E-02	3320364558.06212
1H-2	1.35	2.85	348.1	78.7	4.429E-02	3320364563.39025
1H-2	1.40	2.90	351.9	78.0	4.415E-02	3320364568.71837
1H-3	0.10	3.10	328.5	80.9	3.579E-02	3320365521.23400
1H-3	0.15	3.15	308.2	84.1	3.821E-02	3320365526.56212
1H-3	0.20	3.20	358.4	81.0	3.607E-02	3320365531.87462
1H-3	0.25	3.25	0.3	75.7	3.696E-02	3320365537.20275
1H-3	0.30	3.30	346.5	77.0	3.827E-02	3320365542.53087
1H-3	0.35	3.35	340.7	77.3	3.995E-02	3320365547.85900
1H-3	0.40	3.40	349.8	79.6	4.217E-02	3320365553.18712
1H-3	0.45	3.45	351.8	80.7	4.315E-02	3320365558.49962
1H-3	0.50	3.50	350.6	80.5	4.374E-02	3320365563.82775
1H-3	0.55	3.55	345.7	80.2	4.493E-02	3320365569.15587
1H-3	0.60	3.60	346.3	79.3	4.621E-02	3320365574.48400
1H-3	0.65	3.65	357.7	79.5	4.672E-02	3320365579.81212
1H-3	0.70	3.70	349.6	77.4	4.765E-02	3320365585.12462
1H-3	0.75	3.75	343.5	77.2	4.885E-02	3320365590.45275
1H-3	0.80	3.80	345.2	78.3	4.816E-02	3320365595.78087
1H-3	0.85	3.85	343.9	79.6	4.701E-02	3320365601.10900
1H-3	0.90	3.90	350.8	80.1	4.683E-02	3320365606.42150
1H-3	0.95	3.95	353.4	78.8	4.743E-02	3320365611.74962
1H-3	1.00	4.00	354.9	79.0	4.688E-02	3320365617.07775
1H-3	1.05	4.05	341.5	85.8	4.553E-02	3320365622.40587
1H-3	1.10	4.10	345.7	81.7	4.604E-02	3320365627.73400
1H-3	1.15	4.15	340.0	79.6	4.899E-02	3320365633.04650
1H-3	1.20	4.20	347.9	82.6	5.254E-02	3320365638.37462
1H-3	1.25	4.25	353.0	83.8	5.465E-02	3320365643.70275
1H-3	1.30	4.30	339.0	81.3	5.306E-02	3320365649.03087
1H-3	1.35	4.35	342.8	78.2	4.638E-02	3320365654.35900
1H-3	1.40	4.40	330.5	82.8	2.155E-02	3320365659.67150
1H-4	0.10	4.60	348.7	81.9	6.082E-02	3320366447.98400
1H-4	0.15	4.65	349.7	84.5	6.157E-02	3320366453.29650
1H-4	0.20	4.70	350.5	85.3	6.132E-02	3320366458.62462
1H-4	0.25	4.75	17.5	87.9	6.054E-02	3320366463.95275
1H-4	0.30	4.80	12.4	87.5	6.067E-02	3320366469.28087
1H-4	0.35	4.85	16.6	88.4	6.063E-02	3320366474.60900
1H-4	0.40	4.90	43.8	89.4	5.854E-02	3320366479.93712
1H-4	0.45	4.95	356.3	87.1	5.930E-02	3320366485.24962

Notes: Time = since 1 January 1904. Only a portion of this table appears here. The complete table is available in [ASCII](#).

Table T20. Paleomagnetic data from archive-half sections, Hole U1331B, at 10 mT AF demagnetization. (See table notes.) (Continued on next three pages.)

Core section	Offset (m)	Depth CSF (m)	Declination (°)	Inclination (°)	Intensity (A/m)	Time (s)
320-U1331B-						
1H-7	0.10	9.10	172.5	18.2	1.314E-03	3320370929.18712
1H-7	0.15	9.15	167.0	18.8	1.310E-03	3320370934.51525
1H-7	0.20	9.20	168.4	29.3	8.813E-04	3320370939.84337
1H-7	0.25	9.25	183.2	48.0	6.595E-04	3320370945.15587
1H-7	0.30	9.30	172.4	45.4	6.980E-04	3320370950.48400
1H-7	0.35	9.35	164.7	44.8	6.425E-04	3320370955.81212
1H-7	0.40	9.40	179.7	47.5	5.432E-04	3320370961.14025
1H-7	0.45	9.45	172.3	45.7	5.529E-04	3320370966.46837
1H-7	0.50	9.50	165.7	65.5	4.109E-04	3320370971.79650
1H-7	0.55	9.55	275.2	70.0	4.560E-04	3320370977.10900
1H-7	0.60	9.60	182.6	37.9	1.044E-03	3320370982.43712
1H-7	0.65	9.65	173.9	8.2	8.768E-04	3320370987.76525
1H-7	0.70	9.70	117.9	-11.3	5.587E-04	3320370993.07775
2H-2	0.10	11.70	257.5	6.9	2.859E-03	3320372318.93712
2H-2	0.15	11.75	260.9	6.2	3.017E-03	3320372324.26525
2H-2	0.20	11.80	261.9	5.5	3.840E-03	3320372329.57775
2H-2	0.25	11.85	256.2	7.7	2.231E-03	3320372334.90587
2H-2	0.30	11.90	105.5	33.1	6.686E-04	3320372340.23400
2H-2	0.35	11.95	84.4	18.1	2.325E-03	3320372345.54650
2H-2	0.40	12.00	83.0	18.1	3.253E-03	3320372350.87462
2H-2	0.45	12.05	81.0	26.1	3.073E-03	3320372356.20275
2H-2	0.50	12.10	79.5	19.9	3.249E-03	3320372361.53087
2H-2	0.55	12.15	77.6	16.9	3.395E-03	3320372366.85900
2H-2	0.60	12.20	78.4	12.6	2.834E-03	3320372372.18712
2H-2	0.65	12.25	77.8	19.5	2.560E-03	3320372377.49962
2H-2	0.70	12.30	77.5	19.5	2.558E-03	3320372382.82775
2H-2	0.75	12.35	77.2	18.9	2.642E-03	3320372388.15587
2H-2	0.80	12.40	78.6	20.7	2.450E-03	3320372393.48400
2H-2	0.85	12.45	80.5	24.3	2.186E-03	3320372398.81212
2H-2	0.90	12.50	81.4	24.0	2.339E-03	3320372404.12462
2H-2	0.95	12.55	81.1	18.2	2.971E-03	3320372409.45275
2H-2	1.00	12.60	82.5	13.3	4.029E-03	3320372414.78087
2H-2	1.05	12.65	82.7	14.4	3.776E-03	3320372420.10900
2H-2	1.10	12.70	84.6	18.5	3.171E-03	3320372425.42150
2H-2	1.15	12.75	83.9	20.4	2.739E-03	3320372430.74962
2H-2	1.20	12.80	82.8	20.6	2.787E-03	3320372436.07775
2H-2	1.25	12.85	82.8	21.1	2.667E-03	3320372441.40587
2H-2	1.30	12.90	82.9	18.5	2.802E-03	3320372446.73400
2H-2	1.35	12.95	81.7	18.9	3.085E-03	3320372452.04650
2H-2	1.40	13.00	81.6	21.1	4.261E-03	3320372457.37462
2H-3	0.10	13.20	92.4	17.7	4.309E-03	3320373682.23400
2H-3	0.15	13.25	96.3	23.9	1.683E-03	3320373687.54650
2H-3	0.20	13.30	237.0	62.7	4.328E-04	3320373692.87462
2H-3	0.25	13.35	262.4	12.3	2.044E-03	3320373698.20275
2H-3	0.30	13.40	260.9	3.6	2.121E-03	3320373703.53087
2H-3	0.35	13.45	263.3	31.4	5.502E-04	3320373708.85900
2H-3	0.40	13.50	100.8	60.4	1.169E-03	3320373714.18712
2H-3	0.45	13.55	94.8	35.8	1.777E-03	3320373719.49962
2H-3	0.50	13.60	90.1	28.6	2.702E-03	3320373724.82775
2H-3	0.55	13.65	89.1	21.5	4.365E-03	3320373730.15587
2H-3	0.60	13.70	89.3	20.0	5.062E-03	3320373735.48400
2H-3	0.65	13.75	89.3	20.9	4.561E-03	3320373740.81212
2H-3	0.70	13.80	89.6	19.7	4.672E-03	3320373746.12462
2H-3	0.75	13.85	88.3	19.6	4.862E-03	3320373751.45275
2H-3	0.80	13.90	87.6	22.0	4.280E-03	3320373756.78087
2H-3	0.85	13.95	88.0	22.8	3.371E-03	3320373762.10900
2H-3	0.90	14.00	86.4	20.9	3.368E-03	3320373767.42150
2H-3	0.95	14.05	86.2	23.5	2.596E-03	3320373772.74962
2H-3	1.00	14.10	86.5	22.7	2.595E-03	3320373778.07775
2H-3	1.05	14.15	85.6	21.3	2.707E-03	3320373783.40587
2H-3	1.10	14.20	88.4	21.5	2.870E-03	3320373788.73400
2H-3	1.15	14.25	87.8	21.9	3.242E-03	3320373794.06212
2H-3	1.20	14.30	87.9	23.4	3.726E-03	3320373799.37462
2H-3	1.25	14.35	88.7	19.9	4.194E-03	3320373804.70275
2H-3	1.30	14.40	88.3	19.1	4.194E-03	3320373810.03087
2H-3	1.35	14.45	88.8	21.0	3.515E-03	3320373815.35900

Table T20 (continued). (Continued on next page.)

Core section	Offset (m)	Depth CSF (m)	Declination (°)	Inclination (°)	Intensity (A/m)	Time (s)
2H-3	1.40	14.50	87.4	32.9	1.827E-03	3320373820.68712
2H-4	0.10	14.70	329.9	29.9	3.120E-03	3320374984.89025
2H-4	0.15	14.75	12.1	17.1	1.683E-03	3320374990.21837
2H-4	0.20	14.80	257.4	19.5	1.101E-03	3320374995.54650
2H-4	0.25	14.85	262.9	7.5	1.252E-03	3320375000.87462
2H-4	0.30	14.90	269.2	7.4	1.748E-03	3320375006.20275
2H-4	0.35	14.95	274.8	6.2	1.473E-03	3320375011.51525
2H-4	0.40	15.00	273.1	5.4	1.955E-03	3320375016.84337
2H-4	0.45	15.05	269.7	6.1	2.067E-03	3320375022.17150
2H-4	0.50	15.10	267.5	3.0	1.675E-03	3320375027.49962
2H-4	0.55	15.15	269.6	-0.6	2.106E-03	3320375032.82775
2H-4	0.60	15.20	270.9	9.0	2.512E-03	3320375038.14025
2H-4	0.65	15.25	270.9	15.8	1.327E-03	3320375043.46837
2H-4	0.70	15.30	269.3	24.3	1.218E-03	3320375048.79650
2H-4	0.75	15.35	268.6	16.6	1.773E-03	3320375054.12462
2H-4	0.80	15.40	268.6	13.3	1.835E-03	3320375059.45275
2H-4	0.85	15.45	262.6	17.7	1.559E-03	3320375064.76525
2H-4	0.90	15.50	263.5	15.3	1.822E-03	3320375070.09337
2H-4	0.95	15.55	268.3	9.3	2.860E-03	3320375075.42150
2H-4	1.00	15.60	267.2	9.6	2.633E-03	3320375080.74962
2H-4	1.05	15.65	267.9	7.8	2.558E-03	3320375086.07775
2H-4	1.10	15.70	268.2	8.5	2.247E-03	3320375091.39025
2H-4	1.15	15.75	267.4	6.6	2.132E-03	3320375096.71837
2H-4	1.20	15.80	268.7	5.9	2.694E-03	3320375102.04650
2H-4	1.25	15.85	268.8	7.4	3.107E-03	3320375107.37462
2H-4	1.30	15.90	268.4	12.7	2.993E-03	3320375112.70275
2H-4	1.35	15.95	268.7	13.5	2.643E-03	3320375118.01525
2H-4	1.40	16.00	262.4	26.8	1.413E-03	3320375123.34337
2H-5	0.10	16.20	142.6	76.5	9.641E-04	3320376261.15587
2H-5	0.15	16.25	115.5	26.8	2.760E-03	3320376266.48400
2H-5	0.20	16.30	114.8	25.2	3.606E-03	3320376271.81212
2H-5	0.25	16.35	117.7	26.9	3.551E-03	3320376277.12462
2H-5	0.30	16.40	117.9	22.3	4.809E-03	3320376282.45275
2H-5	0.35	16.45	117.4	18.3	6.725E-03	3320376287.78087
2H-5	0.40	16.50	116.9	19.3	7.113E-03	3320376293.10900
2H-5	0.45	16.55	116.5	19.3	6.786E-03	3320376298.43712
2H-5	0.50	16.60	117.4	19.9	6.882E-03	3320376303.74962
2H-5	0.55	16.65	119.7	17.4	7.892E-03	3320376309.07775
2H-5	0.60	16.70	118.4	17.3	7.678E-03	3320376314.40587
2H-5	0.65	16.75	118.8	17.6	7.425E-03	3320376319.73400
2H-5	0.70	16.80	112.5	19.4	5.614E-03	3320376325.04650
2H-5	0.75	16.85	121.7	23.4	3.999E-03	3320376330.37462
2H-5	0.80	16.90	126.0	34.7	2.294E-03	3320376335.70275
2H-5	0.85	16.95	230.7	62.7	1.133E-03	3320376341.03087
2H-5	0.90	17.00	299.1	41.0	1.536E-03	3320376346.35900
2H-5	0.95	17.05	304.4	10.1	2.347E-03	3320376351.68712
2H-5	1.00	17.10	299.5	14.8	2.192E-03	3320376356.99962
2H-5	1.05	17.15	288.7	26.3	1.178E-03	3320376362.32775
2H-5	1.10	17.20	290.3	15.8	1.365E-03	3320376367.65587
2H-5	1.15	17.25	292.4	7.9	2.952E-03	3320376372.98400
2H-5	1.20	17.30	298.1	3.1	3.337E-03	3320376378.29650
2H-5	1.25	17.35	296.1	3.1	4.116E-03	3320376383.62462
2H-5	1.30	17.40	301.0	4.2	4.209E-03	3320376388.95275
2H-5	1.35	17.45	301.2	4.8	4.712E-03	3320376394.28087
2H-5	1.40	17.50	299.2	3.8	5.145E-03	3320376399.60900
2H-6	0.10	17.70	297.4	4.2	4.935E-03	3320377648.20275
2H-6	0.15	17.75	296.9	2.3	4.834E-03	3320377653.53087
2H-6	0.20	17.80	300.6	3.9	3.518E-03	3320377658.85900
2H-6	0.25	17.85	301.3	6.5	2.661E-03	3320377664.18712
2H-6	0.30	17.90	301.3	2.2	3.034E-03	3320377669.51525
2H-6	0.35	17.95	303.2	0.9	3.340E-03	3320377674.84337
2H-6	0.40	18.00	300.1	-1.6	4.208E-03	3320377680.17150
2H-6	0.45	18.05	303.2	-0.6	3.996E-03	3320377685.48400
2H-6	0.50	18.10	303.1	0.4	3.681E-03	3320377690.81212
2H-6	0.55	18.15	301.5	-0.2	3.262E-03	3320377696.14025
2H-6	0.60	18.20	300.5	-1.2	3.602E-03	3320377701.45275
2H-6	0.65	18.25	301.4	-1.1	4.042E-03	3320377706.78087
2H-6	0.70	18.30	303.0	1.1	3.486E-03	3320377712.10900
2H-6	0.75	18.35	301.9	1.7	3.429E-03	3320377717.43712

Table T20 (continued). (Continued on next page.)

Core section	Offset (m)	Depth CSF (m)	Declination (°)	Inclination (°)	Intensity (A/m)	Time (s)
2H-6	0.80	18.40	302.6	1.0	3.860E-03	3320377722.76525
2H-6	0.85	18.45	303.4	0.9	3.796E-03	3320377728.09337
2H-6	0.90	18.50	314.4	3.1	2.613E-03	3320377733.42150
2H-6	0.95	18.55	304.5	4.6	2.930E-03	3320377738.73400
2H-6	1.00	18.60	304.2	3.4	3.081E-03	3320377744.06212
2H-6	1.05	18.65	303.5	1.2	3.158E-03	3320377749.39025
2H-6	1.10	18.70	304.8	0.7	2.582E-03	3320377754.70275
2H-6	1.15	18.75	306.9	1.8	2.449E-03	3320377760.03087
2H-6	1.20	18.80	305.4	0.7	2.720E-03	3320377765.35900
2H-6	1.25	18.85	304.1	-2.4	3.304E-03	3320377770.68712
2H-6	1.30	18.90	306.3	-5.1	3.799E-03	3320377776.01525
2H-6	1.35	18.95	310.0	-3.8	3.825E-03	3320377781.34337
2H-6	1.40	19.00	313.4	-1.4	5.128E-03	3320377786.67150
2H-7	0.10	19.20	308.9	-7.4	3.660E-03	3320379769.79650
2H-7	0.15	19.25	309.0	-8.7	3.372E-03	3320379775.10900
2H-7	0.20	19.30	307.6	-9.9	3.420E-03	3320379780.43712
2H-7	0.25	19.35	307.4	-10.3	3.480E-03	3320379785.76525
2H-7	0.30	19.40	306.8	-9.6	3.868E-03	3320379791.07775
2H-7	0.35	19.45	308.2	-10.3	4.173E-03	3320379796.40587
2H-7	0.40	19.50	316.6	-11.9	3.172E-03	3320379801.73400
2H-7	0.45	19.55	273.2	-4.5	7.143E-03	3320379807.06212
2H-7	0.50	19.60	284.9	-22.2	4.429E-03	3320379812.39025
2H-7	0.55	19.65	310.9	-10.4	4.011E-03	3320379817.71837
10H-2	0.10	87.70	258.7	30.2	5.277E-03	3320447104.84337
10H-2	0.15	87.75	237.1	30.8	1.011E-02	3320447110.17150
10H-2	0.20	87.80	211.7	33.9	9.061E-03	3320447115.49962
10H-2	0.25	87.85	240.2	37.0	3.032E-03	3320447120.82775
10H-2	0.30	87.90	269.3	30.7	2.514E-03	3320447126.15587
10H-2	0.35	87.95	322.6	31.2	7.238E-03	3320447131.46837
10H-2	0.40	88.00	94.6	80.9	8.598E-03	3320447136.79650
10H-2	0.45	88.05	199.0	58.1	5.144E-03	3320447142.12462
10H-2	0.50	88.10	250.0	42.0	6.699E-03	3320447147.43712
10H-2	0.55	88.15	224.4	25.7	3.587E-03	3320447152.76525
10H-2	0.60	88.20	254.8	29.4	1.477E-03	3320447158.09337
10H-2	0.65	88.25	328.0	9.1	2.756E-03	3320447163.42150
10H-2	0.70	88.30	114.9	-11.2	6.415E-03	3320447168.74962
10H-2	0.75	88.35	182.9	-52.9	5.292E-03	3320447174.07775
10H-2	0.80	88.40	339.4	-5.0	1.589E-03	3320447179.39025
10H-2	0.85	88.45	70.2	16.8	2.363E-03	3320447184.71837
10H-2	0.90	88.50	67.2	24.8	2.354E-03	3320447190.04650
10H-2	0.95	88.55	93.9	29.7	2.580E-03	3320447195.37462
10H-2	1.00	88.60	86.5	31.6	2.086E-03	3320447200.70275
10H-2	1.05	88.65	77.0	20.5	2.592E-03	3320447206.01525
10H-2	1.10	88.70	77.2	20.7	2.560E-03	3320447211.34337
10H-2	1.15	88.75	78.4	17.2	3.104E-03	3320447216.67150
10H-2	1.20	88.80	80.1	15.4	1.674E-03	3320447221.99962
10H-2	1.25	88.85	90.5	14.7	1.803E-03	3320447227.32775
10H-2	1.30	88.90	117.3	21.4	2.080E-03	3320447232.64025
10H-2	1.35	88.95	77.4	16.2	2.336E-03	3320447237.96837
10H-2	1.40	89.00	65.4	13.1	1.842E-03	3320447243.29650
10H-5	0.10	92.20	89.6	11.4	3.668E-03	3320454345.79650
10H-5	0.15	92.25	88.6	9.4	3.706E-03	3320454351.12462
10H-5	0.20	92.30	88.2	8.1	4.041E-03	3320454356.45275
10H-5	0.25	92.35	86.0	9.7	3.537E-03	3320454361.78087
10H-5	0.30	92.40	87.2	15.0	2.474E-03	3320454367.10900
10H-5	0.35	92.45	91.1	21.1	2.671E-03	3320454372.42150
10H-5	0.40	92.50	92.7	24.6	2.898E-03	3320454377.74962
10H-5	0.45	92.55	91.2	22.2	3.013E-03	3320454383.07775
10H-5	0.50	92.60	90.1	19.8	2.940E-03	3320454388.40587
10H-5	0.55	92.65	90.1	17.7	2.475E-03	3320454393.73400
10H-5	0.60	92.70	92.1	10.1	3.926E-03	3320454399.04650
10H-5	0.65	92.75	90.9	8.1	4.593E-03	3320454404.37462
10H-5	0.70	92.80	91.5	13.1	3.419E-03	3320454409.70275
10H-5	0.75	92.85	92.2	14.5	3.450E-03	3320454415.03087
10H-5	0.80	92.90	92.0	19.7	2.473E-03	3320454420.35900
10H-5	0.85	92.95	89.6	24.9	1.574E-03	3320454425.68712
10H-5	0.90	93.00	87.3	22.0	1.447E-03	3320454430.99962
10H-5	0.95	93.05	86.5	16.8	1.529E-03	3320454436.32775
10H-5	1.00	93.10	85.2	14.3	1.417E-03	3320454441.65587

Table T20 (continued).

Core section	Offset (m)	Depth CSF (m)	Declination (°)	Inclination (°)	Intensity (A/m)	Time (s)
10H-5	1.05	93.15	84.2	14.4	1.360E-03	3320454446.98400
10H-5	1.10	93.20	84.7	17.3	1.201E-03	3320454452.29650
10H-5	1.15	93.25	86.2	24.5	9.479E-04	3320454457.62462
10H-5	1.30	93.40	88.8	29.0	8.368E-04	3320454473.60900
10H-5	1.35	93.45	88.7	28.2	8.386E-04	3320454478.93712
10H-5	1.40	93.50	87.8	27.4	8.482E-04	3320454484.24962

Notes: Time = since 1 January 1904. This table is also available in [ASCII](#).

Table T21. Paleomagnetic data from archive-half sections, Hole U1331B, at 15 mT AF demagnetization. ([See table notes](#).)

Core, section	Offset (m)	Depth CSF (m)	Declination (°)	Inclination (°)	Intensity (A/m)	Time (s)
320-U1331B-						
2H-6	0.10	17.70	296.1	2.6	4.465E-03	3320378520.06212
2H-6	0.15	17.75	296.8	0.9	4.345E-03	3320378525.39025
2H-6	0.20	17.80	298.1	1.9	3.270E-03	3320378530.71837
2H-6	0.25	17.85	299.4	4.0	2.493E-03	3320378536.04650
2H-6	0.30	17.90	300.0	-1.5	2.798E-03	3320378541.37462
2H-6	0.35	17.95	301.9	-0.8	3.045E-03	3320378546.70275
2H-6	0.40	18.00	302.0	-1.3	3.427E-03	3320378552.01525
2H-6	0.45	18.05	302.7	-1.8	3.595E-03	3320378557.34337
2H-6	0.50	18.10	302.9	-0.9	3.356E-03	3320378562.67150
2H-6	0.55	18.15	300.9	-1.5	2.977E-03	3320378567.99962
2H-6	0.60	18.20	300.6	-2.2	3.271E-03	3320378573.32775
2H-6	0.65	18.25	300.6	-1.9	3.659E-03	3320378578.64025
2H-6	0.70	18.30	302.0	-0.2	3.165E-03	3320378583.96837
2H-6	0.75	18.35	302.3	0.5	3.091E-03	3320378589.29650
2H-6	0.80	18.40	302.7	0.0	3.481E-03	3320378594.62462
2H-6	0.85	18.45	303.3	-0.2	3.423E-03	3320378599.95275
2H-6	0.90	18.50	304.8	1.1	2.917E-03	3320378605.26525
2H-6	0.95	18.55	304.7	2.8	2.705E-03	3320378610.59337
2H-6	1.00	18.60	304.5	1.9	2.817E-03	3320378615.92150
2H-6	1.05	18.65	303.7	0.1	2.863E-03	3320378621.24962
2H-6	1.10	18.70	304.1	-0.7	2.368E-03	3320378626.57775
2H-6	1.15	18.75	305.4	0.4	2.238E-03	3320378631.90587
2H-6	1.20	18.80	304.9	-0.3	2.475E-03	3320378637.21837
2H-6	1.25	18.85	304.4	-8.4	3.018E-03	3320378642.54650
2H-6	1.30	18.90	305.5	-5.9	3.443E-03	3320378647.87462
2H-6	1.35	18.95	308.4	-5.2	3.494E-03	3320378653.20275
2H-6	1.40	19.00	307.1	-4.1	3.894E-03	3320378658.53087

Notes: Time = since 1 January 1904. This table is also available in [ASCII](#).



Table T22. Paleomagnetic data from archive-half sections, Hole U1331B, at 20 mT AF demagnetization. (See table notes.)

Core, section	Offset (m)	Depth CSF (m)	Declination (°)	Inclination (°)	Intensity (A/m)	Time (s)	Core mean (°)	Declination	
								Geographical coordinates 0°–360°	–90°–270°
320-U1331B-									
1H-1	1.40	1.40	177.1	12.6	3.251E-03	3320364096.57775	348.55	188.6	188.6
1H-2	0.10	1.60	179.8	19.5	2.289E-03	3320364901.43712	348.55	191.3	191.3
1H-2	0.15	1.65	181.9	17.5	2.282E-03	3320364906.76525	348.55	193.4	193.4
1H-2	0.20	1.70	153.7	10.2	3.311E-03	3320364912.07775	348.55	165.2	165.2
1H-2	0.25	1.75	166.5	3.6	3.358E-03	3320364917.40587	348.55	178.0	178.0
1H-2	0.30	1.80	180.3	7.6	3.544E-03	3320364922.73400	348.55	191.8	191.8
1H-2	0.35	1.85	176.5	10.1	3.483E-03	3320364928.06212	348.55	188.0	188.0
1H-2	0.40	1.90	175.2	9.6	3.342E-03	3320364933.39025	348.55	186.7	186.7
1H-2	0.45	1.95	175.4	8.7	3.324E-03	3320364938.70275	348.55	186.9	186.9
1H-2	0.50	2.00	178.3	9.7	2.895E-03	3320364944.03087	348.55	189.8	189.8
1H-2	0.55	2.05	179.6	15.8	2.309E-03	3320364949.35900	348.55	191.1	191.1
1H-2	0.60	2.10	174.6	13.2	2.370E-03	3320364954.67150	348.55	186.1	186.1
1H-2	0.65	2.15	178.3	8.3	2.796E-03	3320364959.99962	348.55	189.8	189.8
1H-2	0.70	2.20	172.1	2.7	4.036E-03	3320364965.32775	348.55	183.6	183.6
1H-2	0.75	2.25	170.7	5.4	3.286E-03	3320364970.65587	348.55	182.2	182.2
1H-2	0.80	2.30	179.4	33.5	1.224E-03	3320364975.98400	348.55	190.9	190.9
1H-2	0.85	2.35	339.2	54.6	9.385E-04	3320364981.29650	348.55	350.7	-9.3
1H-2	0.90	2.40	350.0	17.0	2.571E-03	3320364986.62462	348.55	1.4	1.4
1H-2	0.95	2.45	349.1	17.3	3.179E-03	3320364991.95275	348.55	0.6	0.6
1H-2	1.00	2.50	347.7	17.6	2.831E-03	3320364997.28087	348.55	359.2	-0.8
1H-2	1.05	2.55	345.3	22.7	1.762E-03	3320365002.60900	348.55	356.8	-3.3
1H-2	1.10	2.60	347.7	25.5	1.423E-03	3320365007.93712	348.55	359.2	-0.8
1H-2	1.15	2.65	345.4	36.3	1.103E-03	3320365013.24962	348.55	356.9	-3.2
1H-2	1.20	2.70	348.8	31.5	1.348E-03	3320365018.57775	348.55	0.3	0.3
1H-2	1.25	2.75	348.4	26.2	1.593E-03	3320365023.90587	348.55	359.9	-0.2
1H-2	1.30	2.80	349.0	21.9	1.870E-03	3320365029.23400	348.55	0.4	0.4
1H-2	1.35	2.85	348.4	16.8	2.422E-03	3320365034.54650	348.55	359.9	-0.2
1H-2	1.40	2.90	352.3	16.9	2.412E-03	3320365039.87462	348.55	3.8	3.8
1H-3	0.10	3.10	346.7	17.7	1.397E-03	3320365971.64025	348.55	358.2	-1.8
1H-3	0.15	3.15	264.5	12.0	2.230E-03	3320365976.96837	348.55	276.0	-84.1
1H-3	0.20	3.20	271.9	7.8	1.435E-03	3320365982.29650	348.55	283.4	-76.7
1H-3	0.25	3.25	352.1	7.1	2.300E-03	3320365987.62462	348.55	3.6	3.6
1H-3	0.30	3.30	349.2	8.0	2.255E-03	3320365992.95275	348.55	0.6	0.6
1H-3	0.35	3.35	346.0	7.3	2.031E-03	3320365998.28087	348.55	357.5	-2.6
1H-3	0.40	3.40	346.5	11.3	1.779E-03	3320366003.59337	348.55	358.0	-2.1
1H-3	0.45	3.45	349.1	11.9	1.954E-03	3320366008.92150	348.55	0.6	0.6
1H-3	0.50	3.50	349.5	12.1	2.115E-03	3320366014.24962	348.55	0.9	0.9
1H-3	0.55	3.55	345.9	17.3	2.352E-03	3320366019.57775	348.55	357.4	-2.7
1H-3	0.60	3.60	341.8	15.1	2.498E-03	3320366024.89025	348.55	353.3	-6.8
1H-3	0.65	3.65	342.6	16.0	2.402E-03	3320366030.21837	348.55	354.1	-5.9
1H-3	0.70	3.70	345.7	14.8	2.721E-03	3320366035.54650	348.55	357.2	-2.8
1H-3	0.75	3.75	344.2	17.0	3.391E-03	3320366040.87462	348.55	355.7	-4.3
1H-3	0.80	3.80	340.9	15.9	3.598E-03	3320366046.20275	348.55	352.4	-7.7
1H-3	0.85	3.85	340.7	17.4	3.263E-03	3320366051.53087	348.55	352.2	-7.8
1H-3	0.90	3.90	342.3	19.0	2.874E-03	3320366056.84337	348.55	353.8	-6.3
1H-3	0.95	3.95	344.4	18.2	2.760E-03	3320366062.17150	348.55	355.9	-4.2
1H-3	1.00	4.00	342.8	17.2	2.897E-03	3320366067.49962	348.55	354.3	-5.8
1H-3	1.05	4.05	335.6	19.5	2.486E-03	3320366072.82775	348.55	347.1	-12.9
1H-3	1.10	4.10	338.1	21.2	2.176E-03	3320366078.14025	348.55	349.6	-10.4
1H-3	1.15	4.15	343.7	13.3	3.624E-03	3320366083.46837	348.55	355.2	-4.8
1H-3	1.20	4.20	334.2	24.4	1.931E-03	3320366088.79650	348.55	345.7	-14.3
1H-3	1.25	4.25	341.3	46.1	9.327E-04	3320366094.12462	348.55	352.8	-7.3
1H-3	1.30	4.30	333.1	27.4	1.761E-03	3320366099.45275	348.55	344.6	-15.4
1H-3	1.35	4.35	338.4	14.9	3.473E-03	3320366104.76525	348.55	349.9	-10.2
1H-3	1.40	4.40	337.6	9.6	2.757E-03	3320366110.09337	348.55	349.1	-10.9
1H-4	0.10	4.60	340.6	17.6	2.629E-03	3320366930.39025	348.55	352.1	-7.9
1H-4	0.15	4.65	11.9	61.6	1.001E-03	3320366935.71837	348.55	23.3	23.3
1H-4	0.20	4.70	171.9	57.5	8.848E-04	3320366941.04650	348.55	183.4	183.4
1H-4	0.25	4.75	172.6	17.3	2.298E-03	3320366946.37462	348.55	184.1	184.1
1H-4	0.30	4.80	162.4	9.1	2.205E-03	3320366951.70275	348.55	173.9	173.9
1H-4	0.35	4.85	161.4	12.4	2.483E-03	3320366957.01525	348.55	172.9	172.9
1H-4	0.40	4.90	155.9	8.8	3.147E-03	3320366962.34337	348.55	167.4	167.4

Notes: Time = since 1 January 1904. Only a portion of this table appears here. The complete table is available in [ASCII](#).



Table T23. Paleomagnetic data from archive-half sections, Hole U1331C, at 0 mT AF demagnetization. ([See table notes](#).)

Core, section	Offset (m)	Depth CSF (m)	Declination (°)	Inclination (°)	Intensity (A/m)	Time (s)
320-U1331C-						
1H-1	0.15	0.15	52.9	76.9	4.201E-02	3320522098.34337
1H-1	0.20	0.20	32.2	77.6	4.390E-02	3320522103.67150
1H-1	0.25	0.25	44.6	82.4	4.288E-02	3320522108.99962
1H-1	0.30	0.30	45.0	81.8	4.473E-02	3320522114.32775
1H-1	0.35	0.35	41.6	82.1	4.639E-02	3320522119.65587
1H-1	0.40	0.40	34.3	82.8	4.772E-02	3320522124.98400
1H-1	0.45	0.45	34.2	82.1	4.834E-02	3320522130.31212
1H-1	0.50	0.50	38.8	83.9	4.819E-02	3320522135.62462
1H-1	0.55	0.55	40.5	85.4	4.786E-02	3320522140.95275
1H-1	0.60	0.60	46.2	85.9	4.666E-02	3320522146.28087
1H-1	0.65	0.65	10.7	87.1	4.603E-02	3320522151.60900
1H-1	0.70	0.70	23.2	86.5	4.463E-02	3320522156.93712
1H-1	0.75	0.75	22.3	85.6	4.387E-02	3320522162.26525
1H-1	0.80	0.80	16.2	85.9	4.272E-02	3320522167.59337
1H-1	0.85	0.85	31.1	87.5	4.126E-02	3320522172.92150
1H-1	0.90	0.90	51.5	89.2	4.007E-02	3320522178.24962
1H-1	0.95	0.95	358.6	88.7	3.930E-02	3320522183.57775
1H-1	1.00	1.00	37.5	88.6	3.872E-02	3320522188.89025
1H-1	1.05	1.05	38.4	88.2	3.812E-02	3320522194.21837
1H-1	1.10	1.10	29.3	88.1	3.735E-02	3320522199.54650
1H-1	1.15	1.15	110.7	89.1	3.591E-02	3320522204.87462
1H-1	1.20	1.20	149.6	89.0	3.558E-02	3320522210.20275
1H-1	1.25	1.25	193.4	88.2	3.544E-02	3320522215.53087
1H-1	1.30	1.30	164.3	87.8	3.544E-02	3320522220.85900
1H-1	1.35	1.35	158.4	88.4	3.510E-02	3320522226.17150
1H-1	1.40	1.40	116.1	87.6	3.516E-02	3320522231.49962
1H-2	0.10	1.60	136.7	88.2	3.479E-02	3320524464.54650
1H-2	0.15	1.65	130.7	88.7	3.403E-02	3320524469.87462
1H-2	0.20	1.70	113.3	87.7	3.229E-02	3320524475.20275
1H-2	0.25	1.75	109.8	85.4	3.072E-02	3320524480.53087
1H-2	0.30	1.80	104.7	85.4	3.146E-02	3320524485.85900
1H-2	0.35	1.85	115.8	87.2	3.286E-02	3320524491.17150
1H-2	0.40	1.90	128.0	87.5	3.368E-02	3320524496.49962
1H-2	0.45	1.95	126.6	86.8	3.394E-02	3320524501.82775
1H-2	0.50	2.00	129.6	86.1	3.430E-02	3320524507.15587
1H-2	0.55	2.05	129.3	86.1	3.512E-02	3320524512.46837
1H-2	0.60	2.10	124.2	86.2	3.626E-02	3320524517.79650
1H-2	0.65	2.15	107.0	86.1	3.709E-02	3320524523.12462
1H-2	0.70	2.20	80.1	86.4	3.821E-02	3320524528.45275
1H-2	0.75	2.25	114.3	86.2	3.854E-02	3320524533.76525
1H-2	0.80	2.30	133.7	85.3	3.834E-02	3320524539.09337
1H-2	0.85	2.35	134.2	85.8	3.870E-02	3320524544.42150
1H-2	0.90	2.40	98.6	87.3	3.927E-02	3320524549.74962
1H-2	0.95	2.45	63.7	85.1	3.968E-02	3320524555.07775
1H-2	1.00	2.50	52.1	84.7	4.026E-02	3320524560.39025
1H-2	1.05	2.55	36.4	83.1	4.090E-02	3320524565.71837
1H-2	1.10	2.60	38.1	82.7	4.101E-02	3320524571.04650
1H-2	1.15	2.65	59.6	83.3	4.044E-02	3320524576.37462
1H-2	1.20	2.70	79.3	84.7	3.829E-02	3320524581.70275
1H-2	1.25	2.75	93.7	86.3	3.570E-02	3320524587.01525
1H-2	1.30	2.80	87.8	86.3	3.434E-02	3320524592.34337
1H-2	1.35	2.85	63.1	85.3	3.599E-02	3320524597.67150
1H-2	1.40	2.90	50.3	84.2	3.683E-02	3320524602.99962
1H-3	0.10	3.10	35.2	78.1	3.299E-02	3320527166.18712
1H-3	0.15	3.15	29.9	79.6	3.286E-02	3320527171.51525
1H-3	0.20	3.20	38.4	80.3	3.225E-02	3320527176.84337
1H-3	0.25	3.25	34.7	79.4	3.246E-02	3320527182.17150
1H-3	0.30	3.30	33.5	79.4	3.395E-02	3320527187.48400
1H-3	0.35	3.35	33.5	80.4	3.584E-02	3320527192.81212
1H-3	0.40	3.40	27.7	82.0	3.709E-02	3320527198.14025
1H-3	0.45	3.45	39.4	80.6	3.719E-02	3320527203.46837
1H-3	0.50	3.50	35.7	77.8	3.872E-02	3320527208.78087
1H-3	0.55	3.55	36.7	77.9	4.043E-02	3320527214.10900

Notes: Time = since 1 January 1904. Only a portion of this table appears here. The complete table is available in [ASCII](#).

Table T24. Paleomagnetic data from archive-half sections, Hole U1331C, at 10 mT AF demagnetization. (See table notes.)

Core, section	Offset (m)	Depth CSF (m)	Declination (°)	Inclination (°)	Intensity (A/m)	Time (s)
320-U1331C-						
17H-3	0.10	187.10	295.3	82.6	2.408E-02	3320622741.16512
17H-3	0.15	187.15	306.8	82.9	2.799E-02	3320622746.49325
17H-3	0.20	187.20	282.6	83.1	2.823E-02	3320622751.82137
17H-3	0.25	187.25	279.2	82.0	2.855E-02	3320622757.14950
17H-3	0.30	187.30	321.2	84.9	3.126E-02	3320622762.47762
17H-3	0.35	187.35	33.0	81.4	3.235E-02	3320622767.79012
17H-3	0.40	187.40	42.7	75.9	3.644E-02	3320622773.11825
17H-3	0.45	187.45	67.9	80.1	3.722E-02	3320622778.44637
17H-3	0.50	187.50	84.8	81.4	3.610E-02	3320622783.77450
17H-3	0.55	187.55	39.8	85.8	3.558E-02	3320622789.10262
17H-3	0.60	187.60	216.6	87.2	2.783E-02	3320622794.41512
17H-3	0.65	187.65	192.5	86.9	1.974E-02	3320622799.74325
17H-3	0.70	187.70	199.1	84.5	1.223E-02	3320622805.07137
17H-3	0.75	187.75	157.5	71.6	5.452E-03	3320622810.39950
17H-3	0.80	187.80	111.5	72.9	3.080E-03	3320622815.72762
17H-3	0.85	187.85	48.6	67.5	2.865E-03	3320622821.05575
17H-3	0.90	187.90	37.2	49.9	4.498E-03	3320622826.36825

Notes: Time = since 1 January 1904. This table is also available in [ASCII](#).



Table T25. Paleomagnetic data from archive-half sections, Hole U1331C, at 20 mT AF demagnetization. (See table notes.)

Core, section	Offset (m)	Depth CSF (m)	Declination (°)	Inclination (°)	Intensity (A/m)	Time (s)	Declination		
							Core mean (°)	Geographical coordinates	
								0°–360°	-90°–270°
320-U1331C-									
1H-1	0.15	0.15	78.1	26.7	2.586E-03	3320522524.96837	45.28	32.8	32.8
1H-1	0.20	0.20	65.7	32.9	2.234E-03	3320522530.29650	45.28	20.4	20.4
1H-1	0.25	0.25	61.5	33.0	2.360E-03	3320522535.62462	45.28	16.2	16.2
1H-1	0.30	0.30	52.5	32.7	2.458E-03	3320522540.95275	45.28	7.2	7.2
1H-1	0.35	0.35	53.3	34.5	2.391E-03	3320522546.28087	45.28	8.0	8.0
1H-1	0.40	0.40	46.3	35.6	2.228E-03	3320522551.59337	45.28	1.0	1.0
1H-1	0.45	0.45	33.7	42.1	1.743E-03	3320522556.92150	45.28	348.4	-11.6
1H-1	0.50	0.50	320.0	54.7	1.322E-03	3320522562.24962	45.28	274.7	-85.3
1H-1	0.55	0.55	218.6	79.7	1.047E-03	3320522567.56212	45.28	173.3	173.3
1H-1	0.60	0.60	231.3	64.7	1.134E-03	3320522572.89025	45.28	186.0	186.0
1H-1	0.65	0.65	250.8	33.3	1.884E-03	3320522578.20275	45.28	205.5	205.5
1H-1	0.70	0.70	232.0	46.6	1.400E-03	3320522583.53087	45.28	186.7	186.7
1H-1	0.75	0.75	230.7	48.8	1.234E-03	3320522588.85900	45.28	185.4	185.4
1H-1	0.80	0.80	200.8	26.1	1.756E-03	3320522594.18712	45.28	155.5	155.5
1H-1	0.85	0.85	214.1	31.8	1.472E-03	3320522599.51525	45.28	168.8	168.8
1H-1	0.90	0.90	214.5	22.4	1.844E-03	3320522604.82775	45.28	169.2	169.2
1H-1	0.95	0.95	215.5	19.7	1.944E-03	3320522610.15587	45.28	170.2	170.2
1H-1	1.00	1.00	213.2	21.6	1.825E-03	3320522615.48400	45.28	167.9	167.9
1H-1	1.05	1.05	208.6	23.8	1.683E-03	3320522620.81212	45.28	163.3	163.3
1H-1	1.10	1.10	204.5	25.5	1.581E-03	3320522626.14025	45.28	159.2	159.2
1H-1	1.15	1.15	204.1	22.7	1.744E-03	3320522631.45275	45.28	158.8	158.8
1H-1	1.20	1.20	202.6	18.5	2.058E-03	3320522636.78087	45.28	157.3	157.3
1H-1	1.25	1.25	204.3	16.0	2.269E-03	3320522642.10900	45.28	159.0	159.0
1H-1	1.30	1.30	205.9	15.3	2.563E-03	3320522647.42150	45.28	160.6	160.6
1H-1	1.35	1.35	202.0	15.5	2.513E-03	3320522652.74962	45.28	156.7	156.7
1H-1	1.40	1.40	194.2	14.4	2.382E-03	3320522658.07775	45.28	148.9	148.9
1H-2	0.10	1.60	191.9	19.9	2.341E-03	3320525834.12462	45.28	146.6	146.6
1H-2	0.15	1.65	195.6	15.5	2.101E-03	3320525839.45275	45.28	150.3	150.3
1H-2	0.20	1.70	185.3	17.0	1.883E-03	3320525844.76525	45.28	140.0	140.0
1H-2	0.25	1.75	172.4	15.0	1.896E-03	3320525850.09337	45.28	127.1	127.1
1H-2	0.30	1.80	167.7	10.5	2.000E-03	3320525855.42150	45.28	122.4	122.4
1H-2	0.35	1.85	177.6	5.6	2.140E-03	3320525860.74962	45.28	132.3	132.3
1H-2	0.40	1.90	185.7	8.2	2.235E-03	3320525866.07775	45.28	140.4	140.4
1H-2	0.45	1.95	185.9	11.5	2.232E-03	3320525871.39025	45.28	140.6	140.6
1H-2	0.50	2.00	176.7	12.0	2.403E-03	3320525876.71837	45.28	131.4	131.4
1H-2	0.55	2.05	175.9	10.5	2.730E-03	3320525882.04650	45.28	130.6	130.6
1H-2	0.60	2.10	179.1	15.4	2.583E-03	3320525887.37462	45.28	133.8	133.8
1H-2	0.65	2.15	171.8	15.8	2.397E-03	3320525892.70275	45.28	126.5	126.5
1H-2	0.70	2.20	163.0	18.9	2.154E-03	3320525898.01525	45.28	117.7	117.7
1H-2	0.75	2.25	166.9	21.1	2.094E-03	3320525903.34337	45.28	121.6	121.6
1H-2	0.80	2.30	175.5	15.4	2.677E-03	3320525908.67150	45.28	130.2	130.2
1H-2	0.85	2.35	178.6	19.1	3.215E-03	3320525913.99962	45.28	133.3	133.3
1H-2	0.90	2.40	176.6	21.8	2.576E-03	3320525919.32775	45.28	131.3	131.3
1H-2	0.95	2.45	154.9	47.1	1.697E-03	3320525924.64025	45.28	109.6	109.6
1H-2	1.00	2.50	115.2	56.8	1.557E-03	3320525929.96837	45.28	69.9	69.9
1H-2	1.05	2.55	52.4	55.8	1.527E-03	3320525935.29650	45.28	7.1	7.1
1H-2	1.10	2.60	43.7	32.1	2.316E-03	3320525940.62462	45.28	358.4	-1.6
1H-2	1.15	2.65	34.8	31.3	2.240E-03	3320525945.95275	45.28	349.5	-10.5
1H-2	1.20	2.70	36.3	31.8	2.087E-03	3320525951.28087	45.28	351.0	-9.0
1H-2	1.25	2.75	36.2	34.0	1.835E-03	3320525956.59337	45.28	350.9	-9.1
1H-2	1.30	2.80	35.0	37.2	1.646E-03	3320525961.92150	45.28	349.7	-10.3
1H-2	1.35	2.85	39.8	46.8	1.373E-03	3320525967.24962	45.28	354.5	-5.5
1H-2	1.40	2.90	35.2	45.7	1.425E-03	3320525972.57775	45.28	349.9	-10.1
1H-3	0.10	3.10	38.4	16.1	2.100E-03	3320527590.03087	45.28	353.1	-6.9
1H-3	0.15	3.15	37.9	15.8	2.003E-03	3320527595.34337	45.28	352.6	-7.4
1H-3	0.20	3.20	35.9	16.9	1.666E-03	3320527600.67150	45.28	350.6	-9.4
1H-3	0.25	3.25	36.4	14.1	1.713E-03	3320527605.99962	45.28	351.1	-8.9
1H-3	0.30	3.30	34.5	16.9	1.913E-03	3320527611.32775	45.28	349.2	-10.8
1H-3	0.35	3.35	36.6	30.7	1.804E-03	3320527616.64025	45.28	351.3	-8.7
1H-3	0.40	3.40	39.7	38.2	1.276E-03	3320527621.96837	45.28	354.4	-5.6
1H-3	0.45	3.45	38.7	26.6	1.514E-03	3320527627.29650	45.28	353.4	-6.6
1H-3	0.50	3.50	36.0	14.1	2.754E-03	3320527632.62462	45.28	350.7	-9.3

Notes: Time = since 1 January 1904. Only a portion of this table appears here. The complete table is available in [ASCII](#).



Table T26. Mean paleomagnetic direction for each core, Site U1331. (See table notes.)

Core	Inclination (°)	Declination (°)	N	R	k	α_{95} (°)
320-U1331A-						
1H	7.01	318.76	80	74.3795	14.1	4.4
2H	6.5	106.42	144	131.6710	11.6	3.6
3H	11.6	152.58	109	105.3198	29.3	2.5
4H	8.39	61.23	125	122.9199	59.6	1.6
5H	10.57	157.05	131	126.2611	27.4	2.4
6H	8.86	313.96	123	120.4516	47.9	1.9
7H	6.14	5.25	160	156.0028	39.8	1.8
8H	-23.1	238.79	192	158.6949	5.7	4.7
9H	-24.47	116.61	133	112.4895	6.4	5.2
10H	-8.09	18.08	107	102.6144	24.2	2.8
11H	-2.39	225.94	119	115.7826	36.7	2.2
12H	8.35	245.7	150	145.0188	29.9	2.1
13H	19.97	61.18	100	89.6990	9.6	4.8
14H	-0.44	195.55	134	128.2915	23.3	2.6
15H	-15.61	312.35	83	35.2078	1.7	18.3
320-U1331B-						
1H	0.9	348.55	134	121.4917	10.6	3.9
2H	6.25	101.68	127	115.7427	11.2	3.9
3H	1.72	109.25	141	139.1949	77.6	1.4
4H	-6.58	58.59	103	100.0984	35.2	2.4
5H	7.91	89.42	129	125.9339	41.7	1.9
6H	9.25	187.88	102	100.8677	89.2	1.5
7H	0.54	308.69	126	123.0955	43.0	1.9
8H	-19.28	159.35	137	114.2817	6.0	5.4
9H	-17.58	39.45	119	93.4522	4.6	6.8
10H	-10.07	264.48	140	130.4034	14.5	3.2
11H	7.64	104.8	139	134.0683	28.0	2.3
12H	11.16	225.9	156	151.8367	37.2	1.9
13H	-2.54	116.86	102	97.8268	24.2	2.9
14H	-11.02	311.93	142	136.4178	25.3	2.4
15H	-16.76	349.94	20	18.8458	16.5	8.3
16H	6.31	338.77	44	42.2418	24.5	4.4
17H	8.39	34.41	145	134.0560	13.2	3.4
320-U1331C-						
1H	3.69	45.28	101	92.7850	12.2	4.2
2H	5.98	163.54	138	130.7829	19.0	2.8
3H	9.98	83.75	135	130.0236	26.9	2.4
4H	-9.6	62.19	106	73.4701	3.2	9.2
6H	2.41	126.43	141	132.2467	16.0	3.1
8H	42.51	214.51	79	75.9211	25.3	3.2
10H	7.38	262.94	109	105.6384	32.1	2.4
12H	5.64	109.41	149	147.9859	145.9	1.0
13H	3.33	215.45	148	142.7156	27.8	2.2
14H	0.11	297.26	148	141.1144	21.3	2.6
16H	7.49	249.12	105	98.5630	16.2	3.5
17H	13.78	41.3	28	20.0352	3.4	17.6

Notes: Mean paleomagnetic directions and statistics calculated using Fisher statistics for each core. We used data from stable polarity intervals.

Reversed polarity intervals were inverted prior to computing mean directions and statistics. Inclination = mean paleomagnetic inclination from stable polarity intervals in core, declination = mean paleomagnetic declination from stable polarity intervals in core. By subtracting this value from observed paleomagnetic declinations measured along core, core can be approximately reoriented back into geographic coordinates. After reorientation, normal polarity intervals will have ~0° declination and reversed polarity intervals will have ~180° declination. N = number of paleomagnetic observations used in calculating mean, R = resultant vector length from summing N vectors (directions or poles), k = precision parameter from Fisher statistical calculations, α_{95} = 95% confidence angle for mean direction.



Table T27. Paleomagnetic results for discrete samples, Hole U1331A. ([See table notes.](#))

Core, section, interval (cm)	Depth CSF (m)	Demag (mT)	Declination				Inclination (°)	Intensity (A/m)
			Azimuthally unoriented (°)	Geographical coordinates				
				0°–360°	–90°–270°			
320-U1331A-								
1H-1, 45	0.45	0	7.2	48.5	48.5	67.6	3.601E-02	
1H-1, 45	0.45	5	11.6	52.8	52.8	40.4	1.199E-02	
1H-1, 45	0.45	10	11.9	53.2	53.2	25.2	8.068E-03	
1H-1, 45	0.45	15	11.1	52.4	52.4	24.4	7.441E-03	
1H-1, 45	0.45	20	11.3	52.5	52.5	26.6	6.409E-03	
1H-1, 45	0.45	25	11.1	52.3	52.3	28.2	5.653E-03	
1H-1, 45	0.45	30	11.6	52.8	52.8	30.8	4.633E-03	
1H-1, 45	0.45	35	8.1	49.4	49.4	32.8	3.595E-03	
1H-1, 45	0.45	40	9.8	51.0	51.0	37.7	2.667E-03	
1H-1, 45	0.45	50	13.4	54.6	54.6	37.2	2.001E-03	
1H-1, 45	0.45	60	8.0	49.2	49.2	48.7	1.929E-03	
1H-1, 45	0.45	70	-174.9	226.4	226.4	61.1	1.485E-03	
1H-1, 45	0.45	80	5.8	47.0	47.0	80.8	1.763E-03	
1H-2, 85	2.37	0	172.4	213.7	213.7	85.7	2.256E-02	
1H-2, 85	2.37	5	144.8	186.0	186.0	37.4	3.774E-03	
1H-2, 85	2.37	10	143.5	184.8	184.8	17.3	3.895E-03	
1H-2, 85	2.37	15	143.4	184.6	184.6	17.0	3.453E-03	
1H-2, 85	2.37	20	146.0	187.3	187.3	16.7	2.933E-03	
1H-2, 85	2.37	25	146.9	188.1	188.1	18.7	2.472E-03	
1H-2, 85	2.37	30	145.0	186.2	186.2	25.8	1.818E-03	
1H-2, 85	2.37	35	150.1	191.3	191.3	25.6	1.433E-03	
1H-2, 85	2.37	40	145.7	187.0	187.0	40.6	1.277E-03	
1H-2, 85	2.37	50	157.5	198.8	198.8	58.1	1.074E-03	
1H-2, 85	2.37	60	135.7	176.9	176.9	69.8	1.183E-03	
1H-2, 85	2.37	70	24.2	65.4	65.4	71.6	1.233E-03	
1H-2, 85	2.37	80	11.3	52.5	52.5	73.3	1.075E-03	
1H-3, 85	3.84	0	-54.5	346.7	-13.3	75.9	2.743E-02	
1H-3, 85	3.84	5	-47.9	353.4	-6.6	20.4	4.532E-03	
1H-3, 85	3.84	10	-47.5	353.7	-6.3	6.3	2.770E-03	
1H-3, 85	3.84	15	-47.9	353.4	-6.6	5.5	2.262E-03	
1H-3, 85	3.84	20	-46.8	354.4	-5.6	3.4	1.786E-03	
1H-3, 85	3.84	25	-46.2	355.0	-5.0	9.0	1.445E-03	
1H-3, 85	3.84	30	-45.9	355.4	-4.6	20.2	1.160E-03	
1H-3, 85	3.84	35	-46.2	355.1	-4.9	18.2	7.570E-04	
1H-3, 85	3.84	40	-56.3	344.9	-15.1	33.9	5.255E-04	
1H-3, 85	3.84	50	-36.7	4.5	4.5	74.4	6.023E-04	
1H-3, 85	3.84	60	-60.3	340.9	-19.1	77.6	8.067E-04	
1H-3, 85	3.84	70	-154.7	246.5	246.5	69.6	6.978E-04	
1H-3, 85	3.84	80	-6.6	34.7	34.7	57.0	1.276E-03	
1H-4, 20	4.7	0	-38.5	2.8	2.8	72.7	4.012E-02	
1H-4, 20	4.7	5	-43.3	358.0	-2.0	21.7	7.552E-03	
1H-4, 20	4.7	10	-44.8	356.4	-3.6	8.2	4.872E-03	
1H-4, 20	4.7	15	-45.6	355.6	-4.4	7.5	3.966E-03	
1H-4, 20	4.7	20	-45.0	356.2	-3.8	8.2	3.158E-03	
1H-4, 20	4.7	25	-45.8	355.4	-4.6	9.6	2.560E-03	
1H-4, 20	4.7	30	-43.5	357.7	-2.3	15.8	2.022E-03	
1H-4, 20	4.7	35	-48.3	352.9	-7.1	15.9	1.518E-03	
1H-4, 20	4.7	40	-49.7	351.5	-8.5	29.0	1.205E-03	
1H-4, 20	4.7	50	-34.9	6.3	6.3	48.8	1.408E-03	
1H-4, 20	4.7	60	-43.4	357.9	-2.1	58.7	1.205E-03	
1H-4, 20	4.7	70	-34.5	6.7	6.7	70.7	1.271E-03	
1H-4, 20	4.7	80	-10.2	31.0	31.0	56.8	1.912E-03	
2H-1, 85	6.05	0	-69.4	184.1	184.1	78.0	1.642E-02	
2H-1, 85	6.05	5	-72.5	181.0	181.0	39.2	2.398E-03	
2H-1, 85	6.05	10	-70.8	182.8	182.8	5.6	1.863E-03	
2H-1, 85	6.05	15	-70.0	183.6	183.6	0.4	1.797E-03	
2H-1, 85	6.05	20	-69.7	183.9	183.9	0.4	1.528E-03	
2H-1, 85	6.05	25	-68.8	184.8	184.8	2.0	1.213E-03	
2H-1, 85	6.05	30	-65.9	187.7	187.7	8.7	9.316E-04	
2H-1, 85	6.05	35	-70.6	183.0	183.0	17.3	7.863E-04	
2H-1, 85	6.05	40	-63.2	190.4	190.4	26.6	6.651E-04	
2H-1, 85	6.05	50	-74.4	179.2	179.2	39.2	5.465E-04	

Notes: Demag = demagnetization step in mT for steps <80 and in °C for steps ≥90. Only a portion of this table appears here. The complete table is available in [ASCII](#).

Table T28. Principal component analysis (PCA) results for paleomagnetic data, Hole U1331A. ([See table notes.](#))
(Continued on next page.)

Core, section, interval (cm)	Depth CSF (m)	PCA						Archive-half section at 20 mT AF demagnetization (°)	
		Declination		Geographical coordinates (0°–360°)	Inclination (°)	MAD (°)	Range (mT)		
		Azimuthally unoriented (°)	Geographical coordinates (0°–360°)				Declination	Inclination	
320-U1331A-									
1H-1, 45	0.45	12.0	53.04	19.6	3.3	10–50	2.6	12.6	
1H-2, 85	2.37	140.8	182.54	10.7	5.0	10–35	138.4	6.3	
1H-3, 85	3.84	312.1	354.84	13.1	14.7	5–50	307.2	12.1	
1H-4, 20	4.70	314.5	357.94	3.4	4.4	10–30	314.8	15.8	
2H-1, 85	6.05	289.5	183.38	-11.6	8.6	10–60	313.1	-38.6	
2H-2, 85	7.57	285.1	178.98	-27.5	6.4	10–50	287.9	-6.9	
2H-3, 85*	9.04	296.7	191.78	11.5	9.5	250–450	282.3	-4.5	
2H-4, 85	10.54	280.5	173.78	-11.2	10.9	10–35	251.1	10.7	
2H-5, 85	12.07	112.2	7.08	8.5	3.6	10–30	113.0	11.0	
2H-6, 85	13.54								
2H-7, 35	14.56	291.1	184.88	-15.9	7.7	10–35	291.9	-2.3	
3H-1, 110	15.79	321.1	172.32	-4.4	9.2	10–30	319.1	-12.0	
3H-2, 110	17.33	323.6	168.42	-14.0	4.1	15–60	322.9	-12.8	
3H-3, 110*	18.79	335.6	180.02	25.3	7.4	250–450	330.1	-15.9	
3H-4, 110	20.29	319.0	167.22	-10.0	7.4	10–60	326.7	-15.9	
3H-5, 110	21.83	334.3	183.12	-10.3	5.1	10–30	339.0	-8.3	
3H-6, 110	23.29	153.7	0.22	-10.7	3.0	5–50	337.5	-12.7	
4H-2, 85	26.58	241.1	181.97	6.5	6.3	10–30	230.3	8.7	
4H-3, 85	28.04	234.3	172.57	-9.8	2.6	10–50	247.9	-3.7	
4H-4, 85	29.55	244.7	183.57	-12.9	2.9	10–40	238.5	-14.4	
4H-5, 85	31.08	240.9	178.07	-26.4	3.9	10–30	243.9	-8.2	
4H-6, 85	32.55	66.7	359.97	7.7	6.5	10–30	58.7	16.4	
5H-1, 85	34.55	115.2	319.45	-3.0	1.8	10–30	113.1	-0.5	
5H-2, 85	36.05	134.8	339.45	13.9	3.8	10–35	122.1	14.8	
5H-3, 85*	37.58	163.5	7.45	30.1	10.2	250–450	158.0	10.2	
5H-4, 85	39.04	351.8	194.55	-18.1	3.6	10–30	341.4	-12.2	
5H-5, 85	40.54	166.4	9.85	17.4	2.8	10–30	164.9	16.9	
5H-6, 85	42.03	170.3	13.25	19.7	2.8	10–50	167.1	14.9	
6H-1, 85	44.04	305.0	356.54	11.9	5.7	10–30	301.0	13.0	
6H-2, 85	45.54	315.6	1.74	4.1	3.4	10–30	300.7	7.8	
6H-3, 85*	47.07	122.5	169.44	34.5	8.6	250–450	127.7	-1.2	
6H-4, 85	48.54	250.8	295.34	2.4	17.9	10–50	303.5	9.2	
6H-5, 85	50.03	313.4	1.14	0.8	5.6	10–40	311.9	4.6	
6H-6, 85	51.55	316.5	7.74	4.3	7.8	10–50	319.0	13.2	
6H-7, 40	52.09	319.2	6.44	10.4	4.9	10–40	307.1	12.0	
7H-1, 85	53.54	352.0	347.05	4.9	5.3	10–35	350.9	0.9	
7H-2, 85	55.05	351.9	346.85	2.2	2.6	10–35	358.3	5.8	
7H-3, 85*	56.57	199.3	192.95	6.3	6.3	250–450	192.7	-11.5	
7H-4, 85	58.04	2.3	356.65	-0.7	2.4	15–40	6.3	-3.4	
7H-5, 85	59.54	6.1	0.45	4.6	1.6	20–40	6.1	10.1	
7H-6, 85	61.04	30.7	26.85	-6.3	3.4	10–35	29.3	9.5	
7H-7, 40	62.09	29.9	25.05	0.9	5.9	10–30	29.1	5.7	
8H-1, 85	63.04	55.6	175.81	3.7	5.4	10–40	54.7	-4.4	
8H-2, 85	64.54	58.7	178.71	-17.0	3.5	10–30	59.7	-11.3	
8H-3, 85*	66.07	63.1	180.21	19.1	7.2	250–450	48.9	-3.8	
8H-4, 85	67.55	62.2	183.21	-5.9	2.7	10–40	51.3	-5.0	
8H-5, 85	69.05	80.1	199.71	-18.1	1.9	10–30	70.6	-1.8	
8H-6, 85	70.54								
8H-7, 55	71.76								
9H-2, 85	74.04	289.2	172.79	1.8	4.3	10–40	290.3	-0.8	
9H-3, 85*	75.57	280.3	163.59	15.1	15.2	300–600	298.4	10.5	
9H-4, 83	77.04	298.4	183.59	0.5	2.7	10–35	305.5	-0.1	
9H-5, 85	78.54								
9H-6, 85	80.04								
9H-7, 85	81.34								
10H-2, 85	83.54								
10H-3, 85*	85.08	23.9	8.52	24.2	7.8	350–550	15.2	0.2	
10H-4, 85	86.54	4.9	347.02	-0.0	5.5	10–40	8.7	-0.5	
10H-5, 85	88.05	199.4	182.92	1.4	7.6	10–40	202.1	20.7	
10H-6, 85	89.54	213.0	194.32	14.2	10.8	10–30	200.7	28.6	
11H-2, 85	92.23	42.6	175.46	-11.8	6.6	10–35	24.6	0.3	
11H-3, 85*	93.75								
11H-4, 85	95.23	43.3	177.36	-6.4	3.6	10–40	33.9	-1.0	



Table T28 (continued).

Core, section, interval (cm)	Depth CSF (m)	PCA					Archive-half section at 20 mT AF demagnetization (°)		
		Declination		Geographical coordinates (0°–360°)	Inclination (°)	MAD (°)	Range (mT)	Declination	Inclination
		Azimuthally unoriented (°)	Geographical coordinates (0°–360°)						
11H-5, 85	96.73	62.7	197.96	1.6	4.8	10–30	54.9	-3.0	
11H-6, 85	98.23	45.3	176.26	-3.4	2.6	10–30	55.3	-6.6	
12H-1, 85	101.05	248.8	1.30	-2.2	5.0	10–30	298.3	1.7	
12H-2, 85	102.54	239.7	352.40	14.3	4.7	10–30	208.9	29.3	
12H-3, 85*	104.07	231.9	345.60	28.7	7.3	300–550	238.9	7.4	
12H-4, 85	105.55	253.1	7.30	3.9	2.5	15–35	234.4	17.0	
12H-5, 85	107.05	255.1	7.60	-4.3	2.0	10–30	248.8	4.1	
12H-6, 85	108.55	260.2	15.10	7.4	6.0	10–30	254.6	10.5	
12H-7, 40	109.59	255.0	10.10	-5.9	5.0	10–30	259.1	20.9	
13H-1, 85	110.54	33.0	333.82	2.5	4.1	10–35	123.7	14.1	
13H-2, 85	112.05	39.5	338.42	11.3	9.3	5–25	72.1	1.6	
13H-3, 85*	113.55								
13H-4, 85	115.05	69.8	2.62	12.3	9.7	5–50	58.1	14.8	
13H-5, 85	116.54	62.4	0.12	-8.4	16.8	10–60	43.1	58.2	
13H-6, 85	118.05	66.2	2.22	13.1	6.6	5–30	68.1	7.1	
13H-7, 40	119.09	262.2	199.82	3.8	4.7	10–35	252.8	-23.2	
14H-1, 85	120.05	358.7	163.15	-2.8	4.4	10–35	0.2	1.7	
14H-2, 85	121.52	7.2	174.45	11.2	6.8	10–30	2.1	18.0	
14H-3, 85*	123.05								
14H-4, 85	124.52	23.7	188.35	-11.9	3.0	5–50	27.0	-12.1	
14H-5, 85	126.02	33.6	198.05	-7.9	5.8	10–30	49.0	4.9	
14H-6, 85	127.02	31.4	195.65	-11.2	4.8	10–30			
14H-7, 25	127.52	37.3	199.95	-26.7	11.9	10–30	32.5	-8.3	
14H-8, 40	129.11	37.1	197.55	-6.3	6.4	10–35	28.8	9.6	
15H-2, 85	131.05								
15H-3, 85*	132.55								
15H-4, 85	134.05	186.7	236.35	7.5	9.7	5–30	165.6	-0.7	
15H-5, 85	135.55	273.0	137.95	49.4	5.8	10–30	118.1	23.4	
15H-6, 85	137.04								
15H-7, 40	138.10	153.1	197.15	-21.8	4.7	10–30	126.0	4.8	
16X-4, 80	138.79	332.0	328.7	-5.0	4.2	10–30			
17X-1, 85	148.44	78.5	79.7	-2.7	2.1	10–30	111.4	20.7	
17X-2, 85	149.94	346.3	349.3	23.7	11.6	5–30	17.2	6.5	
17X-3, 85	151.45								
17X-4, 50	152.60	274.5	274.1	18.5	4.4	5–25	287.9	7.1	
17X-5, 60	154.45	220.7	219.1	-16.4	8.8	5–40	237.5	8.0	
17X-6, 85	155.70	60.0	57.6	12.2	7.8	5–30	228.4	5.9	
17X-7, 50	156.60	155.1	155.7	16.1	5.4	10–30	134.2	19.2	

Notes: MAD = maximum angular deviation. * = samples thermally demagnetized.



Table T29. Magnetic susceptibility of discrete samples, Hole U1331A. (See table notes.) (Continued on next page.)

Core, section	Depth CSF (m)	LIMS ID	Susceptibility (SI)	Total mass (g)	Bulk density (g/cm ³)	Volume (cm ³)	Susceptibility			
							Volume normalized (SI)	Mass normalized (m ³ /kg)	Whole core (raw values)	Scale factor
320-U1331A-										
1H-1	0.45	CUBE554121	1.818E-04	11.66	1.10	6.45	1.974E-04	1.091E-07	28.0	7.050E-06
1H-2	2.37	CUBE554131	1.618E-04	11.04	1.16	5.57	2.033E-04	1.026E-07	26.8	7.584E-06
1H-3	3.84	CUBE554141	1.768E-04	11.59	1.20	5.85	2.116E-04	1.068E-07	27.2	7.779E-06
1H-4	4.70	CUBE554151	2.334E-04	11.99	1.08	6.85	2.386E-04	1.363E-07	34.0	7.018E-06
2H-1	6.05	CUBE557101	1.313E-04	11.72	1.21	5.87	1.565E-04	7.845E-08	20.6	7.598E-06
2H-2	7.57	CUBE557111	7.942E-05	13.51	1.35	6.62	8.395E-05	4.115E-08	13.4	6.265E-06
2H-3	9.04	CUBE557121	1.857E-04	13.77	1.48	6.20	2.096E-04	9.440E-08	24.0	8.735E-06
2H-4	10.54	CUBE557131	4.813E-05	11.71	1.57	4.54	7.417E-05	2.877E-08	10.0	7.417E-06
2H-5	12.07	CUBE557141	1.364E-04	12.35	1.55	4.99	1.912E-04	7.731E-08	20.0	9.562E-06
2H-6	13.54	CUBE557151	9.418E-05	14.59	1.49	6.70	9.834E-05	4.519E-08	13.4	7.339E-06
2H-7	14.56	CUBE557161	1.586E-04	11.35	1.49	4.53	2.450E-04	9.781E-08	28.6	8.566E-06
3H-1	15.79	CUBE559281	6.331E-05	12.73	1.43	5.70	7.776E-05	3.480E-08	16.5	4.713E-06
3H-2	17.33	CUBE559291	3.518E-05	13.37	1.34	6.56	3.754E-05	1.842E-08	9.2	4.080E-06
3H-3	18.79	CUBE559301	4.960E-05	14.03	1.31	7.20	4.823E-05	2.475E-08	12.1	3.986E-06
3H-4	20.29	CUBE559311	6.744E-05	11.24	1.26	5.26	8.974E-05	4.199E-08	16.9	5.310E-06
3H-5	21.83	CUBE559321	9.438E-05	13.15	1.26	6.77	9.760E-05	5.024E-08	20.1	4.856E-06
3H-6	23.29	CUBE559331	8.761E-05	13.00	1.26	6.65	9.222E-05	4.717E-08	18.7	4.931E-06
4H-2	26.58	CUBE560031	2.448E-04	10.90	1.22	5.18	3.308E-04	1.572E-07	45.1	7.334E-06
4H-3	28.04	CUBE560041	1.597E-04	12.68	1.19	6.79	1.647E-04	8.818E-08	23.8	6.920E-06
4H-4	29.55	CUBE560051	2.782E-04	12.88	1.20	6.90	2.821E-04	1.512E-07	36.6	7.707E-06
4H-5	31.08	CUBE560061	1.922E-04	10.15	1.24	4.47	3.008E-04	1.326E-07	39.2	7.675E-06
4H-6	32.55	CUBE560071	9.288E-05	9.99	1.19	4.53	1.435E-04	6.508E-08	20.1	7.138E-06
5H-1	34.55	CUBE560431	1.448E-04	11.47	1.16	5.91	1.715E-04	8.834E-08	24.2	7.085E-06
5H-2	36.05	CUBE560441	1.470E-04	12.18	1.16	6.52	1.579E-04	8.446E-08	23.1	6.834E-06
5H-3	37.58	CUBE560461	1.503E-04	11.93	1.13	6.50	1.617E-04	8.819E-08	24.2	6.683E-06
5H-4	39.04	CUBE560471	1.472E-04	12.49	1.16	6.78	1.519E-04	8.249E-08	22.3	6.812E-06
5H-5	40.54	CUBE560481	1.194E-04	11.91	1.18	6.22	1.345E-04	7.019E-08	19.8	6.791E-06
5H-6	42.03	CUBE560491	9.125E-05	11.31	1.20	5.60	1.141E-04	5.649E-08	17.2	6.636E-06
6H-1	44.04	CUBE560921	1.480E-04	11.28	1.20	5.55	1.866E-04	9.184E-08	26.4	7.068E-06
6H-2	45.54	CUBE560931	1.312E-04	10.75	1.16	5.33	1.724E-04	8.543E-08	24.9	6.925E-06
6H-3	47.07	CUBE560941	1.574E-04	12.08	1.07	7.01	1.571E-04	9.121E-08	23.8	6.601E-06
6H-4	48.54	CUBE560951	9.574E-05	10.39	0.95	6.11	1.096E-04	6.453E-08	19.8	5.538E-06
6H-5	50.03	CUBE560961	9.257E-05	11.85	1.20	6.05	1.071E-04	5.468E-08	14.3	7.492E-06
6H-6	51.55	CUBE560971	9.897E-05	11.83	1.20	6.03	1.149E-04	5.856E-08	15.8	7.270E-06
6H-7	52.09	CUBE560981	1.094E-04	12.09	1.20	6.25	1.226E-04	6.334E-08	16.1	7.613E-06
7H-1	53.54	CUBE561351	1.334E-04	12.34	1.23	6.30	1.482E-04	7.570E-08	18.3	8.099E-06
7H-2	55.05	CUBE561361	9.473E-05	12.08	1.19	6.30	1.053E-04	5.489E-08	15.4	6.837E-06
7H-3	56.57	CUBE561371	9.801E-05	11.89	1.03	7.07	9.704E-05	5.770E-08	16.1	6.027E-06
7H-4	58.04	CUBE561381	8.645E-05	11.53	1.17	5.92	1.022E-04	5.246E-08	14.3	7.149E-06
7H-5	59.54	CUBE561391	8.033E-05	12.21	1.15	6.62	8.494E-05	4.605E-08	12.1	7.020E-06
7H-6	61.04	CUBE561401	8.321E-05	11.45	1.19	5.75	1.014E-04	5.087E-08	14.3	7.088E-06
7H-7	62.09	CUBE561411	2.475E-05	11.43	1.18	5.80	2.989E-05	1.516E-08	5.9	5.067E-06
8H-1	63.04	CUBE561671	6.867E-05	11.54	1.16	6.01	8.002E-05	4.164E-08	-4.4	-1.819E-05
8H-2	64.54	CUBE561681	5.746E-05	12.08	1.22	6.13	6.566E-05	3.330E-08	8.8	7.461E-06
8H-3	66.07	CUBE561691	8.321E-05	12.38	1.19	6.55	8.889E-05	4.705E-08	11.0	8.081E-06
8H-4	67.55	CUBE561701	6.872E-05	11.89	1.08	6.77	7.104E-05	4.045E-08	10.3	6.897E-06
8H-5	69.05	CUBE561711	5.045E-05	12.25	1.18	6.47	5.460E-05	2.883E-08	9.2	5.934E-06
8H-6	70.54	CUBE561721	8.394E-05	12.41	1.11	7.04	8.347E-05	4.735E-08	14.3	5.837E-06
8H-7	71.76	CUBE561661	8.691E-05	12.28	1.20	6.41	9.496E-05	4.954E-08	11.0	8.633E-06
9H-2	74.04	CUBE562391	8.472E-05	11.62	1.20	5.86	1.012E-04	5.102E-08	14.3	7.077E-06
9H-3	75.57	CUBE562401	7.005E-05	11.79	1.36	5.29	9.268E-05	4.159E-08	14.3	6.481E-06
9H-4	77.04	CUBE562411	9.841E-05	12.50	1.32	5.99	1.151E-04	5.512E-08	18.7	6.154E-06
9H-5	78.54	CUBE562421	8.722E-05	13.15	1.21	7.09	8.611E-05	4.643E-08	16.1	5.348E-06
9H-6	80.04	CUBE562431	8.920E-05	13.13	1.29	6.61	9.450E-05	4.756E-08	15.4	6.137E-06
9H-7	81.34	CUBE562441	8.498E-05	12.54	1.31	6.07	9.806E-05	4.744E-08	9.9	9.905E-06
10H-2	83.54	CUBE562471	7.124E-05	12.39	1.34	5.80	8.604E-05	4.026E-08	12.5	6.883E-06
10H-3	85.08	CUBE562481	1.074E-04	12.38	1.22	6.38	1.178E-04	6.073E-08	16.9	6.970E-06
10H-4	86.54	CUBE562491	9.195E-05	12.28	1.28	6.02	1.069E-04	5.240E-08	14.7	7.272E-06
10H-5	88.05	CUBE562501	1.050E-04	12.67	1.29	6.28	1.171E-04	5.800E-08	17.6	6.651E-06
10H-6	89.54	CUBE562511	1.306E-04	12.60	1.11	7.19	1.272E-04	7.256E-08	23.4	5.434E-06
11H-2	92.23	CUBE563241	1.370E-04	12.07	1.19	6.26	1.532E-04	7.947E-08	21.6	7.092E-06
11H-3	93.75	CUBE563251	1.133E-04	12.11	1.23	6.10	1.300E-04	6.549E-08	18.0	7.220E-06
11H-4	95.23	CUBE563261	1.445E-04	12.32	1.23	6.30	1.606E-04	8.211E-08	21.2	7.578E-06
11H-5	96.73	CUBE563271	8.320E-05	11.89	1.20	6.11	9.539E-05	4.898E-08	15.4	6.194E-06



Table T29 (continued).

Core, section	Depth CSF (m)	LIMS ID	Susceptibility (SI)	Total mass (g)	Bulk density (g/cm ³)	Volume (cm ³)	Susceptibility			
							Volume normalized (SI)	Mass normalized (m ³ /kg)	Whole core (raw values)	Scale factor
11H-6	98.23	CUBE563281	1.102E-04	12.09	1.19	6.30	1.224E-04	6.380E-08	18.0	6.802E-06
12H-1	101.05	CUBE563941	1.258E-04	12.59	1.22	6.56	1.343E-04	6.997E-08	19.0	7.070E-06
12H-2	102.54	CUBE563961	9.047E-05	12.36	1.19	6.55	9.670E-05	5.124E-08	16.5	5.861E-06
12H-3	104.07	CUBE563971	1.059E-04	12.15	1.36	5.55	1.337E-04	6.101E-08	17.2	7.772E-06
12H-4	105.55	CUBE563981	6.936E-05	11.43	1.19	5.76	8.428E-05	4.247E-08	14.3	5.894E-06
12H-5	107.05	CUBE563991	7.589E-05	11.75	1.20	5.95	8.923E-05	4.521E-08	14.3	6.240E-06
12H-6	108.55	CUBE564001	7.968E-05	12.33	1.09	7.07	7.892E-05	4.524E-08	14.3	5.519E-06
12H-7	109.59	CUBE563951	6.737E-05	12.26	1.21	6.36	7.415E-05	3.847E-08	11.0	6.741E-06
13H-1	110.54	CUBE564901	4.432E-05	12.38	1.22	6.38	4.865E-05	2.506E-08	11.0	4.423E-06
13H-2	112.05	CUBE564911	5.755E-05	12.13	1.26	5.97	6.753E-05	3.321E-08	11.4	5.924E-06
13H-3	113.55	CUBE564921	6.836E-05	12.15	1.13	6.67	7.175E-05	3.940E-08	12.1	5.930E-06
13H-4	115.05	CUBE564931	7.117E-05	12.23	1.18	6.46	7.711E-05	4.073E-08	13.2	5.846E-06
13H-5	116.54	CUBE564941	1.287E-04	12.59	1.16	6.90	1.305E-04	7.156E-08	23.1	5.651E-06
13H-6	118.05	CUBE564951	4.502E-05	12.27	1.16	6.63	4.757E-05	2.568E-08	11.0	4.324E-06
13H-7	119.09	CUBE564961	6.558E-05	11.63	1.20	5.86	7.827E-05	3.947E-08	14.3	5.474E-06
14H-1	120.05	CUBE565411	5.514E-05	11.56	1.20	5.80	6.650E-05	3.340E-08	10.3	6.456E-06
14H-2	121.52	CUBE565421	7.610E-05	12.13	1.22	6.17	8.627E-05	4.392E-08	11.0	7.843E-06
14H-3	123.05	CUBE565431	1.091E-04	12.52	1.24	6.39	1.196E-04	6.100E-08	14.3	8.363E-06
14H-4	124.52	CUBE565441	8.067E-05	12.36	1.03	7.51	7.522E-05	4.568E-08	13.9	5.412E-06
14H-5	126.02	CUBE565451	6.212E-05	11.50	1.22	5.65	7.698E-05	3.781E-08	13.6	5.660E-06
14H-6	127.02	CUBE565461	9.757E-05	11.91	1.20	6.10	1.120E-04	5.735E-08	17.6	6.363E-06
14H-7	127.52	CUBE565471	7.256E-05	12.25	1.20	6.36	7.983E-05	4.146E-08	18.3	4.363E-06
14H-8	129.11	CUBE565481	7.231E-05	11.88	1.09	6.66	7.603E-05	4.261E-08	5.1	1.491E-05
15H-2	131.05	CUBE566391	8.800E-05	11.56	1.19	5.87	1.049E-04	5.327E-08	13.6	7.711E-06
15H-3	132.55	CUBE566401	6.647E-05	12.02	1.21	6.15	7.564E-05	3.871E-08	9.9	7.640E-06
15H-4	134.05	CUBE566411	8.735E-05	12.13	1.20	6.30	9.705E-05	5.040E-08	12.5	7.764E-06
15H-5	135.55	CUBE566421	9.177E-05	12.23	1.16	6.57	9.784E-05	5.253E-08	13.9	7.039E-06
15H-6	137.04	CUBE566431	1.085E-04	12.34	1.20	6.46	1.176E-04	6.155E-08	14.7	8.002E-06
15H-7	138.10	CUBE566441	1.065E-04	12.24	1.20	6.37	1.170E-04	6.091E-08	16.1	7.265E-06
16X-1	138.79	CUBE567411	6.613E-05	11.39	1.22	5.59	8.283E-05	4.066E-08	13.9	5.959E-06
17X-1	148.44	CUBE567941	9.297E-05	12.06	1.16	6.43	1.012E-04	5.398E-08	14.3	7.078E-06
17X-2	149.94	CUBE567951	8.837E-05	12.07	1.20	6.23	9.927E-05	5.125E-08	12.5	7.941E-06
17X-3	151.45	CUBE567961	9.969E-05	11.26	1.20	5.56	1.256E-04	6.197E-08	15.4	8.155E-06
17X-4	152.60	CUBE567971	1.140E-04	11.68	1.20	5.91	1.351E-04	6.831E-08	16.1	8.390E-06
17X-5	154.45	CUBE567981	8.471E-05	12.32	1.20	6.44	9.208E-05	4.813E-08	11.0	8.371E-06
17X-6	155.70	CUBE567991	7.615E-05	12.06	1.20	6.22	8.565E-05	4.420E-08	11.0	7.787E-06
17X-7	156.60	CUBE568001	9.154E-05	11.55	1.20	5.80	1.105E-04	5.548E-08	17.2	6.425E-06

Mean scale factor:

6.61E-06

Notes: Depth = depth to middle of discrete sample measured in meters using the core depth below seafloor, method A (CSF), depth scale. LIMS ID = sample identification within the Laboratory Information Management System (LIMS) database. Susceptibility = volume magnetic susceptibility of discrete sample measured in KappaBridge with volume of cube assumed to be 7 cm³. Mass = mass of sample including mass of plastic cube, which has a mean of 4.5921 g. Bulk density = density from moisture and density (MAD) measurements. When these were not available or were obviously anomalous, we used a density of 1.20 m³/kg. Volume = volume of sediments, calculated by subtracting mass of plastic cube from total mass and then dividing by bulk density. Volume normalized susceptibility = susceptibility of discrete samples normalized by true sample volume. These are unitless in the SI unit system. Mass normalized susceptibility = susceptibility of discrete samples normalize by mass of sediments in each sample cube. Scale factor = factor whole-core raw susceptibility values would need to be multiplied by to convert them to SI volume normalized susceptibilities.



Table T30. Magnetostratigraphy, Site U1331. (See table notes.) (Continued on next two pages.)

Polarity chron	Age (Ma)	Hole U1331A			Measurement type
		Range CSF (m)	Best estimate CSF (m)	Best estimate core, section, interval (cm)	
0	0.000	0.00–0.00	0.000	Mudline	
Normal-reversed, possibly C2n–C2r or younger		1.70–1.90	1.800	1H-2, 30	Split core
C2r–C2An.1n	2.581	3.20–3.25	3.225	1H-3, 22.5	Split core
C2An.1n–C2An.1r	3.032			Not identified	
Excursion (?)				Not identified	
C2An.1r–C2An.2n*	3.116			Not identified	
C2An.2n-1r (t)*				Not identified	
C2An.2n-1r (o)*				Not identified	
C2An.2n–C2An.2r*	3.207			Not identified (should occur in upper part of Section 2H-1)	
Hiatus			6.640	Hiatus at 2H-1, 144	Erosional contact
C10n.2n–C10r	28.318			Not identified	
C10r–C11n.1n	29.166	10.85–10.95	10.900	2H-4, 120	Split core
C11n.1n–C11n.1r	29.467	12.15–12.15	12.150	2H-5, 95	Split core
C11n.1r–C11n.2n	29.536	12.45–12.50	12.475	2H-5, 127.5	Split core
C11.2n–C11r	29.957	13.40–13.40	13.400	2H-6, 70	Split core
C11r–C12n	30.617			Not well recorded	Split core
C12n–C12r	31.021			Not well recorded	Split core
C12r–C13n	33.232	24.00–25.35	24.675	Between Cores 3H and 4H	Split core
C13n–C13r	33.705	25.80–25.80	25.800	4H-2, 10	Split core
C13r-1n (t)		28.45–28.45	28.450	4H-3, 125	Split core
C13r-1n (o)		28.55–28.55	28.550	4H-3, 135	Split core
C13r–C15n	35.126	30.05–30.05	30.050	4H-4, 135	Split core
C15n–C15r	35.254	30.85–30.85	30.850	4H-5, 65	Split core
C15r–C16n.1n	35.328	31.95–32.00	31.975	4H-6, 27.5	Split core
C16n.1n–C16n.1r	35.554	32.60–32.60	32.600	4H-6, 90 or lower (?)	Split core
C16n.1r–C16n.2n	35.643	34.00–34.00	34.000	5H-1, 30 or higher (?)	Split core
C16n.2n–C16r	36.355	37.85–38.00	37.925	5H-3, 122.5	Split core
C16r–C17n.1n	36.668	39.50–39.60	39.550	5H-4, 135	Split core
C17n.1n–C17n.1r	37.520	42.65–43.30	42.975	Between Cores 5H and 6H	Split core
C17n.1r–C17n.2n	37.656	43.95–43.95	43.950	6H-1, 75	Split core
C17n.2n–C17n.2r	37.907	44.45–44.45	44.450	6H-1, 125 or lower (?)	Split core
C17n.2r–C17n.3n	37.956	45.20–45.20	45.200	6H-2, 50 or higher (?)	Split core
C17n.3n–C17r	38.159	46.35–46.35	46.350	6H-3, 15 or higher (?)	Split core
C17r–C18n.1n	38.449	47.50–47.80	47.650	6H-3, 145	Split core
C18n.1n–C18n.1r	39.554	56.00–56.30	56.150	7H-3, 45	Split core
C18n.1r–C18n.2n	39.602	57.30–57.30	57.300	7H-4, 10	Split core
C18n.2n–C18r	40.084	62.85–63.00	62.925	8H-1, 72.5	Split core
C18r–C19n	41.358	81.35–84.80	83.075	10H-2, 7.5	Split core
C19n–C19r	41.510	87.90–88.10	88.000	10H-5, 80	Split core
C19r–C20n	42.536	98.78–98.98	98.880	11H-6, 150	Split core
C20n–C20r	43.789	118.60–118.90	118.750	13H-7, 5	Split core
C20r–C20r-1n(t)		136.40–136.40	136.400	15H-6, 20	Split core
C20r-1n(o)–C20r		136.85–136.85	136.850	15H-6, 65	Split core
C20r–C21n	46.264			Not identified	
C21n–C21r	47.906			Not identified	
C21r–C22n	49.037			Not identified	
C22n–C22r	49.714			Not identified	
C22r–C23n.1n	50.778			Not identified	
C23n.1n–C23n.1r	50.946			Not identified	
C23n.1r–C23n.2n	51.047			Not identified	
C23n.2n–C23r	51.743			Not identified	

Notes: * = correlation is uncertain. (t) = termination of magnetozone or chronozone, (o) = onset of magnetozone or chronozone.



Table T30 (continued). (Continued on next page.)

Polarity chron	Age (Ma)	Range CSF (m)	Best estimate CSF (m)	Hole U1331B	
				Best estimate core, section, interval (cm)	Measurement type
0	0.000			Not recovered	
Normal-reversed, possibly C2n–C2r or younger				Not recorded owing to coring deformation	
C2r–C2An.1n	2.581	2.30–2.35	2.325	1H-2, 82.5	Split core
C2An.1n–C2An.1r	3.032	4.60–4.70	4.650	1H-4, 15	Split core
Excursion (?)		5.10–5.10	5.100	1H-4, 60	Split core
C2An.1r–C2An.2n*	3.116	5.45–5.50	5.475	1H-4, 97.5	Split core
C2An.2n–1r (t)*				Between Sections 1H-4 and 5 (?)	
C2An.2n–1r (o)*				Between Sections 1H-4 and 5 (?)	
C2An.2n–C2An.2r*	3.207	6.35–6.35	6.350	1H-5, 35	Split core
Hiatus			7.170	Hiatus at 1H-5, 116	Erosional contact
C10n.2n–C10r	28.318			Not identified	
C10r–C11n.1n	29.166	11.85–11.95	11.900	2H-2, 30	Split core
C11n.1n–C11n.1r	29.467	13.20–13.30	13.250	2H-3, 15	Split core
C11n.1r–C11n.2n	29.536	13.45–13.55	13.500	2H-3, 40	Split core
C11.2n–C11r	29.957	14.50–14.80	14.650	2H-4, 5	Split core
C11r–C12n	30.617	16.20–16.25	16.225	2H-5, 12.5	Split core
C12n–C12r	31.021	16.90–17.00	16.950	2H-5, 85	Split core
C12r–C13n	33.232	24.50–24.60	24.550	3H-4, 45	Split core
C13n–C13r	33.705	26.00–26.10	26.050	3H-5, 45	Split core
C13r–1n (t)				Not identified	
C13r–1n (o)				Not identified	
C13r–C15n	35.126	29.10–29.20	29.150	Between Cores 3H and 4H	Split core
C15n–C15r	35.254	29.40–29.50	29.450	4H-1, 35	Split core
C15r–C16n.1n	35.328	30.35–30.50	30.425	4H-1, 132.5	Split core
C16n.1n–C16n.1r	35.554	31.40–31.45	31.425	4H-2, 82.5	Split core
C16n.1r–C16n.2n	35.643	33.20–33.50	33.350	4H-3, 125 (identification uncertain)	Split core
C16n.2n–C16r	36.355	35.85–35.95	35.900	4H-5, 80 (identification uncertain)	Split core
C16r–C17n.1n	36.668	38.85–39.25	39.050	Between Cores 4H and 5H (?)	Split core
C17n.1n–C17n.1r	37.520	44.45–44.70	44.575	5H-4, 147.5	Split core
C17n.1r–C17n.2n	37.656	45.05–45.15	45.100	5H-5, 50	Split core
C17n.2n–C17n.2r	37.907	46.25–46.35	46.300	5H-6, 20	Split core
C17n.2r–C17n.3n	37.956	46.60–46.60	46.600	5H-6, 50	Split core
C17n.3n–C17r	38.159	47.60–47.60	47.600	5H-7, 50	Split core
C17r–C18n.1n	38.449			Between Cores 5H and 6H (?)	
C18n.1n–C18n.1r	39.554			Probably between Cores 6H and 7H (?)	
C18n.1r–C18n.2n	39.602	58.85–58.85	58.850	7H-1, 125 or higher (?)	Split core
C18n.2n–C18r	40.084	64.85–64.85	64.850	7H-5, 125	Split core
C18r–C19n	41.358			Between Cores 9H and 10H (?)	
C19n–C19r	41.510	88.20–88.45	88.325	10H-2, 72.5	Split core
C19r–C20n	42.536	96.95–97.90	97.425	11H-2, 32.5	Split core
C20n–C20r	43.789	119.00–119.00	119.000	13H-3, 140	Split core
C20r–C20r–1n(t)				Not identified	
C20r–1n(o)–C20r				Not identified	
C20r–C21n	46.264	150.50–150.50	150.500	16H-5, 140	Split core
C21n–C21r	47.906			Not identified	
C21r–C22n	49.037			Not identified	
C22n–C22r	49.714			Not identified	
C22r–C23n.1n	50.778			Not identified	
C23n.1n–C23n.1r	50.946			Not identified	
C23n.1r–C23n.2n	51.047			Not identified	
C23n.2n–C23r	51.743			Not identified	



Table T30 (continued).

Polarity chron	Age (Ma)	Hole U1331C			Measurement type
		Range CSF (m)	Best estimate CSF (m)	Best estimate core, section, interval (cm)	
0	0.000	0.00–0.00		Mudline	
Normal-reversed, possibly C2n–C2r or younger		0.45–0.55	0.500	1H-1, 50.0	Split core
C2r–C2An.1n	2.581	2.50–2.55	2.525	1H-2, 102.5	Split core
C2An.1n–C2An.1r	3.032	5.05–5.10	5.075	1H-4, 57.5	Split core
Excursion (?)		5.40–5.55	5.475	1H-4, 97.5	Split core
C2An.1r–C2An.2n*	3.116	5.90–6.00	5.950	1H-4, 145	Split core
C2An.2n–1r (t)*		6.30–6.30	6.300	1H-5, 30.0	Split core
C2An.2n–1r (o)*		6.40–6.45	6.425	1H-5, 42.5	Split core
C2An.2n–C2An.2r*	3.207	6.75–6.75	6.750	1H-5, 75	Split core
Hiatus			7.580	Hiatus at 1H-6, 5	Erosional contact
C10n.2n–C10r	28.318			Not identified	
C10r–C11n.1n	29.166	10.30–10.35	10.325	2H-1, 82.5	Split core
C11n.1n–C11n.1r	29.467	11.55–11.60	11.575	2H-2, 57.5	Split core
C11n.1r–C11n.2n	29.536	11.80–11.80	11.800	2H-1, 80	Split core
C11.2n–C11r	29.957	12.80–12.80	12.800	2H-3, 30	Split core
C11r–C12n	30.617	14.20–14.50	14.350	2H-4, 35.0	Split core
C12n–C12r	31.021	15.10–15.10	15.100	2H-4, 110.0	Split core
C12r–C13n	33.232	25.10–25.25	25.175	3H-5, 17.5	Split core
C13n–C13r	33.705	26.60–26.65	26.625	3H-6, 12.5	Split core
C13r–1n (t)				Not cored	
C13r–1n (o)				Not cored	
C13r–C15n	35.126			Not cored	
C15n–C15r	35.254			Not cored	
C15r–C16n.1n	35.328			Not cored	
C16n.1n–C16n.1r	35.554			Not cored	
C16n.1r–C16n.2n	35.643			Not cored	
C16n.2n–C16r	36.355			Not cored	
C16r–C17n.1n	36.668			Not cored	
C17n.1n–C17n.1r	37.520			Not cored	
C17n.1r–C17n.2n	37.656			Not cored	
C17n.2n–C17n.2r	37.907			Not cored	
C17n.2r–C17n.3n	37.956			Not cored	
C17n.3n–C17r	38.159			Not cored	
C17r–C18n.1n	38.449			Not cored	
C18n.1n–C18n.1r	39.554			Not cored	
C18n.1r–C18n.2n	39.602			Not cored	
C18n.2n–C18r	40.084	61.85–61.90	61.875	6H-2, 137.5	Split core
C18r–C19n	41.358			Not cored	
C19n–C19r	41.510			Not cored	
C19r–C20n	42.536			Not cored	
C20n–C20r	43.789			Not cored	
C20r–C20r–1n(t)				Not cored	
C20r–1n(o)–C20r				Not cored	
C20r–C21n	46.264	148.65–148.70	148.675	14H-1, 67.5	Split core
C21n–C21r	47.906			Not identified	
C21r–C22n	49.037			Not identified	
C22n–C22r	49.714			Not identified	
C22r–C23n.1n	50.778			Not identified	
C23n.1n–C23n.1r	50.946			Not identified	
C23n.1r–C23n.2n	51.047	179.20–179.25	179.225	16H-2, 72.5	Split core
C23n.2n–C23r	51.743	186.05–186.10	186.075	17H-2, 57.5	Split core



Table T31. Interstitial water data from squeezed whole-round samples, Site U1331. (See table notes.)

Core, section, interval (cm)	Depth (m)		Alkalinity (mM)	Salinity (mM)	Cl ⁻ (mM)	Na ⁺ (mM)	SO ₄ ²⁻ (mM)	HPO ₄ ⁻ (μM)	H ₄ SiO ₄ (μM)	Mn ²⁺ (μM)	Fe ²⁺ (μM)	Ca ²⁺ (mM)	Mg ²⁺ (mM)	B (μM)	Sr ²⁺ (μM)	Ba ²⁺ (μM)	Li ⁺ (μM)	K ⁺ (mM)	
	CSF	CCSF-A																	
320-U1331A-																			
1H-2, 145–150	2.95	2.95	7.41	2.58	34.0	559	486	27.3	BDL	473	BDL	BDL	10.1	50.1	490	81.2	1.9	28.5	10.3
2H-2, 145–150	8.15	9.65	7.39	2.57	—	560	498	27.4	1.1	493	BDL	BDL	8.9	46.0	437	69.5	2.9	23.7	9.2
2H-5, 145–150	12.65	14.15	7.44	2.51	34.0	561	497	28.3	BDL	562	BDL	BDL	9.5	47.2	468	73.7	1.6	25.0	9.8
3H-2, 145–150	17.65	20.56	7.41	2.64	34.0	557	472	27.9	0.7	586	BDL	BDL	9.6	49.8	436	73.1	1.6	23.3	9.8
3H-5, 145–150	22.15	25.06	7.43	2.62	34.0	565	503	29.2	BDL	616	BDL	BDL	9.5	47.2	457	76.4	1.8	24.4	9.8
4H-2, 145–150	27.15	30.41	7.49	2.95	34.5	563	493	29.2	BDL	605	BDL	BDL	10.3	50.3	473	82.9	2.0	27.7	10.2
4H-5, 145–150	31.65	34.91	7.53	3.02	34.5	566	492	28.7	BDL	635	BDL	BDL	10.6	51.1	470	80.9	1.8	27.2	10.7
5H-3, 145–150	38.15	43.74	7.52	2.97	34.5	563	492	29.5	BDL	498	BDL	BDL	10.3	50.7	462	79.6	2.0	25.8	10.8
6H-3, 145–150	47.65	55.15	7.52	2.94	34.5	562	487	28.8	BDL	567	BDL	BDL	10.7	51.8	451	78.9	1.7	25.5	10.4
7H-3, 145–150	57.15	66.20	7.49	2.97	34.0	564	492	28.9	BDL	610	BDL	BDL	10.6	50.5	440	81.1	2.0	25.2	10.3
8H-3, 145–150	68.10	77.96	7.49	2.94	34.0	560	483	28.3	—	643	BDL	BDL	10.7	52.4	435	80.2	1.9	24.4	10.4
9H-3, 145–150	76.15	86.60	7.51	2.77	34.0	558	483	28.5	—	590	BDL	BDL	10.4	51.8	429	80.1	1.8	25.3	10.2
10H-3, 145–150	85.65	94.17	7.43	2.66	34.0	560	490	27.7	—	632	BDL	BDL	9.8	49.1	453	78.8	1.7	25.4	9.9
11H-3, 145–150	94.33	105.34	7.43	2.72	34.0	562	492	27.8	—	645	BDL	BDL	10.1	49.3	446	77.7	1.7	23.7	9.7
12H-3, 145–150	104.65	117.87	7.51	2.97	34.5	558	490	27.9	—	535	BDL	BDL	10.0	48.5	437	77.4	1.8	23.1	9.3
13H-3, 145–150	114.15	129.21	7.53	3.08	34.5	562	495	28.1	—	761	BDL	BDL	10.1	48.7	413	75.6	1.7	22.6	9.2
14H-3, 145–150	123.62	139.80	7.49	3.01	34.0	563	490	27.9	—	689	BDL	BDL	10.6	50.3	407	73.0	1.7	21.3	9.8
15H-3, 145–150	133.15	149.33	7.55	2.78	34.5	560	487	28.3	—	661	BDL	BDL	10.5	50.8	407	70.0	1.7	22.1	9.8
17X-3, 145–150	152.05	167.12	7.46	2.96	34.5	563	490	27.5	—	658	BDL	BDL	10.4	50.2	413	71.0	1.6	22.6	10.1
320-U1331B-																			
15H-3, 140–150	138.00	154.67	7.56	3.04	34.5	561	480	27.4	—	701	BDL	BDL	10.9	53.2	416	74.1	1.9	22.6	10.8
17H-1, 140–150	154.00	169.56	7.55	3.00	34.5	565	491	30.2	—	620	BDL	BDL	10.6	52.7	436	77.0	1.7	22.2	10.7

Notes: — = no data. BDL = below detection limit (HPO₄⁻ = 0.6 μM, Mn²⁺ = 0.1 μM, Fe²⁺ = 0.4 μM, B = 2 μM, Sr²⁺ = 1 μM, Ba²⁺ = 0.3 μM, Li⁺ = 3 μM) calculated as three times the standard deviation of multiple measures of a blank. H₄SiO₄ values measured by different techniques during Expeditions 320 and 321 disagree significantly, especially for low values. Therefore, caution should be used concerning the H₄SiO₄ data and comparison between the different expeditions.



Table T32. Interstitial water data from rhizone samples, Section 320-U1331B-1H-6. (See table notes.)

Core, section, interval (cm)	Depth (m)		Alkalinity (mM)	Cl ⁻ (mM)	Na ⁺ (mM)	SO ₄ ²⁻ (mM)	H ₄ SiO ₄ (µM)	Mn ²⁺ (µM)	Fe ²⁺ (µM)	Ca ²⁺ (mM)	Mg ²⁺ (mM)	B (µM)	Sr ²⁺ (µM)	Ba ²⁺ (µM)	Li ⁺ (µM)	K ⁺ (mM)	
	CSF	CCSF-A	pH	Salinity													
320-U1331B-																	
1H-6, 10	7.61	8.46	ND	ND	556	488	28.3	459	BDL	BDL	9.5	48.8	471	73.1	1.6	23.7	10.5
1H-6, 20	7.71	8.56	ND	ND	560	483	27.8	477	BDL	BDL	10.2	52.0	471	73.3	1.5	23.6	11.3
1H-6, 30	7.81	8.66	ND	ND	556	476	27.4	470	BDL	BDL	10.4	52.7	468	72.6	1.5	23.2	11.4
1H-6, 40	7.91	8.76	ND	ND	556	477	27.3	474	BDL	BDL	10.3	52.2	478	76.8	1.6	24.5	11.0
1H-6, 50	8.01	8.86	ND	ND	558	480	27.5	492	BDL	BDL	10.2	52.1	467	74.0	1.6	23.8	10.8
1H-6, 60	8.11	8.96	ND	ND	558	483	27.5	468	BDL	BDL	9.9	51.1	463	73.5	1.6	23.7	10.8
1H-6, 70	8.21	9.06	ND	ND	553	479	27.9	438	BDL	BDL	9.8	51.0	467	75.0	1.6	24.4	10.7
1H-6, 80	8.31	9.16	ND	ND	556	481	27.7	354	BDL	BDL	9.9	51.3	444	71.6	1.5	23.2	10.8
1H-6, 90	8.41	9.26	ND	ND	556	481	27.5	451	BDL	BDL	9.8	51.3	462	73.8	1.6	23.8	10.6
1H-6, 100	8.51	9.36	ND	ND	559	482	27.9	454	BDL	BDL	9.9	52.4	452	70.8	1.5	22.7	10.9
1H-6, 110	8.61	9.46	ND	ND	559	482	27.8	476	BDL	BDL	10.3	52.1	438	69.3	1.6	22.3	10.9
1H-6, 120	8.71	9.56	ND	ND	561	491	28.2	479	BDL	BDL	9.5	49.9	452	70.6	1.5	22.8	10.3
1H-6, 130	8.81	9.66	ND	ND	560	484	27.7	433	BDL	BDL	10.0	51.7	472	73.7	1.6	24.2	11.0
1H-6, 140	8.91	9.76	ND	ND	556	481	27.9	504	BDL	BDL	9.9	51.5	464	73.0	1.5	23.7	10.7

Notes: ND = not determined. BDL = below detection limit (Mn²⁺ = 0.1 µM, Fe²⁺ = 0.4 µM, B = 2 µM, Sr²⁺ = 1 µM, Ba²⁺ = 0.3 µM, Li⁺ = 3 µM) calculated as three times the standard deviation of multiple measures of a blank. H₄SiO₄ values measured by different techniques during Expeditions 320 and 321 disagree significantly, especially for low values. Therefore, caution should be used concerning the H₄SiO₄ data and comparison between the different expeditions.

Table T33. Inorganic geochemistry of solid samples, Site U1331. (See table notes.)

Core, section, interval (cm)	Depth CSF (m)	Major element oxide (wt%)								Trace element (ppm)									
		SiO ₂	Al ₂ O ₃	Fe ₂ O ₃ T	MnO	MgO	CaO	Na ₂ O	K ₂ O	TiO ₂	P ₂ O ₅	Ba	Cr	Cu	Sc	Sr	V	Y	
320-U1331A-																			
13H-2, 65–66	111.85	9.75	0.47	0.45	0.03	0.32	41.68	1.16	0.27	0.01	0.26	2,723	BDL	53	0.6	2,009	BDL	15.9	17.9
320-U1331C-																			
16H-4, 0–3	181.50	76.75	0.42	1.29	0.10	1.05	0.41	4.08	0.30	0.02	0.21	1,530	5.1	66	2.7	63.8	9.0	29.4	17.9
16H-4, 48–50	181.98	79.84	0.72	3.32	0.79	1.66	0.47	4.68	0.39	0.04	0.25	1,356	10.1	194	4.2	92.2	25.0	29.2	34.4
16H-4, 116–118	182.66	72.55	1.13	4.46	1.38	2.63	0.58	3.67	0.51	0.06	0.32	3,350	13.8	268	5.6	131.9	31.7	49.4	42.3
16H-4, 133–135	182.83	63.60	1.72	6.66	2.34	3.35	0.74	3.75	0.64	0.10	0.41	4,433	14.4	415	8.1	180.2	45.5	67.0	55.2
17H-2, 53–60	186.03	72.91	0.49	1.42	0.23	1.36	0.37	4.28	0.31	0.02	0.19	2,765	BDL	79	2.6	92.4	11.0	22.5	21.8
17H-2, 90–98	186.40	48.87	3.98	13.33	5.13	9.05	1.87	3.10	0.97	0.23	1.07	6,604	18.2	1,015	19.1	292.4	70.7	204.7	111.2
17H-3, 35–42	187.35	44.90	7.25	13.83	4.93	4.69	6.24	3.05	1.69	0.39	3.60	13,442	25.3	1,191	39.6	621.8	154.5	579.6	186.4
17H-3, 90–97	187.90	7.24	0.85	1.22	0.14	0.78	37.95	1.09	0.25	0.07	0.71	BDL	7.6	99	3.8	501.6	BDL	27.2	25.3
17H-4, 83–84	189.33	44.31	10.93	6.34	0.30	4.54	10.26	3.44	2.16	0.60	4.69	BDL	28.8	209	26.1	218.5	20.7	75.3	63.2

Notes: BDL = below detection limit (SiO₂ = 3.5 wt%, Al₂O₃ = 0.04 wt%, Fe₂O₃ T = 0.003 wt%, MnO = 0.0004 wt%, MgO = 0.007 wt%, CaO = 0.1 wt%, Na₂O = 0.02 wt%, K₂O = 0.004 wt%, TiO₂ = 0.001 wt%, P₂O₅ = 0.1 wt%, Ba = 28 wt%, Cr = 5 wt%, Cu = 16 wt%, Sc = 0.4 wt%, Sr = 3 wt%, V = 4 wt%, Y = 1.7 wt%, Zr = 4 wt%). See Table T9 in the "Methods" chapter for maximum values of calibration.

Table T34. Calcium carbonate and organic carbon data, Site U1331. (See table notes.) (Continued on next page.)

Core, section, interval (cm)	Depth (m)		CaCO ₃ (wt%)	IC (wt%)	TC (wt%)	TOC (wt%)	
	CSF	CCSF-A				Normal	Acid
320-U1331A-							
1H-1, 65–66	0.65	0.65	BDL	BDL	0.24	0.24	ND
1H-2, 65–66	2.16	2.16	BDL	BDL	0.52	0.52	ND
1H-3, 65–66	3.65	3.65	BDL	BDL	0.14	0.14	ND
2H-1, 65–66	5.85	7.35	3.2	0.38	0.18	ND	0.04
2H-2, 65–66	7.36	8.86	51.6	6.19	6.84	0.66	0.03
2H-3, 65–66	8.84	10.34	51.3	6.15	6.76	0.60	BDL
2H-4, 65–66	10.33	11.83	77.0	9.25	9.59	0.35	BDL
2H-5, 65–66	11.86	13.36	80.6	9.68	9.87	0.19	BDL
2H-6, 65–66	13.34	14.84	63.2	7.59	7.95	0.37	BDL
2H-7, 15–16	14.34	15.84	34.2	4.11	5.64	1.53	BDL
3H-1, 105–106	15.74	18.65	76.2	9.15	8.20	ND	BDL
3H-2, 105–106	17.28	20.19	77.3	9.27	8.74	ND	BDL
3H-3, 105–106	18.74	21.65	82.3	9.87	10.01	0.13	BDL
3H-4, 105–106	20.24	23.15	72.8	8.74	8.53	ND	0.03
3H-5, 105–106	21.78	24.69	48.9	5.87	6.56	0.69	BDL
3H-6, 105–106	23.24	26.15	41.0	4.92	5.05	0.13	BDL
4H-2, 65–66	26.37	29.63	BDL	BDL	0.19	0.19	ND
4H-3, 65–66	27.85	31.11	BDL	BDL	0.98	0.98	ND
4H-4, 65–66	29.35	32.61	BDL	BDL	0.25	0.25	ND
4H-5, 65–66	30.87	34.13	BDL	BDL	0.14	0.14	ND
4H-6, 60–61	32.30	35.56	BDL	BDL	0.24	0.24	ND
4H-7, 60–61	33.81	37.07	35.6	4.28	4.67	0.39	BDL
5H-1, 65–66	34.35	39.94	BDL	BDL	0.27	0.27	ND
5H-2, 65–66	35.85	41.44	BDL	BDL	0.22	0.22	ND
5H-3, 65–66	37.38	42.97	BDL	BDL	0.23	0.23	ND
5H-4, 65–66	38.85	44.44	BDL	BDL	0.97	0.97	ND
5H-5, 65–66	40.34	45.93	BDL	BDL	0.92	0.92	ND
5H-6, 65–66	41.83	47.42	BDL	BDL	0.28	0.28	ND
5H-7, 20–21	42.40	47.99	BDL	BDL	0.26	0.26	ND
6H-1, 65–66	43.85	51.35	BDL	BDL	0.14	0.14	ND
6H-2, 65–66	45.34	52.84	BDL	BDL	0.30	0.30	ND
6H-3, 65–66	46.87	54.37	BDL	BDL	0.14	0.14	ND
6H-4, 65–66	48.34	55.84	BDL	BDL	0.27	0.27	0.05
6H-5, 65–66	49.83	57.33	14.1	1.70	1.45	ND	BDL
6H-6, 50–51	51.20	58.70	27.3	3.27	3.30	0.03	BDL
6H-7, 20–21	51.90	59.40	10.0	1.20	2.14	0.95	BDL
7H-1, 65–66	53.34	62.39	6.0	0.72	1.17	0.44	ND
7H-2, 65–66	54.85	63.90	BDL	BDL	0.53	0.53	ND
7H-3, 65–66	56.37	65.42	BDL	BDL	0.42	0.42	ND
7H-4	57.85	66.90	BDL	BDL	0.58	0.58	ND
7H-5, 65–66	59.34	68.39	BDL	BDL	0.50	0.5	ND
7H-6, 65–66	60.84	69.89	BDL	BDL	0.13	0.13	ND
7H-7, 65–66	62.34	71.39	BDL	BDL	0.48	0.48	ND
8H-1, 64–65	62.84	72.70	BDL	BDL	0.95	0.95	ND
8H-3, 64–65	65.86	75.72	BDL	BDL	0.25	0.25	ND
8H-4, 64–65	67.34	77.20	BDL	BDL	0.28	0.28	ND
8H-5, 64–65	68.84	78.70	BDL	BDL	0.47	0.47	ND
8H-6, 64–65	70.34	80.20	32.1	3.86	4.35	0.50	BDL
8H-7, 30–31	71.50	81.36	30.6	3.67	5.36	1.69	BDL
9H-2, 65–66	73.85	84.30	BDL	BDL	0.49	0.49	ND
9H-3, 65–66	75.37	85.82	16.0	1.92	2.24	0.32	ND
9H-4, 65–66	76.85	87.30	63.1	7.57	7.74	0.17	BDL
9H-5, 45–46	78.15	88.60	42.6	5.12	5.36	0.24	BDL
9H-6, 45–46	79.64	90.09	44.5	5.35	5.53	0.19	BDL
9H-7, 45–46	81.14	91.59	43.5	5.22	5.21	ND	BDL
10H-2, 65–66	83.34	91.86	41.5	4.98	5.27	0.29	BDL
10H-3, 65–66	84.87	93.39	27.2	3.26	2.97	ND	BDL
10H-4, 65–66	86.34	94.86	20.2	2.43	3.01	0.58	BDL
10H-5, 65–66	87.85	96.37	15.9	1.90	2.82	0.92	BDL
10H-6, 65–66	89.34	97.86	43.5	5.22	5.74	0.53	ND
11H-2, 65–66	92.03	103.04	18.0	2.16	2.93	0.77	BDL
11H-3, 65–66	93.55	104.56	25.0	3.01	3.71	0.70	BDL
11H-4, 65–66	95.03	106.04	BDL	BDL	0.19	0.19	ND
11H-5, 65–66	96.53	107.54	BDL	BDL	0.04	0.04	ND
11H-6, 65–66	98.03	109.04	BDL	BDL	0.12	0.12	ND
12H-1, 65–66	100.85	114.07	11.1	1.33	1.78	0.44	ND

Table T34 (continued).

Core, section, interval (cm)	Depth (m)		CaCO ₃ (wt%)	IC (wt%)	TC (wt%)	TOC (wt%)	
	CSF	CCSF-A				Normal	Acid
12H-2, 65–66	102.34	115.56	BDL	BDL	0.12	0.12	ND
12H-3, 65–66	103.86	117.08	BDL	BDL	0.88	0.88	ND
12H-4, 65–66	105.35	118.57	BDL	BDL	0.45	0.45	ND
12H-5, 65–66	106.85	120.07	BDL	BDL	0.27	0.27	ND
12H-6, 65–66	108.35	121.57	BDL	BDL	0.17	0.17	ND
12H-7, 20–21	109.40	122.62	BDL	BDL	0.51	0.51	ND
13H-1, 65–66	110.34	125.40	6.0	0.72	0.74	0.03	BDL
13H-2, 65–66	111.85	126.91	BDL	BDL	0.20	0.20	BDL
13H-3, 65–66	113.35	128.41	BDL	BDL	0.88	0.88	ND
13H-4, 65–66	114.85	129.91	BDL	BDL	1.12	1.12	ND
13H-5, 65–66	116.35	131.41	26.0	3.12	3.78	0.66	BDL
13H-6, 65–66	117.85	132.91	18.0	2.15	2.84	0.69	ND
13H-7, 50–51	119.19	134.25	21.3	2.55	3.29	0.74	BDL
14H-1, 65–66	119.85	136.03	BDL	BDL	0.26	0.26	ND
14H-2, 65–66	121.32	137.50	BDL	BDL	0.18	0.18	ND
14H-3, 65–66	122.84	139.02	7.0	0.84	1.43	0.59	ND
14H-4, 65–66	124.32	140.50	BDL	BDL	0.19	0.19	ND
14H-5, 65–66	125.82	142.00	BDL	BDL	0.19	0.19	ND
14H-6, 65–66	126.93	143.11	BDL	BDL	0.20	0.20	ND
14H-7, 33–34	127.6	143.78	BDL	BDL	0.23	0.23	ND
14H-8, 16–17	128.37	144.55	BDL	BDL	0.20	0.20	ND
15H-1, 114–115	129.84	146.02	BDL	BDL	0.23	0.23	ND
15H-3, 114–115	132.84	149.02	BDL	BDL	0.19	0.19	ND
15H-4, 105–106	134.25	150.43	BDL	BDL	0.22	0.22	ND
15H-5, 114–115	135.84	152.02	BDL	BDL	0.19	0.19	ND
15H-6, 116–117	137.35	153.53	BDL	BDL	0.21	0.21	ND
15H-7, 20–21	137.90	154.08	BDL	BDL	0.20	0.20	ND
16X-1, 60–61	138.80	154.98	BDL	BDL	0.18	0.18	ND
17X-1, 64–65	148.23	163.30	BDL	BDL	0.18	0.18	ND
17X-2, 64–65	149.74	164.81	BDL	BDL	0.03	0.03	ND
17X-3, 64–65	151.24	166.31	BDL	BDL	0.06	0.06	ND
17X-4, 25–26	152.35	167.42	BDL	BDL	0.04	0.04	BDL
17X-5, 64–65	154.24	169.31	BDL	BDL	0.03	0.03	BDL
17X-6, 40–41	155.50	170.57	BDL	BDL	0.20	0.20	ND
17X-7, 30–31	156.40	171.47	BDL	BDL	0.20	0.20	ND
320-U1331C-							
17H-2, 20–21	185.7	201.12	BDL	BDL	—	—	ND
17H-4, 83–84	189.33	204.75	2.7	0.32	—	—	ND

Notes: IC = inorganic carbon, TC = total carbon, TOC = total organic carbon, Acid = determined by acidification method. BDL = below detection limit ($\text{CaCO}_3 < 1 \text{ wt\%}$, TOC by either method = $< 0.03 \text{ wt\%}$) as determined by three times the standard deviation of replicate measures of a low concentration sample. When CaCO_3 is BDL, TOC is reported as equal to TC. ND = not determined (negative TOC wt%), — = no data.



Table T35. Moisture and density measurements, Hole U1331A.

Core, section, interval (cm)	Depth CSF (m)	Water content (%)	Density (g/cm ³)			Water content (%)	Density (g/cm ³)		
			Wet bulk	Dry bulk	Grain		Wet bulk	Dry bulk	Grain
320-U1331A-									
1H-2, 75–76	2.25	80.2	1.16	0.23	2.44	90.6	9H-6, 75–76	79.95	64.4
1H-3, 75–76	3.75	75.3	1.20	0.30	2.45	87.9	9H-7, 55–56	81.25	62.3
2H-1, 75–76	5.95	74.7	1.21	0.31	2.67	88.5	10H-2, 75–76	83.45	63.2
2H-2, 75–76	7.45	49.4	1.49	0.75	2.67	71.7	10H-3, 75–76	84.95	72.9
2H-3, 75–76	8.95	37.7	1.84	1.15	3.58	67.9	10H-4, 75–76	86.45	66.8
2H-4, 75–76	10.45	22.0	2.33	1.82	3.66	50.3	10H-5, 75–76	87.95	67.8
2H-5, 25–26	11.95	49.8	1.48	0.74	2.64	71.9	11H-2, 75–76	92.13	74.6
3H-1, 100–101	15.70	53.4	1.43	0.67	2.61	74.5	11H-3, 75–76	93.63	72.0
3H-5, 100–101	21.70	61.2	1.34	0.52	2.59	79.9	11H-4, 75–76	95.13	73.8
3H-6, 100–101	23.20	63.4	1.31	0.48	2.55	81.2	11H-5, 75–76	96.63	70.4
4H-2, 75–76	26.45	72.2	1.22	0.34	2.39	85.8	11H-6, 75–76	98.13	74.2
4H-3, 75–76	27.95	74.7	1.19	0.30	2.30	86.9	12H-1, 75–76	100.95	73.4
4H-4, 75–76	29.45	36.8	2.10	1.32	5.35	75.2	12H-2, 75–76	102.45	75.3
4H-5, 75–76	30.95	69.0	1.24	0.39	2.37	83.7	12H-3, 75–76	103.95	58.2
4H-6, 75–76	32.45	74.3	1.19	0.31	2.26	86.4	12H-4, 75–76	105.45	74.3
5H-3, 75–76	37.45	77.7	1.16	0.26	2.23	88.4	12H-5, 75–76	106.95	76.0
5H-4, 75–76	38.95	77.7	1.16	0.26	2.23	88.4	12H-7, 30–31	109.50	72.1
5H-6, 75–76	41.95	77.9	1.16	0.26	2.26	88.6	13H-1, 75–76	110.45	70.4
5H-7, 8–9	42.28	76.0	1.18	0.28	2.23	87.3	13H-2, 75–76	111.95	70.5
6H-1, 75–76	43.95	74.0	1.20	0.31	2.42	87.1	13H-4, 75–76	114.95	74.3
6H-4, 75–76	48.45	78.6	1.16	0.25	2.20	88.7	13H-7, 30–31	119.00	75.0
6H-7, 30–31	52.00	73.3	1.22	-0.33	2.52	87.1	14H-1, 75–76	119.95	74.0
7H-1, 75–76	53.45	72.4	1.23	0.34	2.58	86.8	14H-3, 75–76	122.92	72.2
7H-2, 75–76	54.95	74.0	1.19	0.31	2.19	85.9	14H-5, 75–76	125.92	72.6
7H-4, 75–76	57.95	77.3	1.17	0.27	2.33	88.6	14H-6, 80–81	127.42	72.1
7H-5, 75–76	59.45	79.3	1.15	0.24	2.19	89.1	14H-7, 15–16	127.47	74.6
7H-6, 75–76	60.95	77.1	1.19	0.27	2.70	89.9	15H-3, 75–76	132.45	75.2
7H-7, 30–31	62.00	76.0	1.18	0.28	2.28	87.6	15H-4, 75–76	133.95	75.0
8H-1, 75–76	62.95	79.3	1.16	0.24	2.30	89.6	15H-5, 75–76	135.45	73.5
8H-2, 75–76	64.45	73.3	1.22	0.33	2.60	87.4	15H-6, 75–76	136.95	78.5
8H-3, 75–76	65.95	78.2	1.19	0.26	2.81	90.8	16X-1, 70–71	138.90	75.9
8H-5, 75–76	68.95	76.2	1.18	0.28	2.37	88.1	17X-1, 75–76	148.35	74.6
9H-3, 75–76	75.45	61.6	1.36	0.52	2.88	81.9	17X-2, 75–76	149.85	68.1
9H-4, 74–75	76.94	62.3	1.32	0.50	2.53	80.3	17X-3, 75–76	151.35	75.5
9H-5, 75–76	78.45	71.6	1.21	0.34	2.19	84.4	17X-4, 33–34	152.43	74.3
							17X-5, 75–76	154.35	74.7
									1.16
									0.29
									1.91
									75.7



Table T36. Split-core *P*-wave velocity measurements, Hole U1331A. ([Continued on next page.](#))

Core, section	Depth CSF (m)	Velocity (m/s)			Core, section	Depth CSF (m)	Velocity (m/s)		
		x-axis	y-axis	z-axis			x-axis	y-axis	z-axis
320-U1331A-									
1H-1	1.20			1514	7H-2	55.52	1609		
1H-1	1.27	1611			7H-3	56.99	1530	1529	
1H-1	1.39		1431	1514	7H-3	57.08	1619		
1H-2	1.39			1526	7H-4	58.41	1535	1529	
1H-2	2.71	1604			7H-4	58.50	1608		
1H-2	2.78		1430	1528	7H-5	60.05	1530	1528	
1H-3	2.91		1543	1485	7H-5	60.14	1618		
1H-3	4.35	1593			7H-6	61.47	1530	1487	
1H-4	4.41		1549		7H-6	61.64	1604		
1H-4	4.84	1625			7H-7	62.31	1551	1538	
2H-1	4.90		1526		7H-7	62.39	1596		
2H-1	6.48	1588			8H-1	63.53	1543	1530	
2H-2	6.57		1514	1453	8H-1	63.63	1586		
2H-2	7.93	1567			8H-2	65.02	1539	1531	
2H-3	8.02			1505	8H-2	65.10	2981		
2H-3	9.46	1572			8H-3	66.46	1542	1534	
2H-4	9.55		1528		8H-3	66.55	1589		
2H-4	10.95	1581			8H-4	68.00	1432	1536	
2H-5	11.07		1525	1516	8H-4	68.10	1597		
2H-5	12.45	1593			8H-5	69.50	1537	1527	
2H-6	13.99		1509	1504	8H-5	69.58	3105		
2H-6	14.08	1565			8H-6	71.01	1532	1526	
3H-1	15.96		1521		8H-6	71.13	1587		
3H-1	16.08	1588			9H-2	74.50	1550	1164	
3H-2	17.48		1517		9H-2	74.59	1611		
3H-2	17.57	1576			9H-3	75.91	1555	1444	
3H-3	19.03		1512	1507	9H-3	76.01	1618		
3H-3	19.12	1560			9H-4	77.51		1484	
3H-4	20.54		1513	1506	9H-4	77.59	1589		
3H-4	20.62	1563			9H-5	79.02	1531	1476	
3H-5	21.97		1522	1471	9H-5	79.11	1580		
3H-5	22.07	1581			9H-6	80.50	1529	1787	
3H-6	23.52		1519	1516	9H-6	80.59	3003		
3H-6	23.62	1581			10H-1	82.52		1519	1480
4H-2	26.96		1553		10H-3	84.20		1547	
4H-2	27.08	1605			10H-3	85.48	1610		
4H-3	28.53		1552		10H-4	87.06		1546	1481
4H-3	28.62	1609			10H-4	87.20	1585		
4H-4	30.03		1549	1476	10H-5	87.20		1546	
4H-4	30.14	1587			10H-5	88.60	1584		
4H-5	31.48		1539	1534	11H-2	92.68		1555	
4H-5	31.57		1608		11H-2	92.77	1599		
5H-1	35.06		1524	1527	11H-3	94.18		1542	
5H-2	36.48		1528		11H-3	94.27	1567		
5H-3	36.61		1533	1531	11H-4	95.69		1560	
5H-4	39.57		1527	1529	11H-4	95.77	1578		
5H-5	41.06		1528	1531	11H-5	97.25	1592		
5H-6	42.13		1531	1528	11H-6	98.73		1565	1547
5H-7	42.68		1546	1531	11H-6	98.81	1597		
6H-1	44.55		1522	1800	12H-1	101.43	1585		
6H-1	44.55		1535		12H-1	101.55		1432	1475
6H-1	44.65	1645			12H-2	102.99		1546	
6H-2	46.05		1528	1531	12H-2	103.23	1614		
6H-2	46.15	1645			12H-3	104.40	1634		
6H-3	47.48		1549	1526	12H-3	104.51		1560	1532
6H-3	47.59		1622		12H-4	105.95		1527	1532
6H-4	48.99		1528	1525	12H-4	105.95			1161
6H-4	49.10		1629		12H-4	106.06	1620		
6H-5	50.51		1522	1526	12H-5	107.44		1552	1538
6H-5	50.62	1604			12H-5	107.62	1624		
6H-6	51.49		1522	1522	12H-6	109.01		1539	1487
6H-6	51.60	1625			12H-6	109.01		1543	
6H-7	52.25		1520	1510	12H-6	109.14	1633		
6H-7	52.34	1594			12H-7	109.74	1622		
7H-1	53.92		1533	1527	12H-7	109.87		1450	1546
7H-1	54.00	1595			13H-1	110.74	1624		
7H-2	55.33		1533		13H-2	112.51		1549	1466
					13H-2	112.51		1554	

Table T36 (continued).

Core, section	Depth CSF (m)	Velocity (m/s)			Core, section	Depth CSF (m)	Velocity (m/s)		
		x-axis	y-axis	z-axis			x-axis	y-axis	z-axis
13H-2	112.61	1627			14H-7	127.79	1627		
13H-3	114.01		1544	1542	14H-8	128.52	1633		
13H-3	114.11	1642			15H-1	129.91	1564		
13H-4	115.48		1553	1466	15H-1	130.01		1533	1534
13H-4	115.61	1617			15H-2	131.50		1534	1534
13H-5	116.99		1539	1433	15H-2	131.60	1535		
13H-5	116.99		1445		15H-3	133.01		1534	1532
13H-5	117.13	1577			15H-3	133.08	1580		
13H-6	118.57		1454	1495	15H-4	134.40		1536	1533
13H-6	118.64	1611			15H-4	134.50	1584		
13H-7	118.82		1554	1542	15H-5	135.99		1545	1540
13H-7	118.94	1619			15H-5	136.12	1630		
14H-1	120.51		1568	1543	15H-6	137.53		1540	1534
14H-1	120.62	1618			15H-6	137.63	1605		
14H-2	121.88	1624			15H-7	138.25		1543	1534
14H-2	121.99		1559	1520	15H-7	138.35	1619		
14H-2	122.12	3098			16X-1	139.12			1540
14H-3	123.42		1554	1541	16X-1	139.20	1598		
14H-3	123.51	1628			17X-2	150.41			1453
14H-4	124.99		1562	1542	17X-2	150.50	1601		
14H-4	125.07	1623			17X-4	153.30	1598		
14H-5	126.52		1547	1539	17X-4	153.39		1545	1487
14H-5	126.61	1629			17X-5	154.97		1543	1536
14H-6	127.65		1567	1548	17X-5	155.05	1607		
14H-6	127.68	1629			17X-6	155.99		1552	1539
14H-7	127.74		1461	1547	17X-6	156.08	1598		

Table T37. Thermal conductivity, Site U1331.

Core, section, interval (cm)	Depth CSF (m)	Thermal conductivity (W/[m·K])
320-U1331A-		
1H-2, 81	2.31	0.770
2H-3, 104	9.24	0.927
3H-3, 115	18.85	1.145
4H-4, 115	29.85	0.776
5H-3, 115	37.85	0.778
6H-3, 115	47.35	0.763
7H-3, 115	56.85	0.749
8H-3, 115	66.35	0.751
9H-3, 115	75.85	0.762
10H-3, 115	85.35	0.823
11H-3, 115	94.03	0.795
12H-3, 115	104.35	0.754
13H-3, 115	113.85	0.760
14H-3, 115	123.32	0.760
15H-3, 115	132.85	0.761
16X-1, 70	138.90	0.738
17X-3, 100	151.60	0.761
19X-2, 30	161.80	0.739
19X-CC, 12	162.20	0.766
22X-1, 30	186.70	0.795
320-U1331B-		
1H-3, 115	4.00	0.767
1H-3, 115	4.15	0.771
2H-3, 115	14.25	0.941
3H-3, 115	23.75	0.824
4H-3, 115	33.26	0.821



Table T38. Shipboard core top, composite, and corrected composite depths, Site U1331.

Core	Depth CSF (m)	Offset (m)	Top depth (m)	
			CCSF-A	CCSF-B
320-U1331A-				
1H	0.0	0.00	0.00	0.00
2H	5.2	1.50	6.70	6.09
3H	14.7	2.91	17.61	16.01
4H	24.2	3.26	27.46	24.96
5H	33.7	5.59	39.29	35.72
6H	43.2	7.50	50.70	46.09
7H	52.7	9.05	61.75	56.14
8H	62.2	9.86	72.06	65.51
9H	71.7	10.45	82.15	74.68
10H	81.2	8.52	89.72	81.56
11H	90.7	11.01	101.71	92.46
12H	100.2	13.22	113.42	103.11
13H	109.7	15.06	124.76	113.42
14H	119.2	16.18	135.38	123.07
15H	128.7	16.18	144.88	131.71
16X	138.2	16.18	154.38	140.34
17X	147.6	15.07	162.67	147.88
19X	160.5	15.07	175.57	159.61
320-U1331B-				
1H	0.0	0.85	0.85	0.78
2H	10.1	0.27	10.37	9.43
3H	19.6	2.98	22.58	20.53
4H	29.1	3.76	32.86	29.87
5H	38.6	5.85	44.45	40.41
6H	48.1	7.43	55.53	50.48
7H	57.6	7.55	65.15	59.22
8H	67.1	9.88	76.98	69.98
9H	76.6	10.09	86.69	78.81
10H	86.1	10.99	97.09	88.26
11H	95.6	12.12	107.72	97.93
12H	105.1	13.63	118.73	107.93
13H	114.6	14.82	129.42	117.66
14H	124.1	14.34	138.44	125.86
15H	133.6	16.67	150.27	136.61
16H	143.1	13.47	156.57	142.34
17H	152.6	15.56	168.16	152.87
320-U1331C-				
1H	0.0	0.54	0.54	0.49
2H	9.5	2.12	11.62	10.57
3H	19.0	2.07	21.07	19.15
4H	28.5	2.64	31.14	28.31
6H	59.0	10.70	69.70	63.36
8H	92.5	12.18	104.68	95.17
10H	102.5	12.18	114.68	104.26
12H	129.0	14.17	143.17	130.16
13H	138.5	14.67	153.17	139.25
14H	148.0	15.42	163.42	148.56
16H	177.0	15.42	192.42	174.92
17H	184.0	15.42	199.42	181.29



Table T39. Splice tie points, Site U1331.

Hole, core, section, interval (cm)	Depth (m)		Hole, core, section, interval (cm)	Depth (m)	
	CSF	CCSF-A		CSF	CCSF-A
320-					
U1331A-1H-3, 102	4.02	4.02	Tie to	U1331C-1H-3, 49	3.49
U1331C-1H-5, 97	6.97	7.50	Tie to	U1331A-2H-1, 80	6.00
U1331A-2H-5, 82	12.02	13.53	Tie to	U1331C-2H-2, 40	11.40
U1331C-2H-6, 25	17.25	19.37	Tie to	U1331A-3H-2, 26	16.46
U1331A-3H-6, 3	22.23	25.14	Tie to	U1331B-3H-2, 106	22.16
U1331B-3H-5, 18	25.78	28.76	Tie to	U1331A-4H-1, 130	25.50
U1331A-4H-5, 128	31.48	34.73	Tie to	U1331B-4H-2, 37	30.97
U1331B-4H-6, 18	36.78	40.54	Tie to	U1331A-5H-1, 125	34.95
U1331A-5H-5, 94	40.64	46.23	Tie to	U1331B-5H-2, 27	40.37
U1331B-5H-7, 66	47.76	53.62	Tie to	U1331A-6H-2, 142	46.12
U1331A-6H-7, 46	52.16	59.66	Tie to	U1331B-6H-3, 113	52.23
U1331B-6H-5, 87	54.97	62.40	Tie to	U1331A-7H-1, 65	53.35
U1331A-7H-7, 32	62.02	71.07	Tie to	U1331C-6H-1, 138	60.38
U1331C-6H-4, 64	64.14	74.84	Tie to	U1331A-8H-2, 128	64.98
U1331A-8H-5, 94	69.14	79.00	Tie to	U1331B-8H-2, 52	69.12
U1331B-8H-6, 51	75.11	84.98	Tie to	U1331A-9H-2, 133	74.53
U1331A-9H-5, 146	79.16	89.61	Tie to	U1331B-9H-2, 142	79.52
U1331B-9H-3, 147	81.07	91.16	Tie to	U1331A-10H-1, 144	82.64
U1331A-10H-6, 19	88.89	97.40	Tie to	U1331B-10H-1, 32	86.42
U1331B-10H-5, 82	92.92	103.91	Tie to	U1331A-11H-3, 3	92.91
U1331A-11H-5, 84	96.72	107.73	Tie to	U1331C-8H-3, 5	95.55
U1331C-8H-6, 3	100.03	112.21	Tie to	U1331B-11H-3, 149	100.09
U1331B-11H-7, 24	104.84	116.96	Tie to	U1331A-12H-3, 54	103.74
U1331A-12H-5, 130	107.50	120.72	Tie to	U1331B-12H-2, 49	107.09
U1331B-12H-6, 70	113.30	126.93	Tie to	U1331A-13H-2, 67	111.87
U1331A-13H-6, 88	118.08	133.14	Tie to	U1331B-13H-3, 72	118.32
U1331B-13H-7, 29	123.89	138.72	Tie to	U1331A-14H-3, 37	122.54
U1331A-14H-5, 104	126.21	142.38	Tie to	U1331B-14H-3, 94	128.04
U1331B-14H-5, 57	130.67	145.01	Tie to	U1331C-12H-2, 34	130.84
U1331C-12H-7, 6	137.86	152.04	Tie to	U1331B-15H-2, 27	135.37
U1331B-15H-3, 67	137.27	153.94	Tie to	U1331C-13H-1, 76	139.26
U1331C-13H-5, 125	145.75	160.42	Tie to	U1331B-16H-3, 85	146.95
U1331B-16H-6, 69	151.29	164.77	Tie to	U1331A-17X-2, 60	149.70



Table T40. Magnetostratigraphic and biostratigraphic datums, Site U1331. (See table note). (Continued on next page.)

Event	Age (Ma)	Depth CCSF-A (m)	Error (m)
C2r–C2An.1n	2.581	3.20	
C2An.1n–C2An.1r	3.032	5.56	
C2An.1r–C2An.2n	3.116	6.41	
C2An.2n–C2An.2r	3.207	7.25	
C10r–C11n.1n	29.166	12.34	
C11n.1n–C11n.1r	29.467	13.62	
C11n.1r–C11n.2n	29.536	13.89	
C11.2n–C11r	29.957	14.91	
C11r–C12n	30.617	16.48	
C12n–C12r	31.021	17.22	
C12r–C13n	33.232	27.39	
C13n–C13r	33.705	28.93	
C13r–C15n	35.126	33.31	
C15n–C15r	35.254	34.11	
C15r–C16n.1n	35.328	35.24	
C16n.1n–C16n.1r	35.554	35.86	
C16n.1r–C16n.2n	35.643	39.59	
C16n.2n–C16r	36.355	43.52	
C16r–C17n.1n	36.668	45.14	
C17n.1r–C17n.2n	37.656	51.45	
C17n.2n–C17n.2r	37.907	52.05	
C17n.2r–C17n.3n	37.956	52.58	
C17n.3n–C17r	38.159	53.65	
C17r–C18n.1n	38.449	55.15	
C18n.1n–C18n.1r	39.554	65.20	
C18n.1r–C18n.2n	39.602	66.38	
C18n.2n–C18r	40.084	72.59	
C18r–C19n	41.358	91.60	
C19n–C19r	41.510	96.52	
C19r–C20n	42.536	109.72	
C20n–C20r	43.789	133.82	
C20r–C21n	47.906	164.03	
C23n.1r–C23n.2n	51.047	194.65	
C23n.2n–C23r	51.743	201.50	
Nannofossils			
B <i>Sphenolithus distentus</i>	30.0	12.65	0.75
T <i>Reticulofenestra umbilicus</i>	32.0	25.46	0.75
T <i>Coccolithus formosus</i>	32.9	26.73	0.52
T <i>Discoaster saipanensis</i>	34.4	32.56	4.00
T <i>Chiasmolithus grandis</i>	37.1	58.35	0.95
B <i>Dictyococcites bisectus</i>	38.0	61.08	0.98
T <i>Chiasmolithus solitus</i>	40.4	71.81	8.26
B <i>Reticulofenestra umbilicus</i> >14 µm	42.5	106.44	0.75
T <i>Nannotetra fulgens</i>	43.4	128.89	2.58
T <i>Tribrachiatius orthostylus</i>	50.7	203.47	0.05
Radiolarians			
B <i>Theocyrtis annosa</i>	28.33	10.75	1.50
T <i>Trityllospyris triceratops</i> > <i>Dorcadospyris ateuchus</i>	28.60	14.28	2.03
B <i>Dorcadospyris circulus</i>	29.96	19.80	2.08
B <i>Dorcadospyris spinosa</i>	30.84	23.36	1.48
B <i>Dorcadospyris pseudopapilio</i>	31.00	28.52	1.49
<i>Lithocyctia aristotelis</i> > <i>Lithocyctia angusta</i>	33.82	28.52	1.49
B <i>Lithocyctia angusta</i>	34.13	31.51	1.50
T <i>Thryscyrtis tetricanthia</i>	35.30	35.11	2.10
B <i>Lophocyrtis hadra</i>	35.34	39.53	2.32
B <i>Calocyctas bandycia</i>	36.74	46.60	1.76
B <i>Cryptocarpium azyx</i>	37.52	54.75	1.50
B <i>Podocyrtis goetheana</i>	40.16	69.38	2.17
<i>Podocyrtis mitra</i> > <i>Podocyrtis chalara</i>	40.70	89.82	2.10
B <i>Sethochytris triconiscus</i>	42.40	106.46	1.50
<i>Podocyrtis sinuosa</i> > <i>Podocyrtis mitra</i>	43.84	128.81	1.50
<i>Podocyrtis phyxis</i> > <i>Podocyrtis ampla</i>	44.77	139.40	1.50
B <i>Eusyringium lagena</i>	47.42	160.34	4.88
<i>Theocotyle nigriniae</i> > <i>Theocotyle cryptocephala</i>	49.00	179.63	2.46
Foraminifers			
T <i>Paragloborotalia opima</i>	26.9	10.39	1.29



Table T40 (continued).

Event	Age (Ma)	Depth CCSF-A (m)	Error (m)
B <i>Paragloborotalia opima</i>	30.8	14.11	2.42
T <i>Acarinina bulbrookii</i>	40.8	91.79	0.25
B <i>Turborotalia pomeroli</i>	42.4	95.26	3.74
T <i>Morozovella subbotinae</i>	50.8	192.16	10.08

Note: B = bottom, T = top.

Table T41. Results from APCT-3 temperature profiles, Hole U1331B. (See table notes.)

Core	Temperature (°C)				
	Average at mudline	Minimum above mudline	Depth DSF (m)	In situ temperature (°C)	Thermal resistance (m ² K/m)
320-U1331B-					
2H	1.550	1.448	19.6	1.88	22.4
3H	1.552	1.452	29.1	1.89	33.7
5H	1.564	1.459	48.1	2.40	58.5
7H	1.609	1.457	67.1	2.21	83.9
10H	1.572	1.461	95.6	2.86	121.1
Average:	1.569	1.455			

Notes: In situ temperatures were determined using the TP-Fit software by Martin Heesemann. Thermal resistance was calculated from thermal conductivity data (see “Physical properties”) corrected for in situ conditions (see “Downhole measurements” in the “Methods” chapter).